Naval Research Laboratory
Stennis Space Center, MS 39529-5004

NRL/FR/7176--96-9650

von WISPR Family Processors: Volume 1

RONALD A. WAGSTAFF
ALLEN E. LEYBOURNE
JACOB GEORGE

Ocean Acoustics Branch
Acoustics Division

July 7, 1997

Approved for public release; distribution unlimited.

REPORT DOCUMENTATION PAGE

Form Approved
OBM No. 0704-0188

Public reporting burden for this collection of information is estimated to average 1 hour per response, including the time for reviewing instructions, searching existing data sources, gathering and maintaining the data needed, and completing and reviewing the collection of information. Send comments regarding this burden or any other aspect of this collection of information, including suggestions for reducing this burden, to Washington Headquarters Services, Directorate for information Operations and Reports, 1215 Jefferson Davis Highway, Suite 1204, Arlington, VA 22202-4302, and to the Office of Management and Budget, Paperwork Reduction Project (0704-0188), Washington, DC 20503.

1. AGENCY USE ONLY *(Leave blank)*

2. REPORT DATE
July 7, 1997

3. REPORT TYPE AND DATES COVERED
Final

4. TITLE AND SUBTITLE
von WISPR Family Processors: Volume 1

5. FUNDING NUMBERS
Job Order No. 571683007
Program Element No.
Project No. 0602435N
Task No.
Accession No.

6. AUTHOR(S)
Ronald A. Wagstaff, Allen E. Leybourne, and Jacob George

7. PERFORMING ORGANIZATION NAME(S) AND ADDRESS(ES)
Naval Research Laboratory
Acoustics Division
Stennis Space Center, MS 39529-5004

8. PERFORMING ORGANIZATION REPORT NUMBER
NRL/FR/7176--96-9650

9. SPONSORING/MONITORING AGENCY NAME(S) AND ADDRESS(ES)
Naval Research Laboratory
Acoustics Division
Stennis Space Center, MS 39529-5004

10. SPONSORING/MONITORING AGENCY REPORT NUMBER

11. SUPPLEMENTARY NOTES

12a. DISTRIBUTION/AVAILABILITY STATEMENT
Approved for public release; distribution unlimited.

12b. DISTRIBUTION CODE

13. ABSTRACT *(Maximum 200 words)*

Fluctuation-based signal processing is a new approach to signal processing. It focuses on the situation in which the signals of interest fluctuate less than signals that are not of interest (clutter) and the background noise they are embedded in. Processors utilizing those fluctuations such as the von WISPR Family Processors discussed herein, are methods or algorithms that preferentially attenuate the fluctuating signals and noise as their fluctuation levels increase. Both amplitude and phase fluctuations can be exploited, the latter requiring novel approaches to coherent processing. The net effects can be significant enhancements in the characteristics, attributes, or products of the signal processor. Some examples include enhancements in signal-to-noise ratio, clutter reduction or elimination, spatial and spectral resolution, and minimum detectable level. Several processors that provide such enhancements are presented and discussed using measured and simulated data. In many cases, the results are independent of the spatial aperture of the measurement apparatus (sensor or array) and the spectral resolution (frequency binwidth) of the spectrum analyzer. The implication is that exploiting fluctuations is a means whereby the signal processor can tap into an additional independent source of gain. The results presented herein provide both qualitative and quantitative measures of the additional gains that can be achieved by exploiting the fluctuations in signal and noise. Although most of the examples presented are for underwater acoustic data, the generality of fluctuation-based processing is demonstrated for other types of data as well.

14. SUBJECT TERMS
signal processing, classification, antisubmarine warfare, underwater acoustics

15. NUMBER OF PAGES
150

16. PRICE CODE

17. SECURITY CLASSIFICATION OF REPORT
Unclassified

18. SECURITY CLASSIFICATION OF THIS PAGE
Unclassified

19. SECURITY CLASSIFICATION OF ABSTRACT
Unclassified

20. LIMITATION OF ABSTRACT
Same as report

NSN 7540-01-280-5500

Standard Form 298 (Rev. 2-89)
Prescribed by ANSI Std. Z39-18
298-102

INTRODUCTION AND OVERVIEW

This Report covers recent NRL research and development related to the AEC laser-pellet fusion program. The work covered in this report was primarily carried out under AEC Contract No. AT(04-3)-878 between July, 1973 and June, 1974. In some cases, for the sake of clarity, work not performed during this period has been included. In addition, the report discusses the large complementary program supported by the Defense Nuclear Agency at NRL on the study of laser produced plasmas in high atomic number materials. A significant part of the soft x-ray experimental studies (Chapter V) and all of the numerical modelling studies (Chapter VIII and Chapter IX) were supported by the DNA program. This work has been included in the present report for the sake of completeness and since many of the results obtained are of direct benefit to the AEC laser-fusion effort.

There is some overlap in time, with the period covered by the last NRL report, which was presented to the Laser-Fusion Coordinating Committee in November, 1973. However, it was felt useful to establish the precedent of fiscal year reporting starting with this Annual Report. In the future, a report on the AEC supported laser-fusion studies at NRL will appear on a semi-annual basis.

Studies of laser produced plasmas began at NRL in 1968. Development of a large Q-switched glass laser facility was carried out under ARPA sponsorship. Additional support for laser development was received as part of a DNA-supported program to study the interactions between an expanding laser-produced plasma and an ambient magnetized plasma background. The DNA program also provided NRL with the genesis of its expertise in the study of laser plasma generation and interactions. The glass laser system was developed under joint ARPA and DNA sponsorship to the point where, by FY 72, it represented the state-of-the-art in high power short pulse lasers. The system included an NRL designed mode-locked YAG oscillator system and a disc amplifier which became a prototype for those now in use and under development in the laser-fusion program.

When a large AEC supported laser-fusion effort began in FY 72, NRL was a logical place to turn to for support in building up the programs of the AEC laboratories. Shortly after the start of AEC-supported work at NRL, a DNA program at NRL was initiated to study laser produced high atomic number plasmas. The aim of this program was to develop a new source of soft x-rays for weapons effect simulation. The combined AEC and DNA supported programs have been known within NRL as the Laser-Matter Interaction (LMI) Program and Dr. John Stamper has served as Program Manager since its inception. The LMI Program has included contributions from a number of divisions at NRL and has involved both experimental and theoretical studies. The funding of the program during FY 74 consisted of $500,000 from the AEC for laser-fusion studies as well as additional funding from DNA for x-ray source investigations.

One of the unique features of the NRL laser-fusion program has been the availability of a reliable Nd:glass laser system which produces exceptionally clean pulses (i.e., spatially, temporally and spectrally pure) at sufficient power levels ($\lesssim$ 0.5 TW) for many studies of interest to laser fusion. Over 1500 laser shots were put on target in FY 74 for our AEC

CONTENTS

1.0 INTRODUCTION 1

1.1 Essence of the von WISPR Family Processors 1
1.2 Fluctuation-Based Processors 5
1.3 Fluctuation Processing: Signal and Noise Suppression 7
1.4 Organization of the Report 8

2.0 EQUATIONS FOR SEVERAL RELATED AND EFFECTIVE PROCESSING ALGORITHMS 9

2.1 Introduction 9
2.2 Magnitude Order in Decibels 10
2.3 The Conventional Processor/Filter (AVGPR) 11
2.4 Fluctuation-Based Processors/Filters Equal to M_r 11
2.5 Fluctuation-Based Processors/Filters Derived from M_r 11

3.0 FUNDAMENTAL CONCEPTS OF FLUCTUATION-BASED PROCESSORS ILLUSTRATED WITH WISPR 12

3.1 Introduction 12
3.2 Fluctuation Amplitude 13
3.3 Fluctuation Modeling 19
3.4 An Example of WISPR Response to a Submerged Shallow-Water Tonal and Noise 25
3.5 Gain Improvement Illustrated Using Synthesized Data 25
3.6 Influence of the Type of Distribution Function on WISPR Processing, Illustrated with Data from a Shallow-Water Environment 32
3.7 Gain Improvement, Illustrated Using Single-Channel Data from a Towed Line Array 41
3.8 Enhancing Resolution of a Horizontal Sonar Array FFT Beamformer 42
3.9 Summary 44

4.0 ADVANCED WISPR SUMMATION PROCESSORS ($AWSUM_k$) 45

4.1 Introduction 45
4.2 Demonstration of WISPR Processing 45
4.3 Comparison of AWSUM Orders 1 and 4 at Five Levels of Spectral Resolution 49
4.4 Comparison of AWSUM Orders 1 and 4 for Nonacoustic Data 52
4.5 $AWSUM_k$: Submerged Source Identification 54
4.6 $AWSUM_k$: Performance for Low SNR 56
4.7 $AWSUM_k$: Performance for $k = 1$ and $k = 4$ for Sonobuoy Data Using Overlapped Processing 59
4.8 Summary 59

5.0 ADDITIONAL SNR GAIN FOR THE WISPR AND $AWSUM_4$ FILTERS USING STANDARD DEVIATION OF THE TIME SERIES: THE WISPR II_k AND $AWSUM_4$ II_k FILTERS 61

5.1 Introduction 61
5.2 Signal Gain Improvement Rationale for the AVGPR Processor 61
5.3 Signal Gain Improvement for the WISPR Filter: WISPR II_k 63
5.4 Signal Gain Improvement for the $AWSUM_4$ Filter: $AWSUM_4$ II_k 63
5.5 Gains Achieved for WISPR II_k Processing 63
5.6 Removal of Clutter Tonals with WISPR II_4 Processing 67
5.7 Comparison of WISPR II_4 Performance with WISPR and $AWSUM_4$ for Specific Signals 67
5.8 Summary 70

6.0 TYPICAL WISPR FILTER APPLICATIONS 71

6.1 Introduction 71
6.2 Robustness to Harsh Transients and Intermittent High-Level Noise 71
6.3 Improvement in Spatial Resolution – A Substitute for Increased Array Aperture 74
6.4 Spectral/Spatial Resolution Enhancement and Compensation for Array Misalignments and Instabilities 78
6.5 Summary 85

7.0 ADVANCED WISPR FILTER APPLICATIONS 86

7.1 Introduction 86
7.2 Multifrequency Matched-Field Processing 86
7.3 WISPR Applied to Frequency Domain Matched Filtering 89
7.4 WISPR and the Active Barrier 90
7.5 WISPR Time History (Gram) Performance/Robustness to Masking 94
7.6 Noise Spectrum Equalization (NSE) via Fluctuation-Based Processing to Enhance Submerged Source Detection and Classification 101
7.7 Summary 109

8.0 WISPR FILTER COHERENT PROCESSING APPLICATIONS, WISPR III_k AND A_kCSDM 109

8.1 Introduction 109
8.2 The WISPR III_k Processor 109
8.3 The AWSUM Cross-Spectral Density Matrix, A_kCSDM Processor, and the WISPR Cross-Spectral Density Matrix, $WCSDM = A_1CSDM$ Processor 112

9.0 COMBINING THE WISPR FILTER WITH OTHER HIGH-RESOLUTION PROCESSORS 117

9.1 Introduction 117
9.2 High Gain and Resolution with the Combined WB^2 and WISPR Processors 117
9.3 High Gain and Resolution with the Combined DIET and WISPR Processors 119

10.0 MEASURES OF WISPR PROCESSOR PERFORMANCE 123

10.1 The Problem with the DI as a WISPR Performance Measure 123
10.2 WISPR Performance Measured by ROC Curves and the Relationship to DI 128

11.0 ACKNOWLEDGMENTS 131

12.0 REFERENCES 131

Appendix A — PROCESSING ALGORITHMS AND RELATED EQUATIONS 133

Appendix B — LIST OF RELATED PUBLICATIONS 143

von WISPR FAMILY PROCESSORS: VOLUME 1

1.0 INTRODUCTION

The philosophical approach that is taken in this document and in all of the fluctuation-based processing research that is reported herein is that there is an important class of signal processing situations of interest to the Navy where the signal of interest fluctuates in amplitude and phase less than other signals that are not of interest (clutter) and noise. A signal processor, or signal processing algorithm, that discriminates against (or attenuates) the highly fluctuating signals and noise less than the signals that have much smaller fluctuations can be of considerable value to the Navy. The von WISPR (**W**agstaff's **I**ntegration **S**ilencing **PR**ocessor) Family Processors perform in that manner, and their potential value to the Navy (as well as the signal processing community in general) is, in a small part, reflected in this document. The significance of this processor family is that previously unimaginable gains in signal processing performance are achieved through exploitation of a new or third signal processing dimension. This new dimension is essentially independent of the two dimensions of frequency binwidth resolution (spectral domain) and aperture size (spatial domain) which have in many cases already been exploited to practical limits. As a result, some of the signal processing needs not currently met by techniques limited to the two dimensions of the spectral domain and spatial domain, may be satisfied when fluctuation gains are added. Additionally, the size of the von WISPR Family Processors presented herein is evidence that there is more than one way to exploit fluctuations and that the area of fluctuation exploitation is fertile territory for new techniques, methods, and applications.

A cogent example of the von WISPR Family Processors' capabilities is provided by the data in Fig. 1.1. Processing for both plots in that figure is for the conventional average power, top-curve designated average power processor (AVGPR); one of the von WISPR Family Processors, middle-curve designated FILTER; and the submerged source detector, designated DETECTOR. The left plot (projector on surface) has fluctuations characteristic of High Fluctuation Amplitude Tonals (HIFAT) or surface ship clutter signals and noise. The right plot (projector submerged) has fluctuations characteristic of Low Fluctuation Amplitude Tonals (LOFAT) from a submerged source. The detector curve will approach 0 dB (usually less than 1.5 dB) on the DETECTOR curve when a submerged source is present. This occurs near "A" in the projector submerged plot, indicating a submerged source, whereas no detection of a submerged source is indicated in the projector on surface plot, just as it should have been. In all aspects, the two projectors and the environmental conditions were identical with the exception that one projector was near the surface and the other was submerged.

1.1 Essence of the von WISPR Family Processors

The essence of the von WISPR Family Processors is embodied in Fig. 1.2. The objective of the measurement for which the results in Fig. 1.2 correspond was the unalerted detection and identification (i.e., classification) of a projected tonal from a distant submerged source.

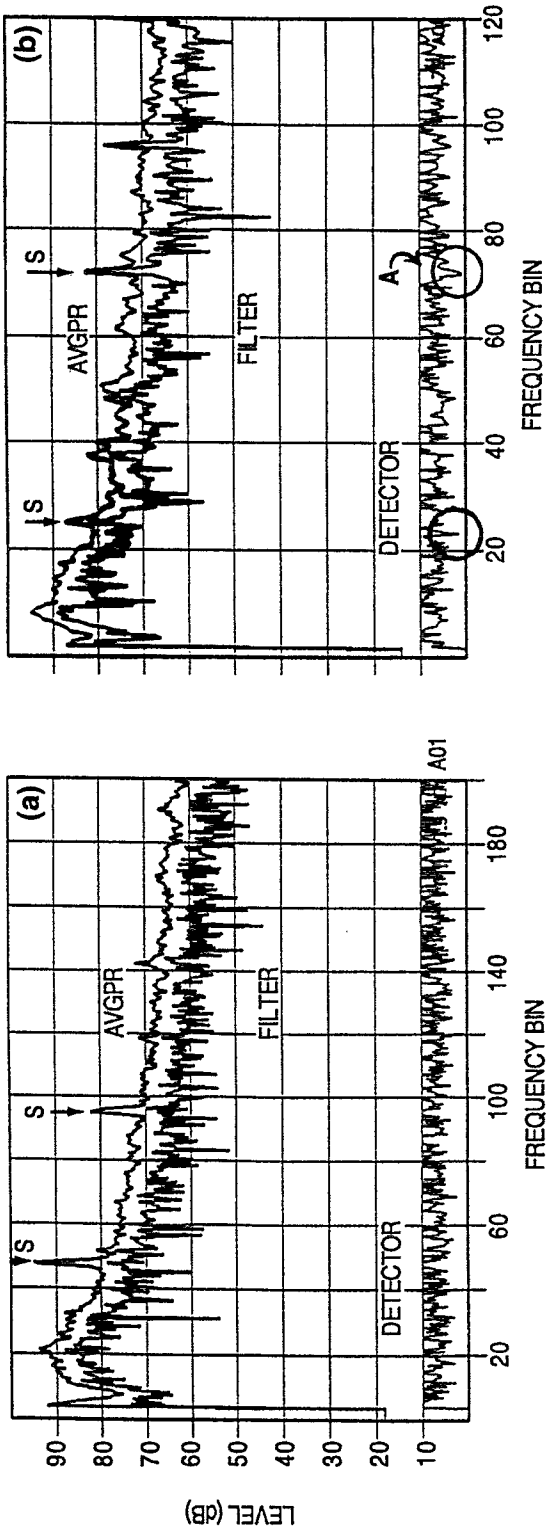

Fig. 1.1 — WISPR submerged tonal discrimination/identification: (a) projector on surface and (b) projector submerged

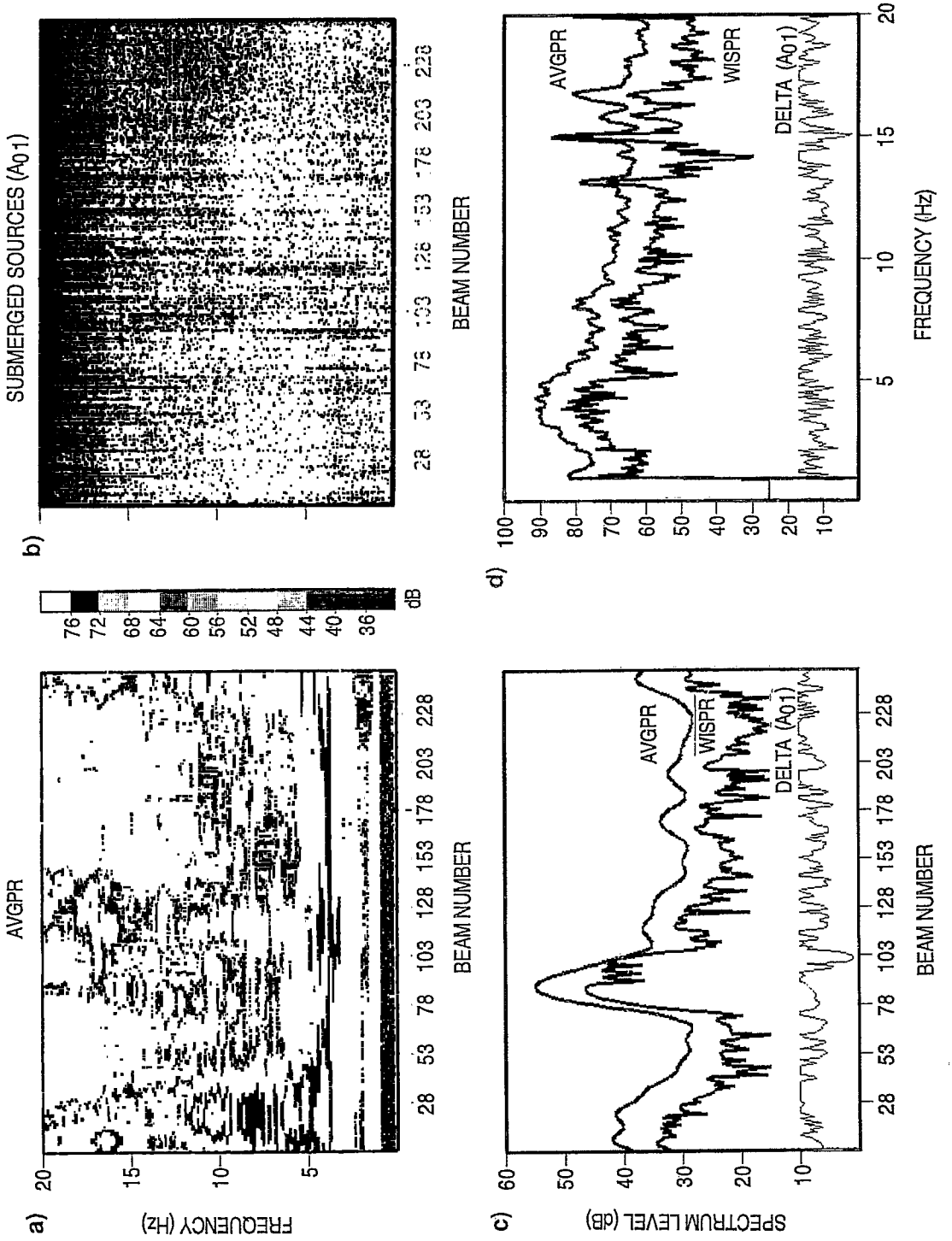

Fig. 1.2 — The essence of the von WISPR Family Processors Products including: (a) average frequency versus beam number surface, (b) corresponding submerged source signal surface, (c) and (d), spatial beams and frequency spectra, respectively, for the AVGPR (top), WISPR (middle), and DELTA (submerged source) curves, respectively

Figure 1.2a contains the beam number versus frequency plot from about 2 min of data acquired by a towed array. Beam numbers are along the x-axis and frequency is along the y-axis. The frequency range is 0 to 20 Hz. The color scale at the right of the plot gives the relative average power levels. Sounds arriving at the array from broadband sources such as ships will appear along vertical lines at a given beam number. There are at least five distinct sources (i.e., ships) in this plot (e.g., along beam numbers 2, 26, 80, 128, and 256). There are considerably more individual sources in the data, but this frequency beam number plot is not the best format for detecting them. However, it does give a qualitative representation of the signals and noise at the time of the measurement. There are many local maxima in this surface plot which could be the projected tonal, but from this plot there is no way of determining which one of them it could be.

Figure 1.2b is a plot that is similar to the frequency beam number plot in Fig. 1.2a, except instead of the average power level being plotted, the location in frequency beam number space is plotted for signals identified to be from submerged sources. Identification is based on an appropriately thresholded value of the difference between the average power level and the WISPR filter result (A_{01} processing, explained more fully in Sec. 2.0). The single dot at 15 Hz and beam number 101 is the only frequency beam number bin of the 5×10^4 bins covered by the plot that has been classified by the A_{01} processor, one of the von WISPR Family Processors, as being a bin that contains a signal from a submerged source. Hence, Fig. 1.2b is a zero clutter display that eliminates all clutter, not just suppresses it.

Figures 1.2c and 1.2d give processing results for a horizontal cut across the average power level surface in Fig. 1.2a at 15 Hz and a vertical cut along beam 101. The top curves in each of these plots are the corresponding power level versus beam number and frequency curves, respectively. The middle curves in these two plots are the corresponding WISPR Filter (one of the von WISPR Family Processors) results. When these two WISPR Filter curves are compared with the corresponding average power curves, there is an obvious suppression or vertical displacement to lower levels for the WISPR Filter curves than for the average power level curves. That suppression can be the source of gain if it is greater for noise than for signals. Such is the case for stable or submerged source signals, of which one is clearly evident at 15 Hz in the spectral plot of Fig. 1.2d. The submerged source signal at 15 Hz has nearly the same level at beam 101 in the average power level curve (top) as it has in the WISPR Filter curve (middle), while the other areas of the WISPR curve are suppressed about 8 dB. Hence, there is a signal-to-noise ratio (SNR) gain for the submerged source signal at 15 Hz of about 8 dB.

The WISPR Filter curve (middle curve) in Fig. 1.2c shows higher resolution than the average power level curve (top curve) and provides an average suppression level of about 9 dB, except near the peak at beam number 101 where the two curves nearly touch. It is interesting that the single, large peak in the average power level results, which ranges from about beam numbers 75 to 105, is divided into four smaller and narrower peaks in the WISPR Filter results. This demonstrates a significant enhancement in spatial resolution of the WISPR Filter processor when compared to the AVGPR. Similar enhancements in spatial resolution are evident at other beam numbers in this plot. There are corresponding enhancements in frequency resolution in the frequency spectrum plot in Fig. 1.2d, but because of the frequency scale, they are not as noticeable as they are in the beam results in Fig. 1.2c.

The bottom curves in Fig. 1.2c and d are the submerged source curves that identify the beam number (Fig. 1.2c) and the frequency (Fig. 1.2d) at which there is a signal from a submerged source. The indicator that identifies those submerged source signals is the location on the plots (e.g., beam number or frequency) where the submerged source curves are less than 1.5 dB. That happens in Fig. 1.2c at beam number 101 and in Fig. 1.2d at a frequency of 15 Hz. Correspondingly,

the submerged source signal is plotted as a dot in the "A_{01} submerged sources" plot in Fig. 1.2b at the frequency and beam coordinates of 15 Hz and beam 101.

The submerged source is not visible in the frequency beam number average power level surface plot in Fig. 1.2a, even though the exact coordinates are now known (15 Hz, beam 101). Similarly, knowing the exact beam number of the submerged source signal does not aid in locating it in the average power level curve of Fig. 1.2c. There is no visual evidence in that curve of the existence of a local maximum near beam 101 that could be a signal. Obviously, the SNR is too small (i.e., below the minimum detectable level). However, the resolution-enhancing character of the WISPR Filter has divided the largest maximum (between beams 75 and 105) into four local maxima, the farthest one on the right (beam 101) being the submerged source signal.

The particular processor of the von WISPR Family Processors that was used in this example (the WISPR Filter) has identified a submerged source signal, both reduced and eliminated all of the clutter (all other signals from surface ships), increased the resolution, and provided a SNR gain enhancement of about 8 dB. The techniques, equations, and algorithms that were used to produce those results are presented and discussed in various sections of this report. In addition, there are other members of the von WISPR Family Processors that are introduced and discussed within this report, many of which produce even more impressive results than those in Fig. 1.2.

1.2 Fluctuation-Based Processors

The specialized branch of science and technology, underwater sound, has received the attention of many investigators, each with varied objectives. In regard to the practical objectives of the Navy, much attention has been devoted to the development of techniques involving processing algorithms and hardware that can classify, detect, and locate signal sources in operational environments contaminated by noise from myriad sources. Much emphasis has been placed on methods that can achieve better spectral and spatial resolution, and gain improvements in the SNR. There are many such methods, e.g., large hydrophone arrays, averaging over time, deconvolution with matched filters, several types of coherent processing, and matched-field processing. The SNR gains that can be achieved by many current methods quickly reach practical limits as a result of signal time instabilities, signal spatial incoherence, operational impracticality, and insufficient knowledge of environmental information upon which many sophisticated signal processors are necessarily based. Therefore, any technique that can provide additional gain and resolution, particularly in conjunction with existing methods, can be expected to find a wide range of applications. "Fluctuation-based processors," a term derived from their unique response to fluctuating signals as opposed to relatively stable ones, offer just such a technique.

Once it was realized that certain forms of processing can strongly attenuate fluctuating signals in favor of the steady signals, thus giving a gain, work was undertaken to demonstrate this for signal magnitude fluctuations in many different environments and myriad applications. It was later realized that fluctuations in signal phase also offer additional opportunities for exploitation. Work exploring this area quickly generated the understanding that the fluctuation processor summations would, of necessity, require preprocessing to ensure that the steady, tonal signals were in phase. This has given rise to a class of coherent, fluctuation-based processors. Although all of these processors are particularly important for the detection of submerged signal sources, they are certainly not limited to this area. They will find applications in any situation that produces differentiated fluctuation levels between signals and noise.

This report is intended to provide a reasonably comprehensive overview of investigations that have been made demonstrating the viability, capability, and features of fluctuation-based processors in a wide range of applications. The comprehensive nature of this report has required an abridged presentation of the original investigations that have been conducted. The reader interested in more detail about some of the topics addressed may refer to the publications listed in App. B (these are not specifically cited otherwise in this report). It is believed that study of this report will reveal that several of the applications presented have required imagination to determine that fluctuation-based processors are applicable. Indeed, it is quite possible that many other such applications await discovery, limited only by the research community's familiarization with and acceptance of these processors and by its time and resources. One of the chief obstacles to acceptance of these processors by the signal processing community is their utter simplicity, which appears to lack appeal to the sophisticated tastes of that community.

Many new and exciting results have been obtained by these potentially important processors, typified by WISPR, which improves SNR gain of signals from submerged sources as depicted in the cartoon shown in Fig. 1.3. Analysis of acoustic data from literally all over the world, obtained from real operational environments, support this view. In a limited number of cases, to have better knowledge of the characteristics of the data, simulations have been used. However, as most conclusions reached rely on observations with real data, the capabilities described can be expected to function in real environments that are strategically and tactically important to the Navy.

To classify, detect, and locate sources of interest and to minimize the number of analysis errors, signature signals must be efficiently extracted from among the ambient noise, much of which may be present at signature frequencies. One type of information more or less independent of frequency and signal magnitude, encoded by nature at the time of generation and during transit to a receiver,

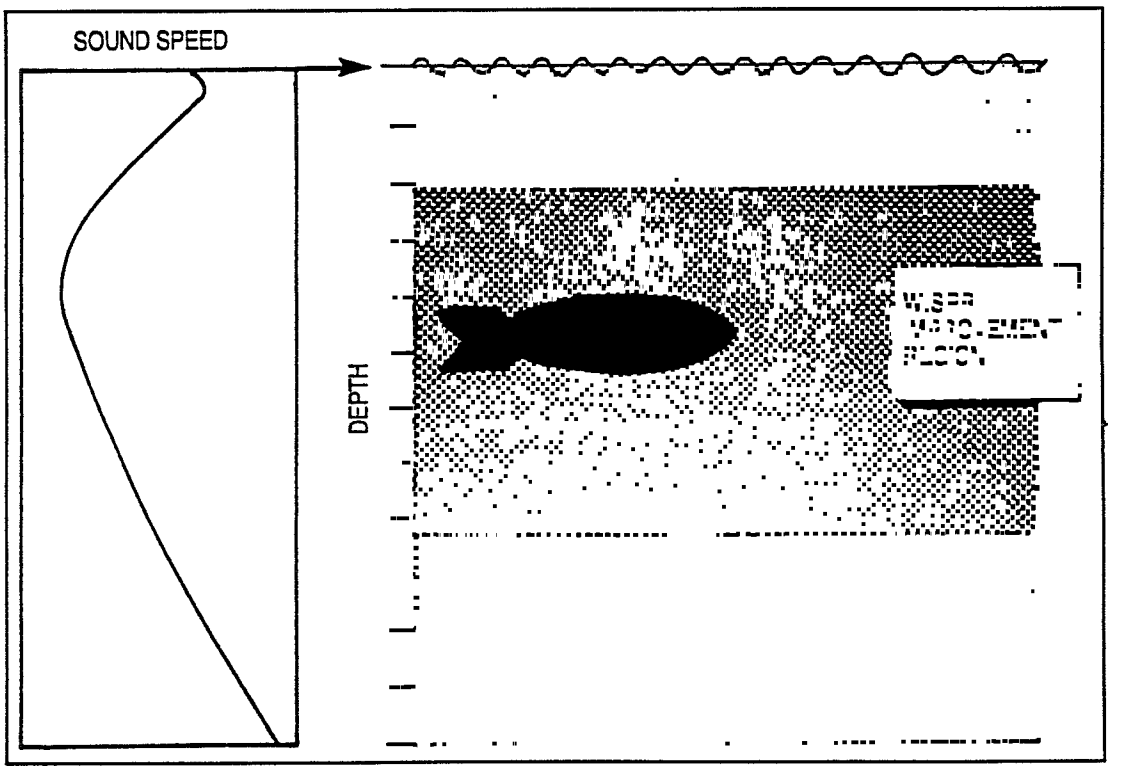

Fig. 1.3 — WISPR Filter improvement depth range

is signal fluctuation. Fortunately, for the purpose of classification, detection, and location of submerged sources, fluctuation level is strongly associated with the source depth. In fact, signals arriving from multiple distant surface sources, such as commercial shipping, have sufficiently high fluctuation levels that they are easily removed (through suppression or outright elimination) by fluctuation-based processors. More than 20 examples are presented throughout the course of this report.

One way of stating an objective that is strategically important to the Navy is that conditions arise wherein it is highly desirable to increase the signal excess or SNR gain of LOFAT signals relative to the background noise and HIFAT clutter signals and noise. The cartoon shown in Fig. 1.3 illustrates qualitatively that this occurs at mid-range depths. Insufficient research has been completed up to now to provide quantitative definition of the depth dependence of signal fluctuation levels. However, qualitatively, sufficient depth dependence has been observed to indicate that future investigation of this area could be quite productive, at least in well understood environments. One observation of importance, somewhat surprising in view of the manner in which fluctuations are induced, is that these processors have been shown to produce favorable results for some types of data even in what is generally considered to be shallow-water environments (e.g., 150 m).

1.3 Fluctuation Processing: Signal and Noise Suppression

A visual representation of how the WISPR Filter exploits fluctuations to achieve gains is provided by the two data sequences in Fig. 1.4. The top sequence represents seven power levels that

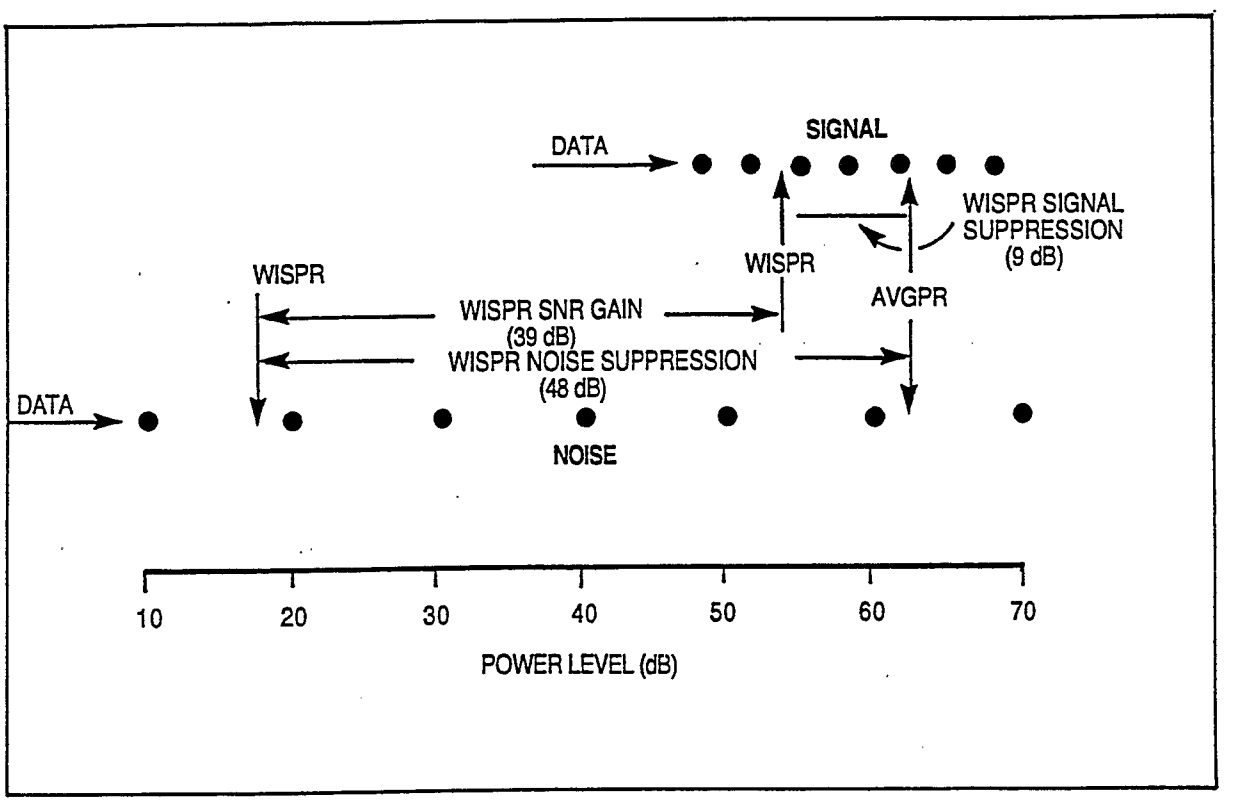

Fig. 1.4 — Fluctuation-based signal processing: signal and noise suppression

will be used to represent a LOFAT signal, in that the spread in the data points is relatively small, suggestive of low fluctuation amplitudes. The conventional averaging processor (AVGPR) and WISPR levels are designated at the appropriate locations relative to the power level axis. The lower sequence of seven points is much more spread out and is used to represent a HIFAT signal or typical noise. The AVGPR and WISPR levels are also designated at the appropriate locations according to the power level axis. For this example, the data points have been chosen in such a manner as to have equal AVGPR values. That being the case, the SNR gain of the WISPR processor would simply be the decibel difference between the WISPR suppression level relative to the AVGPR level for the noise (48 dB) minus the corresponding WISPR suppression level for the signal (9 dB), or 39 dB.

Although gains achieved with actual data may be somewhat less than in this hypothetical example, the anticipated results should be clear. The signal and noise data sets may have any consistent origin, e.g., the spectra from Fourier transforms of sequential data sets, a series of beamformer outputs, etc.

1.4 Organization of the Report

This report is intended as a survey of the results of several years of ongoing efforts in the development of fluctuation-based processors. Various nomenclature which may have been used earlier has been standardized to clarify the presentation. The nomenclature is introduced in Sec. 2.0 along with the definition of most processors, devoid of unnecessary developmental details. Most of Sec. 2.0 is repeated in App. A where more detail is presented relating to the origin, rationale, and mathematical properties of these processors. In that appendix, quantitative results are presented relating to a wider range of processors than the semi-quantitative presentation of Fig. 1.4. Sec. 10.0 contains a discussion relating to evaluation techniques for these processors, and during that discussion, another rather convincing example is provided showing how these processors differentiate between the fluctuation levels of steady tonals and fluctuating signals and noise.

The initial presentation in Sec. 3.0, centered on the WISPR Filter, explains the motivation to pursue the development of the WISPR Filter and related processors. Examples for mechanisms that produce acoustical fluctuations in the ocean are discussed along with a rationale for their distribution in depth. Quantitative processor response to the fluctuation level of noise and steady tonals is provided through simulations wherein the data set statistical properties are known, followed by several examples of detection of steady tonals from known submerged sources. The most important properties, such as SNR gain and resolution enhancement, are demonstrated.

The concept of fluctuation processor order, k, is introduced for the Advanced **W**ISPR **SUM**mation Filters ($AWSUM_k$) and demonstration of their abilities for acoustic as well as nonacoustic data is presented. A method for data presentation and interpretation that allows a robust determination of the detection threshold setting is presented with numerous examples which show that known submerged sources are actually detected, often at multiple frequencies, even in the presence of noise at levels nearly equal to the submerged source signal strength. The fluctuation statistic, standard deviation, may be used in conjunction with the WISPR Filter to produce additional SNR gain. Examples for this new class of filters, the WISPR II_k Filters, are presented for several types of data and for the $AWSUM_4$ II_k Filters. Dramatic suppression of noise produced by the clutter tonals associated with surface shipping is presented.

Although the detection of submerged sources has been presented as one of the main motivations for WISPR and related filter development, additional applications of merit are described and

demonstrated including tolerance to masking by intermittent, high-level electronic noise; tolerance to transients such as seismic prospecting; and compensation for fluctuations introduced at the receiver, e.g., from receiving array meanders during towing. These topics are treated in the section describing typical WISPR Filter applications. Several advanced applications of the WISPR Filter show how it may be coupled with other well known forms of processing, such as matched-field processing, matched filtering, and active barrier detection. WISPR processing is illustrated as a preprocessor substitute for noise spectrum equalization (NSE) algorithms and in conjunction with tactical decision aids such as the gram chart. These topics provide a feel for the breadth of the applications that should benefit from the utilization of fluctuation-based processors.

Coherent processing is described in Sec. 8.0 for two types of beamforming. One is a WISPR preprocessor to a cross-spectral density matrix beamformer (WCSDM) and the others are the unique beamformer post processors and the WISPR III_k processors. These processors exploit the fluctuation content of the phase information as well as the magnitude. In Sec. 9.0, WISPR processing is shown to enhance the performance of two other processors that were independently developed to improve beamformer spatial resolution, the Wagstaff-Berrou (WB^2) and the **D**irectivity **I**mproved **E**stimate **T**echnique (DIET) algorithms. DIET, in combination with the WISPR Filter (denoted the DIET WISPR algorithm), is an especially good example of a signal processing gem that is quite obscure. It is unlikely that such applications will be developed universally until the properties and advantages of fluctuation-based processors are widely distributed, understood, and universally accepted by the signal processing community.

Finally, in Sec. 10.0, the detection index (DI) and receiver operating characteristic (ROC) curves are investigated as measures of fluctuation-based processor SNR gain. When evaluated for data having the types of distribution actually associated with ocean acoustic noise, each of these measures indicates that the WISPR and related fluctuation-based filters perform considerably better than the AVGPR processor. The rationale for this is presented, along with an explanation of why (under some conditions) they both fail to produce results that can be interpreted meaningfully. The failure is associated with the low SNR levels of approximately 0 dB and less—the very region where the WISPR filter can detect submerged sources that are simply not indicated at all by the AVGPR processor. For this reason, the signal excess of fluctuation-based processors (e.g., WISPR Filter) is believed to be a better measure of the SNR gain. In any case, for the evaluation of fluctuation-based processors, better measures of performance are needed than historical benchmarks such as the DI and ROC curves.

2.0 EQUATIONS FOR SEVERAL RELATED AND EFFECTIVE PROCESSING ALGORITHMS

2.1 Introduction

To interpret data, particularly when in the form of rapidly acquired real-time data streams, it is both reasonable and necessary to develop methodologies (algorithms) that reduce the original data to more easily interpretable (derived) quantities. The statistical community commonly computes familiar quantities, such as measures of central tendency (e.g., average), standard deviation, and higher order statistics. A somewhat more detailed development of the relationships introduced below is given in App. A. The equations presented here are all for power in the original data units. Subsequently, in this report, for effective plotting and other reasons, the symbols defined here will be used interchangeably when the values are convertered to decibels (note divisions become subtractions when these quantities are in decibels). It is intended that the context in later discussions will enable the reader to make the appropriate distinction.

Some of the computational methods pertinent to this report are evolved from the generalized function

$$M_r = M_r(a) = \left[\frac{1}{n} \sum_{j=1}^{j=n} a_j^r \right]^{\frac{1}{r}} . \tag{2.1.1}$$

Where the data stream is the sequence, a

$$a = (a_1, a_2, a_3, \ldots a_n), \; a_j \geq 0. \tag{2.1.2}$$

Because of the possibility of numerical overflow, use of Eq. 2.1.1, when $r < 0$, is restricted to nonzero data values. Two practical approaches that avoid numerical overflow are: (1) to force nearly zero values to a small, numerically convenient value, or alternatively (2) to simply delete any data less than a small, numerically convenient value from the original data set. The latter approach is preferred as it also provides for automated removal of data from periods of time where the data acquisition system is malfunctioning or otherwise unavailable without biasing the results obtained from the data actually processed. As analog to digital (A/D) converters are not usually significant in the lowest order bits, a logical choice is to set this minimum value of a_j to the value implied by some small multiple of the A/D converter least-significant bit.

Equation 2.1.1 can be used quite generally, and for particular choices of r, defines several familiar statistical quantities.[1] For example, compare

When $r = 1$, the average is: $a_{avg} \equiv M_1 = \left[\frac{1}{n} \sum_{j=1}^{j=n} a_j \right]$,

when $r = 2$, the root mean square is: $a_{rms} \equiv M_2 = \left[\frac{1}{n} \sum_{j=1}^{j=n} a_j^2 \right]^{\frac{1}{2}}$,

when $r = -1$, the harmonic mean is: $a_{harm} \equiv M_{-1} = \left[\frac{1}{n} \sum_{j=1}^{j=n} a_j^{-1} \right]^{-1}$.

Though not obvious from the above, the geometric mean, a_{geom}, is identically equal to M_0.

2.2 Magnitude Order in Decibels

It can be shown[1] that the magnitude order in decibels with the original data in power is

$$\mathrm{dB}(a_{harm}) \leq \mathrm{dB}(a_{geom}) = \mathrm{dB}(a_{avg \; in \; dB}) \leq \mathrm{dB}(a_{avg}) \leq \mathrm{dB}(a_{rms}) . \tag{2.2.1}$$

Similarly, the decibel magnitude order is preserved for other values of r, a property which is extensively utilized by fluctuation-based processors.

2.3 The Conventional Processor/Filter (AVGPR)

The average power is referred to as the conventional processor or filter. Thus, when the sequence, a, is power, average power is

$$AVGPR = M_1 . \tag{2.3.1}$$

2.4 Fluctuation-Based Processors/Filters Equal to M_r

2.4.1 The WISPR Filter

When the sequence, a, is power, then

$$WISPR = M_{-1} . \tag{2.4.1}$$

It may be noted that $WISPR$ is notationally equivalent to $AWSUM_1$ below.

2.4.2 The $AWSUM_k$ Filters

Usually, for $k = 2$, 3, or 4, when the sequence, a, is power, then

$$AWSUM_k = M_{-k} . \tag{2.4.2}$$

2.5 Fluctuation-Based Processors/Filters Derived from M_r

Several processors that are related to the M_r class may be obtained by simple combination of those described previously.

2.5.1 The A_{0k} Processors

Examples for A_{0k} processors, for $k = 1$ and 4, are

$$A_{01} = AVGPR/WISPR = M_1/M_{-1} , \tag{2.5.1}$$

$$A_{04} = AVGPR/AWSUM_4 = M_1/M_{-4} , \tag{2.5.2}$$

or more generally

$$A_{0k} = AVGPR/AWSUM_4 = M_1/M_{-k}. \tag{2.5.3}$$

2.5.2 The A_{jk} Processors

The A_{jk} processors, for $j = 1$ and $k > 1$, are defined as

$$A_{1k} = WISPR/AWSUM_k = M_{-1}/M_{-k} , \tag{2.5.4}$$

and for $j > 1$ and $k > j$ are defined as

$$A_{jk} = AWSUM_j/AWSUM_k = M_{-j}/M_{-k} . \tag{2.5.5}$$

3.0 FUNDAMENTAL CONCEPTS OF FLUCTUATION-BASED PROCESSORS ILLUSTRATED WITH WISPR

3.1 Introduction

The terminology, "fluctuation-based processors/filters," stems from their unique response to fluctuating signals as opposed to relatively stable ones. One motivation to pursue development of filters that exploit fluctuations to enhance the performance of signal processors is provided by the results from a relatively simple experiment which dramatically demonstrates the nature and presence of signal fluctuations. Figure 3.1 illustrates two different types of fluctuations in a sonar system output. The left side of the plot shows the amplitude time series from a narrow-band processor during a time period when a signal from a deep underwater sound projector was being received by a deep sensor. The total amplitude excursion is approximately 2 dB during the time required to collect the 68 samples designated as "signal." Only ambient noise was present beyond sample 69 after the projector had been turned off. The difference in the character of the amplitude fluctuations of the remaining signal (ambient noise) should be of great interest. The excursions in the amplitude during the noise period are approximately 7 dB and are of a much more erratic character than those during the previous signal part, even though the underlying ambient noise was still present.

Figure 3.2 illustrates one mechanism that generates fluctuations in signals that originate near the sea surface from such sources as ships. As ray paths reflect off the moving sea surface, the reflection angle will change, causing ray bundle splitting and different ray paths with different lengths. As the split-off ray paths travel through a cycle and return to the surface, they will be varying degrees out of phase and constructively or destructively interfere when recombined. The result will be the generation of fluctuations. There are other mechanisms such as internal waves, multiple path interference, etc., that also contribute to fluctuations.

Another interesting example of fluctuations is provided by time histories from six contiguous beams due to a double FFT (Fast-Fourier Transform) beamformer shown in Fig. 3.3. The top and bottom traces are dominated by ambient noise. The third trace from the top is dominated by a relatively stable signal, and the others correspond to varying degrees of signal and noise. The scale along the bottom of the plot corresponds to time, and the vertical scale is relative levels. Statistics

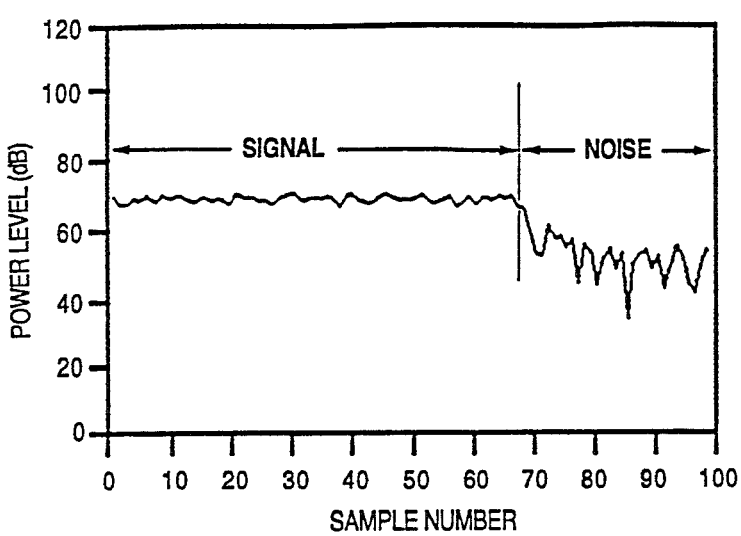

Fig. 3.1 — Example of sonar system output when a tonal is received from a deep projector (signal) and when the projector is turned off (noise)

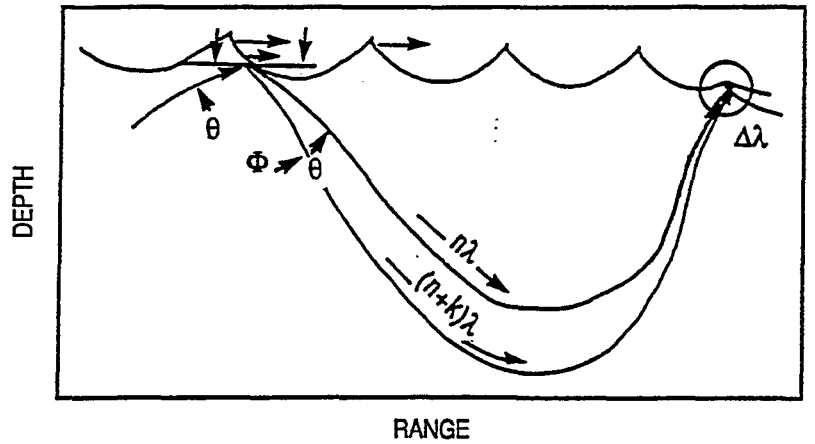

Fig. 3.2 — Illustration of ray-path interaction with a moving irregular sea surface as a source for generating amplitude fluctuations

that correspond to each trace are given above each trace. The average power level is AVGPR. The WISPR level is designated WISPR. The standard deviation is SIGMA, and DELTA is the average power level minus the WISPR level (A_{01} = AVGPR – WISPR). The beam number (BEAM) associated with each trace is also indicated.

When considering the temporal character of the traces in Fig. 3.3, the extreme difference between the pure signal (beam 70) and pure noise (beams 67 and 72) is remarkable. The noise traces have numerous deep fades, while the signal does not. These fades are the fluctuations that are caused by the various mechanisms operating on the noise that is radiated by moving ships and other sources near the sea surface. The parameter DELTA is a measure of the extent of the fluctuations. In the case of the signal beam (beam 70), the DELTA is 0.3 dB. The corresponding values for the two beams of pure noise is 14 and 10 dB. The DELTAs for the beams adjacent to the signal beam are 1.0 and 0.4 dB. Their relatively low values suggest that they are dominated more by the signal than by the noise. The reduction in the magnitudes of the fades is indicative of a bottom threshold or "floor" being established by a stable signal.

The two examples just presented should be sufficient to establish that fluctuation levels do vary significantly. In this section, several fluctuation mechanisms affecting signals of interest to the Navy are presented. There are many contributors to these variations. It is important to firmly establish that fluctuation-based filters achieve their benefits through the differentiated effect on data in relation to its fluctuation magnitude. The discussions that follow are intended to provide an insight into the importance and effectiveness of processors which can robustly differentiate between sources having different fluctuation levels.

The results of investigations utilizing field data, demonstrating myriad applications of these filters, will be presented in subsequent sections. Here, some of their attractive general properties are illustrated by the WISPR Filter, defined by Eq. 2.4.1. The results of WISPR processing of synthesized data, of acoustic data from a single phone of a towed line array, and of the FFT beamformed output of a horizontal sonar line array are discussed.

3.2 Fluctuation Amplitude

If all signal and noise had identical statistics, fluctuation-based processors would be of little benefit. However, environments important to the Navy exist that contain signals of very different

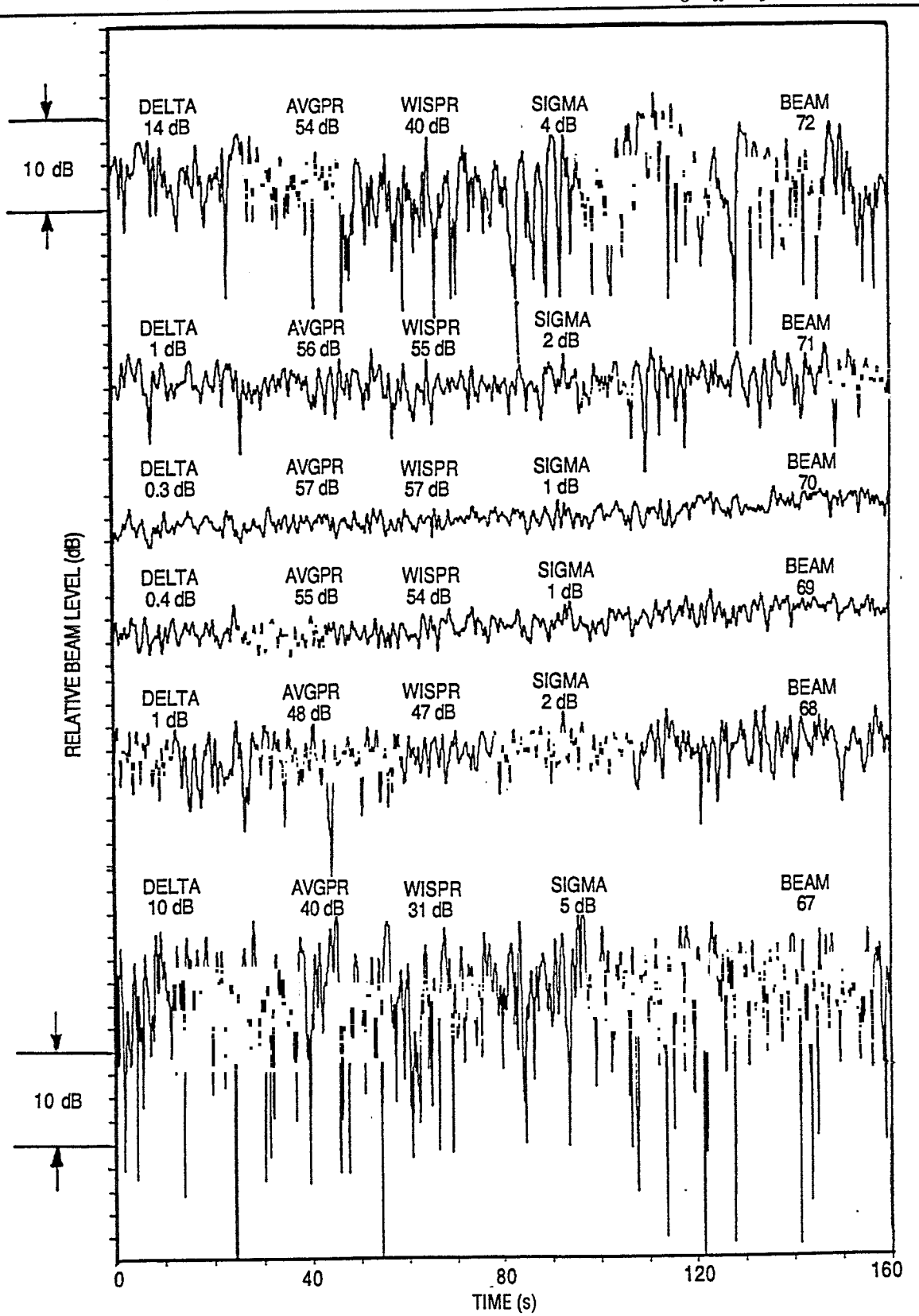

Fig. 3.3 — Time history of array signal and noise level

characteristics. As an example, one characteristic that has been used to distinguish spectral lines due to submerged sources from spectral lines, due to sources at the ocean surface, is the amplitude of their temporal fluctuations. This is possible since the amplitude fluctuations of spectral lines from submerged sources are generally small compared to those of many types of noise and of spectral lines from sources near the ocean surface, especially noise from distant shipping.

3.2.1 Surface Source Fluctuation Mechanisms

Exclusive of fluctuations induced at the receiver, there are several mechanisms responsible for amplitude fluctuations of the sound pressure received from sources located at the surface. Depending upon local condition, these may include:

(a) rocking dipole effect of the radiation directivity pattern of a ship at the sea surface,

(b) ray-path and wave-front reflection from the moving irregular sea surface,

(c) interference from multipath arrivals,

(d) variability in sound generation as the components of the engineering plant of a ship underway interacts with seas containing swells,

(e) variable sea surface height above the source due to sea surface motion,

(f) source vertical motion, and

(g) other.

A discussion of two of these should be sufficient to focus attention on the sea surface as a very significant source of acoustic signal fluctuations. The upper subplot in Fig. 3.4 illustrates fluctuations that occur from ships at two different locations on the ocean surface, or from the same ship at two different times when the surface shapes are different. The temporal history of the sound from these surface ships received on a deep sensor is presented in the top insert plot. It shows a fluctuation range from 36 to 66 dB.

The rocking dipole mechanism is illustrated by the radiation patterns (represented by the two circles at the stern of each ship) shown in Fig. 3.4. The radiated noise level from each ship increases as the radiation angle measured from the tangent to the sea surface increases, being maximum perpendicular to the surface and nearly zero parallel to it. As the ship rocks with the passing waves and the sea surface changes shape (and reflection angles), amplitude fluctuations are induced upon a signal that may already have fluctuations due to other factors, such as an unsteady generation mechanism (e.g., motor). Hence, the shape of the sea surface and the response of ships to the sea surface could make a substantial contribution to the fluctuation content of sound received from sources near the surface. Following this line of logic, one might predict that as the sea surface becomes calmer, or as the ship becomes longer, more stable, and has a deeper sound radiation point (e.g., propeller), the fluctuations induced due to the ocean surface would decrease. This suggests that small ships ought to induce higher fluctuation amplitudes than supertankers.

Another mechanism is illustrated in Fig. 3.2, where the ray path interacts with a moving and irregular sea surface. At one instant of time, the surface has a given reflection angle and speed. At a small time later, both the reflection angle and the speed have changed. This results in ray-path splitting with a different ray path and Doppler shift for the signal that travels the split-off path. Signals arriving together at the surface will have traversed paths of slightly different acoustic length. There will be either a constructive or destructive interference that will be compounded with increasing range and number of surface interactions.

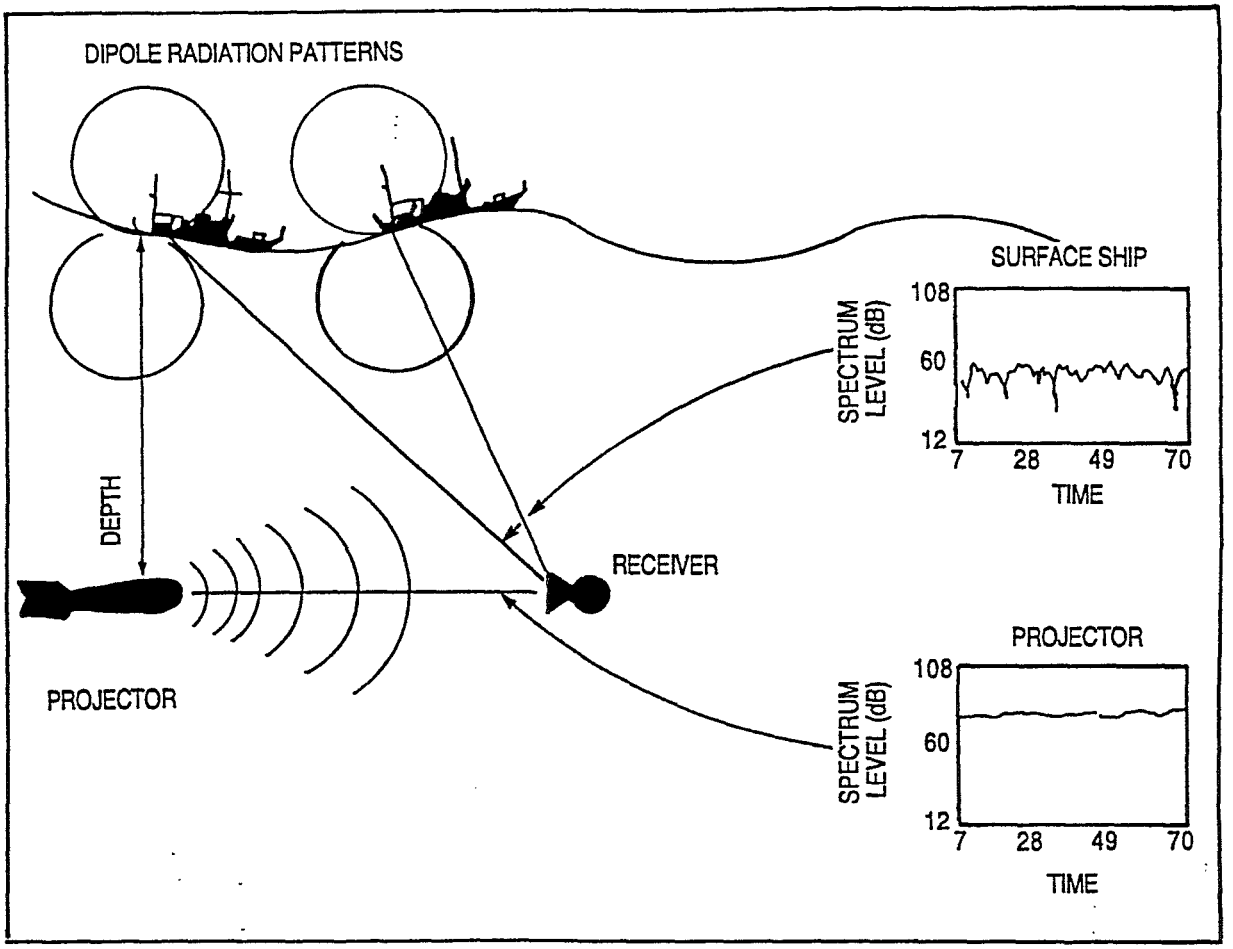

Fig. 3.4 — Noise/signal source fluctuation generation

3.2.2 Submerged Sources

A submerged source is also illustrated in Fig. 3.4 with its sound propagation path to the receiver. In a typical summer deep-ocean situation, that path would be by continuously refracted propagation. In the case of long distances, only those would be detectable. The other paths that interact with the ocean surface or bottom would be attenuated too severely to be detectable. The corresponding measured time history trace for a submerged source is presented in the bottom inset plot of Fig. 3.4. The amplitude fluctuations range from about 78 to 88 dB, a very small temporal variation. Because of the greater attitude stability of a submerged source (lack of interaction with surface waves), its radiation pattern should be more stable over time than surface ships.

3.2.3 Fluctuations Resulting from Sensor Motion

Fluctuations are also induced by mechanisms occurring at the sensor. These mechanisms should cause additional fluctuation in signals received, contaminating the signals from both submerged and surface sources. The apparent SNR will be decreased by these mechanisms. However, the original difference in fluctuation level would still persist.

Surface effects – If the sensor is near the surface of the ocean and within the surface decoupling range, vertical motion of the sea surface relative to the sensor will change the level of the received sound with the change in the decoupling associated with variable sensor depth below the sea surface. However, this only applies within the decoupling range, which is about two wavelengths (about 300 m at 10 Hz). This depth includes most sonobuoys and sometimes towed arrays.

Signal angle of arrival at the array – Another form of sensor-motion-dependent fluctuations that can affect signals received on arrays, is due to the relative time variation of the signal arrival angle at the array, varying as a result of the array motion. Consider the effects that would occur as illustrated with the cartoon representation of this situation in the figures used for the following discussion. In the case of vertical or horizontal line arrays, the motion may be caused by water flow past the array (i.e., towing or currents). The beamformer response to the signal changes as the signal arrival angle relative to the array changes, inducing fluctuations in the received signal.

The two signals, S_1 and S_2 (as shown in Fig. 3.5), are being received by the array whose beam response pattern is given for one configuration as the array moves on a meandering path through the water. The azimuthal variability of the sources, in the present context, is considered to be only due to the array motion (rotation or distortion, or both). As the relative arrival angles of the sources change, the signals received from them traverse regions of the beam response curve that have different levels of response. This will induce fluctuations in the received signal that has magnitudes that depend on the locations of the signals relative to the beam response curve. For example, signal S_1 and S_2 are at different locations on the response curve. For the small change in angle, $\Delta\Theta_2$ of S_2, a larger range in response level is traversed than for the signal S_1 as it changes in angle $\Delta\Theta_1$. This is illustrated by the time history plots in Fig. 3.5 that correspond to the beamformer output signals from these two sources.

As a result of the mechanism of array motion, one would project that the magnitude of the fluctuations induced by array motion would increase as the source angle off-beam boresight increases, increase with the magnitude of the relative motion and distortion of the array, and decrease as the width of the beam increases (aperture or frequency decrease). These effects could be quantified theoretically and experimentally.

3.2.4 Fluctuation Amplitude versus Signal-to-Noise Ratio

Experience and the previous discussion suggests that the signal from a submerged source will have smaller amplitude fluctuations than the signal from a source near the surface. Thus, signals originating from a surface source or a submerged source, if free of noise, could be distinguished by measurement of the fluctuation magnitude of spectral lines that are not shared. However, noise composed of spectral clutter originating from distant shipping (surface sources) and other sources is also present. When the submerged source signal amplitude fluctuations are small and the noise amplitude fluctuations are large, the magnitude of the combined fluctuations will depend on the relative magnitude of the signal energy compared to the noise energy or SNR. To illustrate the SNR effect, varying degrees of SNR are shown in Fig. 3.6. In that figure, the addition of signal and noise should be interpreted only qualitatively. The signal is shown with small fluctuation amplitude. The noise is shown with a much larger amplitude of fluctuation. Four different levels of SNR are depicted, from that of being nearly all noise (signal well below the noise) to signal dominated (noise level well below the signal level). As the SNR increases, the fluctuation amplitude approaches that of the pure signal case. Conversely, as the SNR decreases, the fluctuation amplitude approaches that of pure noise. Hence, even though a submerged signal is present, it cannot be identified from a consideration of amplitude fluctuations alone.

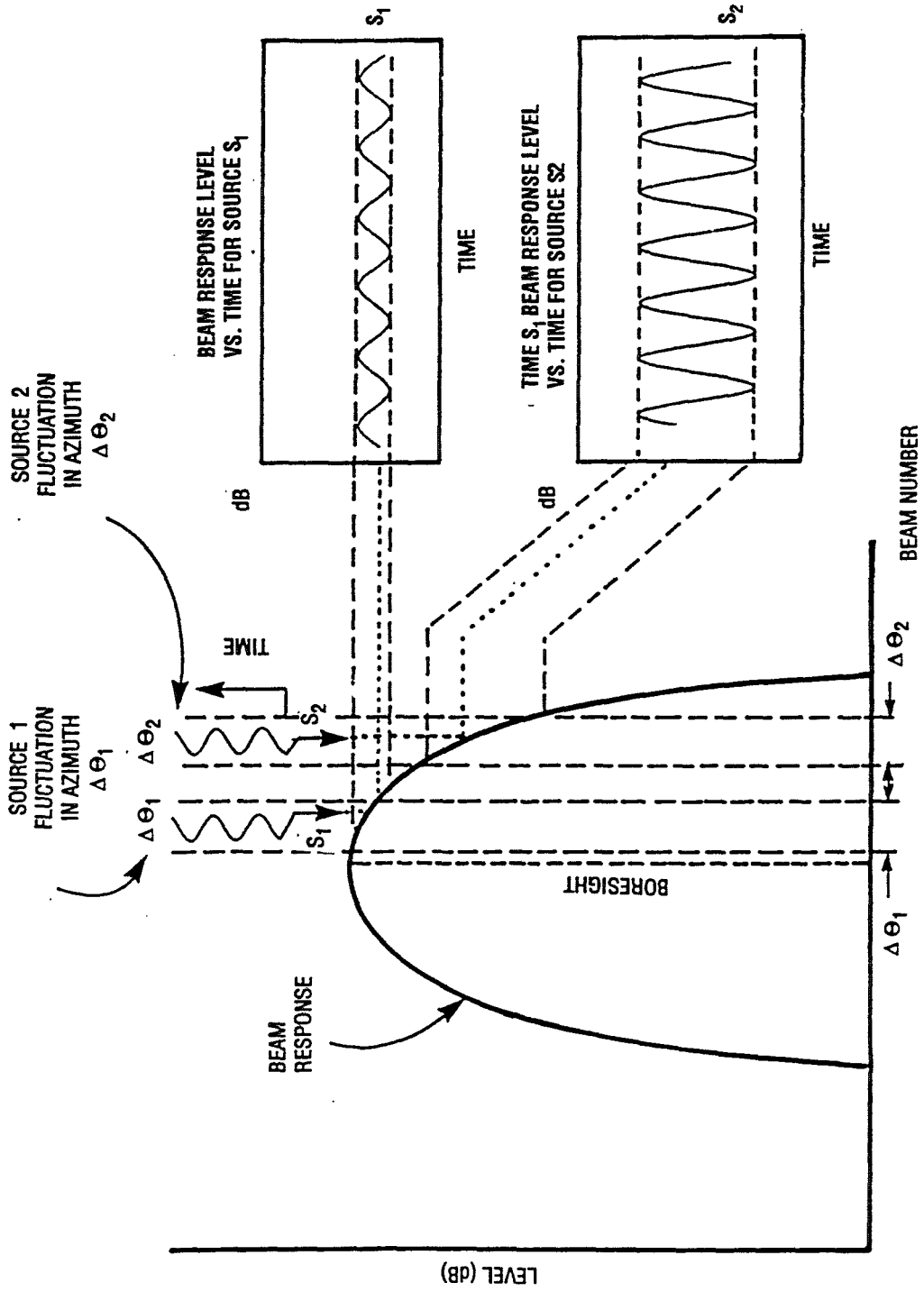

Fig. 3.5 — Beam signal/noise fluctuation generation

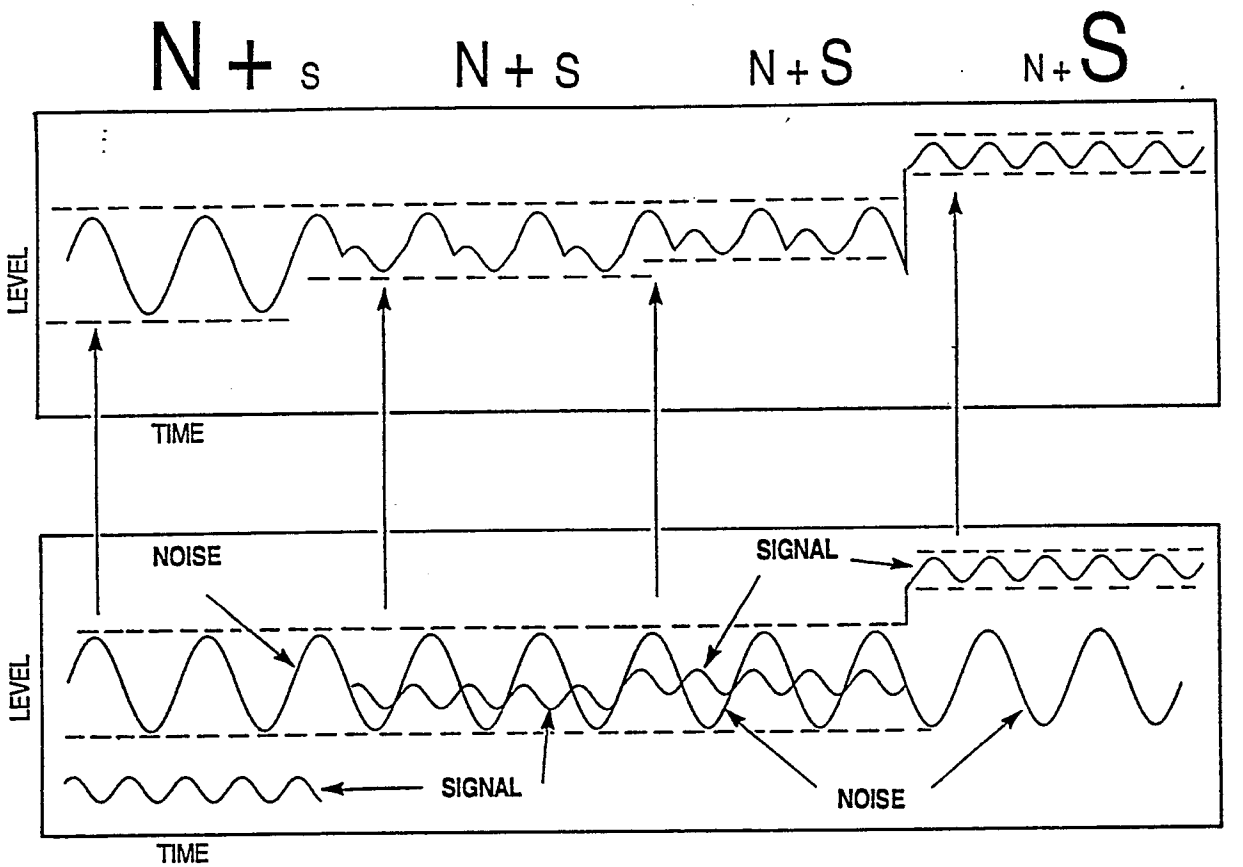

Fig. 3.6 — Fluctuation amplitude versus SNR

3.2.5 Fluctuation Depth Dependence

In the case of surface-decoupling-induced fluctuations or those induced as a result of the source approaching the surface, it should be possible to estimate the depth of the source (assuming a sufficiently high initial SNR). The diagram shown in Fig. 3.7 schematically illustrates this fluctuation depth dependence. In principle, in defined environments, it should be possible to develop quantitative relationships between the WISPR SNR enhancement, source depth, and source frequency, such as is shown schematically in Fig. 3.8. With this information in hand, in addition to determining that a source is submerged, it may be possible to estimate its depth as well. In extremely well characterized environments, it may be possible to determine the approximate depth of the source, even at low SNR.

3.3 Fluctuation Modeling

One mechanism for generating fluctuations is the selective attenuation of acoustic signals (and noise) as the ray path proximity to the surface decreases. There are several specific mechanisms that behave this way. One is the forward and out-of-path scattering when bubble clouds are encountered just below the sea surface. Another is the actual reflection from the moving, irregular sea surface. The combined sea and swell can account for more than 4 m change in the elevation of the sea surface. Patches of thermal inhomogeneities and internal waves are other possible causes.

The combined effects due to these fluctuation generators were modeled in an ad hoc manner by starting with a broadband signal that was measured by a sensor that was well within a deep

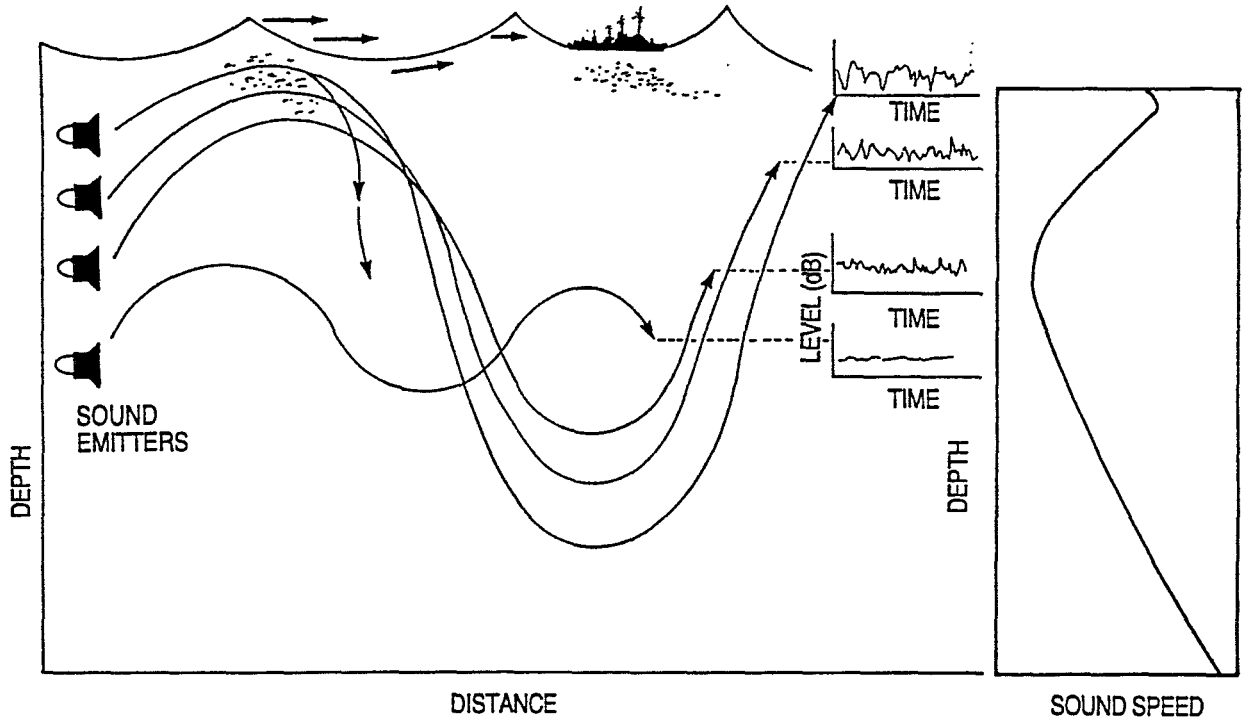

Fig. 3.7 — Fluctuation generation source depth dependence

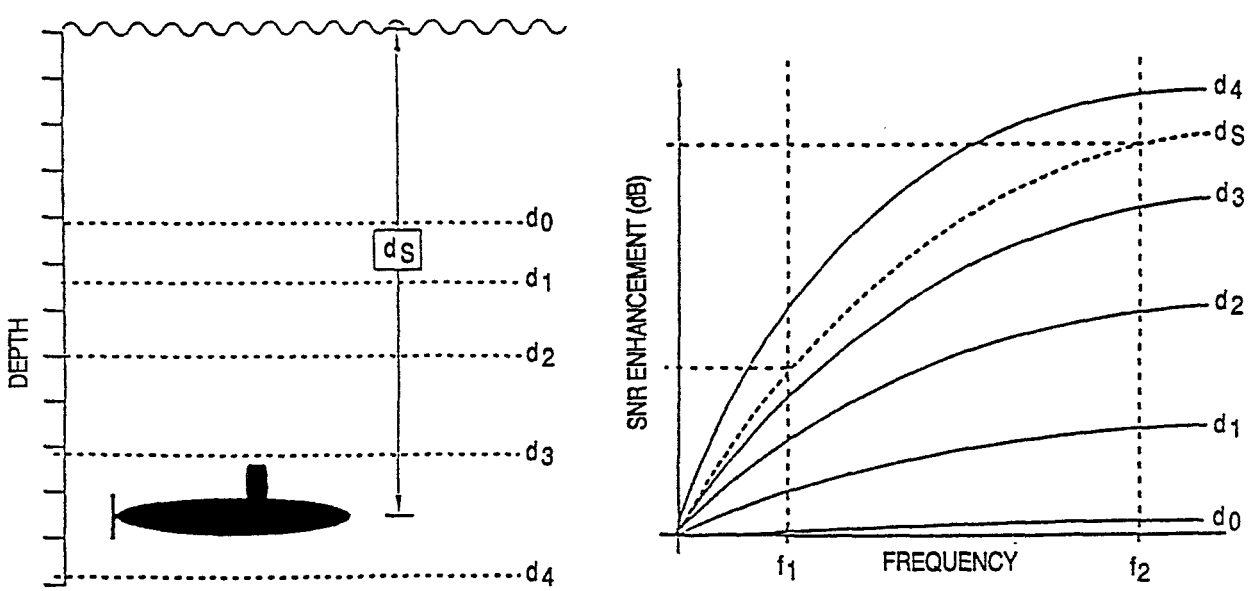

Fig. 3.8 — WISPR hypothetical SNR depth dependence function

channel of the Northeast Pacific Ocean. Embedded in that broadband signal was a narrow-band tonal at 45 Hz. The remainder of the broadband signal was typical of the noise that might be measured by a hydrophone in the deep sound channel. Figure 3.9a shows the amplitude time series of the measured broadband acoustic pressure. There are several high amplitude transient events that are of no consequence for the present discussion. Figure 3.9c shows the spectrum of the broadband signal that is represented in Fig. 3.9a. The narrow-band tonal at 45 Hz is clearly evident. In this case, the SNR of the tonal is approximately 15 dB.

Figures 3.9b and 3.9d give ray-trace diagrams for a receiver depth of 100 m and for source depths of 6 m and 100 m, respectively. The bottom depths are denoted by the double horizontal lines near 5200 m, and the sound speed profiles are to the right of the ray diagrams. Only enough ray paths have been included in these figures to give an idea of the characteristic differences between ray paths that correspond to the two different source depths. Basically, the most important difference is that the ray paths for the 6-m source depth begin near the surface and return to the surface after traveling through the water column, at least as deep as a particular ray path goes. On the other hand, the ray paths for the 100-m source start well below the surface (100 m) and a large number of them do not ever reach the surface during a complete ray cycle. Those latter ray paths are the ones that will not be attenuated as much as will the former ones that approach within a few meters of the sea surface or reflect from it. It turns out that the ray paths that get near the sea surface or reflect from it are the main ones responsible for the fluctuations.

Figure 3.10a shows the amplitude spread that has taken place in the signal that was originally as shown in Fig. 3.9a when the amplitudes of the signal that travel the various ray paths from the source at 6-m depths to a receiver at 100-m depth are selectively attenuated, with the severity of the attenuation increasing with the increasing proximity of the ray paths to the sea surface. On the other hand, the time history of the signal transmitted from the source at 100-m depth and received on a sensor at 100-m depth is given in Fig. 3.10c. This figure indicates that there is almost no change in the amplitude spread from that shown in Fig. 3.9a. Figures 3.10b and 3.10d give the spectra that results from the broadband time histories in Figs. 3.10a and 3.10c, respectively. Of particular importance in these two figures is the fluctuation-induced attenuation that has taken place in the 45 Hz signal in the 6 m result (Fig. 3.10b), but not in the 100 m result (Fig. 3.10d). The SNR of the tonal measured by the sensor at 6-m depth has decreased about 5 to 10 dB, while the SNR of the tonal measured by the sensor at 100-m depth has not decreased. Furthermore, the ambient noise background in the spectrum for the 6-m depth sensor is more erratic (noisy) than it is in the corresponding spectrum for the 100-m depth sensor. The added noisy appearance is a result of the fluctuations that were induced by the ray paths that were selectively attenuated as the ray path distance to the sea surface decreased.

Here a minor digression from the point of this section is made to assist a reader unfamiliar with interpretation of fluctuation-based processor results. There is a tendency when studying the type of plots depicted in Figs. 3.11a and 3.11b for the first time to lose sight of what is actually important. One may be initially somewhat overwhelmed by the noisy appearance of the data, especially the difference between the AVGPR and the WISPR curves, shown at the bottom of those figures. It is precisely the interpretation of this difference that is critical to understanding. Only steady signals with low fluctuation can produce nearly convergent results for the AVGPR and WISPR processors. This is a direct result of their mathematical properties, discussed in detail in App. A. Therefore, the most important detail to observe is the location of those positions where the differences are almost zero, rather than being distracted by what appears at first glance to be an unruly data set.

Figures 3.11a and 3.11b give the results that compare WISPR processing (middle curves) with AVGPR (top curves) for a 6-m source depth and a 100-m source depth, respectively. The curves at

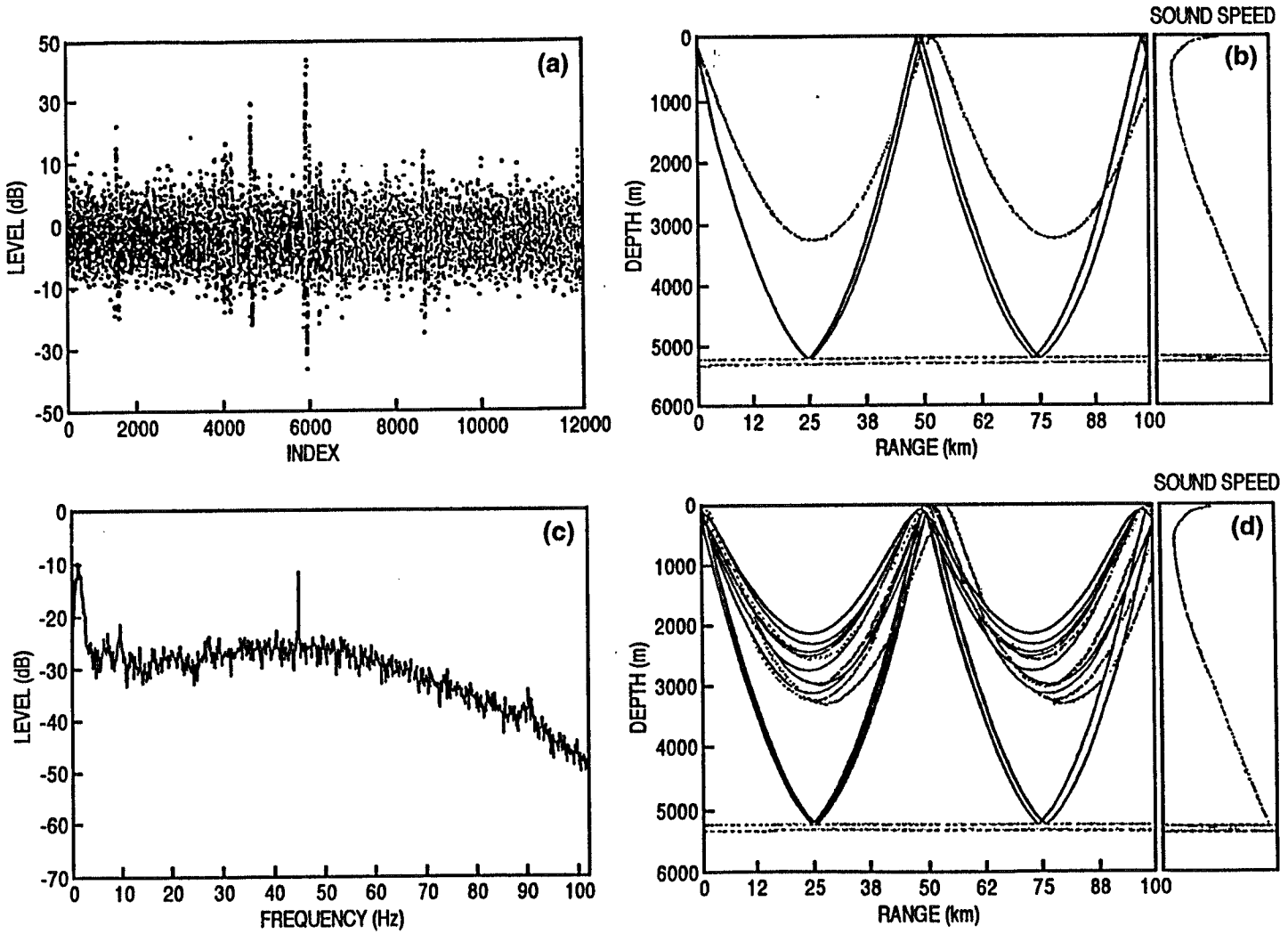

Fig. 3.9 — Illustration of (a) broadband noise with a 45-Hz embedded tonal and (c) the associated spectrum and raytrace diagrams for a 100-m receiver depth; (b) a shallow (6-m) source and (d) a deep (100-m) source

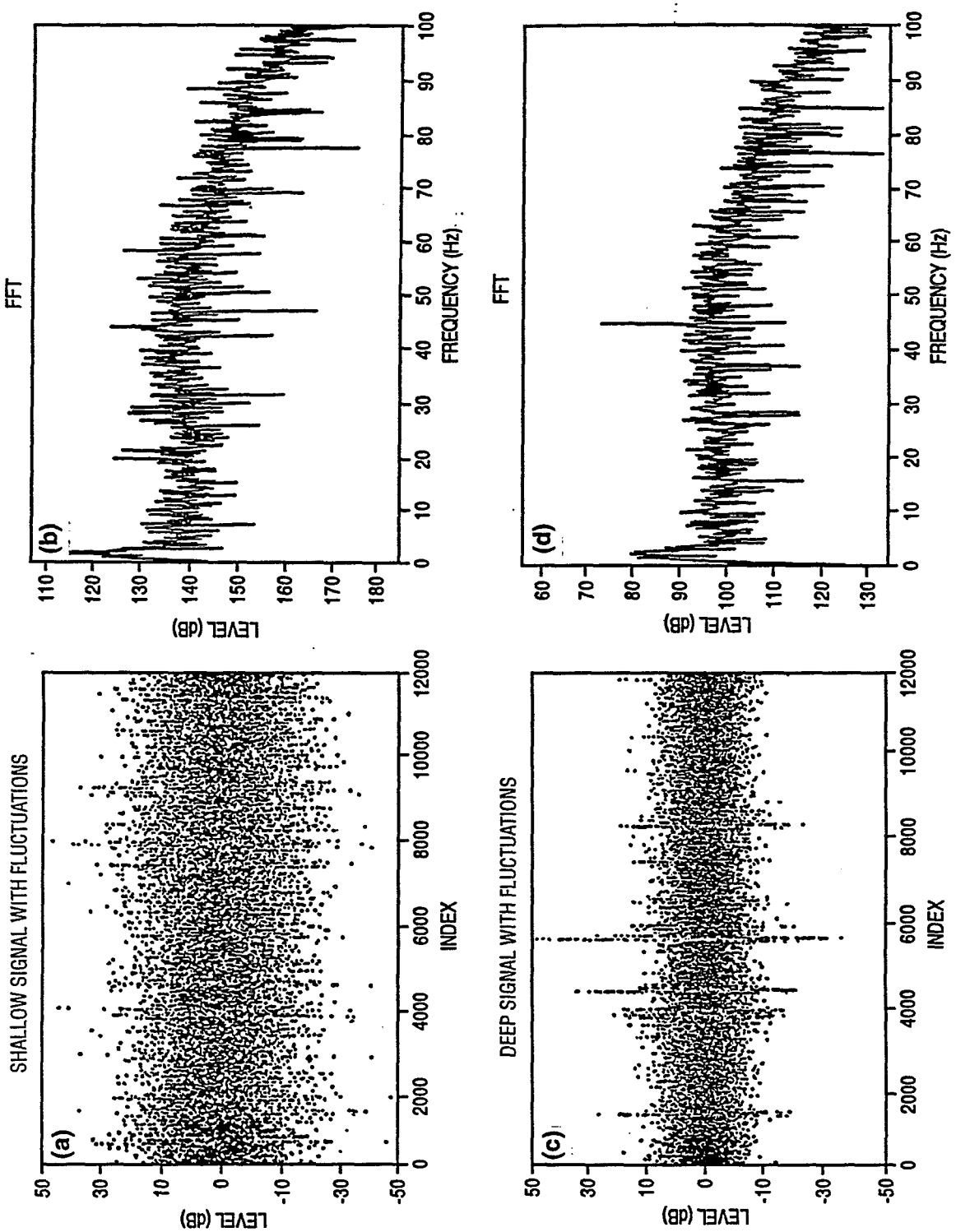

Fig. 3.10 — Signal pressure time series and corresponding transform for a shallow source at 6 m (top row) and a deep source at 100 m (bottom row)

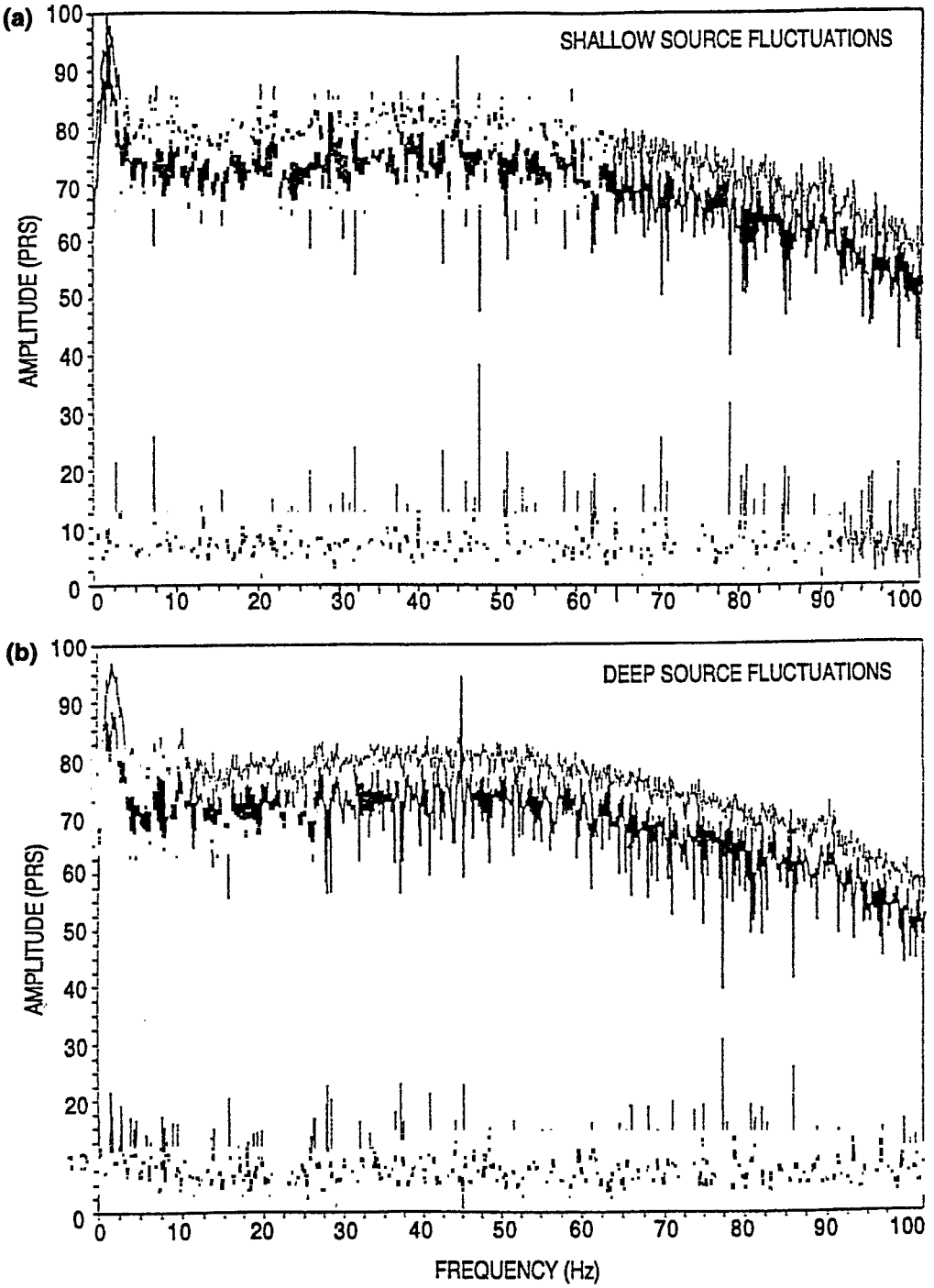

Fig. 3.11 — (a) 6-m source depth showing AVGPR and WISPR processing results and (b) 100-m source depth showing AVGPR and WISPR processing results

the bottom of each plot are the differences between the two other curves in each plot. In Fig. 3.11a, the WISPR curve is on the average less than the power average curve. However, at some frequencies, the differences between the two results are very small. The difference curve at the bottom of that plot indicates that average difference between the average power levels and the WISPR levels is about 7 dB. In Fig. 3.11b, for the sensor at 100 m, the average difference is also about 7 dB. However, the curves for the average power result and the WISPR result are easily identifiable as two separate curves, whereas they are not as well separated in the plot for the 6 m result. Furthermore, the difference curve in the 100 m result clearly shows that the 45 Hz tonal can be attributed to a submerged tonal, while in the 6 m result it cannot.

This example serves to illustrate that selective attenuation can be a source of fluctuations. In this case, signals traveling near the sea surface a subjected to more variability of attenuation than those traveling at greater depths. Even though the actual mechanisms were not modeled, this example provides some insight into how some of the mechanisms might be handled in a modeling situation when attempting to account for the overall effects of fluctuations on a signal processor.

3.4 An Example of WISPR Response to a Submerged Shallow-Water Tonal and Noise

A clear example of the way fluctuation processors function is provided by a shallow-water test conducted near the Juan de Fuca Strait, off the coast of the state of Washington, in an area where the depth is about 145 m and the bottom relatively flat. Steady pilot tonals were produced by a moored source at 61-m depth and recorded by the sensors in a vertical array at 100-m depth separated from the source by 14.7 km. The acoustic data included tonal and ambient noise. Figure 3.12 illustrates the temporal history of suppression by the WISPR Filter in shallow water. The left plot is noise suppression versus time for a noise frequency bin and the right plot is the pilot tone suppression versus time for the tonal frequency bin. Note the difference in the suppression scale of each plot. The noise plot has a much larger scale than that of the signal plot. The suppression of the pilot tone is sufficiently small so that if it were plotted with the same scale as the noise suppression, the details would be obscured.

The pilot tonal is an example of a signal whose fluctuation level is very small. For all practical purposes, the suppression of the pilot tone is negligible, only about 0.001 to 0.015 dB. However, the ambient noise, having much greater fluctuations, is significantly suppressed, approximately 4 to 15 dB. In this case, it follows that the SNR enhancement would be determined almost entirely by the magnitude of the noise suppression and be nearly equal to it (i.e., 4 to 15 dB).

3.5 Gain Improvement Illustrated Using Synthesized Data

The SNR performance of the WISPR Filter is determined by the fluctuation amplitudes of the spectral time series of the signal and the noise. Since the WISPR Filter produces an attenuated estimator, with the severity of the attenuation increasing as the fluctuation amplitudes increase, a SNR enhancement can be expected when the fluctuation amplitudes of the signal are less than the fluctuation amplitudes of the noise.

Log-normal illustration – To illustrate the SNR enhancement capability of the WISPR Filter, consider the case of a propagation medium in which the signal has small amplitude fluctuations in the spectral time series. Such a spectral time series can be generated by a log-normal random number generator with a mean of any arbitrary value and a standard deviation indicative of a signal from a submerged source of about 2 dB. The three plots in Fig. 3.13 correspond to that time series for 25,000 points.

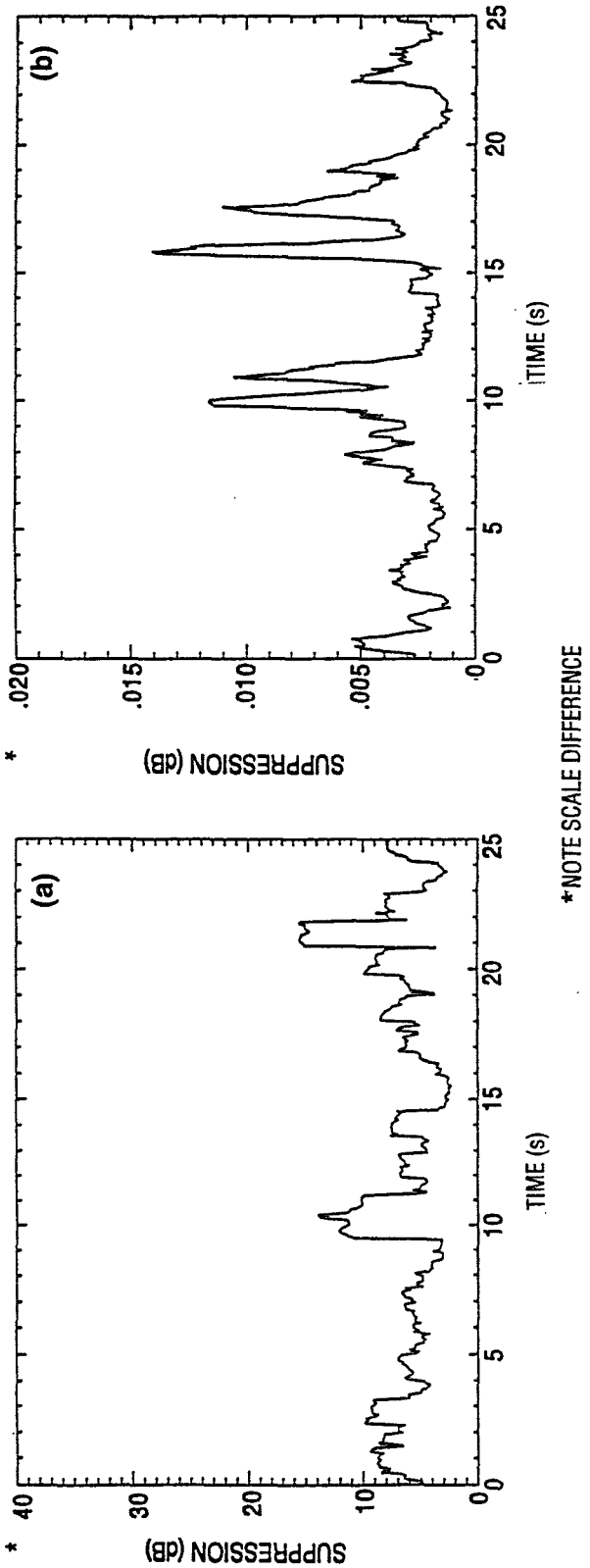

Fig. 3.12 — WISPR filter development and evaluation in a shallow-water environment: (a) noise suppression and (b) pilot tone suppression

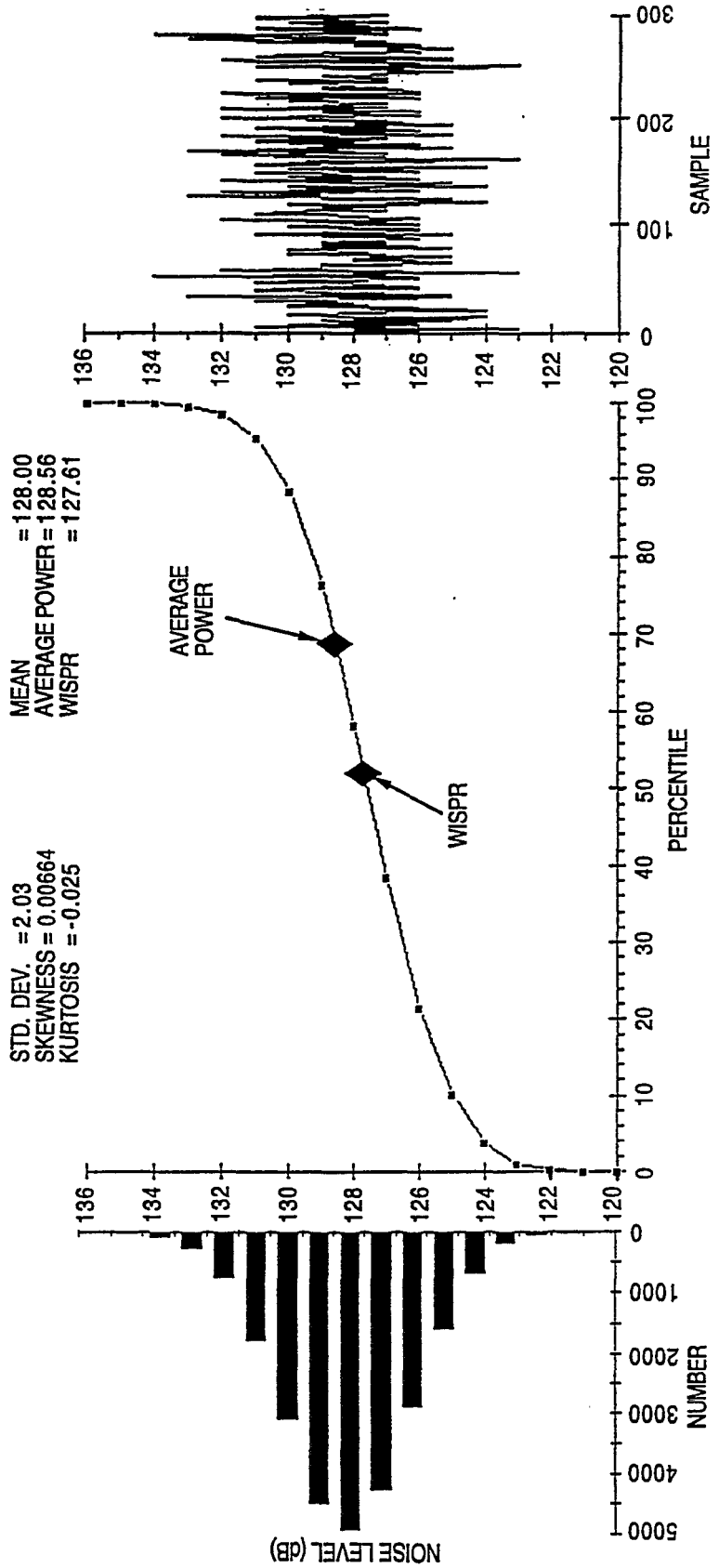

Fig. 3.13 — WISPR performance, 25,000 points, log-normal noise

The right plot in Fig. 3.13 shows the first 300 points of the 25,000 points in the series, the left plot is the corresponding histogram of the series, and the center plot is the cumulative distribution function (CDF). The mean, standard deviation, skewness, kurtosis, AVGPR, and the WISPR value (all in decibels) are listed at the top of the plots. The two diamonds on the CDF plot at 70 and 52% correspond to the AVGPR and the WISPR levels, respectively. In this case, the plot and the tabulation above the plot indicates that the AVGPR level is about 1 dB more than the WISPR level. Hence, a processor that utilized the AVGPR filter would provide an average signal level 1 dB greater than one that utilized a WISPR Filter.

Now consider a similar case in which the fluctuations correspond to something representative of ambient noise with, for example, a standard deviation of about 5.7 dB. In this case, the AVGPR level obtained from a similar time series of 25,000 points, Fig. 3.14, is about 127 dB, near the 80 percentile level, and the WISPR level is about 119 dB, near the 28 percentile level. Hence, a processor that utilized the AVGPR filter would produce an average ambient noise level 8 dB greater than one that utilized the WISPR Filter.

When the results in Fig. 3.13 are considered to be the signal and the results in Fig. 3.14 are considered to be the noise, the corresponding SNR for a processor that utilizes AVGPR in decibels is

$$(S - N)_{AVGPR} = 128.56 - 126.83 = 1.73 \text{ dB},$$

and for the WISPR Filter in decibels it is

$$(S - N)_{WISPR} = 127.61 - 119.27 = 8.34 \text{ dB}.$$

Hence, the WISPR enhancement over conventional, AVGPR processing is

$$8.34 - 1.73 = 6.61 \text{ dB}.$$

The SNR enhancement is independent of the absolute level of the signal or the noise. Although only an imprecise estimate of the noise and signal fluctuation level can be obtained for real data, in this synthesized case, the two different standard deviations used guarantees that the fluctuations are at two different levels. Therefore, as was shown, the controlling quantity of interest is the amplitude of the fluctuations, and the SNR gain result is a direct consequence of that difference.

Chi-squared illustration – A similar test was conducted for Chi-squared distributions for both signal and noise. In this case, a signal-like standard deviation (about 2 dB) was achieved with 4° of freedom, and a noise-like standard deviation (about 5.8 dB) was achieved with 34° of freedom. As before, 25,000 points in each time series were generated. The resulting histogram plots, CDF plots, and plots of the first 300 points of the time series are presented in Figs. 3.15 and 3.16. The diamonds show the locations of the AVGPR levels and the WISPR levels and their values, along with other statistics tabulated above the plots. The SNR determined from the AVGPR in decibels is

$$(S - N)_{AVGPR} = 4.56 - 38.63 = -34.07 \text{ dB}.$$

The SNR of the WISPR Filter in decibels is

$$(S - N)_{WISPR} = 3.59 - 30.63 = -27.04 \text{ dB}.$$

Hence, the SNR enhancements of the WISPR processor compared to the AVGPR processor is

$$-27.04 - (-34.07), \text{ or } 7 \text{ dB}.$$

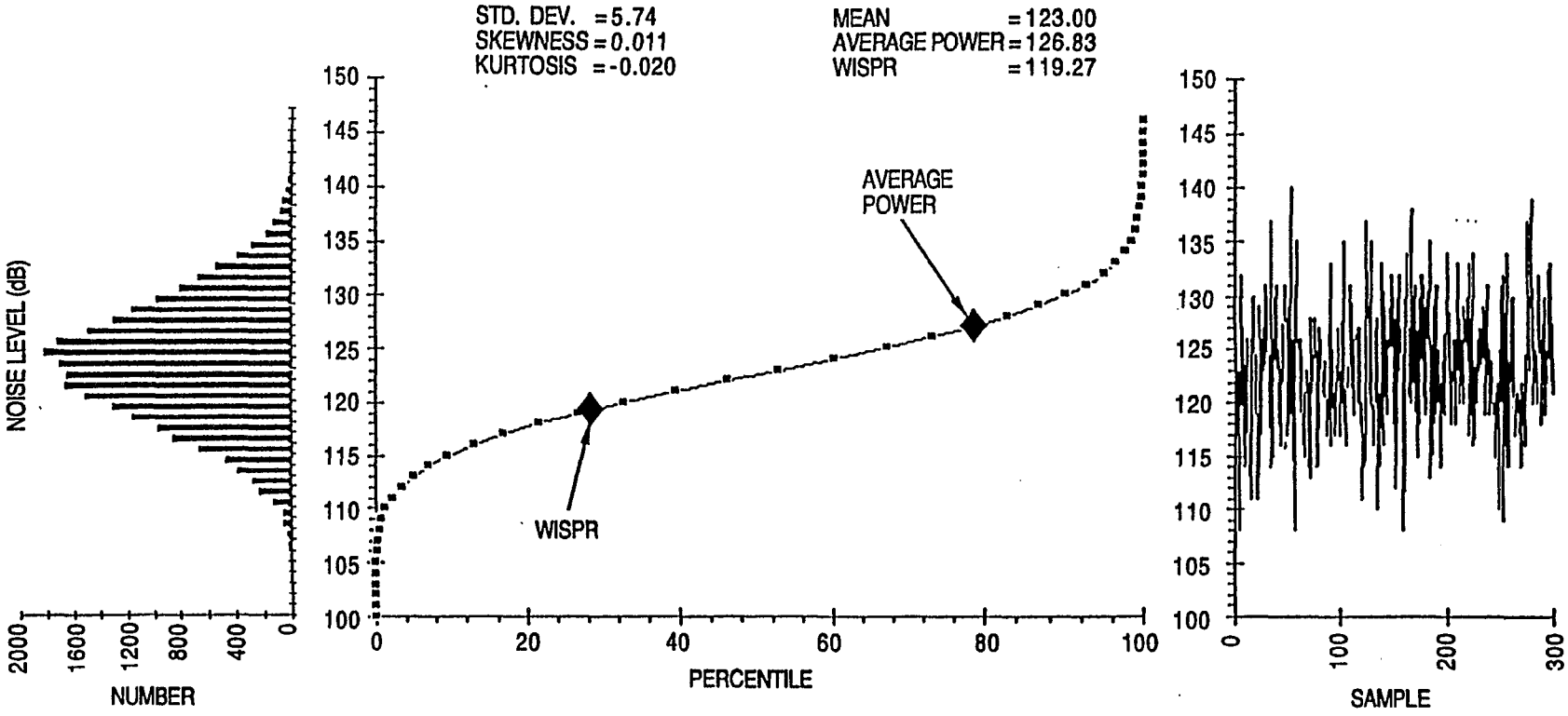

Fig. 3.14 — WISPR performance, 25,000 points, log-normal noise

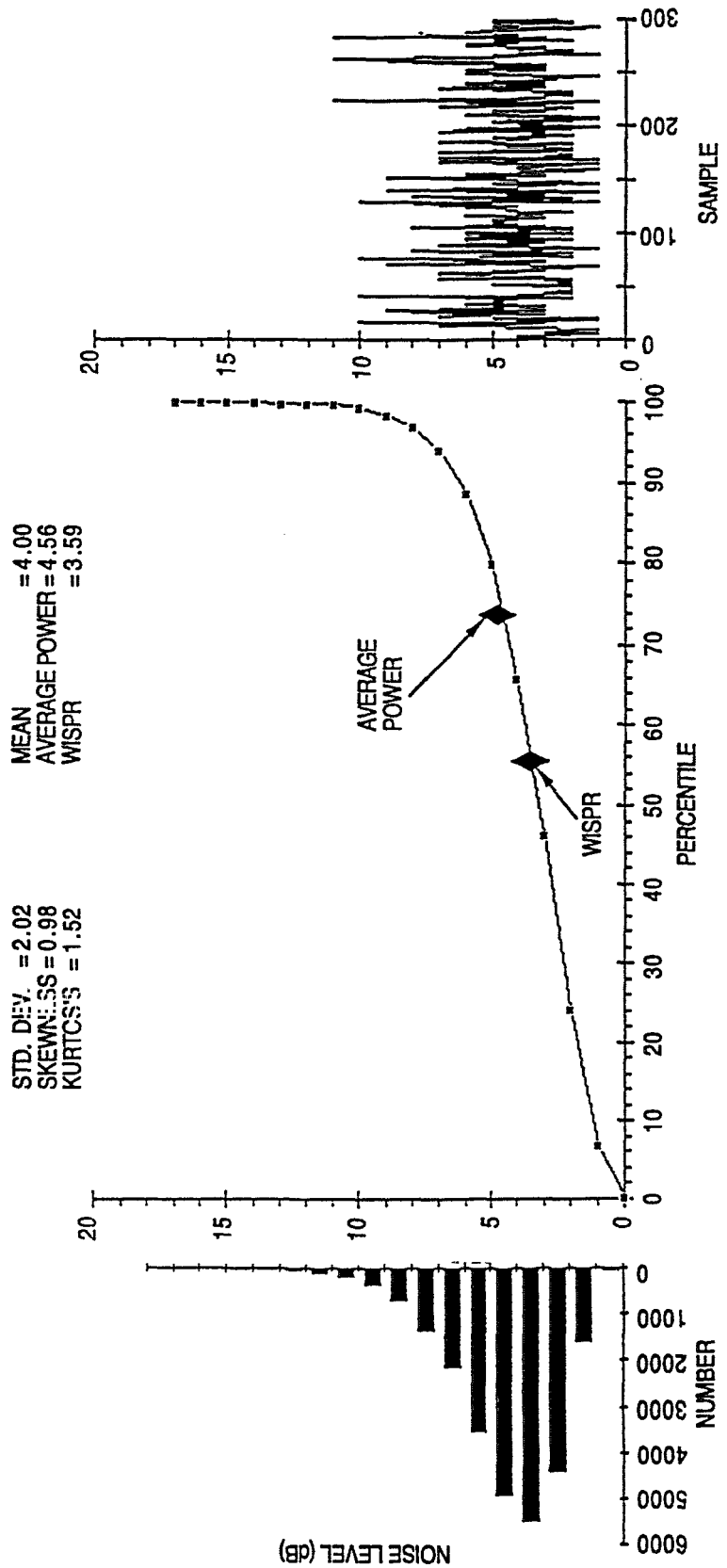

Fig. 3.15 — WISPR performance, 25,000 points, Chi-squared noise power, 4 degrees of freedom

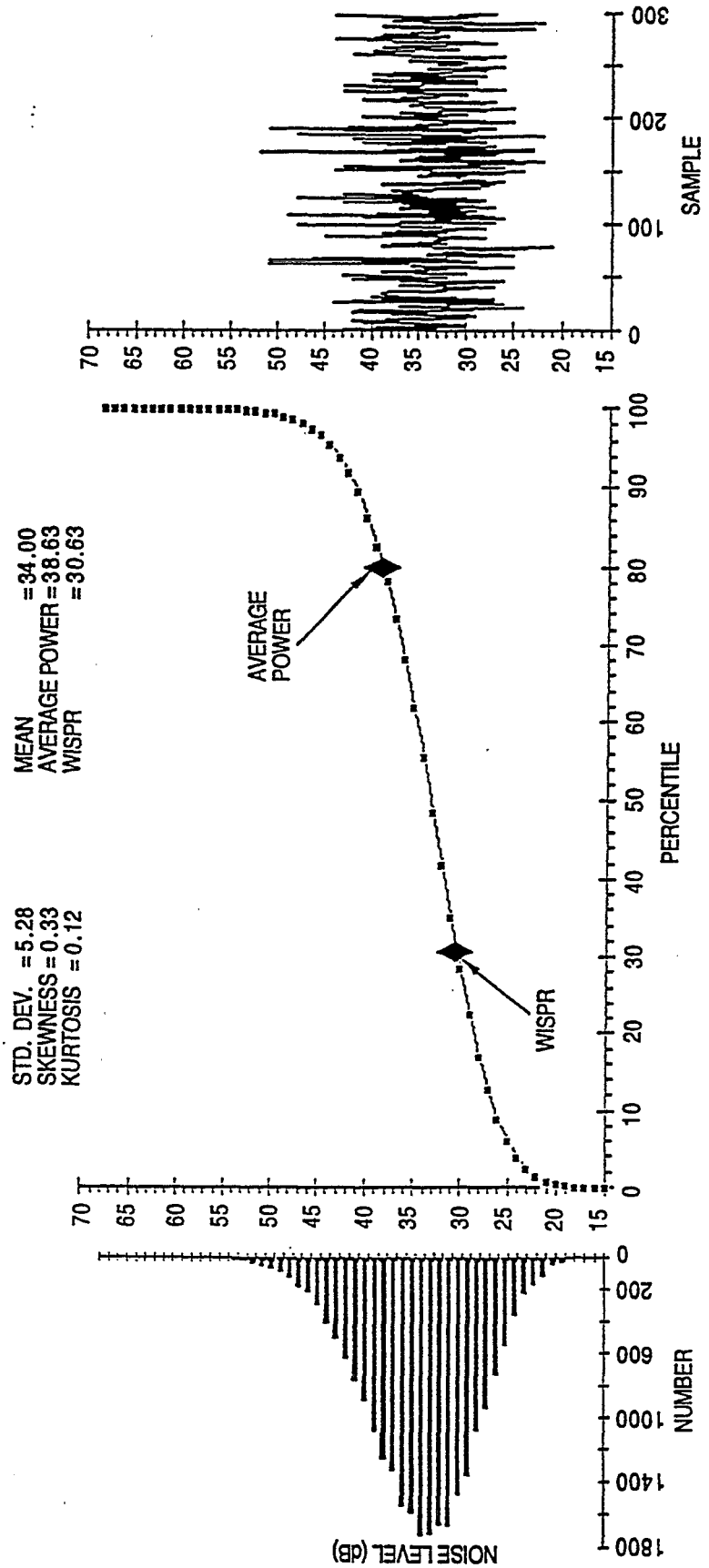

Fig. 3.16 — WISPR performance, 25,000 points, Chi-squared noise power, 34 degrees of freedom

Comparison – Figures 3.13 through 3.16 for the two different distributions presented show that the WISPR level is less than the AVGPR level. The reason for this, discussed in App. A, Sec. A.1, is that the AVGPR calculation is biased upward by the high levels in the distribution and are relatively insensitive to the low levels, while the WISPR level calculation is biased downward by the low values in the time series and is relatively insensitive to the high levels.

The tendency of WISPR to bias toward low values versus AVGPR to bias toward high values can be further visualized by examining Figs. 3.17, 3.18, and 3.19, which are the same as Figs. 3.13, 3.14, and 3.16 except for additional annotations. Two horizontal lines have been added to the plots and two corresponding statistics have been added to the statistics tabulation above the plots. The top and bottom lines indicate the boundary where data cutoffs produce WISPR and AVGPR values within 90% of the values that would be calculated using all of the data. Since these are CDF plots, the percent of data discarded can be obtained directly from the abscissa. Table 3.1, prepared from these figures, clearly shows this bias. The same effects are denoted on the figures by the arrows marked 90% range of XXX domination, where XXX is either AVGPR or WISPR.

An additional important observation is that the amount of bias is strongly influenced by the type of distribution, e.g., almost half of the data can be discarded in the case of the Chi-squared distribution, affecting the result by only 10%, while the change is about proportional to the amount of data discarded for the log-normal distribution. One would therefore anticipate that the level of signal gain between WISPR and AVGPR processing depends on the underlying distribution.

3.6 Influence of the Type of Distribution Function on WISPR Processing, Illustrated with Data from a Shallow-Water Environment

The WISPR Filter result has been compared to the AVGPR result to evaluate or quantify its performance. Such things as SNR gain and spectral and spatial resolution are typical examples. Such comparisons, when actual acoustic data are used, still require careful interpretation. The reason is that the average power level is a statistic that depends upon the distribution function of the data from which it was derived. Similarly, the WISPR level also depends on the distribution function. For example, consider the four CDF plots in Fig. 3.20. The left plot in the top row is an ambient noise CDF plot for sensor 1 near the top of the hydrophone string in a shallow-water area that has a depth of approximately 140 m. The scale on the y-axis is percentile arranged according to a normal or Gaussian probability distribution. The x-axis is signal (or noise) level in decibels. A log-normal distribution would appear as a straight line on this type of plot. The top two plots are for noise in frequency bin 4. In the single-sensor noise plot (bin 4), the curve bows downward, which indicates that the ambient noises on these sensors are not log-normally distributed. When all of the CDF results for each noise bin are suitably normalized to remove mean level differences from sensor to sensor and are plotted together, the top right composite plot is for the noise on about 26 sensors at various depths. The close agreement in the noise CDF curves among the various sensors is significant and establishes both the creditability of the results for the individual sensor to the left in Fig. 3.20, and also indicates that the type of the distribution function of the noise does not significantly change over the depth of the hydrophone string.

The bottom two plots in Fig. 3.20 correspond to the same sensors, but the frequency bin contains a stable tonal with a sufficiently high SNR for it to be essentially dominated by the tonal. In this case, the individual CDF curve, as well as those for all sensors combined, form nearly straight lines, at least over the majority of the percentile range (excluding the extremes at the high and low percentiles). As mentioned previously, a straight line indicates that the probability distribution of the signal is log-normal. Hence, the CDF plots of the signal are significantly different from the

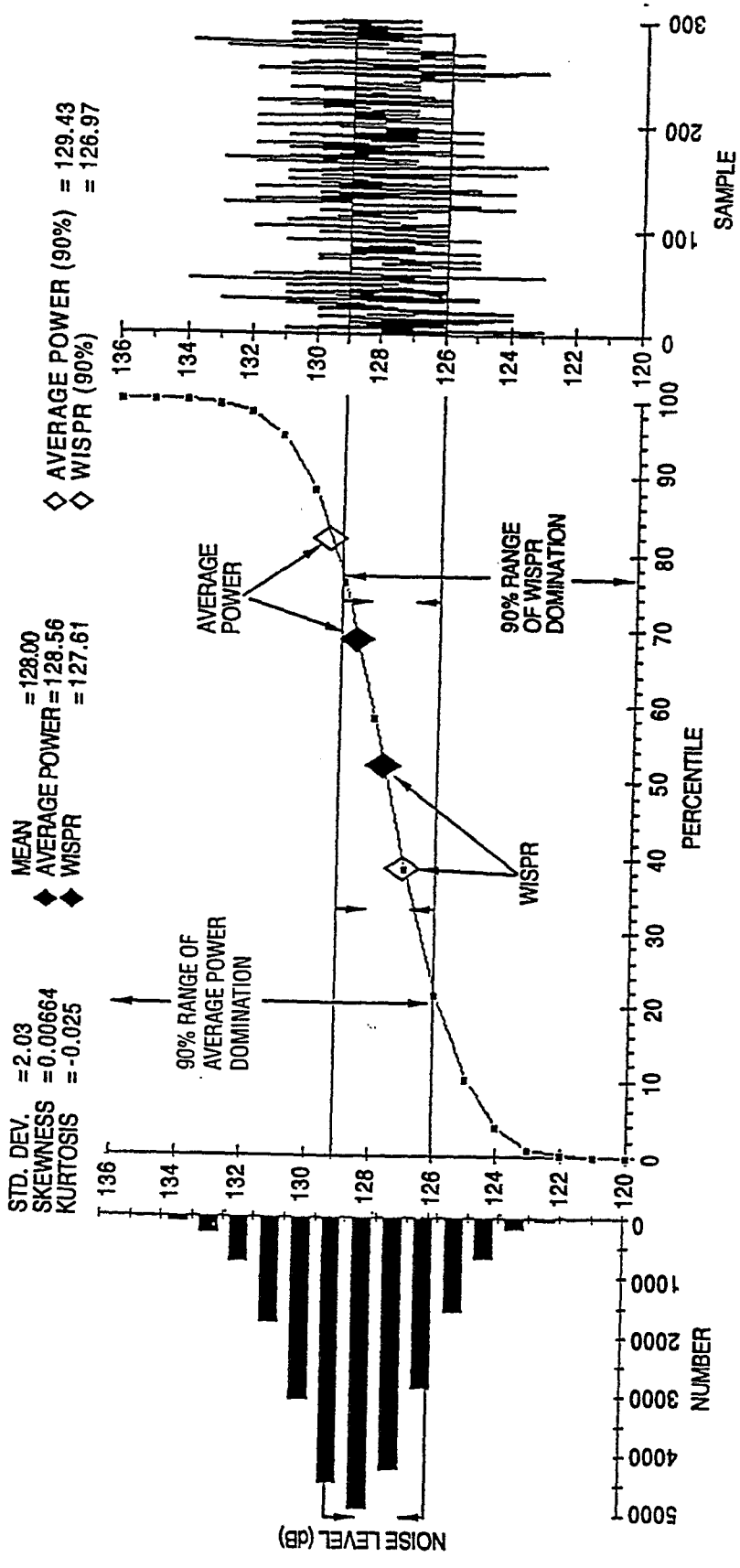

Fig. 3.17 — WISPR performance, 25,000 points, log-normal noise

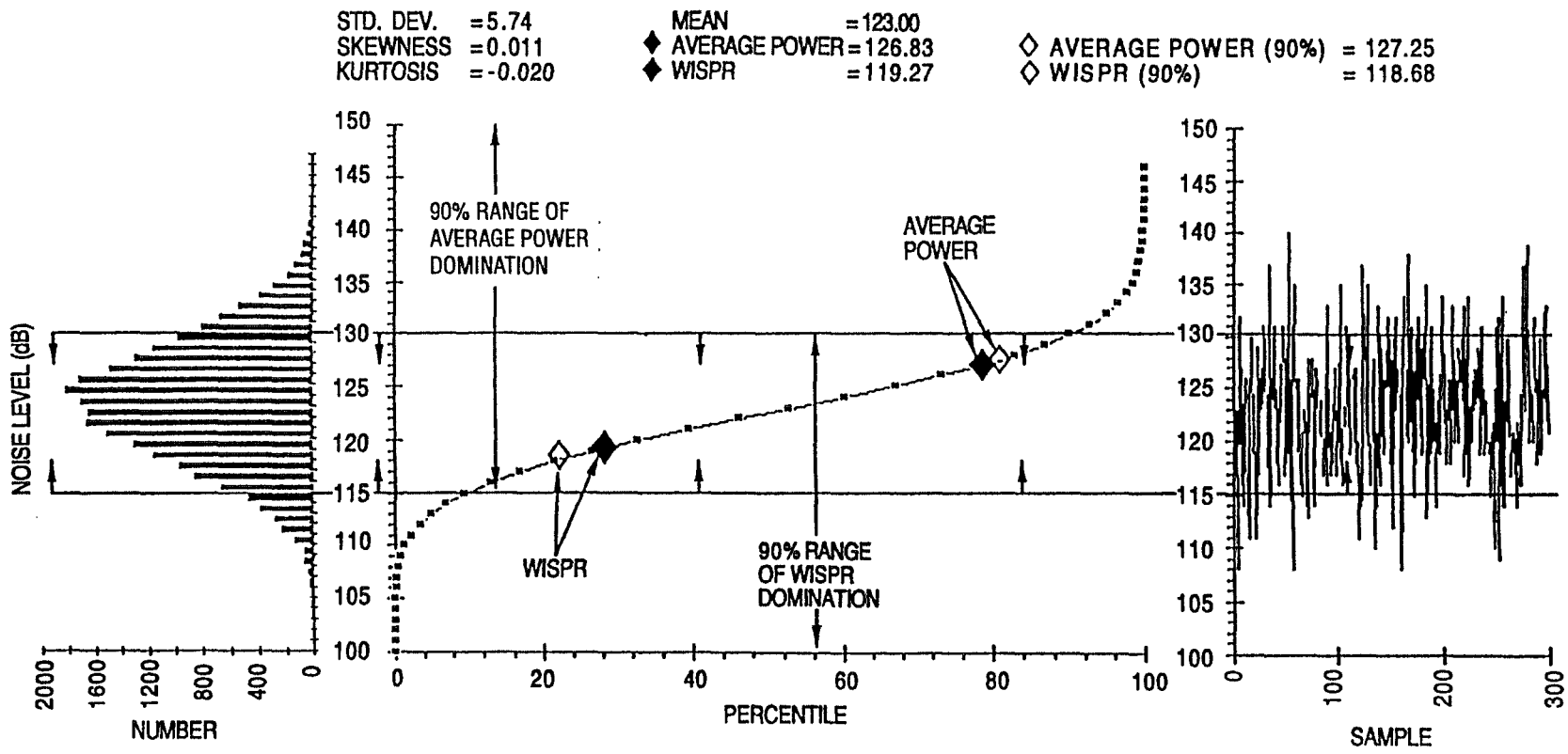

Fig. 3.18 — WISPR performance, 25,000 points, log-normal noise

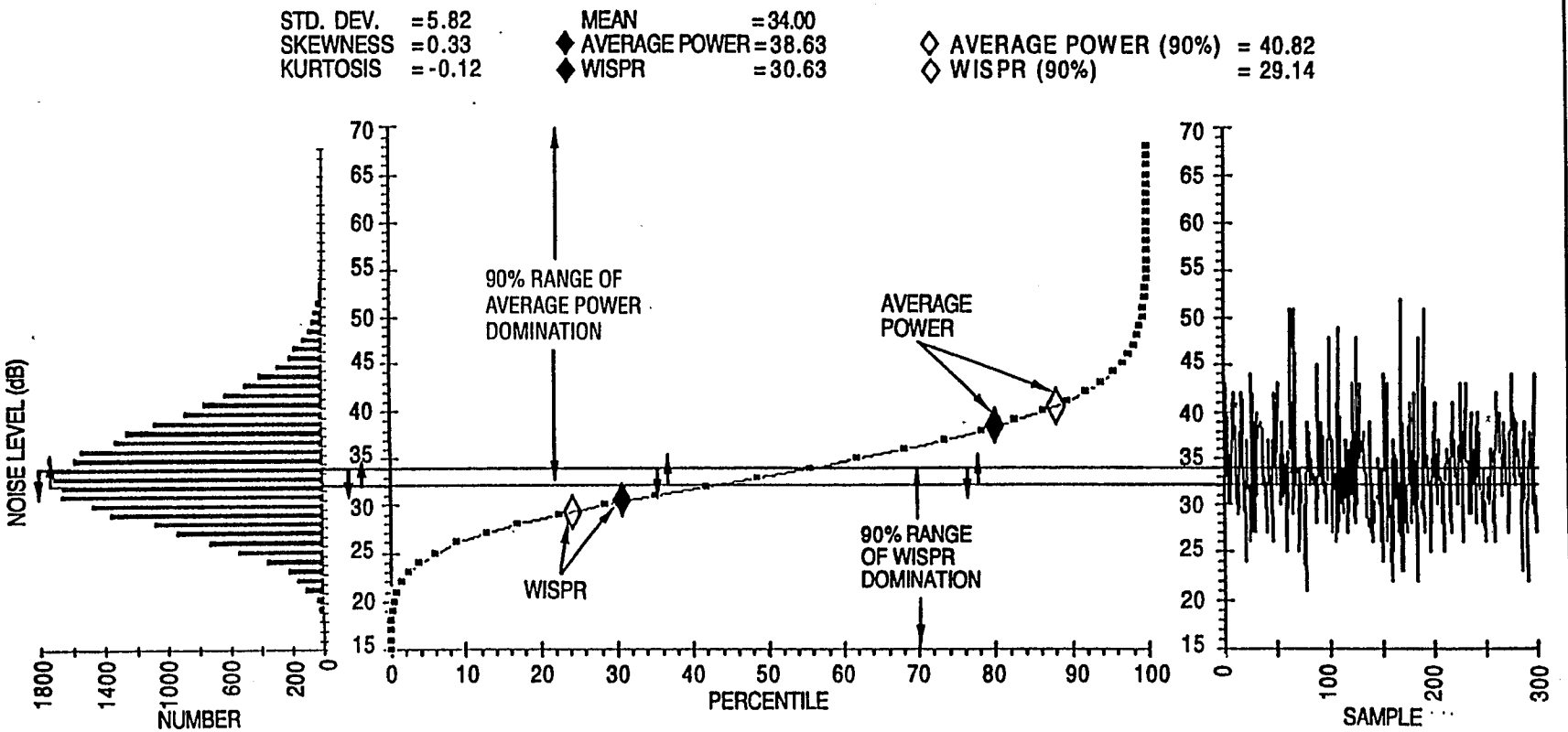

Fig. 3.19 — WISPR performance, 25,000 points, Chi-squared noise power, 34 degrees of freedom

Table 3.1

FIGURE NO.	AVGPR USING ALL DATA	% LOW VALUES DISCARDED	FINAL AVGPR VALUE	WISPR USING ALL DATA	% HIGH VALUES DISCARDED	FINAL WISPR VALUE
3.17	128.6	22	129.4	127.6	23	127.0
3.18	126.8	10	127.3	119.3	11	118.7
3.19	38.6	44	40.8	30.6	45	29.1

ambient noise CDF plots in the first two rows of Fig. 3.20. The steady tonal for which the results in Fig. 3.20 correspond originated from a mid-depth source (about 78 m) at a distance of 14 km. The bottom along the sound propagation path was approximately flat and level between the source and the sensors. It is interesting to note that the signal has a log-normal (straight line) CDF, while the shallow-water ambient noise CDF has a line that bows downward. The significance of such a difference for a fluctuation-based signal processor such as WISPR is that because of the downward bow in the CDF curves, the WISPR suppression (AVGPR minus WISPR level) will be large, while for the log-normal CDF of the signal, the WISPR suppression will be small. Since the SNR gain of the WISPR processor, relative to the conventional (AVGPR) processor, is equal to the level of the noise suppression minus the level of the signal suppression, the SNR gain will be even larger than when the noise and signal are from the same distribution, as was shown in Sec. 3.5 using simulated data.

The magnitude of the SNR gain of the WISPR Processor, for the shallow-water environment from which the data in Fig. 3.20 were obtained, is quantified in Tables 3.2 and 3.3. Table 3.2 gives various statistics calculated on 240 samples of noise frequency bin number 4 for each of the 46 hydrophones in the hydrophone string. Hydrophones 32, 36, and 45 were anomalous and should be ignored. The rows in each table include, in the following order, the hydrophone numbers (PHONE) the average power level (AVGPR), the WISPR level (WISPR), the mean level (MEAN), the standard deviation (STDEV), the Skew (SKEW), the Kurtosis (KURTOS) and the 10, 25, 50, 75, and 90 percentile levels. The focus of this discussion will be on the AVGPR level, the WISPR level (WISPR), and the percentile levels. Of particular interest is the noise suppression level determined by the difference, AVGPR – WISPR (A_{01} processing), the total SNR gain, and the approximate location within the percentile range that the WISPR level and the AVGPR level fall.

As a typical example, consider hydrophone 20. The AVGPR is 35.90 dB, WISPR is 29.76 dB, and the difference is 6.14 dB. That difference is the WISPR noise suppression gain relative to the conventional processor (AVGPR). When comparing the values to the percentiles in the distribution, it is seen that the WISPR level generally falls somewhere between the 10 and 25 percentile levels, while the average power level, AVGPR, lies between the 50 and 75 percentile levels. The greater the spread between these two, the greater the noise suppression gain will be.

A similar comparison to that above for the signal data in Table 3.3, shows that the differences between the AVGPR and the WISPR levels (i.e., the signal suppression levels) are generally less than 0.3 dB, and in many cases, less than 0.1 dB. Furthermore, both the WISPR level and the AVGPR level are within 0.1 dB of the 50 percentile level. Hence, in this case, the SNR gain of the WISPR processor, relative to the AVGPR is dominated by noise suppression. The distribution function of the noise compared to the distribution function of the signal has a much more pronounced low-level tail. This results in even greater noise suppression than would arise from the fluctuation

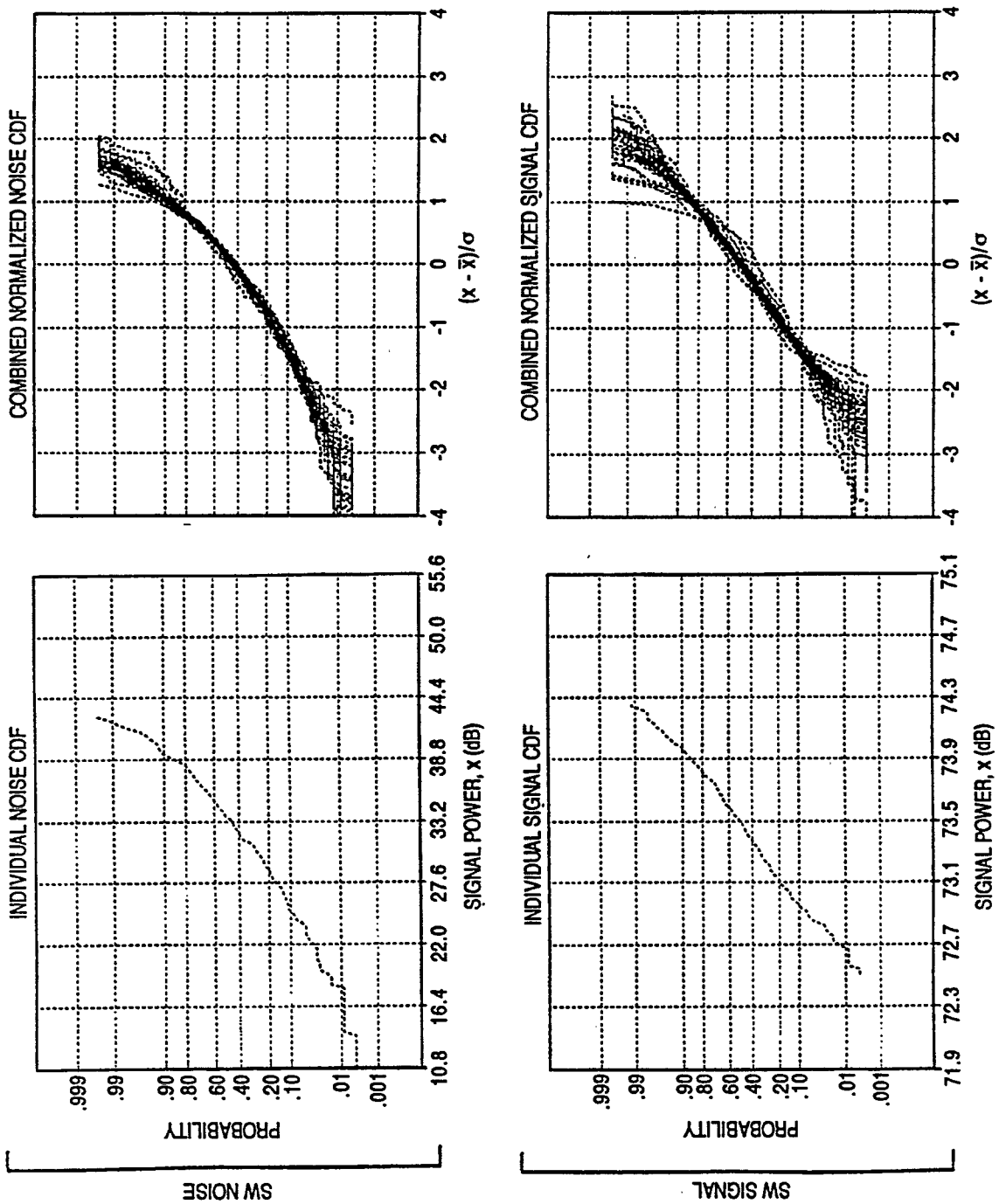

Fig. 3.20 — CDF for shallow-water signal and noise power levels where $\bar{x}$ = average power level and σ = power level standard deviation

Table 3.2 — Statistics for NOISE (Bin No. 4), 240 Samples for a 46-Element Hydrophone Array

PHONE	AVGPR	WISPR	MEAN	STDEV	SKEW	KURTOS	10%	25%	50%	75%	90%
1	35.88	27.84	33.19	5.63	−0.83	3.94	25.22	30.14	33.75	37.36	39.33
2	33.30	20.65	30.59	5.88	−1.38	7.17	23.12	27.28	31.02	34.77	36.85
3	33.47	22.06	30.81	5.96	−1.42	6.48	24.58	28.47	31.58	35.47	37.03
4	39.74	28.99	34.87	7.21	−0.19	2.48	25.05	29.61	34.78	40.25	45.42
5	33.00	24.53	30.36	5.80	−1.08	4.24	22.19	27.76	31.59	34.37	36.46
6	31.75	26.03	29.68	4.83	−0.82	3.87	23.99	27.06	30.41	33.20	35.71
7	30.73	23.91	28.52	5.25	−1.05	4.06	21.05	25.55	29.75	32.15	34.25
8	34.96	25.62	32.63	5.42	−1.22	5.67	25.30	29.46	33.62	36.64	38.53
9	33.83	24.36	31.22	5.70	−1.11	5.04	24.37	28.44	31.77	35.47	37.32
10	31.66	18.07	29.42	5.44	−1.66	9.16	22.41	26.78	30.28	33.34	35.09
11	33.21	23.06	30.79	5.63	−1.38	6.13	24.28	27.84	32.20	34.57	36.55
12	35.83	30.34	34.17	4.47	−1.28	5.59	28.09	31.86	35.05	36.79	39.11
13	32.11	21.86	29.54	5.80	−1.24	5.47	22.05	26.19	30.34	33.36	35.62
14	35.30	27.81	32.94	5.44	−1.05	4.17	25.78	30.05	34.01	36.45	38.89
15	32.63	24.81	30.14	5.43	−0.97	4.50	22.94	27.43	31.22	33.98	36.05
16	38.97	29.44	36.72	5.44	−1.37	6.18	29.41	33.77	37.76	40.66	42.48
17	37.03	31.21	35.07	4.84	−1.01	4.14	28.00	32.66	35.67	38.68	40.33
18	33.40	23.57	30.67	6.03	−1.19	4.80	21.93	27.85	32.03	34.81	36.90
19	30.49	9.84	27.89	6.20	−2.06	11.53	20.29	25.48	29.12	31.71	34.31
20	35.90	29.76	34.14	4.70	−1.31	5.47	27.49	31.77	35.47	37.18	38.89
21	33.80	24.97	31.30	5.62	−1.20	5.20	24.86	28.28	32.04	35.12	37.17
22	33.78	24.89	31.08	5.69	−1.01	4.83	24.47	28.03	31.94	34.79	37.28
23	37.76	31.16	35.70	4.90	−0.96	4.53	29.37	32.90	36.44	39.32	41.25
24	32.67	21.69	30.11	5.88	−1.43	6.26	23.35	27.61	31.09	34.58	36.12
25	32.28	24.92	29.79	5.49	−0.91	3.80	22.03	26.56	30.79	33.81	35.62
26	34.60	26.97	31.98	5.64	−0.88	3.70	23.88	28.77	33.09	35.97	38.56
27	33.45	26.16	31.04	5.19	−0.83	4.50	24.08	27.69	31.62	34.58	36.87
28	34.83	28.46	32.68	5.03	−0.95	4.14	25.67	30.18	33.28	36.38	38.64
29	34.40	27.73	32.06	5.23	−0.86	3.80	25.19	29.27	33.08	35.52	37.97
30	44.18	29.67	42.09	5.59	−2.06	10.56	34.18	40.17	43.17	46.16	47.45
31	37.09	29.89	35.16	4.99	−1.42	6.06	29.10	32.43	35.77	38.80	40.01
32	63.80	63.64	63.72	0.82	−0.05	2.49	62.71	63.10	63.80	64.31	64.90
33	34.68	25.88	32.09	5.61	−0.98	4.50	24.17	28.96	33.02	36.34	38.19
34	36.27	28.05	33.42	5.90	−0.83	3.43	24.98	29.90	34.82	37.45	40.07
35	34.93	28.57	32.55	5.25	−0.70	3.05	25.11	29.10	33.38	36.80	38.51
36	35.90	28.33	33.49	5.46	−1.00	4.13	26.57	30.06	34.82	37.67	39.25
37	35.57	28.43	33.05	5.52	−0.88	3.47	25.15	29.90	34.35	37.03	38.81
38	35.76	26.65	33.17	5.76	−1.09	4.60	25.23	29.84	34.46	37.30	39.43
39	37.00	22.93	34.35	6.20	−1.70	7.70	27.00	31.81	35.74	38.80	40.11
40	32.98	25.79	30.78	5.12	−1.07	5.03	24.82	28.20	31.27	34.65	36.80
41	36.13	28.53	33.53	5.48	−0.87	4.12	26.17	30.71	33.95	37.51	40.10
42	46.58	40.67	44.54	4.87	−0.92	4.03	37.20	41.47	45.46	48.03	50.31
43	33.94	24.01	31.40	5.80	−1.34	5.68	24.04	28.39	32.37	35.26	37.44
44	34.21	16.18	31.37	6.31	−1.73	9.28	23.97	27.99	32.51	36.02	38.03
45	55.57	49.44	53.40	5.14	−0.90	3.36	45.70	50.49	54.52	57.29	59.05
46	39.75	28.89	37.56	5.45	−1.62	7.65	30.56	35.26	38.78	40.73	43.47

Table 3.3 — Statistics for SIGNAL (Bin No. 6), 240 Samples for a 46-Element Hydrophone Array

PHONE	AVGPR	WISPR	MEAN	STDEV	SKEW	KURTOS	10%	25%	50%	75%	90%
1	71.56	71.42	71.49	0.78	−0.08	2.38	70.39	70.91	71.51	72.10	72.49
2	72.50	72.38	72.44	0.73	−0.05	2.53	71.50	71.91	72.48	72.99	73.30
3	73.46	73.39	73.43	0.52	−0.29	2.80	72.69	73.11	73.39	73.81	74.09
4	74.67	74.64	74.66	0.39	−0.46	3.01	74.10	74.40	74.61	75.01	75.09
5	74.11	74.08	74.09	0.38	−0.32	2.75	73.60	73.91	74.11	74.39	74.59
6	74.55	74.51	74.53	0.43	−0.48	2.91	73.90	74.30	74.51	74.91	74.99
7	73.92	73.83	73.88	0.61	−0.16	2.70	73.11	73.39	73.91	74.29	74.69
8	72.24	67.59	70.80	4.23	−1.37	5.23	64.74	69.16	71.49	73.59	75.22
9	74.94	74.89	74.92	0.49	0.07	2.59	74.29	74.59	74.89	75.21	75.59
10	74.73	74.42	74.58	1.16	−0.62	2.33	72.99	73.58	75.00	75.59	75.79
11	68.49	64.18	67.08	4.04	−1.17	5.19	61.77	65.01	67.50	69.74	71.73
12	76.57	76.55	76.56	0.29	−0.21	2.10	76.21	76.30	76.60	76.81	76.90
13	77.14	77.12	77.13	0.32	−0.20	2.22	76.70	76.89	77.10	77.40	77.60
14	77.02	76.99	77.01	0.34	−0.33	2.52	76.50	76.71	76.99	77.30	77.40
15	77.20	77.18	77.19	0.35	−0.20	2.44	76.71	77.00	77.20	77.40	77.60
16	77.17	77.15	77.16	0.35	−0.13	2.32	76.70	76.90	77.21	77.40	77.59
17	75.83	75.80	75.81	0.37	−0.11	2.49	75.30	75.50	75.81	76.10	76.30
18	74.23	74.20	74.22	0.40	−0.01	2.53	73.70	73.89	74.20	74.50	74.69
19	71.27	71.23	71.25	0.40	0.15	2.69	70.70	71.00	71.20	71.51	71.79
20	70.96	70.91	70.93	0.46	−0.35	2.71	70.30	70.59	71.00	71.31	71.50
21	69.08	68.98	69.03	0.66	−0.15	2.61	68.08	68.60	69.01	69.49	69.91
22	66.07	65.90	65.98	0.88	0.44	2.28	64.89	65.32	65.79	66.61	67.41
23	65.30	65.06	65.18	1.01	−0.04	2.74	63.91	64.50	65.10	65.91	66.61
24	64.30	63.98	64.15	1.17	−0.80	3.21	62.61	63.41	64.38	65.12	65.42
25	63.35	62.99	63.18	1.25	−0.31	2.32	61.30	62.31	63.32	64.22	64.78
26	63.05	62.75	62.90	1.15	−0.12	2.06	61.22	62.00	62.88	63.92	64.39
27	64.13	63.98	64.05	0.78	−0.05	2.54	63.01	63.52	64.10	64.69	65.11
28	63.95	63.80	63.87	0.82	−0.17	2.24	62.78	63.30	63.90	64.50	64.90
29	66.65	66.48	66.57	0.84	−0.05	2.50	65.40	65.91	66.69	67.12	67.58
30	69.52	69.39	69.45	0.77	0.45	2.77	68.50	68.88	69.42	69.91	70.52
31	73.59	73.56	73.57	0.41	−0.21	2.64	73.00	73.29	73.61	73.90	74.09
32	73.88	72.85	73.40	2.14	−0.39	1.84	70.18	71.41	73.79	75.43	75.92
33	73.70	73.66	73.68	0.38	−0.16	2.39	73.19	73.39	73.70	74.00	74.20
34	73.54	73.51	73.53	0.39	−0.05	2.44	73.00	73.19	73.50	73.80	73.99
35	73.45	73.42	73.43	0.38	−0.12	2.30	72.90	73.10	73.49	73.70	73.90
36	73.11	73.07	73.09	0.38	−0.14	2.49	72.59	72.79	73.10	73.40	73.60
37	74.41	74.38	74.39	0.38	−0.21	2.65	73.89	74.09	74.40	74.70	74.90
38	73.12	73.08	73.10	0.39	−0.40	2.92	72.61	72.80	73.09	73.41	73.60
39	73.46	72.77	73.18	1.71	−1.52	5.11	70.77	72.29	73.89	74.42	74.69
40	73.94	73.89	73.91	0.44	−0.36	2.66	73.29	73.59	73.89	74.21	74.49
41	73.10	73.05	73.07	0.46	−0.36	2.57	72.40	72.79	73.10	73.41	73.61
42	54.08	53.53	53.83	1.55	−0.73	3.37	51.72	52.94	53.99	55.03	55.81
43	73.67	73.61	73.64	0.51	−0.25	2.38	72.91	73.29	73.70	74.01	74.30
44	73.10	73.04	73.07	0.51	−0.20	2.55	72.39	72.71	73.10	73.41	73.69
45	72.81	72.75	72.78	0.52	−0.21	2.75	72.10	72.39	72.80	73.10	73.39
46	73.46	73.40	73.43	0.53	−0.09	2.62	72.81	73.01	73.41	73.81	74.21

level alone. Since the signal suppression is negligible and the noise suppression is large, the SNR gain due to WISPR processing of approximately 6 dB is obtained.

Similar results to those discussed above were obtained in two other shallow-water areas. However, in those cases, the receivers were sonobuoys at 90 and 400 ft, and the source was being towed away from the sonobuoys at approximately 4 kt. The separation between the source and the sonobuoys at the time of the measurement was greater than 5 nmi. The bottom depths were 400 m (Fig. 3.21) and 150 m (Fig. 3.22), respectively. The time history traces for the signal channel (left side) and the noise channel (right side) are given for the sonobuoys at 90 ft (top set of plots) and 400 ft (bottom set of plots) in each of Figs. 3.21 and 3.22. The time history characteristics of the signal and noise data can easily be compared in these plots, and the statistics that are displayed are the signal or noise suppression levels denoted DELTA (AVGPR – WISPR in the previous discussion regarding Tables 3.2 and 3.3) and the standard deviation denoted SIGMA (STDEV in Tables 3.2 and 3.3). Of considerable significance is the relatively low values of DELTA for the signal and relatively high values for the noise. The differences between the two, for a given sensor depth and site, indicate that the SNR gain of the WISPR processor relative to AVGPR ranges from about 5 to 12 dB. Such results combined with the previous results suggest that substantial SNR gain can be achieved from WISPR processing of shallow-water data. Furthermore, some of that gain comes from the differences in the probability distributions of the signals and the noise, where the long, low-level tails on the ambient noise bias the WISPR processor to significantly lower levels than are achieved by the average power processor, and by the signal being of a different probability distribution,

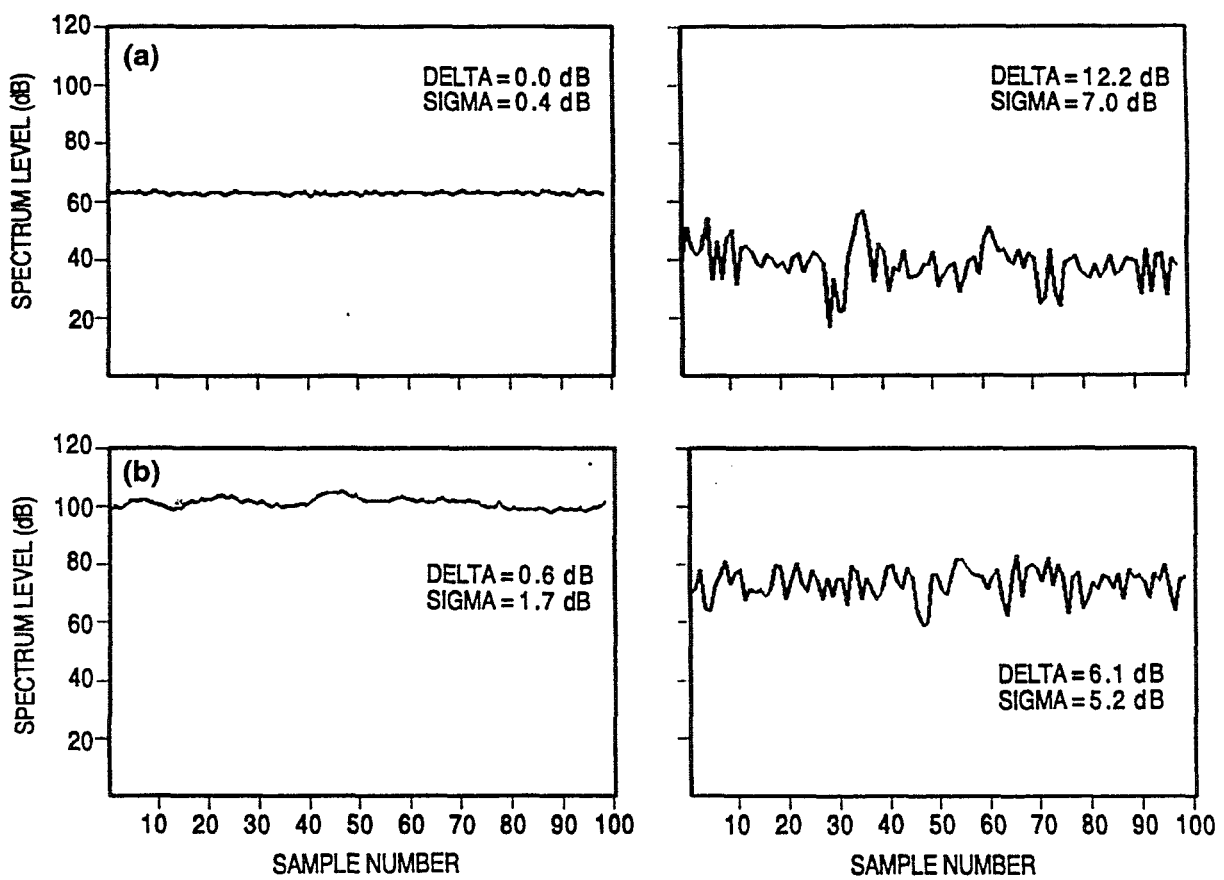

Fig. 3.21 — Shallow-water (400 m) sonobuoy noise data, sensor depths (a) 90 ft and (b) 400 ft

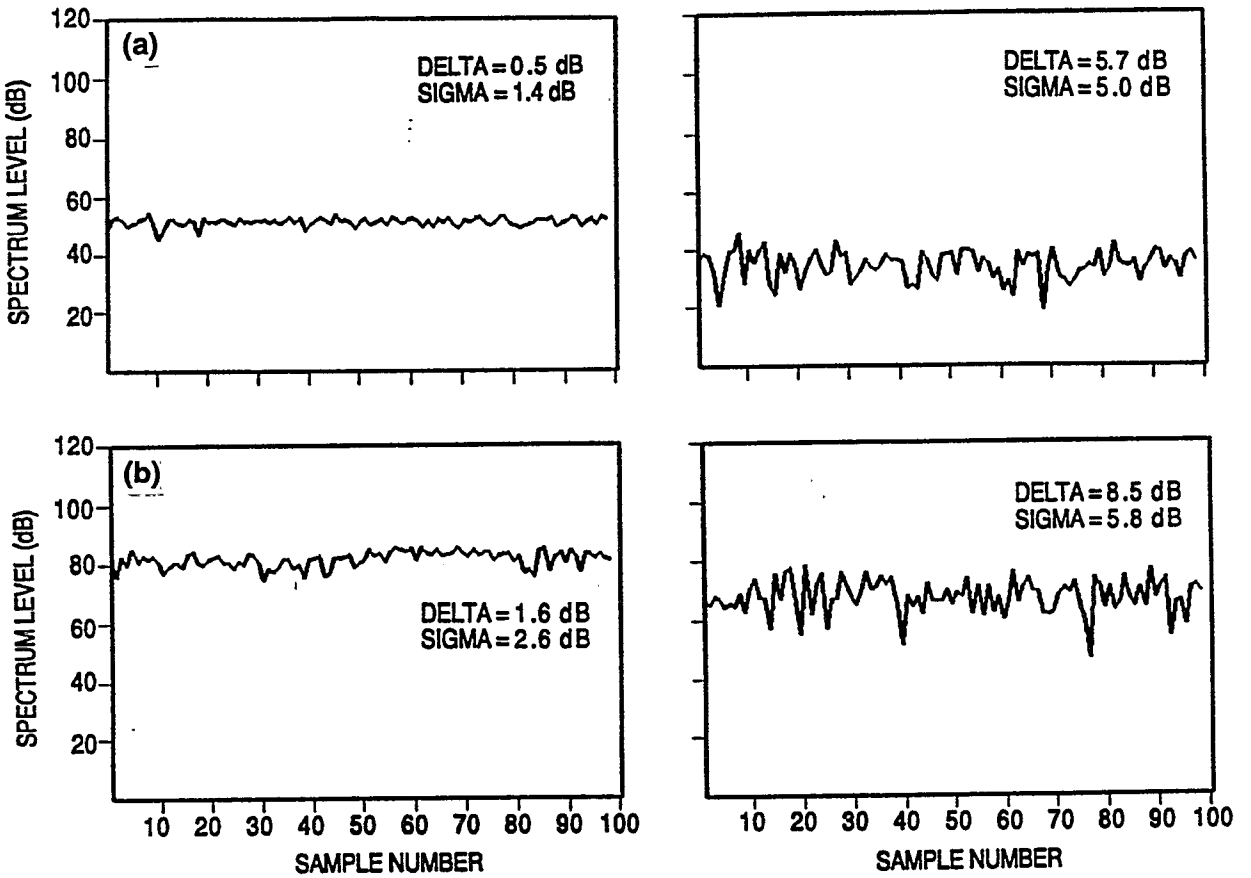

Fig. 3.22 — Shallow-water (150 m) sonobuoy noise data, sensor depths (a) 90 ft and (b) 400 ft

one for which the WISPR and the average power levels are not significantly different. In other words, the distribution function of the noise significantly increases WISPR suppressions relative to the distribution function of the signal. The net result, relative to the AVGPR processor, is a SNR enhancement of about 6 dB for the WISPR processor in shallow water.

3.7 Gain Improvement, Illustrated Using Single-Channel Data from a Towed Line Array

Data were obtained from a single channel of a towed line array for a time period when a submerged source was projecting several tonals. Tonals were also being radiated by the projector ship as a natural consequence of its being there and towing the source. Figure 3.23, prepared using these data, has three plots illustrating several attractive properties of the WISPR filter. The WISPR processing and conventional processing (AVGPR) plots are for the same data. The other plot contains a superposition of the AVGPR and WISPR results. To facilitate comparison, the WISPR results have been shifted a small amount in frequency. The tonal and broadband structures are quite similar, but some significant differences are also apparent:

(a) Some of the tonals are about the same magnitude in both results. This suggests that the WISPR Filter does not attenuate tonals that were emitted by the submerged source.

(b) The broadband noise background has been reduced by about 8 dB by WISPR. The property of not attenuating signals from submerged sources while attenuating the broadband noise by about 8 dB results in a SNR enhancement of 8 dB for signals from submerged sources.

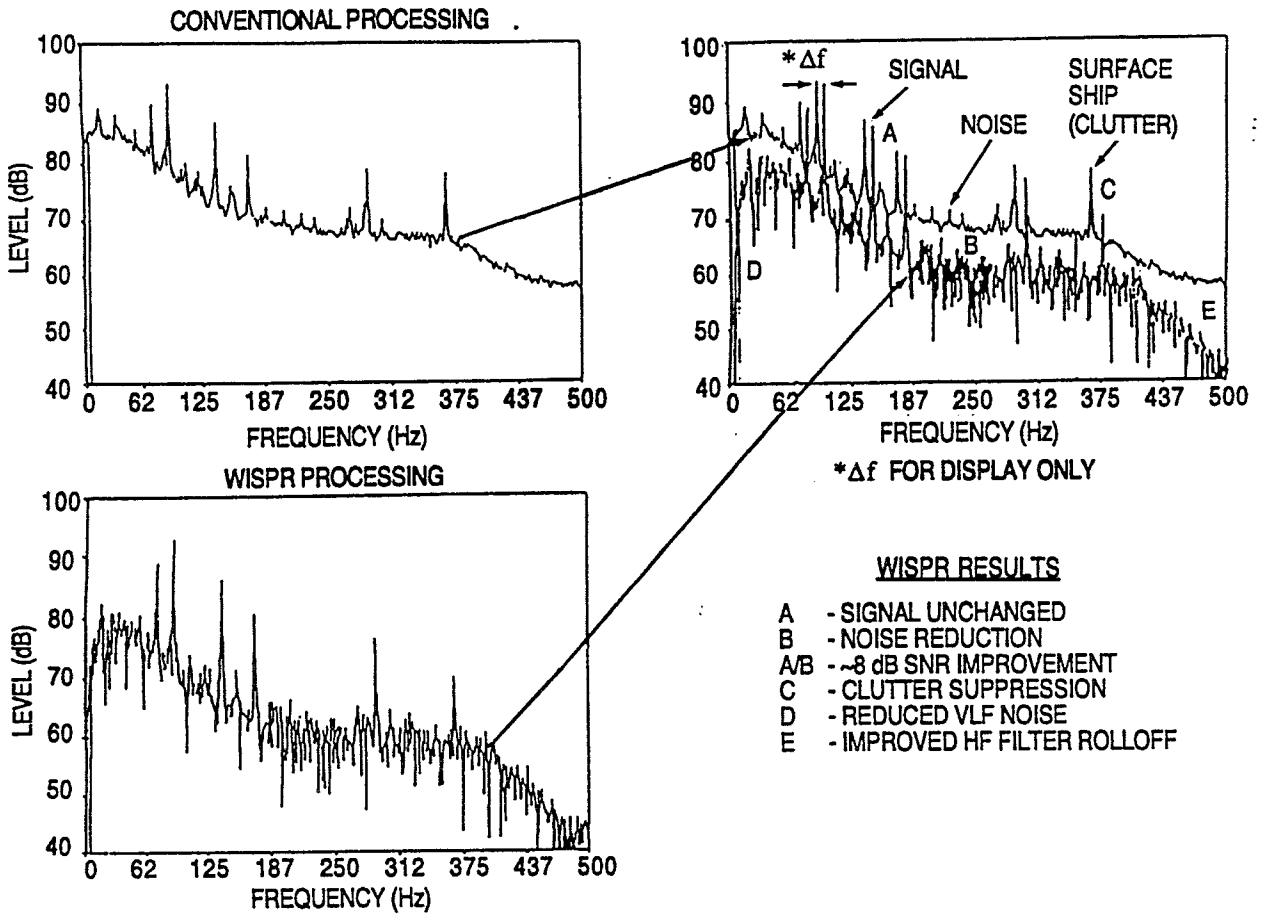

Fig. 3.23 — WISPR SNR improvements

(c) The tonals at the two highest frequencies originated from the source ship and not the submerged source. They have been attenuated by WISPR from 3 to 9 dB. Since surface ship tonals represent narrow-band clutter, this demonstrates that WISPR reduces clutter.

(d) The very low frequency (VLF) broadband noise in the WISPR result below about 30 Hz is suppressed about 15 dB compared to the AVGPR result. This suggests that WISPR has an even greater noise suppression capability at VLF than at the higher frequencies, even though the 8 dB achieved at those frequencies is rather impressive.

(e) Finally, the increased filter roll-off observed in the WISPR results at frequencies above 375 Hz is more indicative of the low-pass filter response of the antibiasing filter than is the output of the conventional processor. This suggests that WISPR is reducing the noise due to the antibiasing filter that adversely affects the AVGPR processor.

3.8 Enhancing Resolution of a Horizontal Sonar Array FFT Beamformer

One common technique for increasing the resolution of a signal processor is to decrease the size of the resolution cells. Examples of that are decreasing the frequency binwidth by increasing the size of an FFT and adding more elements of an array to increase its spatial aperture and, thus, decrease its beamwidths. These and other techniques work well in some applications, but they do not work in all situations. For example, there may be engineering, technology, monetary, or size

constraints that prevent unlimited expansion of the array in the spatial dimension as a means for achieving the desired beamwidth and spatial resolution, or the data may not extend in time long enough or be sufficiently stationary to allow a long FFT to be performed to increase the spectral resolution. In such cases, an alternate, independent approach would be valuable. Achieving enhanced resolution through fluctuation-based processing is one possibility for achieving the needed resolution in both the spatial and the spectral domains.

Fluctuation-based processing provides another dimension that can be exploited that is independent of both the frequency domain (i.e., spectral resolution) and the spatial domain (i.e., beamwidth). In a manner that is similar in both of these domains, fluctuation-based processing can differentiate the fluctuation in one bin (e.g., frequency bin and beam number) from those in another, and then enhance the one bin output relative to the other to achieve improved resolution. Such a case is illustrated by the plot in Fig. 3.24.

The plot in Fig. 3.24 contains three beam response curves. The top curve is the response of an undersea horizontal line array sonar, with an aperture of 1× (a given number of wavelengths), to the noise and signal field in the ocean. The abscissa is beam number from an FFT beamformer. The ordinate is the output level for each beam. The local maxima indicate concentrations of high-level signals and noise in beam number space. The middle curve is the corresponding FFT beamformer output when the number of elements in the array and the aperture have been increased by a factor of four (4× aperture) to increase the spatial resolution. The enhanced spatial resolution of the larger array (middle curve) is demonstrated by the appearance of additional local maxima and the apparent

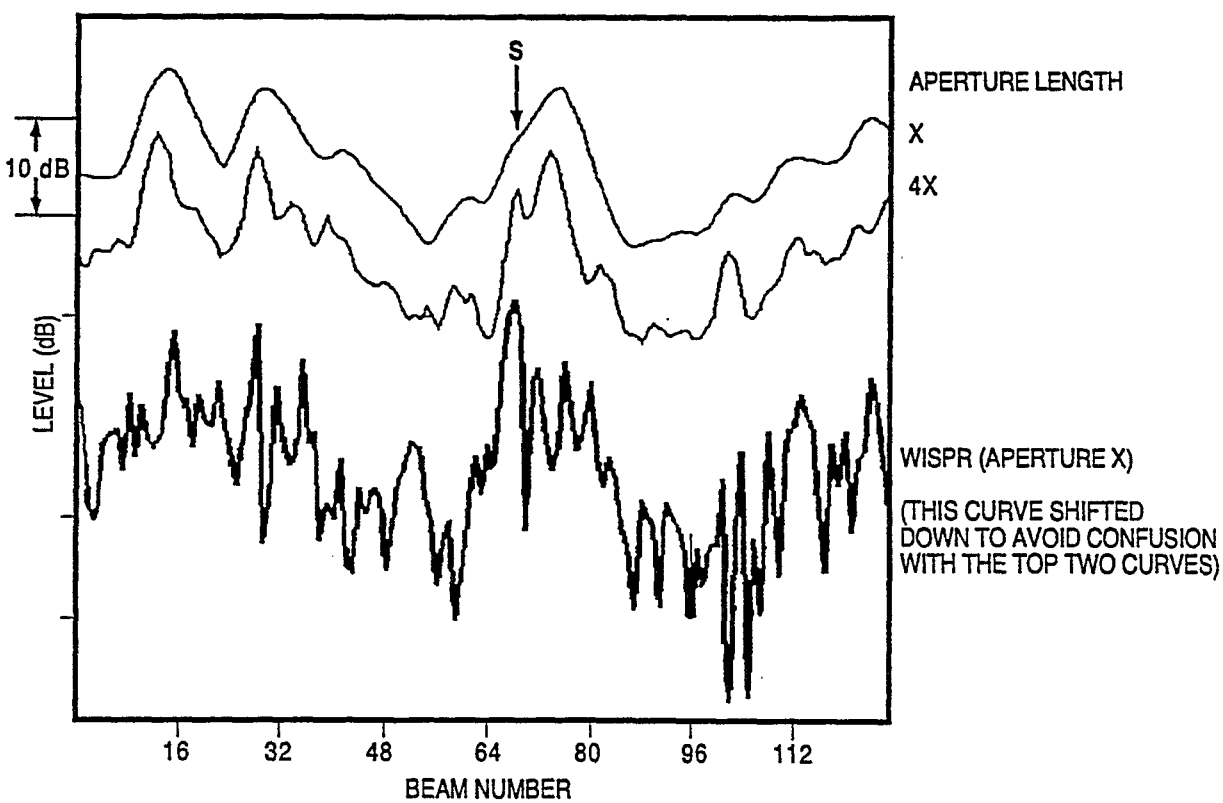

Fig. 3.24 — WISPR filter: enhanced spatial resolution

separation of clumps of signal and noise that are combined in the previous lower resolution results (1× aperture) of the top curve. Some of the local maxima that are in the middle curve are not resolved by the 1× aperture array (top curve).

The bottom curve in Fig. 3.24 is the result of performing WISPR processing on the FFT time history data in each beam number resolution cell that was processed by the conventional technique, AVGPR, to give the 1× aperture result (top curve). The curve has been plotted at a lower average level to minimize the confusion that might be introduced if the various curves have numerous intersections.

The rationale for superimposing the three curves in Fig. 3.24 is that the top curve is a low-resolution output (1×). The middle curve came from an array with four times the aperture, and therefore has four times the resolution (4×). Finally, the bottom curve (WISPR operating on the 1× data), judging from its appearance, has the greatest resolution of the three curves. The credibility of these high-resolution WISPR processor results can be judged, to some degree, by comparing them to the results for the 4× aperture (middle curve). Many of the peaks in the WISPR curve have a direct correspondence with peaks in the 4× results, although some have no correspondence. However, this is also the situation when the 4× results and the 1× results are compared. For example, the signal near beam number 70 in the 4× aperture results does not have a corresponding peak in the 1× aperture results. Even though the signal was present when the 1× aperture data were taken, only the largest aperture, 4×, was able to resolve it using AVGPR. However, when the 1× aperture data were processed by the WISPR Processor, the LOFAT from a submerged source was resolved, and many other signals were also resolved, several of which are evident in the 4× results and some that are not.

Based on the comparison of the three beam response plots in Fig. 3.24, it is evident that the WISPR Processor is providing significantly greater resolution than conventional processing on the 1× aperture data, and even greater than the corresponding 4× aperture results. Perhaps a rough estimate of the enhanced resolution that is being achieved by the WISPR processor is about a factor of 6 to 10 in equivalent increased aperture length (i.e., 6× to 10× aperture).

3.9 Summary

(a) Signal fluctuation content is important to the successful operation of fluctuation-based processors as opposed to the actual level of the signal. Several environments have been illustrated which generate significant differences between signal fluctuations arriving from them. In particular, signals from nearby surface ships can be expected to have greater fluctuation than those from submerged sources at approximately the same distance. Signal clutter from more distant shipping sources should contribute significantly to the noise background, with fluctuations typical of those from surface sources. Fluctuations from distant surface sources may be even greater than from those nearby due to mutual signal interference and a greater likelihood for the signal to be affected by medium inhomogeneities, etc.

(b) Through an analysis of signal ray-trace paths and their associated attenuations, it was shown that the origin (depth) and path taken by acoustic signals strongly influences the fluctuation level. Those signals that travel near the surface typically have greater fluctuation level than signals traveling at greater depths. This is consistent with the observation that signals generated at the surface tend to have greater fluctuation levels than those originating from submerged sources.

(c) Using synthesized data of known characteristics, the conventional processor (AVGPR) was contrasted to the WISPR Filter, demonstrating that AVGPR is biased toward the high values,

whereas the WISPR Filter is biased toward the lower values, giving rise to WISPR gain improvements. Similar effects would be expected for distributions other than those presented, even though the specific levels of gain obtained would be affected. It should be expected that WISPR processing can achieve additional improvements in gain when the noise probability distributions have a longer low-level tail than the one for signal. This situation often arises with acoustic data of interest to the Navy.

(d) Utilizing acoustic data from a single phone, it was shown that WISPR achieves significant gain improvement over the AVGPR processor.

(e) Using FFT beamformed output from a horizontal array, AVGPR and WISPR processing at 1× aperture were compared to show the WISPR capabilities. The WISPR's spatial resolution at 1× aperture even exceeded that achieved by AVGPR processing of concurrently obtained 4× aperture data.

(f) Although perhaps a little premature to mention here, it will later be shown that difference (gain) between the AVGPR and WISPR (M_1 and M_{-1}) Filters, c.f., App. A, Sec. A.1, extends as a continuum for other filter pairs based upon M_r, e.g., for $r = -4, -3, -1, 0, 1$. Though all choices of r do not necessarily produce useful results in all situations, a number of combinations have been investigated with much success for many types of data, including data of nonacoustic origin.

4.0 ADVANCED WISPR SUMMATION PROCESSORS ($AWSUM_k$)

4.1 Introduction

Why not simply utilize the WISPR Filter, which has already been shown to be an effective processor? Examined in this section are results comparing orders of processing (as designated by k) for the $AWSUM_k$ fluctuation-based filter algorithms as defined by Eq. 2.4.2. What will be shown is that additional gain can be achieved with the higher order filters. Several different types of data are used to show the versatility of these processors for a variety of cases and to provide guidance as to how processor order can be varied/combined to achieve optimal results. Before proceeding to the more advanced processors, Sec. 4.2 will present an in-depth example of $AWSUM_1$ (WISPR) processing. Capabilities of the advanced processors generally arise from the same principles as those in evidence for the WISPR Filter. Final interpretation of gain results generally utilize the processors in pairs, e.g., using power, the gain ratio of processors A_{01} and A_{04} is defined by Eqs. 2.5.1 and 2.5.2, respectively. For convenience, these ratios are commonly converted to decibels where the decibel differences are used.

Equation 2.1.1 defines the generalized filter, M_r. An important property, more fully discussed in App. A, is that M_r increases strictly monotonically with increasing r for nonzero data. The additional gains that are achieved by the higher $AWSUM_k$ processors are fundamentally related to this property.

4.2 Demonstration of WISPR Processing

Hypothetical data and preprocessing – Hypothetical shallow-water data are shown in Fig. 4.1a. These data might, e.g., represent a frequency-time sequence of many successive spectral realizations (perhaps the transformed output from an FFT of each time domain realization). Those spectra contain both LOFAT (f_2 and f_3) and HIFAT (f_1 and f_4) signals and background ambient noise (f_n).

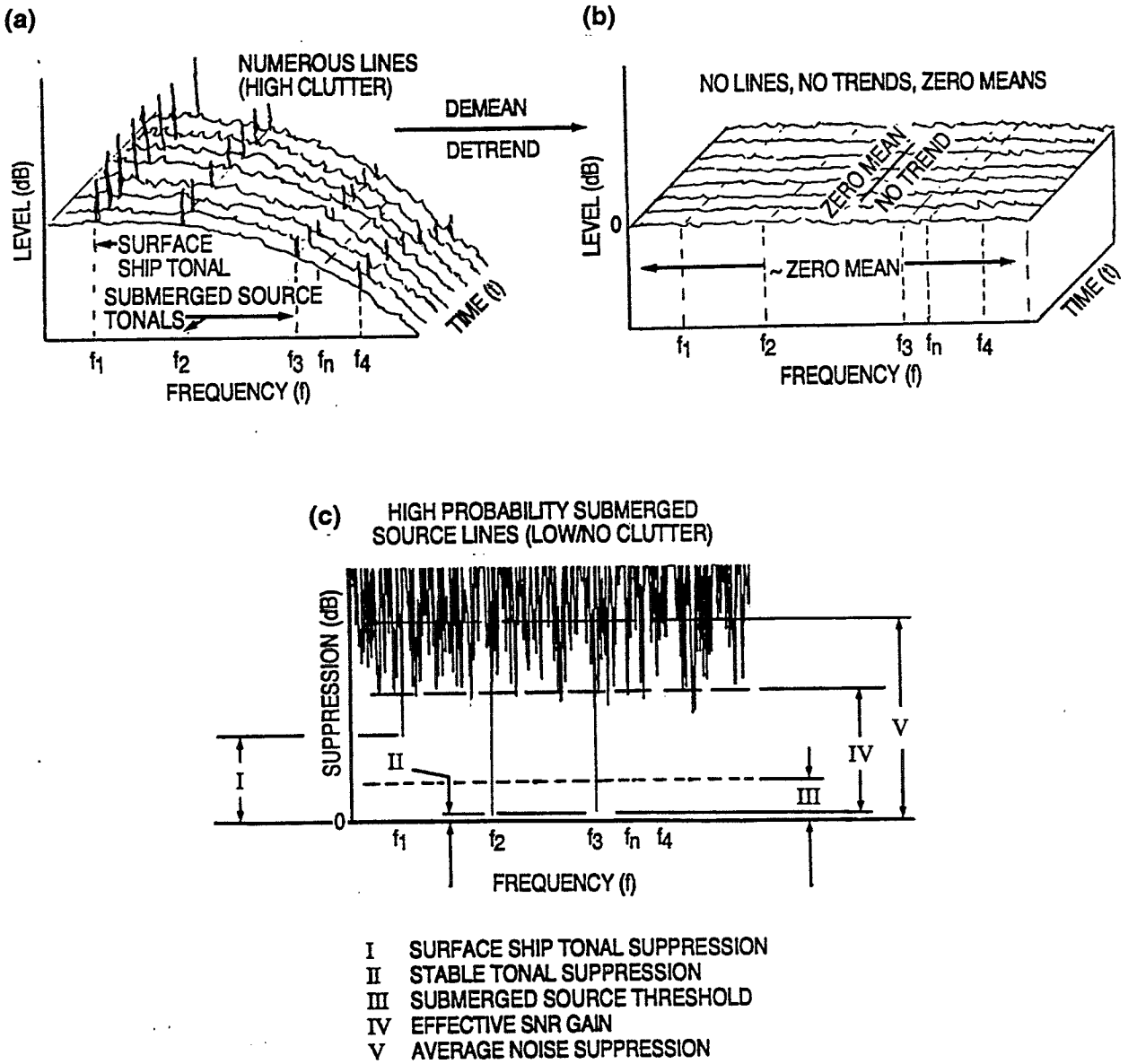

Fig. 4.1 — Fluctuation-based processing: SNR gain and stable signal (submerged source) identification based strictly on fluctuation content: (a) unprocessed frequency-time surface, $F(f,t)$, (b) normalized-detrended frequency-time surface, $G(f,t)$, and (c) submerged source curve, $S(f)$, resulting from the AVGPR–WISPR difference (A_{01} processing)

If the spectral realizations in a given frequency bin for all time increments are passed through a filter that removed the temporal trends and normalized the average to a given level (e.g., zero decibel), a flat surface with a rough texture would result such as that depicted in Fig. 4.1b. The texture of the surface is caused by the fluctuation content that is preserved by the filter, while the trend is removed and the mean is normalized. In addition, none of the tonals would be identifiable by their signal excess after filtering, as they are in Fig. 4.1a, because the normalization makes the average values of all frequency bins equal. With the exception that the fluctuation character of signal plus noise in a particular bin may change as the SNR changes, the flat rough surface in Fig. 4.1b could represent a realistic case of what often happens in the real world. For

example, consider the case where a submerged source is entering a shadow zone or traveling away from the sensor. At some point, the signal will go from a positive SNR to a negative SNR (in decibels). Somewhere in between, a case will exist for which the surface in Fig. 4.1b is a reasonable representation of reality.

4.2.1 WISPR Filter Processing

Now if the data that comprise that averaged and normalized surface are processed with a conventional processor, AVGPR, a flat response across frequency would be the result, the same as before (the previously averaged and normalized values). There would be no SNR excess to indicate that tonals are present, whether they are LOFAT or HIFAT as this was already removed by the normalization of each bin to, e.g., zero decibel. Thus a second application of the AVGPR processor does not give additional SNR gain. On the other hand, if the same data were processed by the WISPR Filter, additional gain would be achieved. The amount of the SNR gain would depend on the differences in fluctuation amplitudes between the LOFAT on one hand and the HIFAT and background noise on the other hand.

The differences between the WISPR outputs and the corresponding outputs from the conventional, AVGPR, processor are shown in Fig. 4.1c. The broad scatter of the curve in this figure is due to the nonuniform fluctuation content in the HIFAT signals and the background noise as measured by the differences between the high degree of fluctuation sensitivity of the WISPR processor compared to the relative insensitivity of the conventional processor to fluctuations. The two lines at f_2 and f_3 that extend downward to nearly zero reflect the difference responses to a LOFAT signal. The difference is expressed in terms of suppression level of the signals. A difference or suppression level of less than an arbitrary level of 1.5 dB may be interpreted in this example as a LOFAT signal from the submerged source. Referring to Fig. 4.1a, note that the surface ship tonal at f_1 is a HIFAT signal as is the tonal at f_4 that is not steady in frequency and all of the background noise such as that in frequency bin f_n. The effective SNR gain (or signal excess) for the LOFAT signals is limited by the large variability in the difference that results more from the WISPR processing than from the conventional processing. However, that variability has a relatively uniform lower end that usually does not interfere with the detection of the LOFAT signals that extend below it (i.e., the signal excess of the line component that extends below the broad scatter of the difference background).

In Fig. 4.1c, the submerged source display that is normally produced whenever A_{01} processing of the data from a single beam or a single sensor is used to obtain the differences between the average power (AVGPR) levels and the WISPR Filter levels. This particular example could be for a single sensor, such as a sonobuoy, or even a single beam of a multibeam beamformer output. A corresponding surface would be obtained when the data for all beams of the beamformer are displayed simultaneously.

4.2.2 Real Shallow-Water Data

Figure 4.2 represents data for a real shallow-water environment when there is one HIFAT signal and one LOFAT signal. Plots 2 and 3 are produced using the same processing described for the previous figure. In plot 3, the bottom curve lowered 60 dB for display purposes, is the A_{01} difference curve that corresponds to the single curve in Fig 4.1a. The top curve is the AVGPR curve for the surface in plot 2, and the center curve is the corresponding WISPR Filter output. This latter curve has also been lowered by 10 dB for display purposes. Note the identification and SNR

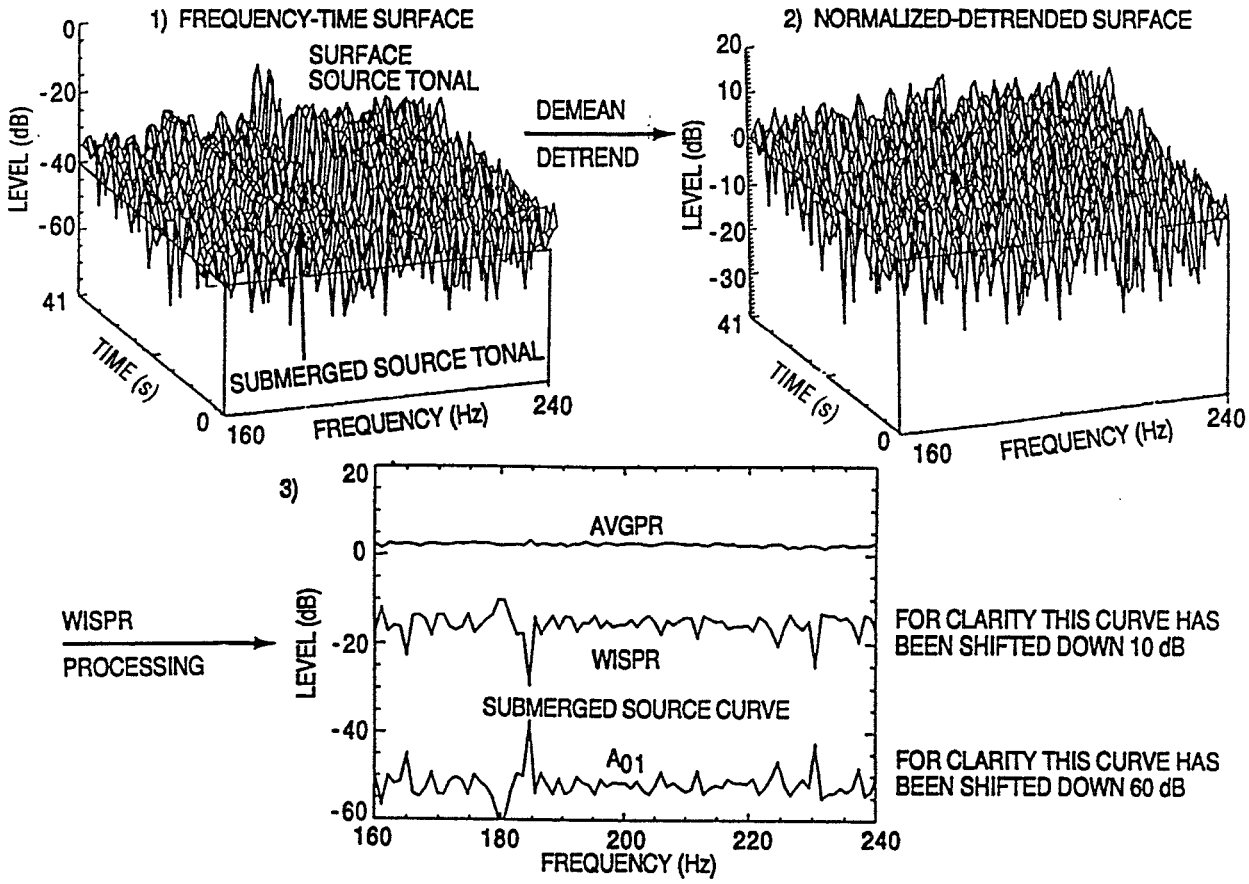

Fig. 4.2 — Fluctuation-based processing: SNR gain and stable signal (submerged source) identification based strictly on fluctuation content

enhancement of the LOFAT signal at 180 Hz in plot 3 and the elimination of the cluttering response of the HIFAT signal at a slightly higher frequency.

4.2.3 Discussion

The similarity of the results obtained for the assumed data where the character of signals can be generated with confidence and the results for the real-world case demonstrates that the hypothetical case presented has a basis in reality. Thus, it may be concluded that the WISPR Filter functions as a fluctuation-based signal processor that enhances the detection, identification, and SNR of LOFAT signals (e.g., tonals from submerged sources). It accomplishes that by attenuating HIFAT signals (e.g., tonals from surface ships) and background ambient noise more than the LOFAT signals. In addition, by thresholding the differences between the AVGPR and WISPR levels at some low value, based on experience with successful detection (e.g., AVGPR – WISPR <1.5 dB), it is possible to identify a submerged source as a consequence of enhancing the SNR of the LOFAT signals and eliminating the clutter due to the HIFAT signals.

These attractive capabilities may be attributed to the unique property of the WISPR Filter as being driven entirely by the fluctuation character of the various signals and noise. The actual levels of the signals and the noise have little direct bearing on the resulting SNR enhancement (except at very low SNR) as contrasted to conventional processors.

4.3 Comparison of AWSUM Orders 1 and 4 at Five Levels of Spectral Resolution

The data set for the example presented here is a little more complex than those discussed previously. However, the additional gain achieved by $AWSUM_4$ compared to WISPR is vividly shown. This gain improvement, typically two to three times greater than the WISPR Filter, is consistently achieved at five levels of spectral resolution, which offers a system designer a number of useful alternates.

Figure 4.3 illustrates the suppression of both signal and noise for three different frequency resolutions that range from 0.2 Hz to 0.012 Hz. Time history sequences are included for the 20-Hz noise bins in the first column. The third column contains time histories for a 45-Hz signal bin. The frequency resolution is improved down each column from 0.2 Hz at the top of the figure to 0.012 Hz at the bottom. The sample rate of the original data was approximately 205 Hz. Approximately 160,000 data points were used, and 400 FFTs were calculated to produce each sequence in Fig. 4.3. To keep the sequences of FFT outputs in Fig. 4.3 a constant length of 400 each, the FFTs were overlapped by increasing amounts as the size of the FFT increased. The results shown at the top of each subplot in that figure are summarized in Tables 4.1 and 4.2, along with the companion results for an FFT sizes of 2048 and 8096. Table 4.1 gives the FFT size, the percentage of the overlap, the frequency binwidth, AVGPR, the WISPR level, and the differences (A_{01}) between those two (AVGPR – WISPR) for the two sets of noise sequences (20 and 35 Hz) and the set of signal sequences (45 Hz). Table 4.2 presents similar results for $AWSUM_4$ (plus AVG A_{04}, which is A_{04} averaged over all frequency bins).

There are several features of the sequences in Fig. 4.3 that are interesting. The most obvious is that as the percentages of overlap and FFT sizes increase (going down each column), the sequences become progressively smoother. However, the dynamic range in level remains relatively constant. The increase in smoothness is a result of the FFTs being less independent as the overlap percentages increase, which increases overlap as the FFT size increases. The A_{01} difference between the AVGPR and the WISPR level is a measure of the dynamic range of each sequence. As can be seen in the last column of Table 4.1, the A_{01} difference for WISPR processing ranges from about 5.7 to 15.6 dB for the noise (20 and 35 Hz) and from about 0.9 to 0.2 for the signal (45 Hz) as the frequency binwidth changes. The corresponding results for $AWSUM_4$ processing in Table 4.2 are 13 dB to 33 dB for noise and 4.0 to 0.4 dB for signal. Less variability would be expected if the results were averaged over more time periods or more frequency bins. That has been done for the $AWSUM_4$ case in Table 4.2, and the result for the noise (AVG A_{04}) is about 21–22 dB.

As the frequency binwidth is reduced by a factor of 2, the average power level of the noise in the 20- and 35-Hz bins decreases by 3 dB as expected. This average power reduction does not occur in the 45-Hz signal bin because the signal is narrower than the binwidth. Therefore, reducing the binwidth of the signal bin does not decrease the signal level. When normalized for binwidth, the signal level will appear to increase by 3 dB each time, while the noise level remains constant. In reality, without binwidth normalization, the noise decreases while the signal remains constant. In either case, the SNR increases by 3 dB each time the binwidth is cut in half.

The A_{01} level for the 45-Hz signal in Table 4.1 decreases from 1.0 dB at 0.2-Hz binwidth to 0.2 dB at 0.012-Hz binwidth. The results in Table 4.2 are similar for $AWSUM_4$ processing. In this case, the signal is narrower than the binwidth. By reducing the binwidth, the signal is not being decreased but the noise is being stripped away. Hence, there is progressively less noise in the same bin with the signal to contaminate it with noise-induced fluctuations.

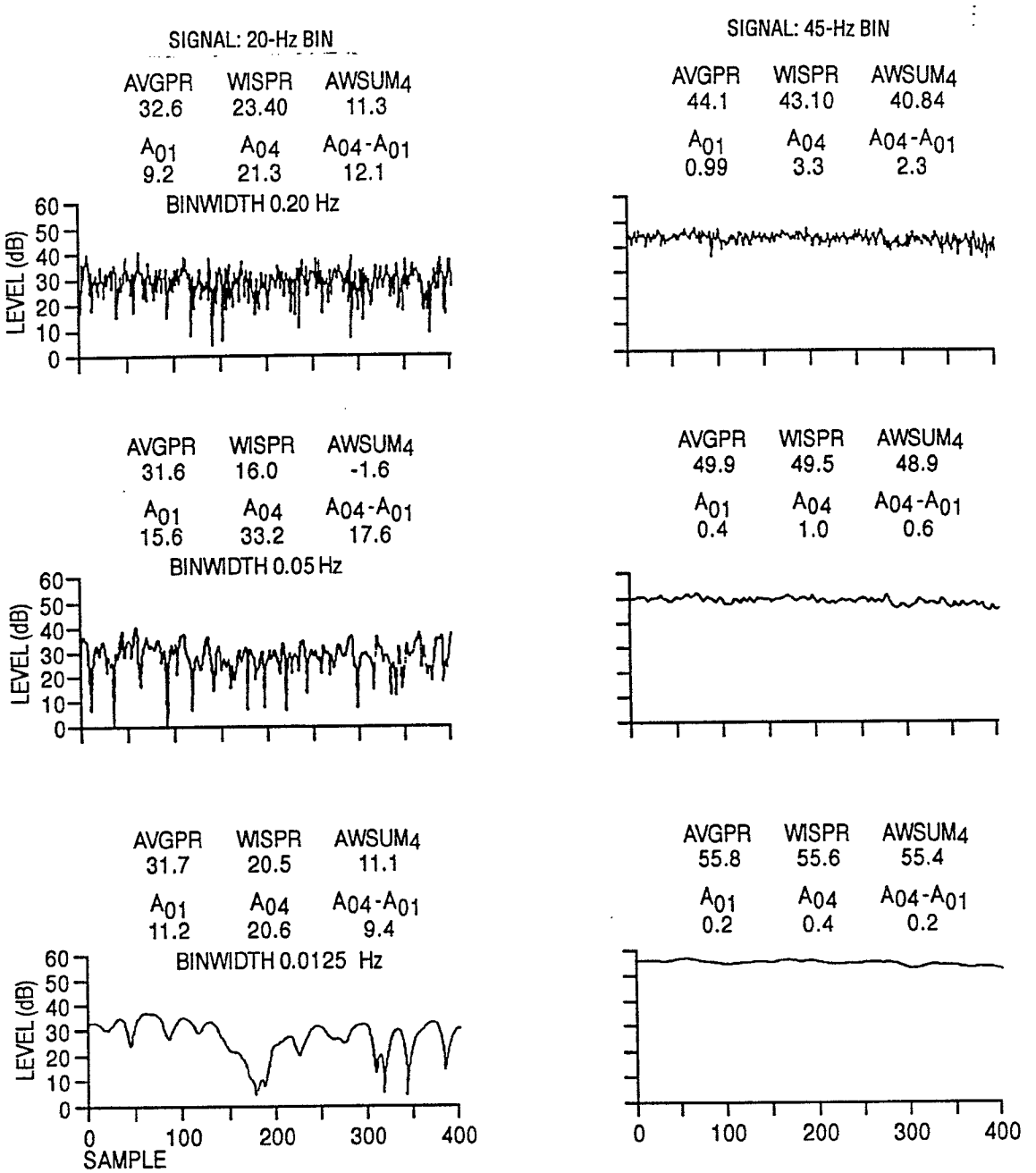

Fig. 4.3 — Signal time history showing fluctuation at three levels of spectral resolution

Table 4.1 — WISPR Processing of the Signal Sequences in Fig. 4.3

$$A_{01} = AVGPR - WISPR$$

FFT SIZE	BINWIDTH (Hz)	OVERLAP (%)	FREQ. (Hz)	AVGPR (dB)	WISPR (dB)	A_{01} (dB)
			20	32.6	23.4	9.2
1024	0.2	56	35	32.0	23.4	8.6
			45	44.1	43.1	1.0
			20	32.3	24.5	7.8
2048	0.1	78	35	31.7	23.8	7.9
			45	46.9	46.4	0.5
			20	31.6	16.0	15.6
4096	0.05	89	35	31.1	21.2	9.9
			45	49.9	49.5	0.4
			20	31.4	25.7	5.7
8192	0.025	95	35	31.2	25.3	5.9
			45	52.8	52.6	0.2
			20	31.7	20.5	11.2
16384	0.012	97	35	31.5	23.0	8.5
			45	55.8	55.6	0.2

Table 4.2 — $AWSUM_4$ Processing of the Signal Sequences in Fig. 4.3

$$A_{04} = AVGPR - AWSUM_4$$

FFT SIZE	BINWIDTH (Hz)	OVERLAP (%)	FREQ. (Hz)	AVGPR (dB)	$AWSUM_4$ (dB)	A_{04} (dB)	AVG A_{04} (dB)
			20	32.6	11.3	21.3	
1024	0.2	56	35	32.0	11.6	20.4	22.5
			45	44.1	40.1	4.0	
			20	32.3	14.4	17.9	
2048	0.1	78	35	31.7	11.8	19.9	22.5
			45	46.9	45.3	1.6	
			20	31.6	−1.6	33.2	
4096	0.05	89	35	31.4	6.1	25.3	22.6
			45	49.9	48.9	1.0	
			20	31.4	18.3	13.1	
8192	0.025	95	35	31.2	15.8	15.4	22.3
			45	52.8	52.2	0.6	
			20	31.7	11.1	20.6	
16384	0.012	97	35	31.5	12.5	19.0	21.0
			45	55.8	55.4	0.4	

4.4 Comparison of AWSUM Orders 1 and 4 for Nonacoustic Data

Figure 4.4a–d illustrates the results of fluctuation-based processors operating on a time segment of nonacoustic data. It is known by other means that tonals from the source exist at several harmonics of 2 Hz.

4.4.1 Power Level Standard Deviation Frequency Plot Locates Frequencies with the Lowest Fluctuation

Figure 4.4a shows the standard deviation of the power of each frequency bin (about 0.1-Hz binwidth) using 87% overlap in the time domain data and 15 averages of the spectrum-analyzed results for all bins in the band from 0 to 10 Hz at 31 min into the processing. The abscissa is frequency in hertz and the ordinate is the magnitude of the standard deviation (0–12 dB) in each bin. The average standard deviation is approximately 4.25 dB with excursions from about 0.25 to 8.3 dB. The relatively low levels for harmonics of 2 Hz (2, 4, 6, 8, and 10), marked with a circle, are of particular interest because the values are all less than 0.8 dB, significantly below the average of all of the others. It can be concluded that these tonals that were known to exist have relatively low-level fluctuations.

4.4.2 Power Level Standard Deviation Time Plot at 2 Hz Locates Time Period with the Lowest Fluctuation

Figure 4.4b shows the time history of the standard deviation in the 2-Hz bin for a time interval of over 30 min (minutes 20 to 50). The results at 2 Hz in Fig. 4.4a correspond to minute 31 in Fig. 4.4b. That time occurs after the standard deviation has reduced from the relatively high values prior to minute 28 and before the standard deviation rapidly increases after about minute 40. Based on the relatively low standard deviations between minutes 28 and 40, one would suspect that period of time to be when the nonacoustic source was at its closest point of approach (CPA).

4.4.3 Detection of Amplitude Stable Tonals Gleaned through WISPR and AWSUM$_4$ Processing

Figure 4.4c shows processing results for a nonacoustic source that are reasonably typical for fluctuation-based processing of acoustic data. At the top of the figure are three power spectrum curves:

1. AVGPR processing – solid curve
2. WISPR processing – dashed curve
3. AWSUM$_4$ processing – dot dashed dot curve

At the bottom of the figure are two inset plots each having a baseline of 0 dB with an ordinate otherwise of the same scale as the main figure. The upper of these plots is for A_{01} processing, i.e., AVGPR – WISPR. The lower of these plots is for A_{04} processing, i.e., AVGPR – AWSUM$_4$.

In Fig. 4.4c, none of the tonals at the harmonics of 2 Hz, which were obvious in Fig. 4.4a, are particularly significant in the curves produced by any of these processors. However, a significant feature of these three curves is that at the harmonics of 2 Hz, all three of the processors produced nearly equivalent results. This is obvious in the two lower plots where the values are less than 0.05 dB at the harmonics of 2 Hz. In this case where the tonals are known to exist and have low fluctuations, c.f., Fig. 4.4a and b, all three processors have produced nearly the same value. It may

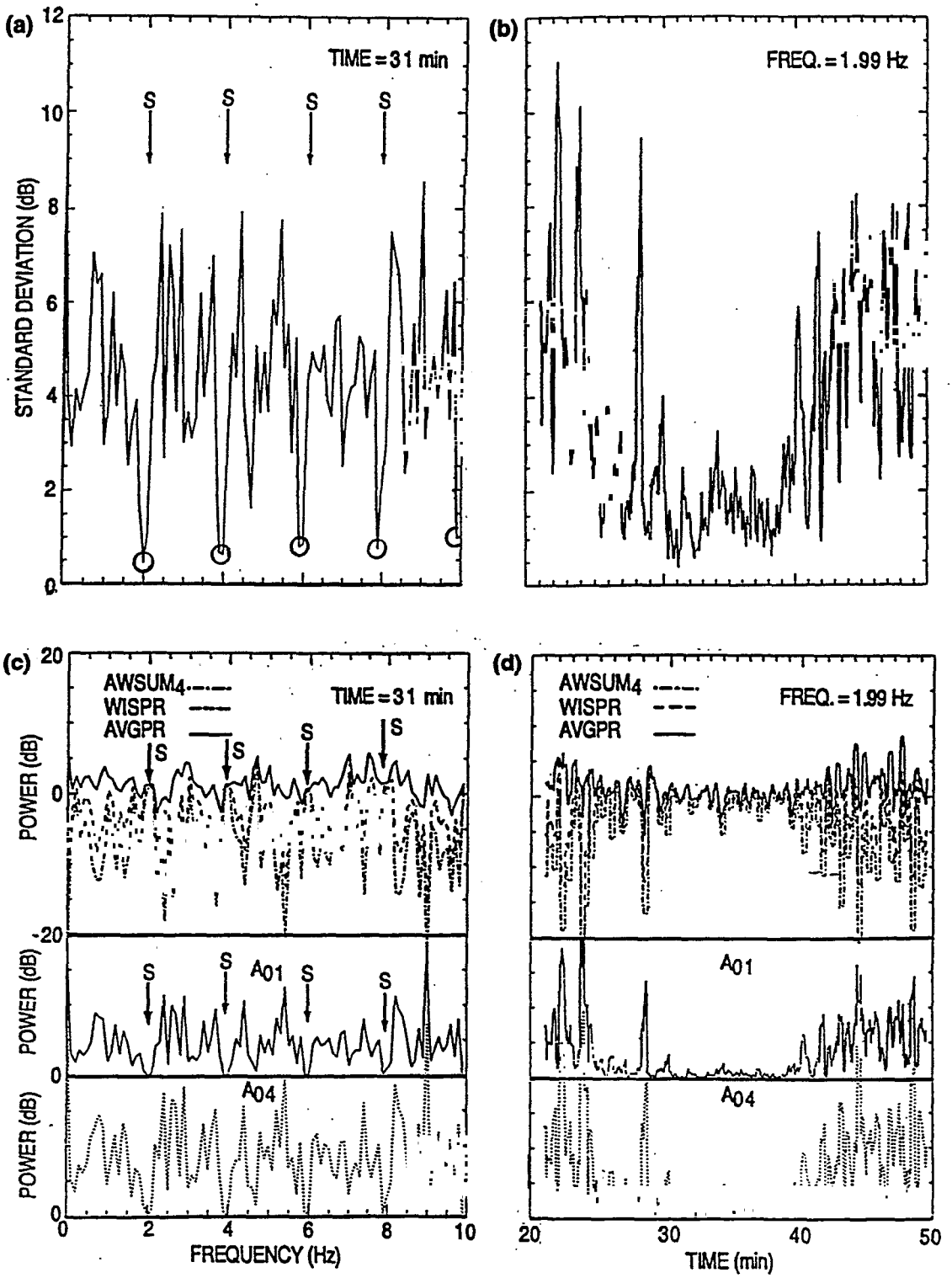

Fig. 4.4 — (a) Standard deviation frequency dependence, (b) standard deviation time dependence, (c) processing frequency dependence, and (d) processing time dependence

be concluded that the steady tonals were not suppressed by the fluctuation-based processors, whereas the fluctuating noise was significantly depressed. This again demonstrates that gain is achieved by fluctuation-based processors.

4.4.4 Interpretation of the A_{01} and A_{04} Plots

Analysis of the A_{01} and A_{04} plots takes some mental adjustment as the identification of low fluctuation signals is associated with the lowest positions on the curves. Persons who are more accustomed to detection based on peaks standing out from the noise background may initially find this a little awkward. They may feel more comfortable by turning the plots upside down. However, the form of presentation in which the low values are pointing down has a distinct advantage. The zero baseline is always in a fixed position. Detection can be associated with any value that is below a threshold value that experience with the type of data and particular processor chosen has been shown to indicate detection. Thus, a reasonable equivalent to complex statistical analysis and interpretation is automatically built in once the processing method and threshold value has been chosen. This alone can be a very substantial advantage when real-time interpretation is required in the field. It also facilitates automated detection schemes. Here, as in the previous section where acoustic data were examined, the A_{04} processor has at least twice the gain of the A_{01} processor.

4.4.5 Extending the Time of Detection

Figure 4.4d gives the time history of the power level of the 2-Hz tonal for the time interval from minute 20 to 50. Recall that Fig. 4.4a and c was for minute 31 in that time history. In this case, the time history is the input data for the same five processors whose outputs were plotted in Fig. 4.4c. The curve for each processor is identified as previously explained for Fig. 4.4d. Of particular significance is the apparent stability, or lack of fluctuations, of the signal during the same time interval identified previously from minute 28 to 40 when the CPA of the source occurred. It is apparent that if either the A_{01} or A_{04} processor is used, that with a properly set threshold, the interval of detection can reasonably be judged to span from minute 26 to 39, broken only for a short interval near minute 28. However, using average power results alone, it is difficult to define any significant interval during which the source could be declared detected with confidence

4.5 $AWSUM_k$: Submerged Source Identification

Figure 4.5 illustrates the capability of AWSUM for submerged source identification in the presence of masking as a function of two different percents of FFT overlap. The left column corresponds to normal data (no masking) and the right column corresponds to a time period when the data were being masked by drop-outs in the sonobuoy radio frequency (RF) carrier. The top row of plots are for 50% overlap in the FFT and the bottom row is for 90% overlap. The total time durations of the data are approximately 240 s for the 50% overlap case and 50 s for the 90% overlap case.

The top curve in each plot is the conventional power average of 240 FFT outputs The middle curves are the $AWSUM_2$ results for the same data as were used in the generation of the top curves. The bottom curves are for five times the difference (in decibels) of the curves for $AWSUM_2$ and $AWSUM_1$, i.e., $5(AWSUM_1 - AWSUM_2)$.

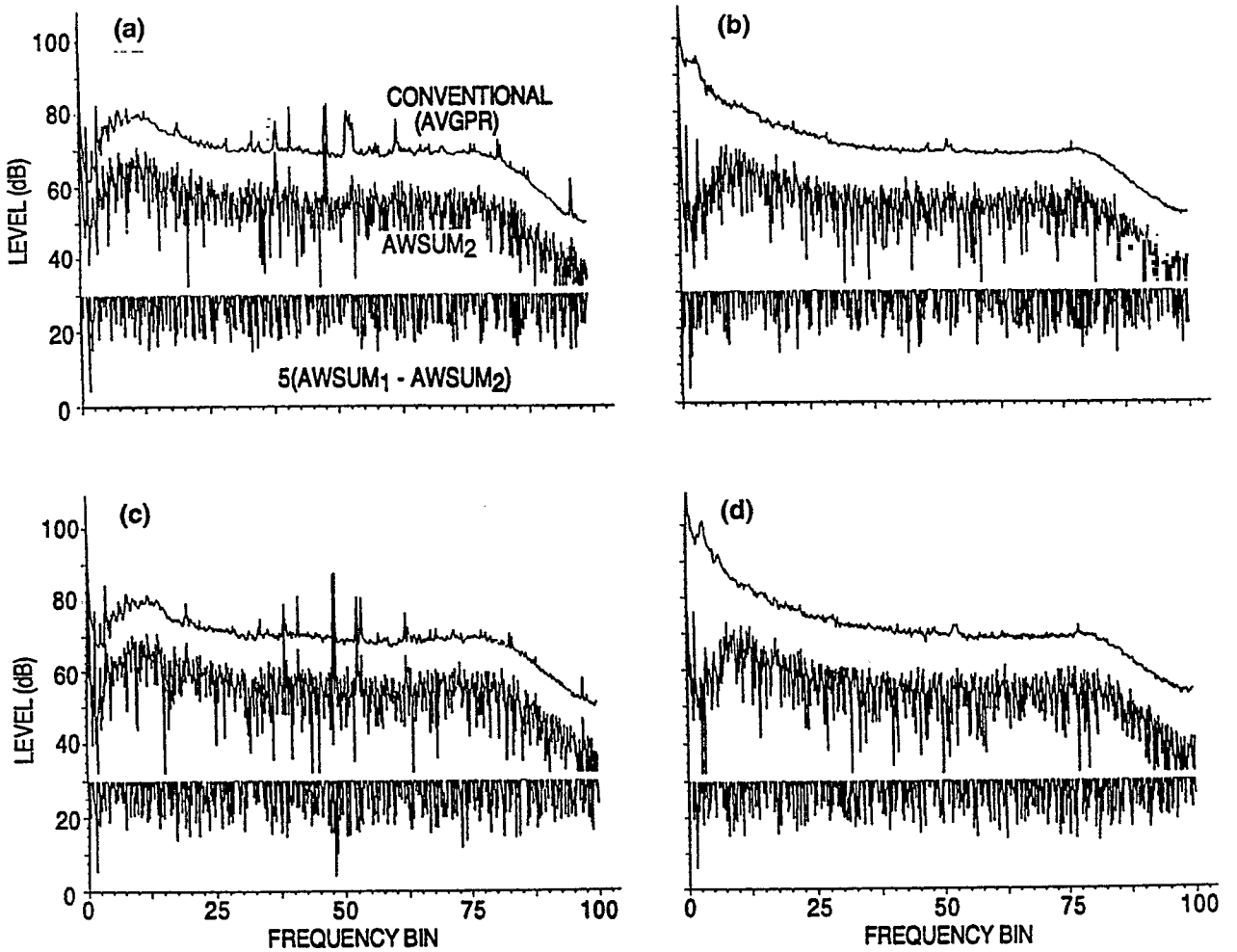

Fig. 4.5 — AWSUM: submerged source identification, FFT size 2048: (a) and (b) 50% overlap, (c) and (d) 90% overlap. The spectra in (b) and (d) are contaminated by high-level transients.

Comparing the 50% overlap results in Fig. 4.5a with the 90% overlap results in Fig. 4.5c reveals several important features listed below:

(a) The overall SNR is about 15.7 for $AWSUM_2$ and 9.2 for $AWSUM_1$.

(b) Because of the shorter time for the 90% overlap results, the SNR of the bin 2 tonal component is approximately 0.2 dB greater than for the 50% overlap results, and there is less frequency smearing of the doublet at bin 48, also of other tonals.

(c) The bin 48 doublet shows up as a submerged source at 90%, whereas at 50%, only the bin 2 signal shows up as a submerged source. The reason is probably due to the amplitude of the fluctuations being small for 50 s (90% overlap) but not for 240 s (50% overlap).

(d) The SNR for the bin 48 doublet is about 14.6 dB for $AWSUM_2$ for 90% overlap and about 5 dB for 50% overlap.

For the case in Fig. 4.5b and d where the masking is present, the following is observed:

(a) $AWSUM_2$ and $AWSUM_1$ gains changed little going from 50% to 90% overlap.

(b) The gains were about 18.6 dB for $AWSUM_2$ at 90% and 18.0 dB for 50%. They were 12 dB for $AWSUM_1$ at 90% and 11.3 dB at 50%.

(c) In both cases, the bin 2 tonal is designated as coming from a submerged source based on the criteria that the ($AWSUM_1$ – $AWSUM_2$) difference is less than 1.5 dB.

The preceding analyses justify the following general observations which apply to the identification of submerged sources.

(a) $AWSUM_1$ minus $AWSUM_2$ can be used to determine if a source is submerged at low SNR when the power average is not a good basis for comparison. The same is true in the presence of masking.

(b) 90% overlap gives better gain than does 50%; more overlap is better.

(c) 240 s (average of 240 FFTs at 50% overlap) is too long for these data to remain stable in amplitude.

4.6 $AWSUM_k$: Performance for Low SNR

Figure 4.6a presents a beam noise level versus beam number plot for 26.9 Hz. The top curve corresponds to the average power level for each of 128 beams from a discrete Fourier transform (DFT) beamformer. The half wavelength design frequency of the array was 30 Hz and the number of hydrophones was 50. Since the hydrophones were uniformly spaced, the beamwidths near broadside were approximately 5°. The bandwidth of the data is 0.2 Hz; 400 time segments were overlapped 95%, an FFT performed on them, and then each spectral bin was averaged over the 400 results. The middle curve is the result obtained from $AWSUM_4$ when the input data are the same 400 spectral estimates that produced the top curve. The bottom curve is the difference between the two previous curves. It has been truncated at 10 dB to prevent it from interfering with either of the two previous curves and complicating the interpretation of the results. Only a small segment shows near beam number 68.

The curve for the AVGPR results (top) shows the presence of high-level signals or noise. There are three peaks that are very prominent at beam numbers 15, 30, and 75, as well as several others that are less prominent. It is not clear from these results whether these high levels are from one source each or multiple sources within a beam summed together due to the relatively broad beamwidths (>5 deg) of the 50-element array.

The middle curve, which corresponds to the $AWSUM_4$ results, shows considerably more resolution than the previous curve. In fact, the number of local maxima has increased by a factor of approximately 4.5 (36 versus 8). It is not possible from these results to determine whether or not the apparent increased resolution is real and is actually an enhancement in the resolving power of the $AWSUM_4$ processor compared to the AVGPR processor. The additional peaks in the $AWSUM_4$ results suggest that it is resolving more sources than the conventional processor. Perhaps the most significant feature in the $AWSUM_4$ results is the maximum at approximately beam number 68. There is no corresponding maximum, or even a local maximum, in the power average results. A tonal was being projected by a submerged source at this frequency at the approximate bearing of beam number 68. The SNR is sufficiently low to be undetectable by the average power processor (top curve). On the other hand, it is clearly indicated with a SNR of approximately 19 dB in the $AWSUM_4$ results.

The differences between the two curves at the top of Fig. 4.6a are truncated at 10 dB and plotted at the bottom of this same plot. The resulting difference curve only appears on the plot near

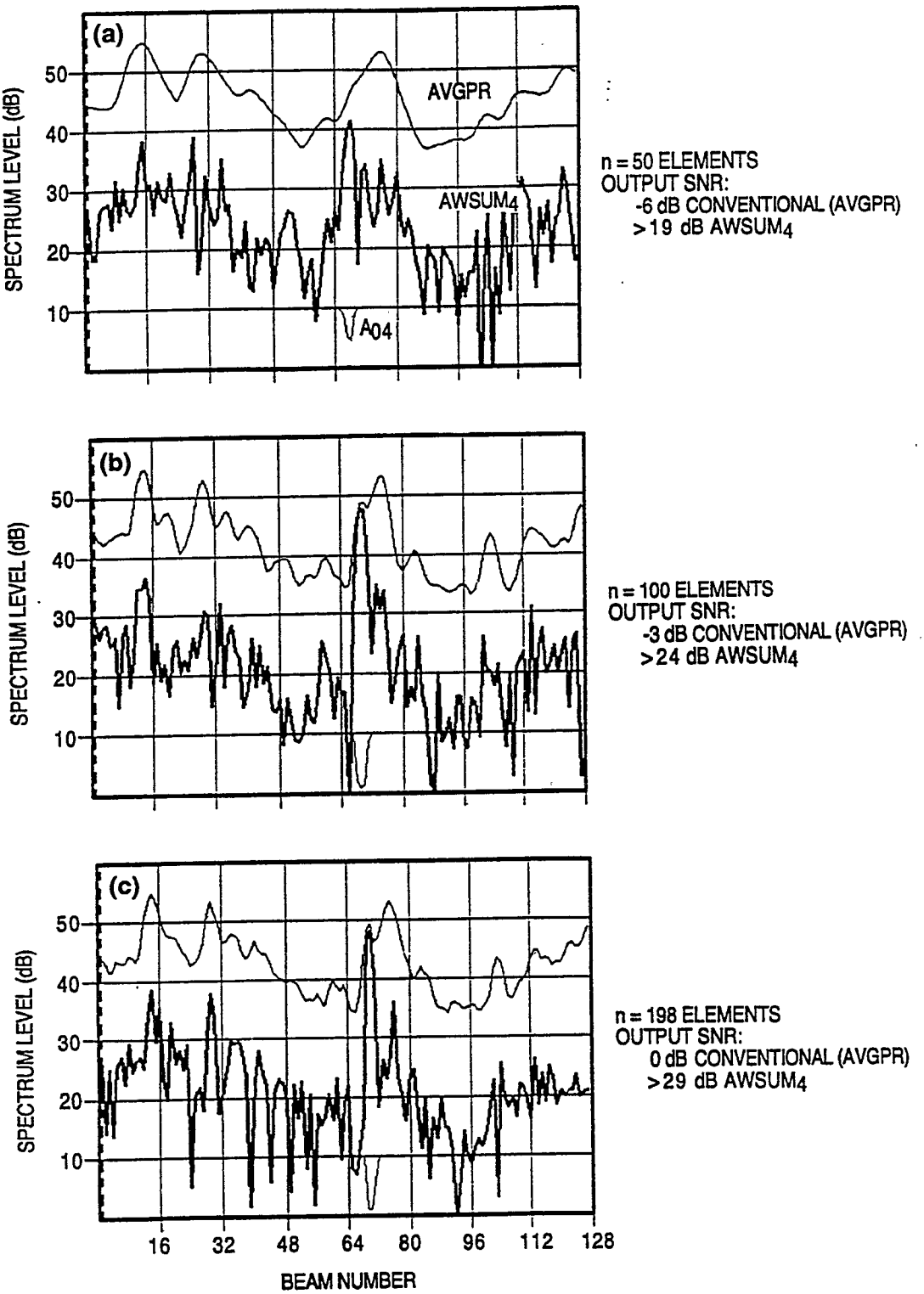

Fig. 4.6 — Comparison of conventional processing, AVGPR (top curves), $AWSUM_4$ processing (middle curves), and the differences between the two (bottom curves) clipped where >10 dB. Bandwidth is 0.2 Hz, 100 s of data and 400 FFTs at 95% overlap.

the beams where the AVGPR – $AWSUM_4$ curve is minimum. The differences are all greater than about 5 dB. Over most of the beam numbers, the differences range from about 15 to 25 dB. The differences increase as the amplitudes of the fluctuations increase. The maxima in the $AWSUM_4$ results correspond to beams for which the amplitudes of the fluctuations are much less than those of the other beams. Such character is indicative of signal or noise that has few interactions with the nonuniform, nonsteady sea surface. The least amount of fluctuations would correspond to a stable tonal traveling along a completely submerged path.

The results in Fig. 4.6a, if verified, show that the $AWSUM_4$ processor significantly enhances the spatial resolving power of the array, is capable of identifying stable tonals from submerged sources, significantly enhances the SNR (>18 dB), and can detect tonals that have SNR too low for the AVGPR processor to detect.

Given a set of data, it is often possible to verify the enhanced performance of a processor by various means. One way is to process the data with a narrower frequency binwidth. Another way, which is more appropriate for this case, is to increase the number of sensors, or in other words, increase the aperture of the array. Fortunately, data for up to 198 hydrophones were available. These data were processed in exactly the same manner as was done to produce Fig. 4.6a, except 100 and 198 hydrophones were used. Figs. 4.6b and 4.6c for 100 and 198 hydrophones, respectively, were produced. Each has the same three different types of curves as discussed earlier.

The average power curves (top curves in Fig. 4.6c) show the presence of a signal at beam number 68. It is barely discernible in the results of the 100-element array in Fig. 4.6b. The $AWSUM_4$ curves in these two plots show maxima at the same beam numbers as they occurred in Fig. 4.6a. In addition, the difference curves clearly show the signal to be from a submerged source (<1.5 dB). This suggests that the minimum in the difference curve of Fig. 4.6a was identifying the signal as being from a submerged source, even though the minimum in the difference was about 5 dB. Such a large difference results from the signal being undetectable in the AVGPR results. Hence, it does not make sense to make the submerged source determination based on the AVGPR. In this case, the smaller amplitude fluctuation of the submerged signal was the essential factor that enabled detection.

Some, but not all, of the enhanced spatial resolution (increased number of local maxima) can be verified by comparison with the corresponding results for increased aperture. The first and most important one is the maximum near beam number 68. It is readily identified in the 198 hydrophone results of Fig. 4.6c, where there is a local maximum of approximately 3 dB. This suggests that in the output of the beamformer and the level of the signal and the noise are approximately equal. In other words, the output SNR is 0 dB. When the number of hydrophones is reduced to 100 (Fig. 4.6b), the output SNR of that signal is approximately –3 dB. The local maximum of the average power, in this case, is about 1 dB. When the number of hydrophones is further reduced to 50, the output SNR must then be approximately –6 dB. Hence, $AWSUM_4$ processing detected a source that was undetectable by the power average processor at –6 dB output SNR and gave a resulting SNR greater than 19 dB. This represents a gain over the conventional summation processor of approximately 25 dB.

It should be noted that the $AWSUM_4$ processor does not produce gain in the usual signal processing sense. Instead, it gives a selective attenuation, c.f., App. A, Figs. A.1.1 and A.1.2. Fortunately, the magnitude of the fluctuations of the noise that is generated near the ocean surface will be greater than the magnitude of the fluctuations of the stable signals that have a small number of interactions or no interaction with the irregular, moving sea surface. Hence, the noise will be attenuated more by $AWSUM_4$ than will the stable signals.

4.7 $AWSUM_k$: Performance for $k = 1$ and $k = 4$ for Sonobuoy Data Using Overlapped Processing

A direct comparison can be made for $AWSUM_k$ processors of different orders by processing data sets at different orders. This has been done for a sequence of sonobuoy data at orders 1 and 4, i.e., $k = 1$ and $k = 4$, at several different percentages of overlapped processing. The results in Fig. 4.7 are for A_{01} processing where the noise suppression has been determined from the average difference between the AVGPR and WISPR processors. Similarly, the results in Fig. 4.8 are for A_{04}, the average difference between the AVGPR and $AWSUM_4$ processing. Comparing the results in these two figures, $AWSUM_4$ processing produced noise suppression at least 3 dB more than the $AWSUM_1$ (WISPR) processing and, depending upon the number of averages and the percentage overlap, this suppression increases to five times that amount. This important result is consistent at all percentages of overlap and number of averages (from 10 to over 1000). An additional observation is that additional noise suppression resulted from the inclusion of a greater number of averages at any particular percentage of overlap as might be anticipated. An understanding of these two figures leads one to realize that if charts of this type are carefully prepared for conditions similar to those that might occur in the field, the expected level of noise suppression can be estimated quantitatively. Using particular combinations of processing parameters, the charts can be used to easily estimate suppression prior to actual tactical employment in the field.

4.8 Summary

(a) A detailed example of how the A_{01} and A_{04} processor plots may be interpreted has been presented. The interpretation technique takes a little mental adjustment from conventional presentations

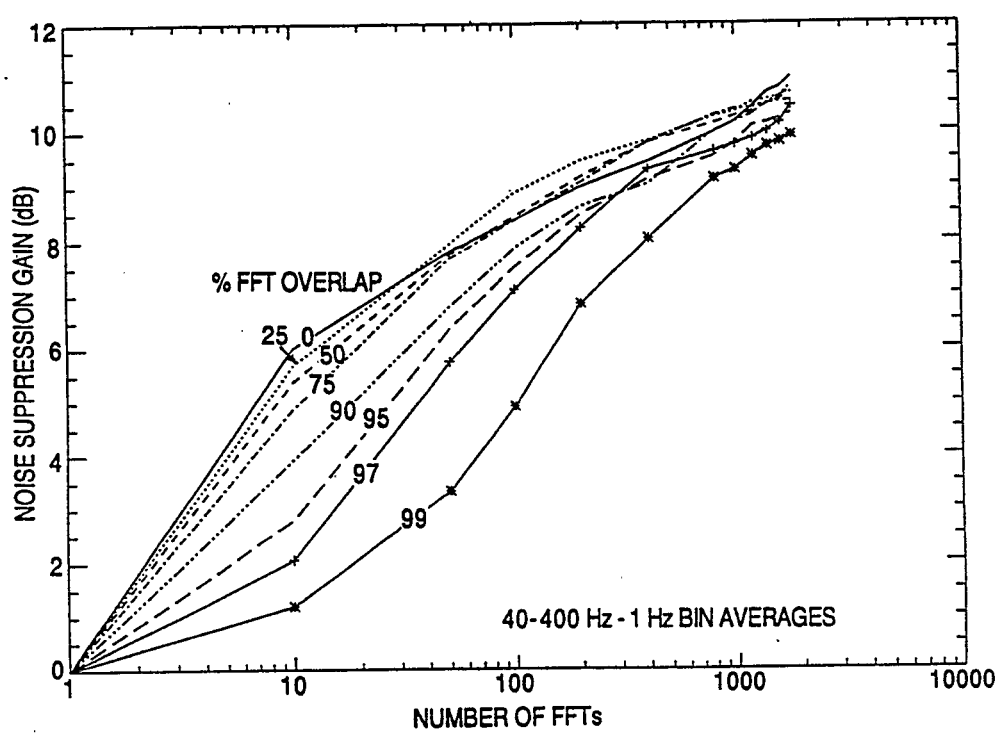

Fig. 4.7 — WISPR (A_{01}) processing of sonobuoy data showing the effects of percentage overlap and the number of temporal data sets averaged (no. of FFTs)

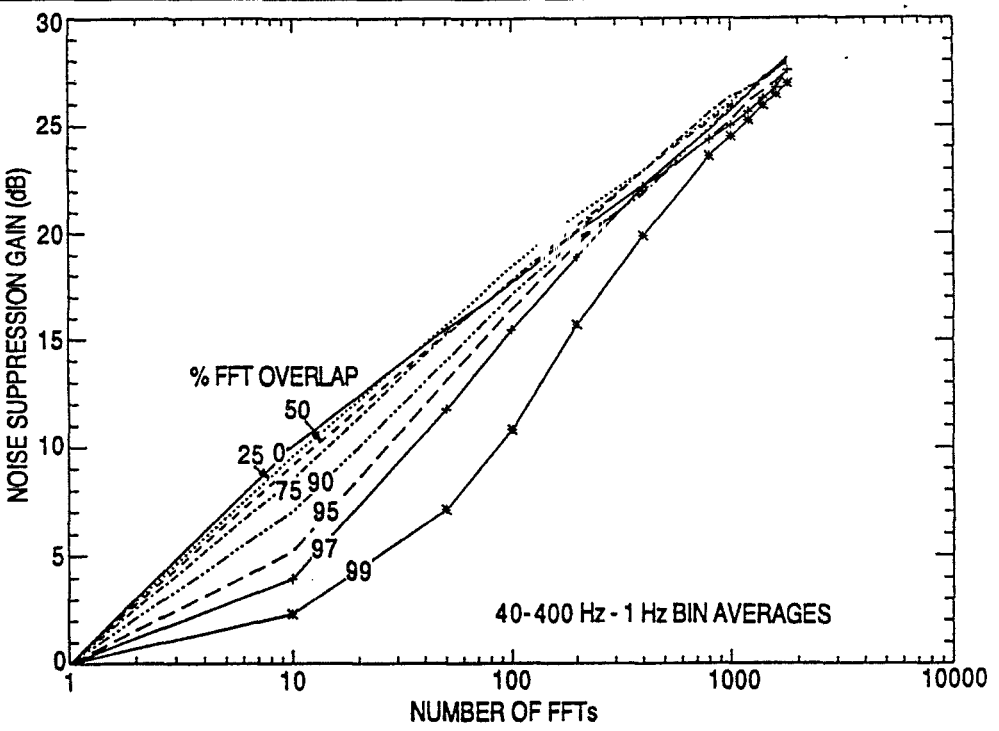

Fig. 4.8 — AWSUM (A_{04}) processing of sonobuoy data showing the effects of percentage overlap and the number of temporal data sets averaged (no. of FFTs)

where the signal is expected to stand out as peaks. However, several advantages of this form of presentation are discussed.

(b) Several examples were provided where it could be determined that the signals of interest had low fluctuation levels relative to the noise. In one case, through a normalization process, the bin magnitude in each bin was equalized, thus removing any signal excess that may have originally existed. SNR gain was then shown to be associated with the difference between fluctuation levels of the LOFAT signals and the combined noise/HIFAT signals.

(c) The higher order A_{04} processor was shown to achieve additional SNR gain over that of the A_{01} processor by 2 to 3 dB. This is achieved through the increased sensitivity of the higher order filters to fluctuations.

(d) To achieve even greater sensitivity, higher orders could be used, eventually at the expense of producing processor instability. In fact, the $AWSUM_k$ order can be increased to absurdity. Order 4 ($k = 4$) appears to achieve a reasonable compromise between fluctuation sensitivity and processor stability for many of the types of data that have been investigated, only a sample of which has been presented here.

(e) The A_{01} and A_{04} processors were also shown to be applicable to nonacoustic data, implying the generality of these processors for fluctuation-based signal processing.

(f) Signals present in the acoustic and nonacoustic examples presented were known to be from submerged sources. Though not the principle point of this section, this provides another confirmation that these processors are effective for the identification of signals from submerged sources.

5.0 ADDITIONAL SNR GAIN FOR THE WISPR AND AWSUM$_4$ FILTERS USING STANDARD DEVIATION OF THE TIME SERIES: THE WISPR II$_k$ AND AWSUM$_4$ II$_k$ FILTERS

5.1 Introduction

Some cases exist that are strategically important to the Navy in which it is highly desirable to increase the signal excess and SNR of LOFAT relative to the background noise and HIFAT. As mentioned in previous sections, an example of that is the detection of a LOFAT signal from a submerged source among HIFAT signal clutter from surface ships and the ambient noise background. The A_{01} and A_{04} processors discussed in Sec. 3.0 were shown to produce significant SNR gain through suppression of HIFAT signals while having little effect on LOFAT signals.

When data exist in the form of a power spectrum time series, an additional statistic that can be used to achieve gain is a modified form of the temporal standard deviation, σ_i, of the time series, a. For the ith spectral bin, where the time series a is in decibels,

$$a = (a_1, a_2, a_3, \ldots a_n), \; a_j \geq 0, \qquad (2.1.2) \text{ (repeated here for convenience)}$$

and

$$\sigma_i = \left[\frac{1}{n-1} \sum_{j=1}^{j=n} (a_j - a_{avg})^2 \right]^{\frac{1}{2}}, \qquad (5.1.1)$$

with $a_{avg} = M_1$ as defined by Eq. 2.1.1 for the ith spectral bin.

There is a distinct advantage of computing the standard deviation of the signal and noise in decibels rather than in power. Fluctuation-based processors achieve gain nearly independent of the signal and noise power levels. Calculation of this modified form of the standard deviation generates values that are indicative of the fluctuation levels, more or less independent of its absolute power level.

The concept utilized to obtain additional gain through use of the standard deviation of the signal time series, although perhaps not particularly obvious, is based upon a rather straightforward extension of fluctuation-based filter concepts. Its rationale is initially presented for the AVGPR processor, then extended in a natural way to the more advanced processors. Examples are presented comparing the WISPR and AWSUM$_4$ Filters to the WISPR II$_k$ processor. Thus far, tests have not been undertaken for the other AWSUM$_4$ II$_k$ processors. However, the rationale presented will demonstrate that they are additional processors that may find useful applications for some types of data.

5.2 Signal Gain Improvement Rationale for the AVGPR Processor

5.2.1 Using the LOFAT and HIFAT Standard Deviations

Observe that LOFAT or HIFAT signals can be associated with certain spectral bins, e.g., let

σ_L = temporal standard deviation that is typical of LOFAT signal bins

and

σ_H = temporal standard deviation that is typical of HIFAT signals and background ambient noise bins.

Using the values commonly observed for these quantities, the decibel difference of the standard deviation of high- and low-level fluctuations that might be anticipated is

$$\sigma_H - \sigma_L \approx 4 \text{ dB}.$$

Extending the concept a little further, for $k > 0$,

$$(\sigma_H - \sigma_L)k \approx 4k \text{ dB} . \tag{5.2.1}$$

Clearly, a significant gain is achieved if either of these results were used to amplify the AVGPR. Note that a choice of k in Eq. 5.2.1, within reasonable limits, implies that the gain can be set to an arbitrary level. Therefore, suppression can be increased (or conversely SNR gain can be improved) by an appropriate choice of k.

5.2.2 Generalization to All Spectral Bins

During signal processing, it is not known, a priori, which are LOFAT or HIFAT bins. Therefore an equivalent method is required. The following procedure exemplifies just such a process:

(a) The LOFAT signal excess Y_L, stipulating that $k > 0$, in LOFAT signal bins is

$$Y_L = AVGPR_L / 10^{\left(\frac{k\sigma_L}{10}\right)}, \tag{5.2.2}$$

(b) and similarly, HIFAT signal excess and/or background noise excess (where σ is approximately the same for these two), Y_H is

$$Y_H = AVGPR_H / 10^{\left(\frac{k\sigma_H}{10}\right)}. \tag{5.2.3}$$

(c) Combining these last two equations yields

$$\frac{Y_L}{Y_H} = \left(\frac{AVGPR_L}{AVGPR_H}\right)\left(10^{\left(\frac{k}{10}(\sigma_H - \sigma_L)\right)}\right). \tag{5.2.4}$$

The last factor in Eq. 5.2.4 utilizes Eq. 5.2.1. Therefore, even though processing is on a bin-by-bin basis, the same gain is realized on the spectrum plots.

(d) Generalizing to the ith spectral bin, the bin statistic's excess, Y_i (whether LOFAT signal, HIFAT signal, or noise), may be expressed for plotting purposes as

$$Y_i = AVGPR_i / 10^{\left(\frac{k\sigma_i}{10}\right)},$$

or on dropping the subscript i, as this is understood to apply to all bin-wise filters,

$$Y \equiv AVGPR / 10^{\left(\frac{k\sigma}{10}\right)}. \tag{5.2.5}$$

(e) Note that when the AVGPR is for a bin having a large standard deviation, Y is suppressed more than for a bin having a small standard deviation. Thus, Eq. 5.2.5 depicts an AVGPR filter that uses the statistic, modified standard deviation, to achieve additional gain through increased relative suppression.

5.3 Signal Gain Improvement for the WISPR Filter: WISPR II_k

The technique just developed for the AVGPR processor, Eq. 5.2.5, can be applied to the WISPR Filter in an analogous manner. Letting WISPR be the WISPR Filter output (a given spectral bin), then $WISPR\ II_k$ becomes

$$WISPR\,II_k \equiv WISPR / 10^{\left(\frac{k\sigma}{10}\right)}. \tag{5.2.6}$$

5.4 Signal Gain Improvement for the $AWSUM_4$ Filter: $AWSUM_4$ II_k

The technique just developed for the AVGPR processor, Eq. 5.2.5, can also be applied generally to higher order processors. As an example of this, for the $AWSUM_4$ Filter in an analogous manner, letting $AWSUM_4$ be the $AWSUM_4$ Filter output for the ith spectral bin, then $AWSUM_4\ II_k$ for that bin is

$$AWSUM_4\,II_k \equiv AWSUM_4 / 10^{\left(\frac{k\sigma}{10}\right)}. \tag{5.2.7}$$

At the present time, evaluation studies have not been conducted with these processors. From the examples that follow for the WISPR II_k processor, by analogy, improvements can be anticipated at least qualitatively. Additional gain would be expected in those situations where $AWSUM_4$ is the appropriate fluctuation discriminator to utilize.

5.5 Gains Achieved for WISPR II_k Processing

The WISPR II Filters are illustrated for data from a sonobuoy, Fig. 5.1, and data from the broadside beam of a vertical line array, Fig. 5.2.

5.5.1 Sonobuoy Data

In the case of the sonobuoy data in Fig. 5.1, there are three plots, each having three curves. The top curve is the spectrum that results from AVGPR processing. The middle curve in the plots from left to right is the spectrum results from WISPR, WISPR II_1, and WISPR II_2. The bottom curve is the difference in decibels between the upper and middle curves.

(a) ***WISPR Filter***

The bottom curve is the A_{01} = (AVGPR – WISPR) processor. The SNR gain of the WISPR processor, compared to AVGPR, is 7.9 dB. The signal at bin 64, clearly visible in all three curves,

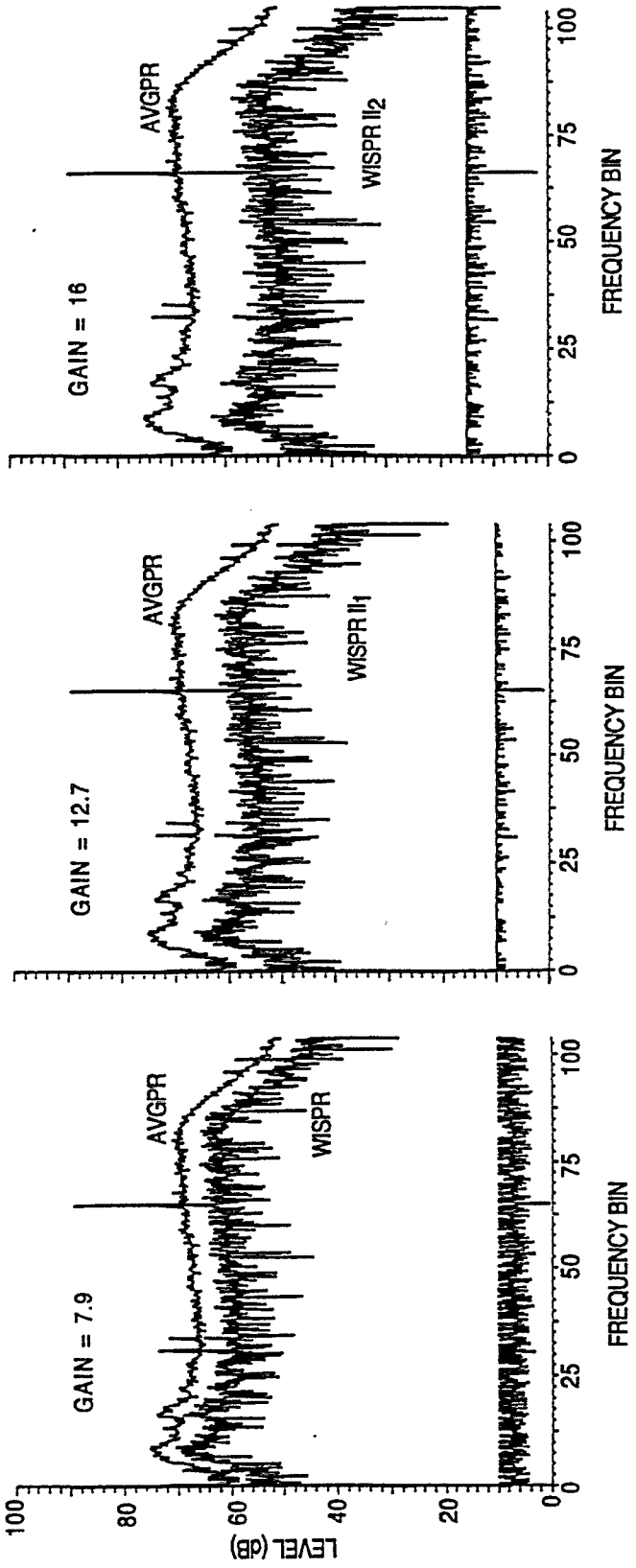

Fig. 5.1 — Fluctuation-based signal processing: SNR and submerged tonal identification for sonobuoy data

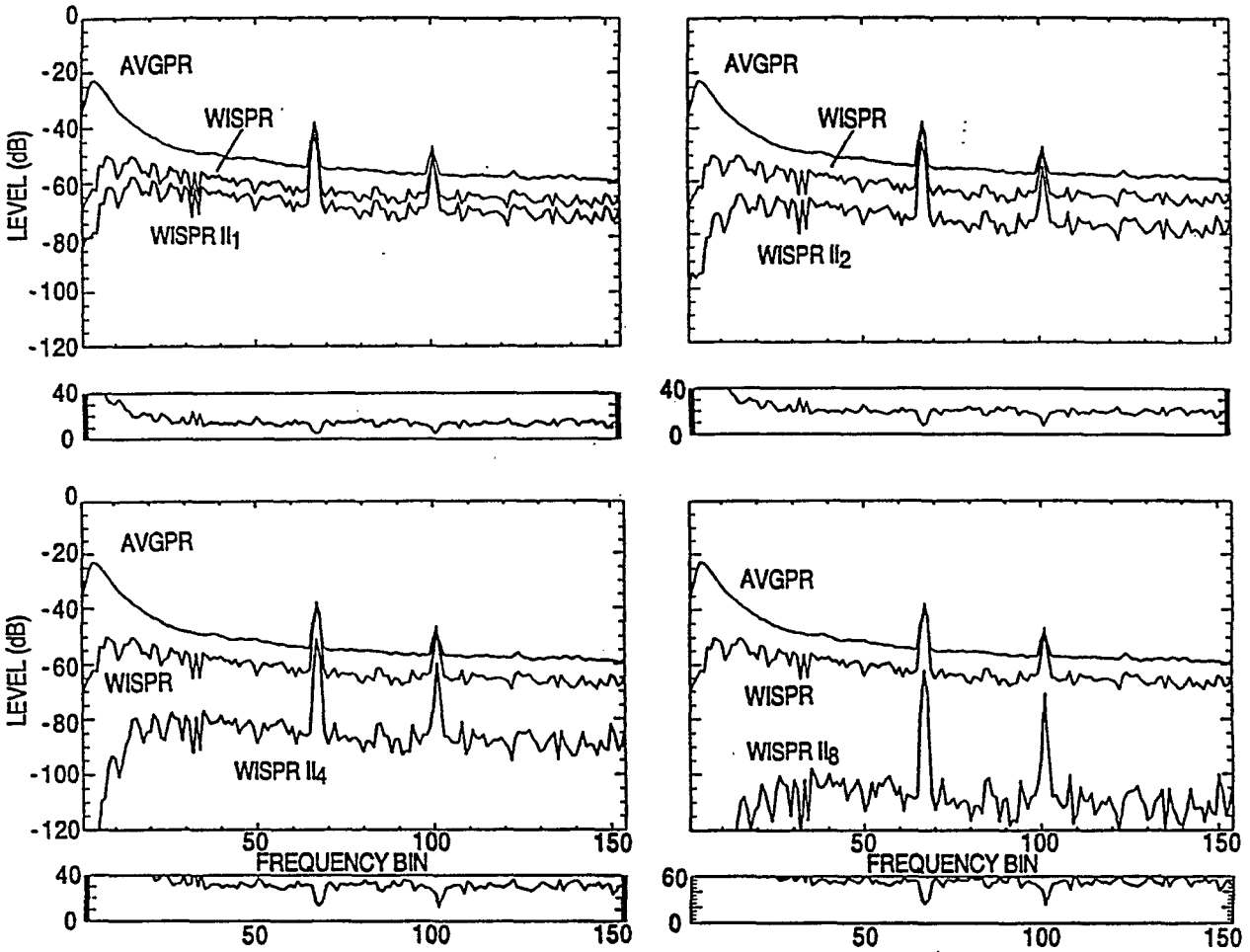

Fig. 5.2 — Fluctuation-based signal processing: SNR and submerged tonal identification for broadside beam of a vertical line array

can be designated a LOFAT signal, as it was not suppressed by the WISPR Filter. It could also be declared that a submerged source has been detected, since the A_{01} curve drops below the empirical 1.5 dB submerged source threshold detection level. Paragraph 4.4 provides a more detailed explanation of the interpretation of this style of plot.

(b) ***WISPR II$_1$***

The noise is suppressed by approximately 14 dB and the signal by about 1 dB, resulting in an added SNR gain of 5 dB over the WISPR Filter. Hence, the total SNR gain of the WISPR II1 Filter is approximately 12 dB more than the AVGPR processor on these data. The bottom curve is the difference (AVGPR – WISPR II_1). Again, the LOFAT signal at bin 64 passes the test for a LOFAT signal that originates from a submerged source.

(c) ***WISPR II$_2$***

Finally, the third plot contains similar results, but for (AVGPR – WISPR II_2). Again, an additional SNR gain of 5 dB has been achieved to make the total about 17 dB. However, the LOFAT signal at bin 64, using the present detection threshold, narrowly misses passing the 1.5-dB threshold

for detection of a submerged source. Perhaps a different threshold would be more appropriate for WISPR II_2.

(d) ***Setting the detection threshold***

Upon initial reflection, it may seem strange that even though greater gain has been achieved, the threshold detection level appears to need increasing as the WISPR II_k order, k, is increased. It is inappropriate to interpret this as a failure of these filters to perform as expected. It can be demonstrated that the detection threshold level should be increased systematically as the order increases to achieve equivalent detection. In fact, with a sensible k-dependent threshold, improved detection can be expected.

Recall that the WISPR and the other fluctuation-based processors discussed thus far identify submerged source signals by their unique property of suppressing fluctuating signals more than stable ones. Therefore, signals that are nearly stable produce mean values that are almost the same for AVGPR and fluctuation-based processors. When the difference is determined, a value near zero is the result. This small difference is what permits setting a detection threshold.

Referring to the previous development of the WISPR II_k Filters:

recall the gain factor, $10^{\left(\frac{k}{10}(\sigma_H - \sigma_L)\right)}$,

and the filter equation, $WISPR\,II_k \equiv WISPR / 10^{\left(\frac{k\sigma}{10}\right)}$.

The gain only becomes apparent when all spectral bins are plotted together (since LOFAT and HIFAT bins are unknown, a priori.) This is an excellent feature for visual data presentation, as a dramatic increase in separation of the top two curves is achieved by the increased gains. Division by $10^{\left(\frac{k\sigma}{10}\right)}$ deflates the plotted value for *WISPR* II_k, which naturally results in the increased difference (bottom curve). Compared to the WISPR plot, the same difference as in the first plot would be achieved if the *WISPR* II_k bin value was multiplied by $10^{\left(\frac{k\sigma}{10}\right)}$. In decibels, this is equivalent to adding $k\sigma$ dB to the final difference that is being compared to the threshold value. Rather than make this somewhat awkward accommodation, a more reasonable approach is to simply add this amount to the detection threshold value; e.g., in this case, the new threshold value would become

New threshold detection value in decibels = $1.5 + k\,\sigma$ dB,

where

σ = the modified standard deviation associated with stable submerged tonals.

5.5.2 Broadside Beam of a Vertical Line Array

In the case of the broadside beam data in Fig. 5.2, there are four main plots, each having three curves with a subplot below it. The top curve is the spectrum that results from AVGPR processing of the beam data. The middle curve is the WISPR Filter results. The third curve in that sequence is the curve that corresponds to the WISPR II_k processing results. The order, k =1, 2, 4, and 8 is indicated at the top of the main plots as NUM = 1, NUM = 2, NUM = 4, or NUM = 8.

In the main plots, the increase in SNR gain is quite obvious as the order is increased, culminating at order, $k = 8$, with noise and HIFAT suppression of approximately 50 dB and with LOFAT signal suppression of approximately 25 dB. The associated SNR gain is approximately 25 dB.

The subplots contain only one curve, the WISPR II_k suppression curve. These curves (e.g., if $k = 4$, AVGPR – WISPR II_4) could be used to indicate detection of submerged sources whenever the appropriate detection thresholds are crossed. As stated in the example in Sec. 5.5.1, in this sequence of plots, it is obvious that it is quite reasonable to use k dependent detection thresholds that increase as k is increases. It is also clear that order $k = 8$ has achieved sufficient gain to produce a clear separation from the AVGPR curve and that little is to be gained by its further increase.

Finally, it could be noted that any order could be utilized that provided sufficient separation from the AVGPR curve to enable reasonable interpretation. These discussions presented a reasonable basis for adapting a successful WISPR detection threshold to the higher order processors. This was done primarily to provide insight as to how these detection thresholds interrelate. In practice, the detection threshold for the processor order chosen should be based on the value found to optimize detection without excess false alarms.

5.6 Removal of Clutter Tonals with WISPR II_4 Processing

Examples have already been provided illustrating the improvements in SNR gain over AVGPR processing that accrue to the WISPR and $AWSUM_4$ processors. Here, an example is shown where the additional gain achieved enables almost complete elimination of clutter tonals. The information plotted in Fig. 5.3 represents 125 consecutive 2048-point temporal FFTs (0.1-Hz binwidth) for each of 256 beams. The AVGPR conventional processor shows a prominent peak near beam number 119. From this curve it is impossible to determine if this represents the signal received from a nearby surface ship, multiple combined high-level tonals due to surface ship clutter, or if there are submerged sources near this beam.

A submerged source tonal is known to be at beam 122, but it is not resolved in the AVGPR results. Even though the effects of the submerged source tonal are evident at beam 122 in the WISPR Filter curve, at this gain level it is difficult to justify the conclusion that either of these peaks represents a submerged source. Proceeding systematically in the order AVGPR, WISPR, $AWSUM_4$, to WISPR II_4, the separation of the two tonals (clutter and submerged source) becomes much more pronounced. Of even greater importance is that as the suppression power of the processor for fluctuating tonals is increasing, the left peak at beam 119 receives more suppression than the peak at beam 122. The strong peak still remaining at beam 122 is strong evidence that a submerged source is in the direction of that beam.

The test for detection is made (previously discussed in Secs. 4.4.3 and 4.4.4) where that curve (bottom of the plot) approaching the zero decibel axis indicates the beam at which the submerged source tonal is found. In this case, it is beam number 122.

5.7 Comparison of WISPR II_4 Performance with WISPR and $AWSUM_4$ for Specific Signals

The frequency domain is where clutter is most easily identified and seems to pose the most challenging problem. It is one thing to reduce the magnitude of the clutter signals, thereby increasing

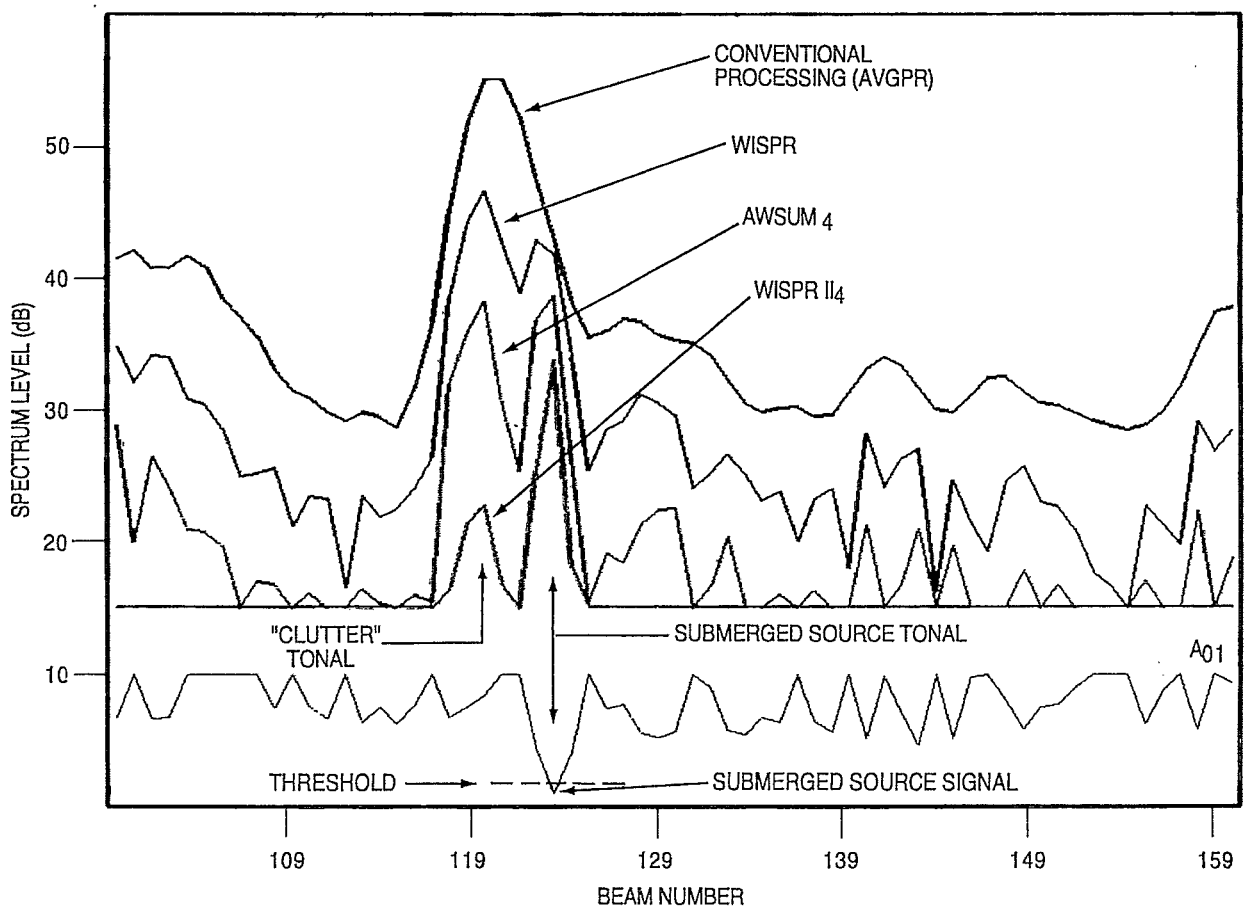

Fig. 5.3 — Fluctuation-based signal processing: SNR gain and submerged tonal identification

the SNR of stable submerged source signals, and it is another thing to eliminate them entirely. The WISPR, AWSUM, and WISPR II_4 filters do both. For example, consider Fig. 5.4 for WISPR, AWSUM, and WISPR II_4 processing. Those results correspond to the spectrum-analyzed beam outputs for a given beam from a long array. Only a small segment in frequency has been plotted for a beam that received signals simultaneously from a submerged source and a surface ship. The top curves are the AVGPR spectrum-analyzed results for a narrow-frequency binwidth, 75% overlap, and 50 averages; about 125 s of data. The middle curves are the corresponding WISPR, $AWSUM_4$, and WISPR II_4 results. The bottom curves are the identifiers of stable signals (normally interpreted as coming from submerged sources) at the frequencies for which the curves are less than 1.5 dB. The first identifier in Fig. 5.4a is the difference between the AVGPR level and the WISPR level, designated the A_{01} processor.

The bottom curve in Fig. 5.4b is the difference between WISPR and $AWSUM_4$, designated the A_{14} processor. It also signifies a stable signal from a submerged source when it is less than 1.5 dB. The bottom curve in Fig. 5.4c, designated A_{0II}, is the difference between AVGPR and WISPR II_4 plus 10 dB. An appropriate submerged source threshold has not yet been determined for A_{0II} processor.

There are two known signals from a submerged source in Fig. 5.4, designated S1 and S2. Some of the more prominent clutter signals have been designated C1, C2, C3, etc. The SNR enhancement

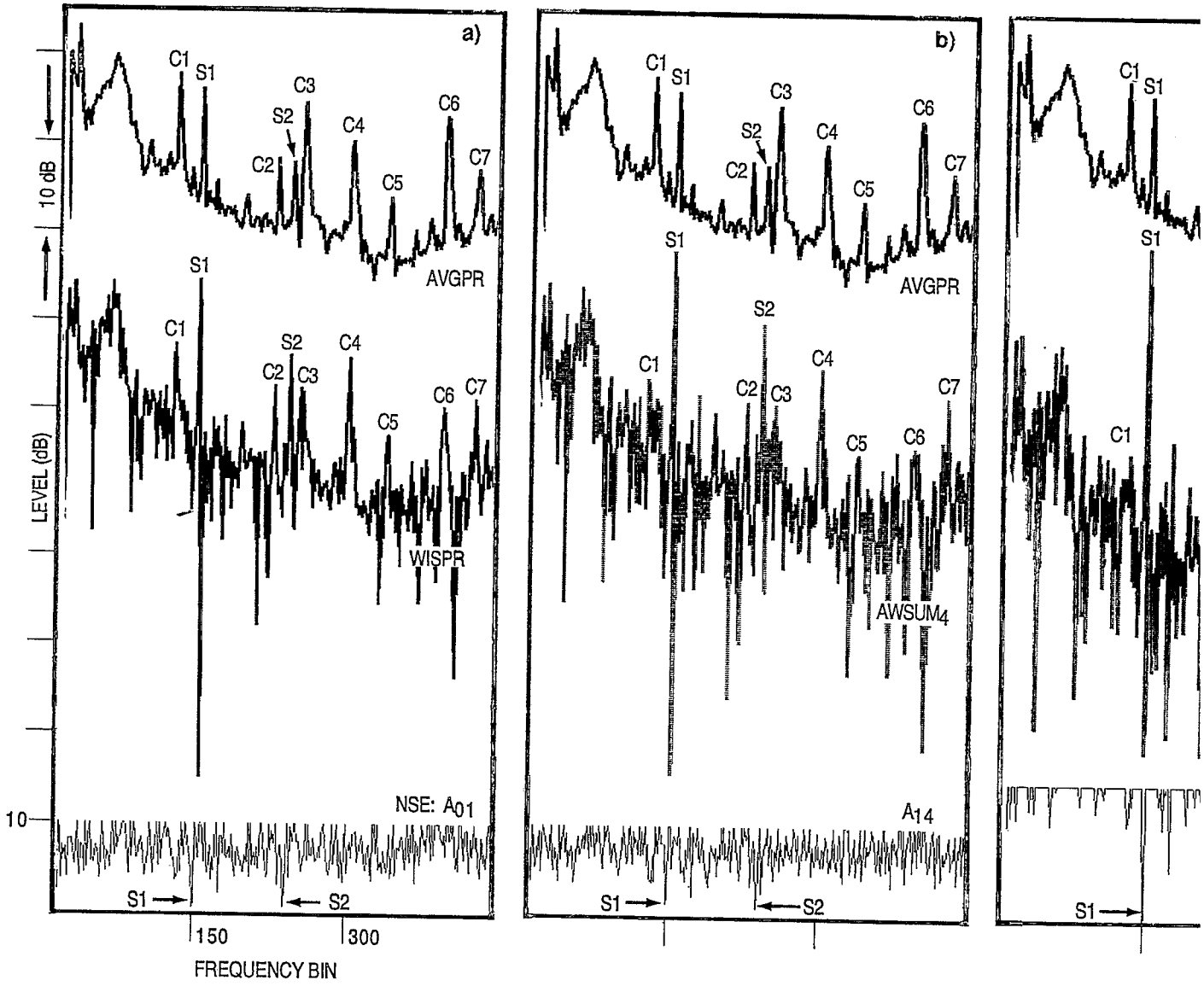

Fig. 5.4 — Fluctuation-based signal processing: clutter (*Ci*) elimination/SNR enhancement/noise spectrum equalization (NSE)/submerg

of the WISPR, $AWSUM_4$, and WISPR II_4 filters are easily seen in Fig. 5.4 by comparing the levels of the clutter signals to the levels of the submerged source signals in each curve. For example, in the AVGPR results, S1 is about 2 dB lower in level than C1, while it is about 8 dB greater in the WISPR results, about 13 dB greater in the $AWSUM_4$ results, and about 26 dB greater in the WISPR II_4 results. That represents an increase or enhancement in the level of S1 relative to C1 of about 10, 15, and 28 dB for WISPR, $AWSUM_4$, and WISPR II_4, respectively. Similarly, for S2 and C3, which have a 6-dB difference in the AVGPR results, S2 is clearly larger in the WISPR, $AWSUM_4$, and WISPR II_4 results, representing an enhancement in SNR of about 11, 15, and 28 dB, respectively. These observations are summarized below.

Filter	SNR Enhancement (dB) S1 Relative to C1	SNR Enhancement (dB) S1 Relative to C6
WISPR	10	10
$AWSUM_4$	15	17
WISPR II_4	28	31

The SNR enhancements for S2 and C3 are 11, 15, and 28 dB for WISPR, $AWSUM_4$, and WISPR II_4, respectively, and for S2 and S6, the corresponding SNR enhancements are 10, 18, and 33 dB, respectively. These observations are summarized below.

Filter	SNR Enhancement (dB) S2 Relative to C3	SNR Enhancement (dB) S3 Relative to C6
WISPR	11	10
$AWSUM_4$	15	18
WISPR II_4	28	33

The bottom curves indicate submerged source signals at frequencies S1 and S2. Both signals are believed to be from a submerged source that was participating in the measurement exercise at a range of about 300 km from the receivers. The complete absence of the clutter signals in the A_{01}, A_{14}, and the A_{0II} curves is rather remarkable. Such behavior of detecting stable submerged source signals and eliminating clutter is worthy of consideration for use as an automatic detection device. An obvious application would be in autonomous detection systems.

The reason for utilizing a detector like A_{14} instead of A_{01} is to enhance the low SNR operation and to increase robustness against high-level transients and some forms of impulsive system or environmental noise degradation.

5.8 Summary

It has been shown that the temporal standard deviation of the time sequence, a direct measure of signal fluctuation level, can be utilized in conjunction with other fluctuation-based filters to achieve additional gain. When the results are displayed visually, this additional gain is directly observable, thus aiding analysis and interpretation. A reasonable technique was developed for adjusting the detection level associated with these processors as the order k is increased. Additional gains possible with the WISPR II_4 processor were demonstrated to be at least 25 dB.

6.0 TYPICAL WISPR FILTER APPLICATIONS

6.1 Introduction

The general properties of the WISPR Filter and related filters have already been introduced in previous sections. Here, a number of applications using real acoustic data to demonstrate their versatility and robustness will be presented. A few of those applications are: the ability to achieve SNR gain even in adverse environments containing harsh transients as occurs near Arctic ice packs; enhanced resolution of peaks that have been masked by fluctuating noise; tolerance to loss of carrier and signal breakup during transmission, as often occurs with sonobuoy data; reduction of masking by off-axis noise; emulation of increased array aperture; and enhancement of spectral resolution.

6.2 Robustness to Harsh Transients and Intermittent High-Level Noise

6.2.1 Detecting Tonals in an Arctic Environment Containing Many High-Level Transients

Figure 6.1 illustrates SNR gain improvements for the WISPR Filter in an adverse ambient noise environment. The data are from the broadside beam of an array that was suspended from an ice cover in the Arctic. The data were acquired during a time when the background ambient noise contained many transient events that caused the standard deviation to range from about 8 to 10 dB. By comparison, the standard deviation for typical deep-water ambient noise, when it is dominated by deep-water shipping, is usually about 6 dB.

Each plot in Fig. 6.1 contains two curves. The top curves correspond to the AVGPR levels in each spectral bin from more than 100 consecutive FFTs. Similarly, the bottom curves correspond to the WISPR Filter output. The binwidths are given in the upper right corners of the plots. The binwidth is 0.6 Hz for the plot in the upper left corner. The binwidth increases by a factor of two for each additional plot, i.e., 1.2 Hz in the upper right corner plot, 2.4 Hz in the lower left corner plot, and 4.8 Hz in the lower right corner plot. The local maxima at 43, 65, and 80 Hz identify tonals from a projector under the ice that was at a range of approximately 40 mi.

In the upper left plot, the local maxima for AVGPR are about 5 dB above the noise background. On the other hand, the SNR of the corresponding local maxima range from 15 to 20 dB above noise background using WISPR processing. This represents a 10 to 15 dB gain over the 5 dB observable for the AVGPR processor.

Reasoning similar to that above can be used to determine the net SNR for the other three plots in Fig. 6.1. By doing that, SNR gains due to WISPR processing of 14 dB are obtained for the upper right plot, 13 to 15 dB for the lower left plot, and 5 to 16 dB for the lower right plot. Such results are well in excess of what would be expected for stable tonals in normal ambient noise. Approximately 7 to 9 dB of SNR gain would be normal. However, in this case, where the source is under an ice cover, the SNR gain is coming mostly from the noise suppression. The noise suppression is more than would be the case for normal ambient noise because of the impulsive nature of the ice noise. On the other hand, the rough undersurface of the ice causes fluctuations in the received signal from a moving projector that to some extent reduces the WISPR Filter output. In this case, the tonals have been suppressed by as little as 3 dB (80 Hz in the upper left plot) and as much as 10 dB (43 Hz in the lower right plot). The suppression of a stable tonal in ice-free water is normally less than 1.5 dB. Even though this excess signal suppression due to the rough underice surface lessens the total amount of SNR gain that can be achieved in a noise environment that has high-level transient ice noise events, the gain improvement under these conditions should still allow more robust target identification.

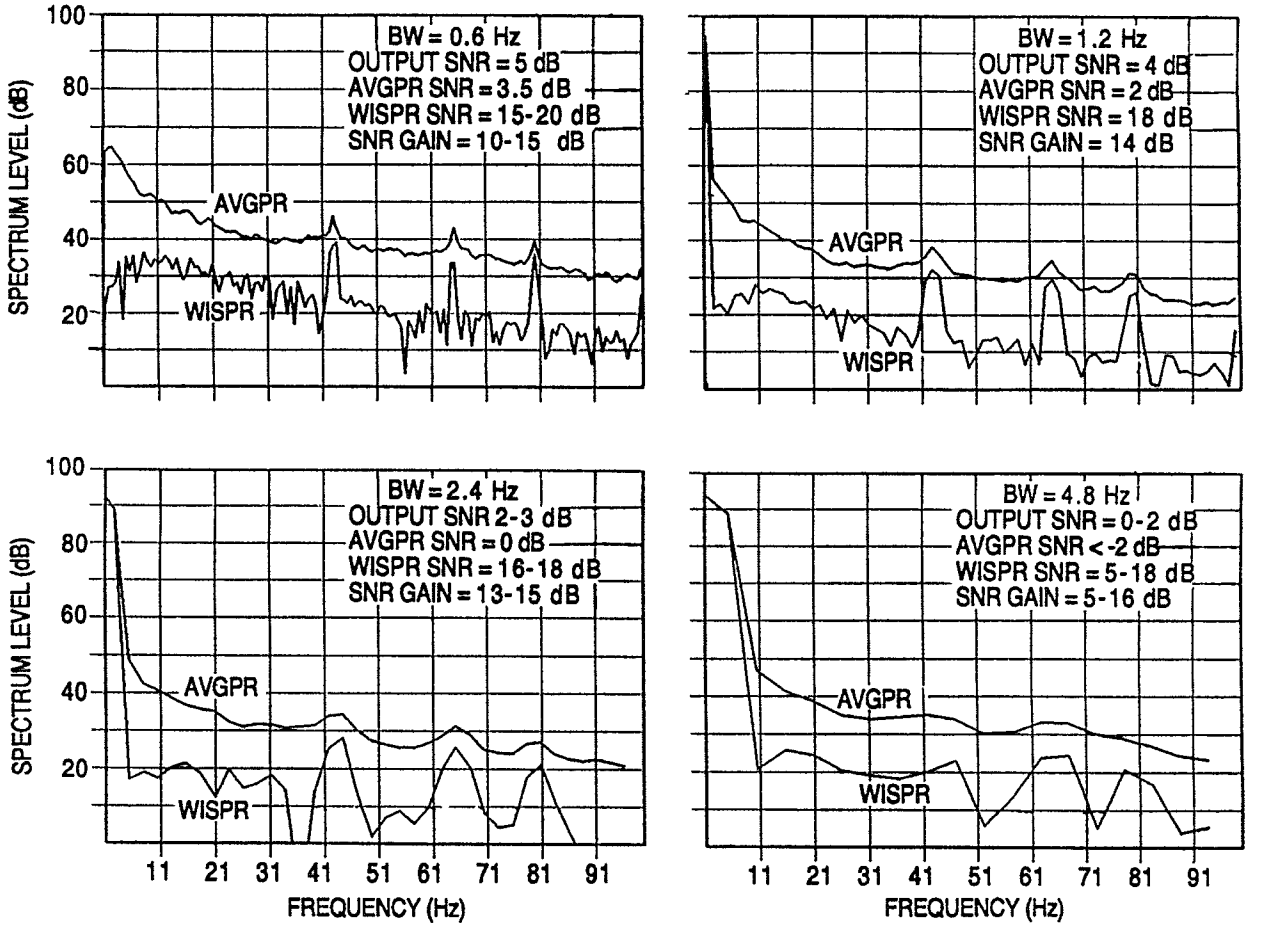

Fig. 6.1 — WISPR processing: SNR gain for low SNR signals versus BW (Arctic data)

6.2.2 Improving Spatial Resolution in the Presence of Seismic Prospecting

The WISPR processor is robust to masking that results from high-level transients, such as the periodic explosions due to seismic prospecting and the frequent loss of the sonobuoy carrier signal, which results in high-level transient noises in the sonobuoy electronics. Figure 6.2 gives an example of results for seismic prospecting. The ordinate is spectrum level in decibels, and the abscissa is the beam number. The plotted data are beamformed output from a towed horizontal line array in about 250 m of water. The top curve, labeled conventional output, was obtained by power averaging (AVGPR) consecutive spectral samples in a given frequency bin during a time period when explosions from seismic exploration were being received every 10 s. The two peaks in the curve are believed to be ambient related, but are contaminated to some degree by the explosions. It is uncertain how much of the remainder of the spatial spectrum is due to the ambient and how much is the effect of the contamination. The bottom curve is the WISPR output for the same data that produced the top curve. The WISPR result shows a spatial structure that is indicative of the ambient noise environment and has magnitudes that are considered to be contamination-free ambient noise at the measurement location. In these more correct results, the WISPR Filter suppression of the masking effects ranges from 14 to 30 dB.

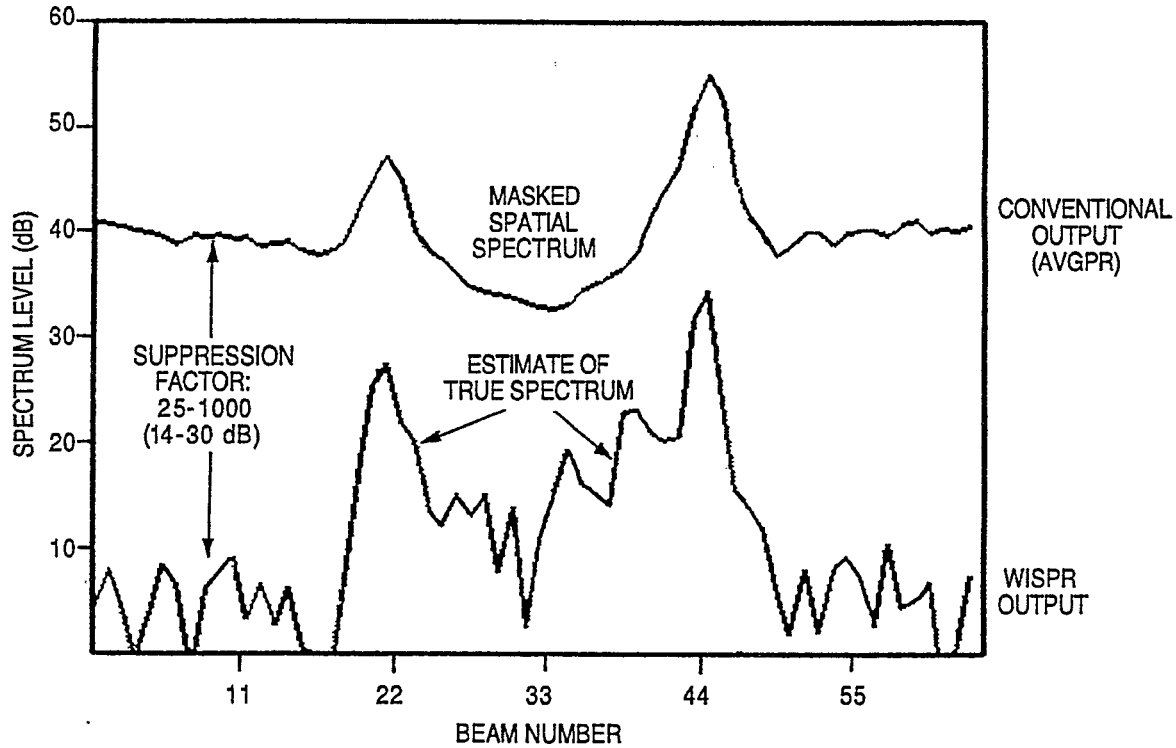

Fig. 6.2 — WISPR robustness to geophysical prospecting (periodic explosions) in shallow water

6.2.3 Identifying a Tonal in the Presence of Masking by Interference from Sonobuoy Electronic Noise

Figure 6.3 illustrates a similar situation as in Fig. 6.2 except the sensor is a sonobuoy. The masking is due to electronic noise when the signal from the sonobuoy is lost. As in the previous case, the top curve is for conventional processing (AVGPR), and the one immediately beneath it is the $AWSUM_4$ output. The difference between the top two curves, what would be A_{04} processing, is about 20 dB. This represents a reduction in masking of about 12 dB over most of the frequency range. The tonal at location B is evidence that the masking was indeed suppressed. In fact, near the frequency of the tonal, the suppression was approximately 50 dB, which left the tonal exposed with a SNR of 30 dB. However, the A_{04} processor result (not shown) would have been too contaminated by the transients for the difference at tonal location B to approach zero, the characteristic of a viable detector. In fact, at tonal location B, the A_{04} processor result would have been about 23 dB.

The versatility of the A_{jk} processors (Eq. 2.5.5) can be illustrated with these data. The bottom curve is five times the difference between $AWSUM_2$ (curve not shown) and $AWSUM_4$ or 5 (A_{24} processor). Clearly, the tonal at location B approaches zero, which would enable a reasonable submerged source detection threshold to be set for this data set masked by sonobuoy electronic noise.

6.2.4 Identifying a Submerged Source Beam at Low SNR in the Presence of High-Level, Off-Axis Masking

Figure 6.4 illustrates the identification of a submerged source when the SNR is low in the presence of off-axis masking. The top curve is the AVGPR result, the middle curve is the WISPR

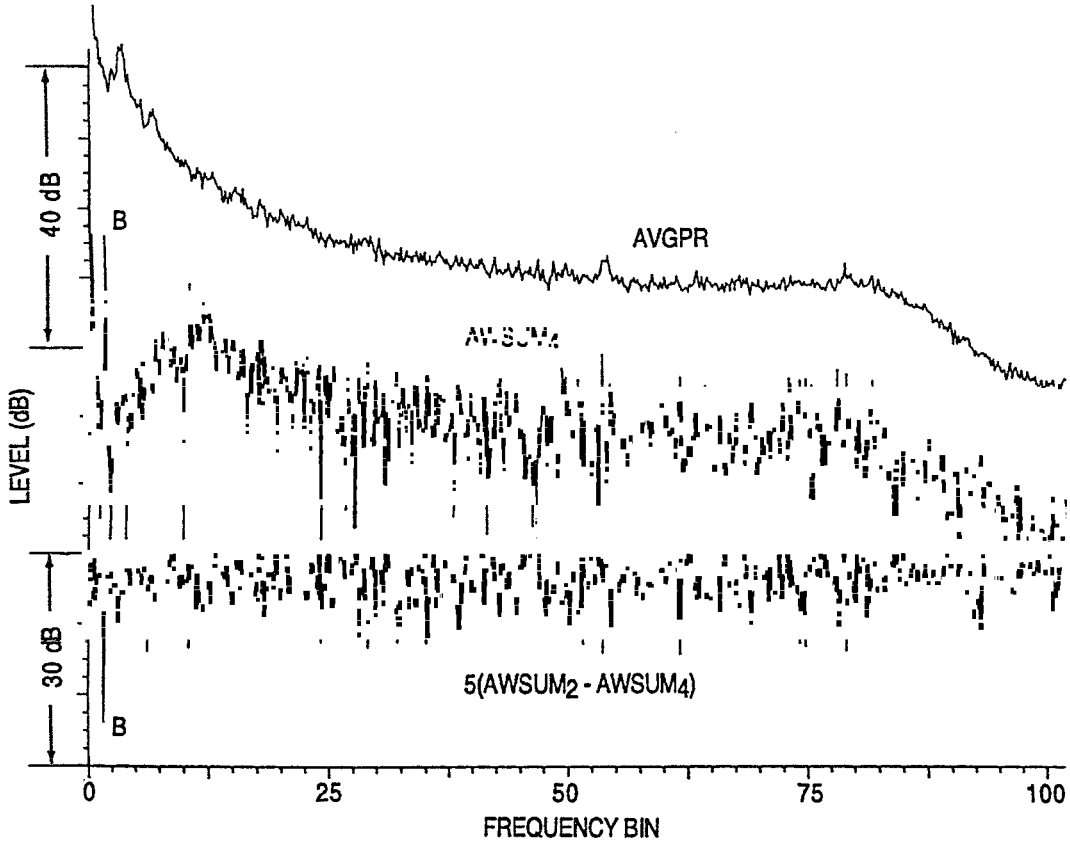

Fig. 6.3 — Noise suppression using higher order AWSUM processors

result, and the bottom curve is the A_{01} processor result in decibels (noise suppression). In this example, a signal could be easily verified at beam 21 by the beam response pattern at a frequency different from the one shown (40 Hz) where little masking was present. At 40 Hz, the signal is masked by the high-level, off-axis noise of source/sources on approximately beam 28. WISPR processing indicates a signal near beam 21, since the A_{01} noise suppression curve is nearly zero there.

The AVGPR curve shows no peak at beam 21. In this case, the signal location could be easily identified at other frequencies, but this is not always possible. The advantage of being able to even partially eliminate the masking by off-axis tonals should find useful applications.

6.3 Improvement in Spatial Resolution - A Substitute for Increased Array Aperture

6.3.1 Aperture Enhancement with the WISPR Filter

In addition to identifying a submerged source signal, as just demonstrated in Sec. 6.2.4, Fig. 6.4 illustrates the spatial resolution enhancement characteristics of WISPR. The top curve is the conventional processing (AVGPR) results for a horizontal line array of approximately 36 wavelengths. The middle curve corresponds to the WISPR results for the same data. The increased resolution of the WISPR results compared to the conventional results is rather dramatic. The amount of detail that is resolved by WISPR processing suggests that the effective aperture after processing is considerably greater than what one would expect for that aperture. The aperture magnification appears to be greater than a factor of 3, i.e., 3×.

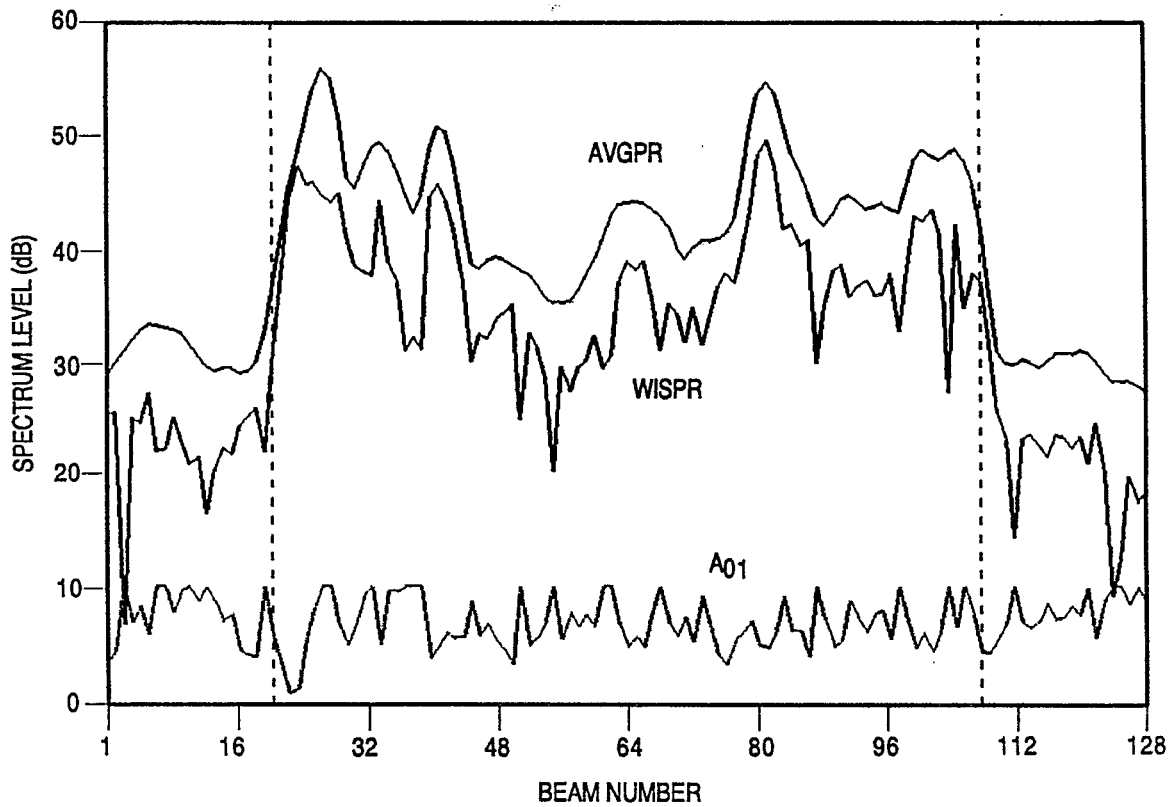

Fig. 6.4 — Identification of a submerged source in the presence of high-level, off-axis masking

Other tests conducted by successively increasing or decreasing the aperture and comparison of the AVGPR and WISPR beam responses indicates that the improved spatial resolution of WISPR is real and not a processing artifact.

6.3.2 A Calibrated Examination of Spatial Resolution Enhancement by the WISPR Filter

The sketch, Fig. 6.5, summarizes the method utilized in acquiring and processing of beamformed data from the NATIVE-1 towed line array data as the aperture of this horizontal line array is successively changed by increasing the number of sensors used from 14 by factors of 2 to 108 sensors. The frequency is 9 Hz, the binwidth is 0.6 Hz, and the number of averages is 30. The increase in resolution obtained as the array aperture is increased (obvious in the sketch) is as expected based on experience and theory.

The original plots from which the sketch in Fig. 6.5 was prepared are shown in Fig. 6.6 where the DI, actual number of sensors, N, and the wavelength, λ, are shown. The abscissa is beam number from 1 to 128. The ordinate on each plot is a relative decibel level that can be made absolute by adding the decibel amount indicated at the lower left of each plot (add: X). The acoustic beams steered into real space are those between the two vertical dashed lines on each plot; those outside that region are nonacoustic or virtual beams. During the acquisition of these data, there was a submerged source along the bearing of beam number 62. It is identifiable only in the lower right plot, wherein the aperture and the spatial resolution are the greatest. Even at this large aperture, from the AVGPR plot, one would expect to find more prominent sources at the bearings indicated by beam numbers 55 and 70.

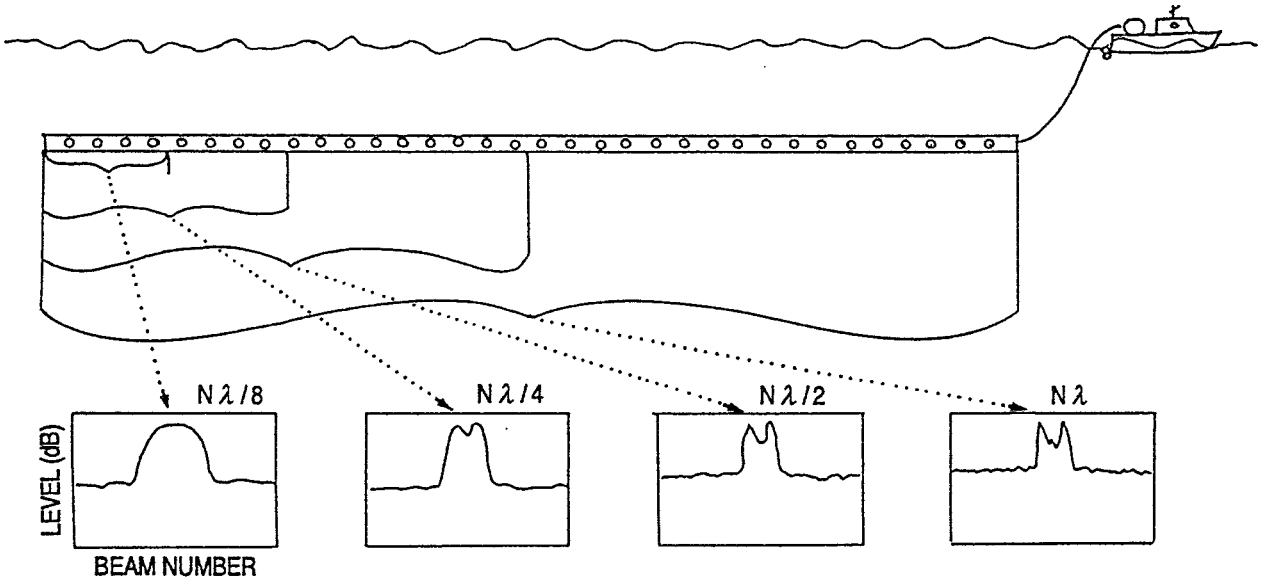

Fig. 6.5 — Spatial resolution versus aperture

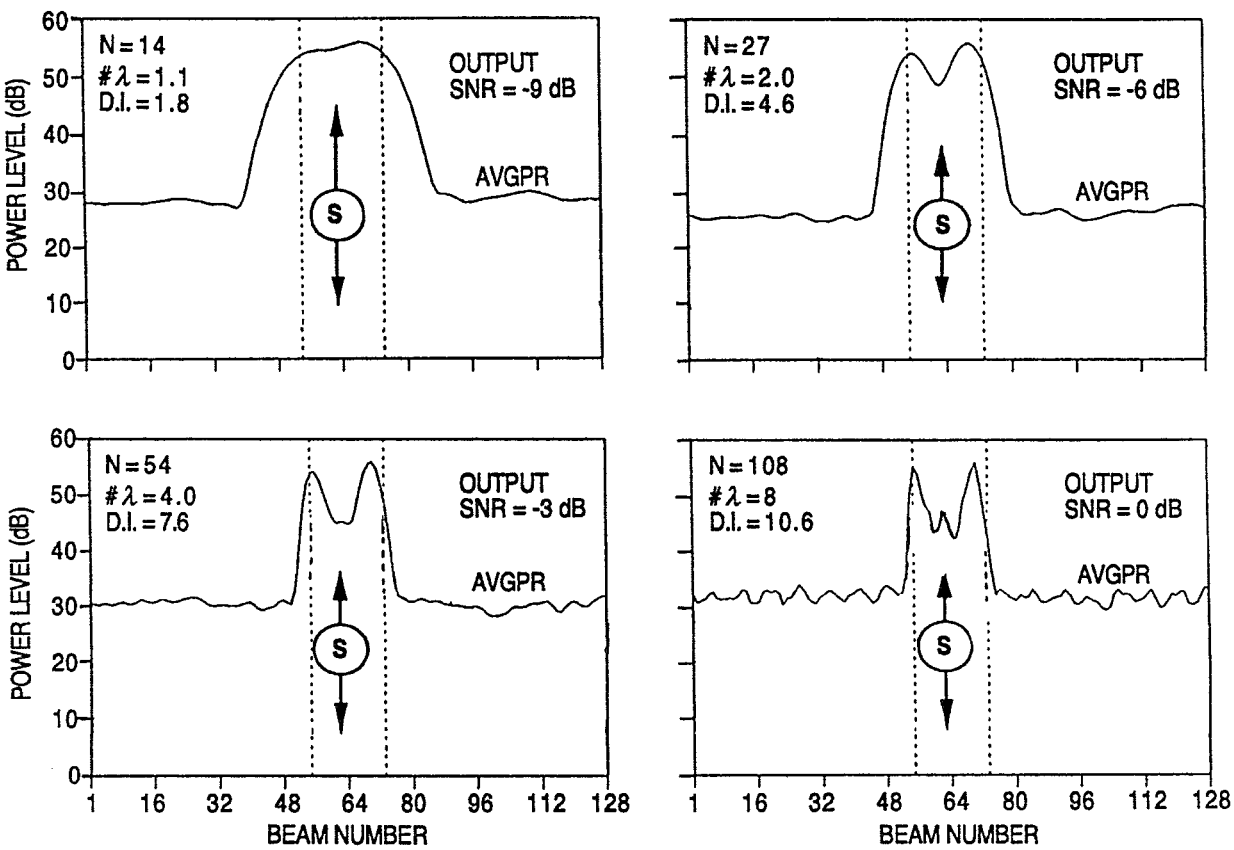

Fig. 6.6 — Spatial resolution versus aperture for power averaging at 9 Hz, 512-point FFT (BW = 0.6 Hz), the source data presented in Fig. 6.5, S = signal (N, #λ, and DI are the number of hydrophones, number of acoustic wavelengths, and the directivity index, respectively)

In Fig. 6.7, the WISPR performance is plotted just below that of the AVGPR processor curve in all four plots. The source along the bearing of beam number 62 shows up as a local peak or maximum of approximately 3 or 4 dB in the AVGPR results. The WISPR results show the source to have about the same level, an indication that it is a submerged source. The relative maxima at beams 55 and 70 are significantly reduced, an indication that their signals contain significant fluctuations and are probably from either surface or transient sources. An additional gain of about 7 to 8 dB over the AVGPR results was achieved.

When the aperture/number of hydrophones is reduced in half ($N = 54$), a local peak corresponding to the known source is no longer evident in the AVGPR results, while it is clearly evident in the WISPR results. The local peak is from 2 to 6 dB. With two more successive factors of 2 reduction in aperture/sensors ($N = 27$ and $N = 14$), the source is also not visible in the AVGPR results, but is visible in the WISPR results. The peak is about 4 to 6 dB for the 27-element aperture and about 1 to 2 dB for the 14-element aperture. In all cases, the signal is discernable in the WISPR results, but it is discernable only for the conventional processor results for the largest aperture ($N = 108$ and SNR = 0). The theoretical difference in the SNR gain for the three factors of 2 would be 10 log 8, or 9 dB. If the SNR of the signal-to-noise beam is 3 dB for the maximum aperture, there must be as much noise as signal or 0 dB SNR, and it must be about –9 dB SNR for the smallest aperture, –6 dB SNR for the next largest, and –3 SNR dB for the second-largest.

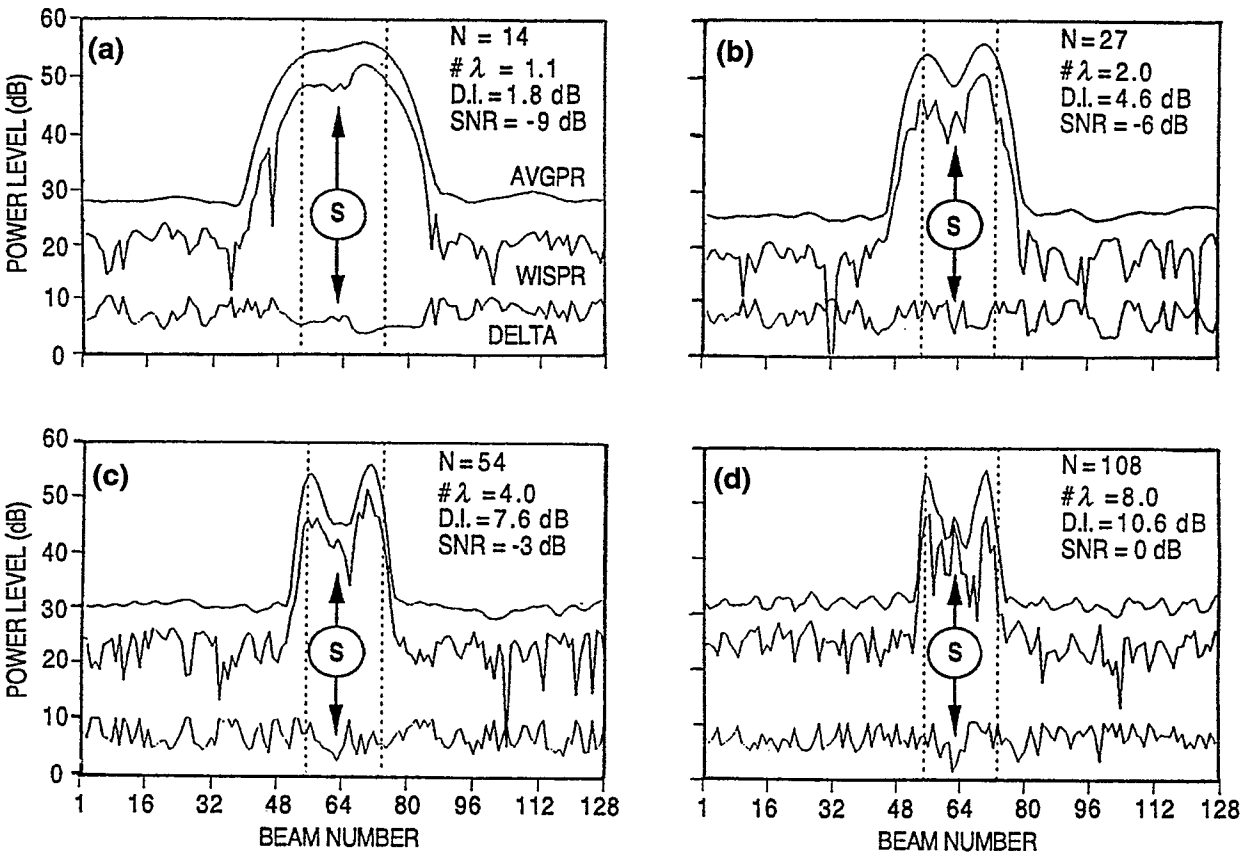

Fig. 6.7 — Spatial resolution versus aperture for power averaging (top) and WISPR processing (middle) at 9 Hz, 512-point FFT (BW = 0.6 Hz)

The bottom curve in Fig. 6.7 gives the average SNR gain of WISPR, about 7 dB in each case, and also indicates whether the WISPR processor can identify the source as being submerged. It does so only in the largest aperture case, where the SNR is about 0 dB. In the other cases where the SNR is equal to –3, –6, and –9 dB, it does not identify them as being submerged. However, it almost does for the –3 dB SNR case. An environmentally and processor-sensitive improved submerged source threshold could be devised for low SNR signals to designate submerged source signals as coming from submerged sources. That is a possibility for future research.

6.4 Spectral/Spatial Resolution Enhancement and Compensation for Array Misalignments and Instabilities

In the previous section, it was shown that WISPR processing achieved improvements in spatial resolution analogous to that achieved by increased array aperture. In that case, the comparison was rather straightforward, as data sets were of equal time. It may appear upon initial reflection that also claiming an additional increase in spectral resolution and SNR gain is an overstatement of the WISPR Filter properties. Clearly, separating these aspects of its performance quantitatively is difficult. However, it is believed that the following examples will show that each of these improvements is possible and that these benefits occur together.

6.4.1 Spectral Resolution Improvements for Nonoverlapped Processing

Section 6.3 was devoted exclusively to improvements in spatial resolution that can be achieved by WISPR processing. It was shown that for signals of low-fluctuation amplitude, the resolution that could be achieved is analogous to an increase of the array aperture. Here, the effect of reduced binwidth (BW) in the frequency domain is contrasted to WISPR processing. Figure 6.8 illustrates the resolution enhancement of WISPR compared to conventional processing for four different BWs. Sixty consecutive data segments were processed to obtain the results shown in these plots. The BW decreases by factors of 2 from 2.4 Hz in plot (a) to 0.3 Hz in plot (d). It is known that there is a signal source in the direction of beam 64.

The top curve in each plot is beam response versus beam number from FFT beamforming using the AVGPR summation. The presence of a source at beam 64 becomes progressively more obvious as the BW is decreased. Knowing that this is the signal location, the SNR determined from the AVGPR curve increases by 3 dB each time BW is halved; from –6 dB in the first plot to 3 dB in the last plot. For example, in the case of plot (c), the local maximum at the known signal location is approximately 3 dB. This indicates that the signal is about the same magnitude as the noise (SNR $\approx$ 0 dB). To place the preceding remarks in perspective, consider for the moment a narrow-band tonal. A familiar feature of an FFT is that most of the tonal's power will be determined to be in the spectral bin whose upper edge is nearest to the tonal frequency; thus, the result is almost unaffected by the BW. On the other hand, the noise power in each spectral bin of noise distributed across the spectrum is proportional to the BW. Thus, when processing statistically independent realizations, each reduction in the BW by a factor of 2 would give a SNR gain of approximately 3 dB and improve spectral resolution as was just noted for the example presented.

The lower curve in each plot is the corresponding WISPR result. Comparing the WISPR result with the AVGPR result in plot (c) in the vicinity marked "A," the peak magnitudes are both about 10 dB above the local minima. Therefore, the WISPR Filter has had about the same effect on gain as a reduction of the BW by a factor of 2. Furthermore, the signal has been better localized in

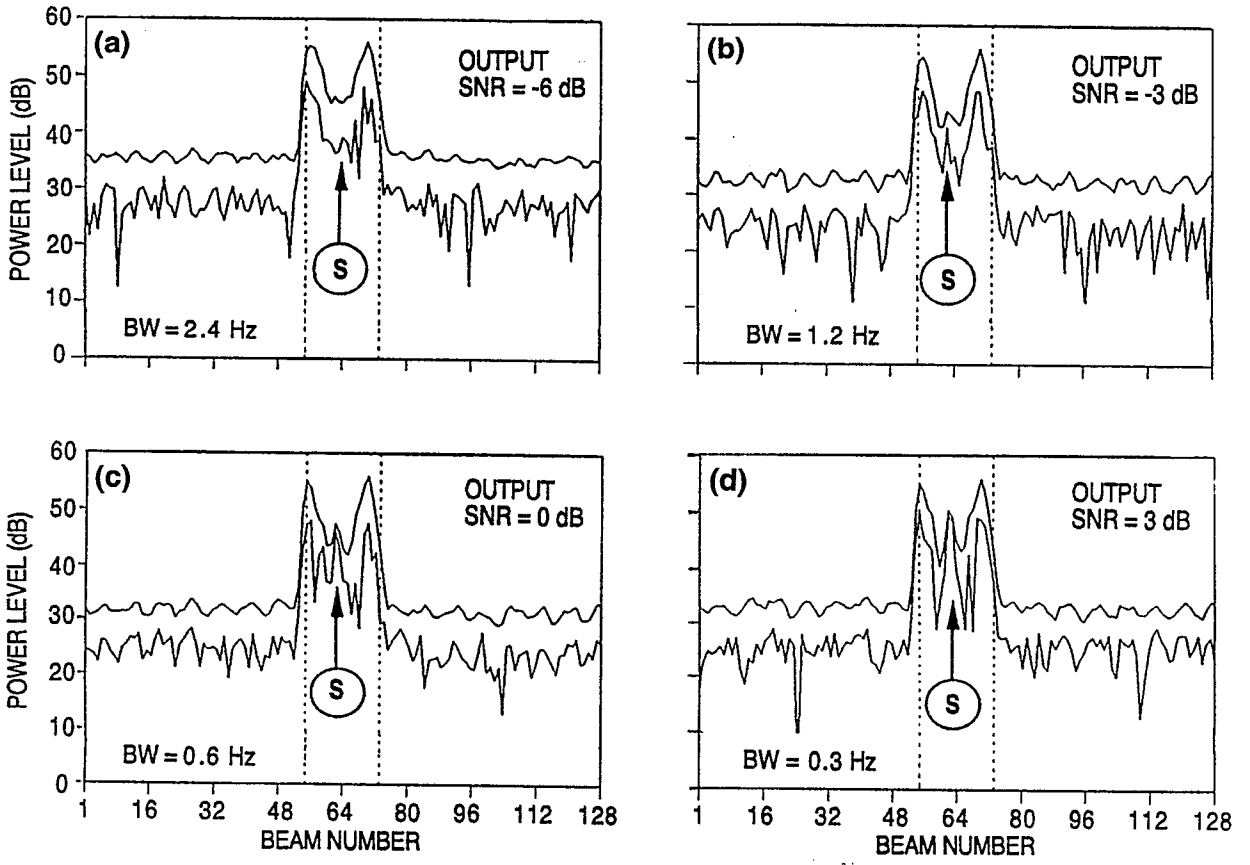

Fig. 6.8 — Spatial resolution versus bandwidth (BW) for power averaging (top) and WISPR processing (bottom). S = signal that is "unmasked" by improved spectral resolution.

azimuth space or beam number at the same time. This is consistent with the enhancement of spatial resolving power observed for the examples presented in the previous section.

In plot (d), where the BW is decreased by a factor of 2 to 0.3 Hz, and the SNR = 3 dB for the conventional results, the local maximum is about 6 dB and 20 dB for the conventional and WISPR results, respectively. As the BW decreases from plot (d) (BW = 0.3 Hz) to plot (a) (BW = 2.4 Hz), the spatial resolution capability of the conventional processing degrades rapidly. There are three identifiable local maxima evident in all of the conventional results. Additional peaks are resolved in the WISPR results in that four to six local maxima are visible in the same region. Furthermore, the sources have been localized better in azimuth (beam number) with a considerable enhancement in spatial (beam number) resolution. From these data, the improvement in spatial resolution resulting from the WISPR processing seems to exceed the conventional results versus BW by more than a factor of eight (8×). That is to say that the spatial resolution in real beam space (i.e., the beam space between the vertical dotted lines) of the WISPR results for a BW of 2.4 Hz exceeds the spatial resolution of the conventional results for 0.3 Hz. Similarly, the WISPR 0.3-Hz BW results might be expected to exceed the conventional results for a considerably narrower BW (say 0.04 Hz). This represents a capability for improved spatial/spectral resolution equivalent to that obtained with the greater FFT lengths. Thus, the longer times required to achieve the number of averages required otherwise can at least be partially avoided.

6.4.2 WISPR and AWSUM Gain and Spectral Resolution Improvements for Time Domain Overlapped Processing

The data cited in this section, the results in Figs. 6.9 and 6.10, are from sonobuoy data. They have been averaged over 361 consecutive frequency bins (40 to 400) to improve the confidence of the results.

Making a case for improvement in spectral resolution and gain over that shown in Sec. 6.4.1 is a little more complex. Since the time available for data acquisition (target position stability, source stability, etc.) is limited, the data set is of finite length. Since the number of statistically independent realizations available for processing is inversely proportional to the FFT length chosen which affects the FFT BW, optimal data utilization implies that tradeoffs are required. For example, when too few realizations are available, even estimates of the standard deviation become unreliable. WISPR and AWSUM processing provides a natural means for utilization of the BW gain and spectral resolution that can be achieved through overlapped processing (which produces narrower BWs), while at the same time enabling the identification of stable, submerged sources. The straight line in Figs. 6.9 and 6.10 represent this idealized BW gain. The rationale for this is discussed in paragraph two of Sec. 6.4.1.

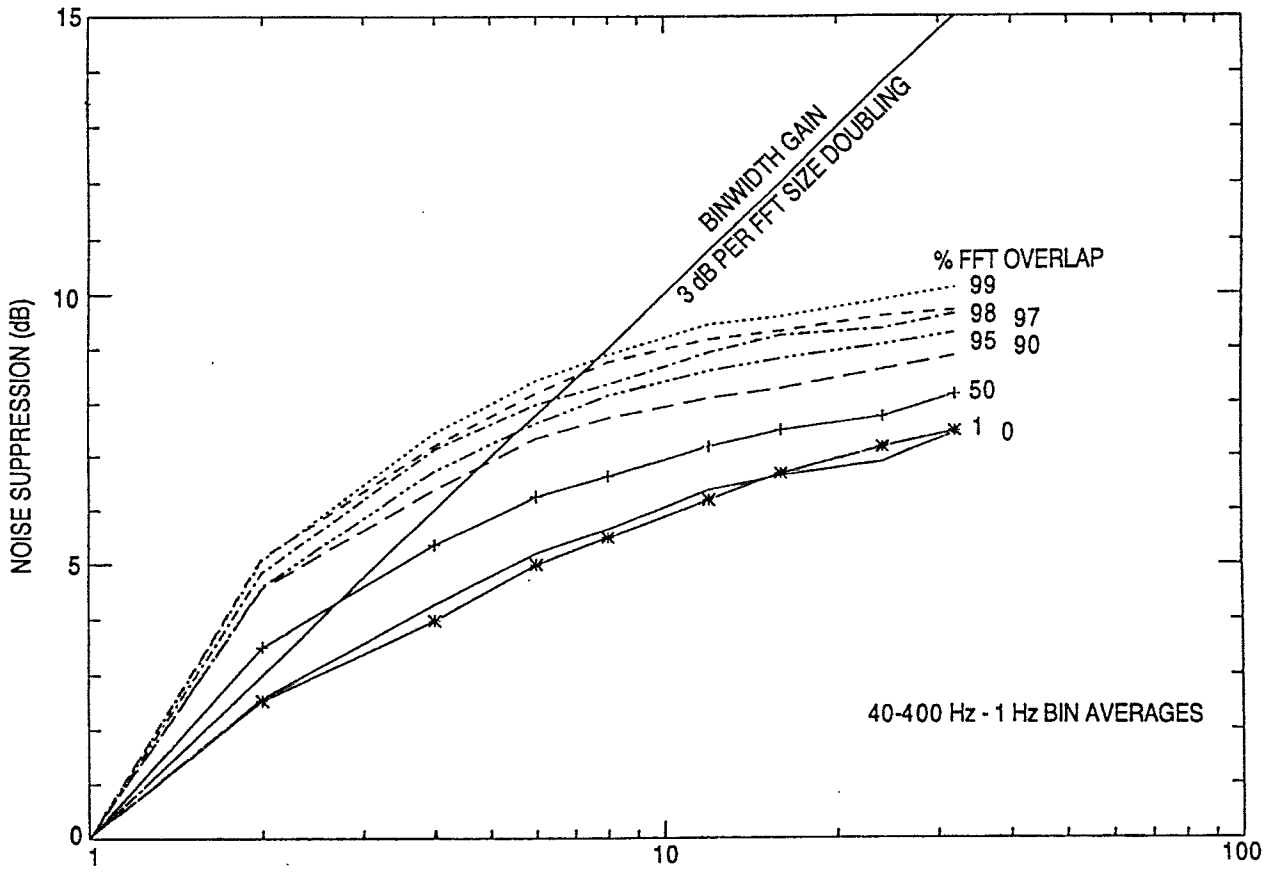

Fig. 6.9 — WISPR sonobuoy processing versus FFT size (binwidth), data length in contiguous FFT time periods

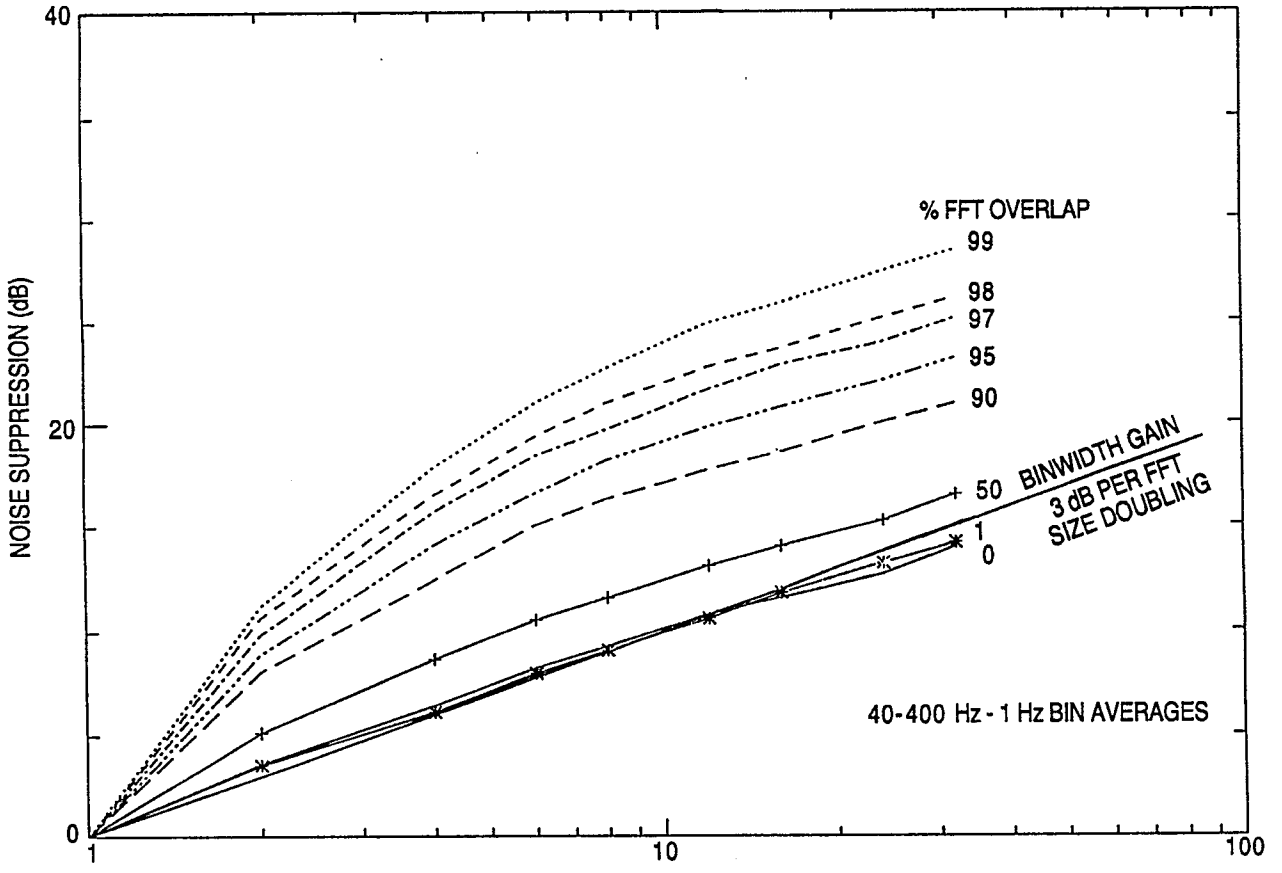

Fig. 6.10 — $AWSUM_4$ sonobuoy processing versus FFT size (binwidth), data length in contiguous FFT time periods

One way of evaluating the gains of the WISPR and AWSUM processors is to compare the noise gain that can be achieved from a given length of data on the basis of simply decreasing the frequency BW. The alternative would be to use the same data to calculate a series of overlapped spectral outputs that have coarser frequency resolution than can be processed by WISPR and AWSUM to achieve the gain. If one thinks in terms of spectral output that is generated by FFTs, the fundamental unit would be the length of data sufficient for one FFT. With that as the reference length, the next size FFT would be twice the size, which would yield a BW of one-half of the size of the reference length FFT. On the other hand, the same lengths of data could be used in WISPR processing to achieve gain instead of using the data to decrease the BW to get BW gain. For example, if the second length of FFT was used to calculate 100 more FFTs that are overlapped 99%, a total of 101 data points could be used in WISPR processing. The result, given as the top (dotted) curve in Fig. 6.9, shows that the WISPR processing of those 101 data points in two FFT lengths would exceed the BW gain for twice the FFT size by approximately 2.5 dB. The WISPR processing continues to exceed the straight line that represents BW gain for a time equal to about seven FFT lengths. Beyond that length, the BW gain exceeds the WISPR gain. Corresponding results are given for 0, 1, 50, 90, 95, 97, and 98% overlaps.

A similar comparison to that of Fig. 6.9 is given for $AWSUM_4$ in Fig. 6.10. In this case, the gain advantage at 99% overlap over that obtained by cutting the BW in half is about 8 dB. Furthermore,

all of the curves for overlaps of 50% and more exceed the BW gain line from about 1.7 dB (50%) to 12 dB (99%). In fact, the maximum total gain for the $AWSUM_4$ processing at 99% overlap is about 27 dB for approximately 32 FFT lengths (about 32 s in the case of the sonobuoy data in Fig. 6.10). When little or no overlap is involved (0 and 1%), the $AWSUM_4$ results are about the same as the BW results.

The results of processing four data sets from sonobuoy 4 data are presented in Fig. 6.11. These results can be utilized to obtain a somewhat better feel for the effect of the number of FFTs available for processing and FFT size (which controls BW). The FFTs were performed, all using 90% overlap, for data lengths of 1024, 2048, 4096, and 8192 points. Therefore, the effect of percentage overlap is constant for these data, in contrast to that effect just discussed in Figs. 6.9 and 6.10. Four fairly distinct sets of curves can be identified, one for each of processors A_{01}, A_{02}, A_{03}, and A_{04} (see Sec. 2.5 for the definition of these processors). Because of the constraints of 80 s of data and 90% overlap, both low and high ends of the number of averages scale have only one datum (8192 at the low end and 1024 at the high end).

The noise suppression increases systematically with the number of averages and the processor order numbers 1 through 4 with a maximum achieved of about 25 dB for A_{04} with 791 averages. Additional gain can probably be achieved at higher order numbers and even more averages. However, the gain increase can be expected to reach a point of diminishing returns for several reasons. First, a greater number of averages requires greater data lengths if the percentage overlap is held constant, which may exceed the temporal stationarity limit of the data; second, as may be observed in Fig. 6.11, even though the amount of gain is systematically increasing, the gain increase (in decibels) with each increase in order number is only about 70% of the previous increase; and third, statistical instabilities will probably occur if the order number becomes too high, since an ever-increasing amount of data is, in effect, rejected as the order number is increased (c.f., Sec. 3.5 and App. A, Sec. A.1).

Perhaps an even more important observation is that suppression level is only weakly influenced by the FFT size, if at all. The BW decibel gain discussed earlier is common to the AVGPR and $AWSUM_k$ filters and is, therefore, removed from the suppression level when the differences are taken. For example, notice that at the number of samples equal to about 100, 200, and 390, there are multiple estimates for the suppression level which agree quite well, differing by as little as 1 dB. Careful examination of these multiple estimates will show that the suppression level is not distributed systematically in FFT size order. For completeness, it should be mentioned that even though the data are all from a common origin, at the points where multiple estimates occur, the data are from slightly different time periods due to the differences in FFT sizes.

Figure 6.11 provides more than the suppression levels of the A_{0k}, $k = 1$ to 4 processors. Since

$$A_{0k} = \frac{AWSUM_0}{AWSUM_4},$$

then

$$A_{jk} = \frac{AWSUM_j}{AWSUM_k} = \left[\frac{AWSUM_0}{AWSUM_k}\right] / \left[\frac{AWSUM_0}{AWSUM_j}\right] = \frac{A_{0k}}{A_{0j}}.$$

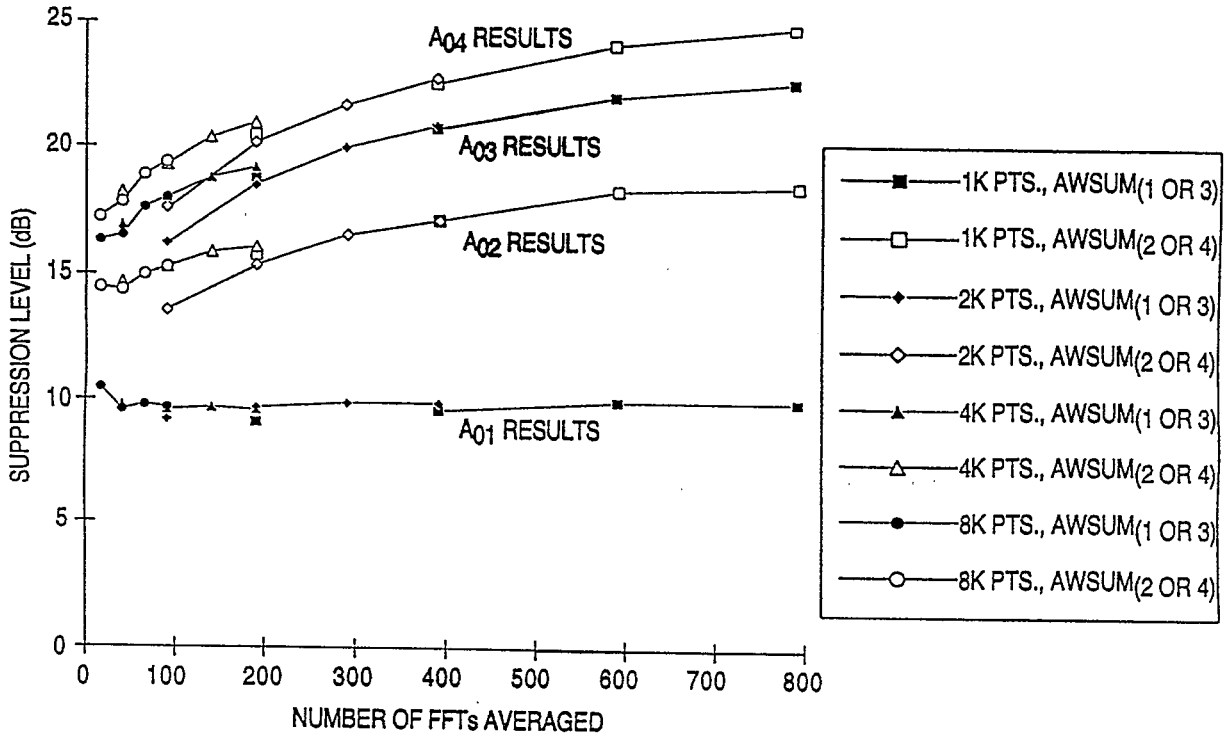

Fig. 6.11 — Summary of suppression level results for overlapped processing with AWSUM Filters

Thus, in decibels, with $k > j$,

$$A_{jk} \text{ in dB} = (A_{0k} \text{ in dB}) - (A_{0j} \text{ in dB}).$$

Hence, the decibel differences (i.e., the spread) between the curves in Fig. 6.11 gives the suppression level as a function of the number of averages for combinations of the four processors.

6.4.3 Spatial Resolution Dependence on Beam Response Overlap

Families of curves have been generated for the WISPR and AWSUM Filters that give the noise suppression gains as a function of the number of averages and the percentage of overlap of successive FFTs in the time domain. The noise suppression gains were as much as 10 dB for WISPR processing and 27 dB for AWSUM processing. Such gains are significant because after a given amount of overlap, the conventional AVGPR does not give a significantly different result. The reason for this is that the dependence between samples is too great, yet the WISPR and AWSUM processors still provide additional gain up to and including overlaps of 99%. Hence, the dependence among the consecutive FFTs does not increase as rapidly as the overlap increases in the fluctuation-based processors (e.g., WISPR and AWSUM) as it does for the AVGPR processor.

The increased fluctuation-based processor (e.g., WISPR and AWSUM) gain due to overlap processing is not unique to the temporal domain. There is a corresponding analogy in the spatial domain. Consider, for example, Fig. 6.12. The three curves plotted in Fig. 6.12a are the AVGPR curve (top), the WISPR Filter curve (middle), and the A_{01} submerged source curve (bottom). These results are for 125 averages and 90% overlap of the FFTs in the time domain. The A_{01} curve

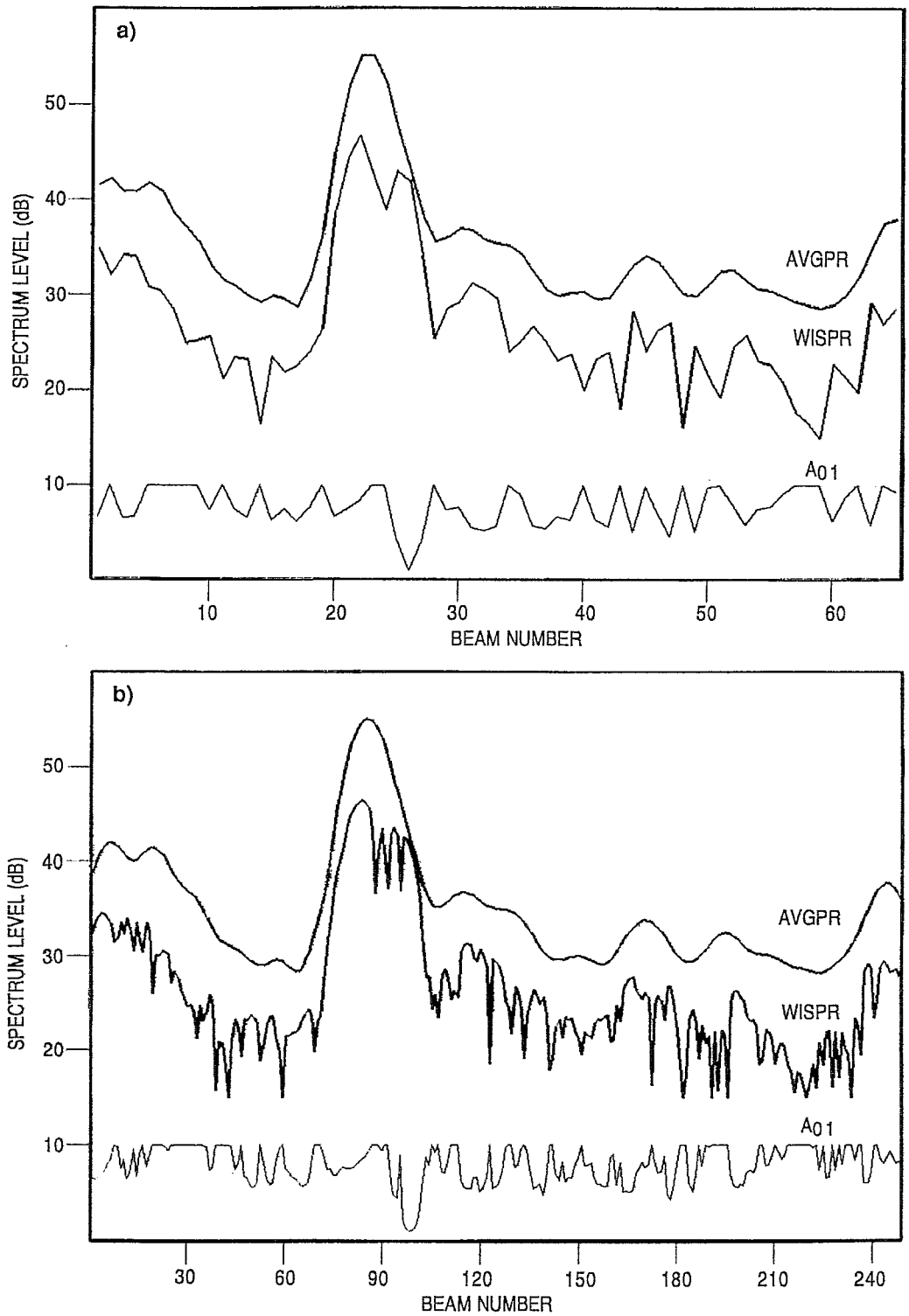

Fig. 6.12 — Spatial resolution dependence on beam response overlap

indicates that there is a submerged source signal at approximately beam number 122. That signal is evident in the WISPR curve, but it is not evident in the AVGPR curve. The submerged source signal is obviously below its minimum detectable level.

Figure 6.12b gives corresponding curves for the three processors (AVGPR, WISPR, and A_{01}), but there is one important difference. The number of beams that is calculated (steered) to cover the same acoustic space is different. There are 63 beams in Fig. 6.12a and 252 beams in Fig. 6.12b. That constitutes an oversampling of the beams in azimuth space for the Fig. 6.12b results by approximately a factor of four. That constitutes a case of consecutive beam response pattern overlap in the spatial domain that is analogous to 75% overlap of consecutive FFTs in the time domain. The effects of the high degree of beam overlap in the spatial domain can be seen by comparing the various curves between the low overlap case in Fig. 6.12a and the high overlap case in Fig. 6.12b. The only effects that are apparent in the AVGPR curve in Fig. 6.12b that are due to increased beam overlap are that some of the straight-line segments between the consecutive beam output values of Fig. 6.12a are more rounded in Fig. 6.12b due to the increased quantization (or interpolation) of the larger number of beams; otherwise, the results are identical. On the other hand, there are significant differences in the WISPR and the A_{01} curves between the two plots. The spatial resolution has increased substantially in the overlapped case in Fig. 6.12b. The prominent peaks of signal and noise in the AVGPR curves between beam numbers 112–123 in Fig. 6.12a and between beam numbers 67 and 105 in Fig. 6.12b are divided into four local maximum in the overlapped case and into only two in the nonoverlapped case. Furthermore, the location of the submerged source in the higher resolution results of Fig. 6.12b corresponds with the fourth local maximum at beam 103.

The spatial resolution in the overlapped case (Fig. 6.12b) has improved over the nonoverlapped case (Fig. 6.12a) sufficiently to localize the source to a much finer degree. Furthermore, it is obvious that the effective beamwidths of the overlapped results are significantly narrower than those of the corresponding nonoverlapped results, perhaps by a reduction factor of as much as two.

6.4.4 Compensation for Array Misalignments and Instabilities

Some of the mechanisms arising at the sensor that are responsible for increased fluctuations of signals and noise alike are discussed in detail in Sec. 3.2.3 (also refer to Fig. 3.5). Two of these occur with towed line arrays, as the relative orientation of signal sources to portions of the array vary through array path meanders and depth variations. The spatial resolution enhancement due to WISPR processing in the time domain can be interpreted as the result of stripping highly fluctuating noise components away from the more stable signal components. The portion of this improvement that can be attributed to the selective attenuation of the fluctuations due to array misalignments and instabilities partially compensates for errors in arrival angle localizations generated at the sensors. No experimental data are currently available that clearly delineate this effect. However, if such fluctuations were added through simulation, such a result would clearly be demonstrated. What should be kept in mind is that fluctuations that are added at the sensor are added to the fluctuating signals and steady signals alike. Thus, fluctuation-based processors can still partially distinguish the difference in fluctuation levels originally present upon arrival.

6.5 Summary

Several interesting applications of WISPR processing have been presented that demonstrate its general utility for processing signals that are differentiated with respect to their fluctuation levels. Spatial resolution, spectral resolution, and SNR gain may be obtained. Reduction of signal masking

from transients, carrier loss, and associated signal intermittent noise; elimination of directional masking from high-level, off-axis noise or surface sources; and even partial compensation for sensor (array) induced noise are possible under favorable conditions. WISPR and AWSUM filters can uniquely take advantage of overlapped processing. In addition to the recovery of signal power ordinarily lost by data windowing that is usually recovered by overlapped processing, improvements in spectral resolution and SNR gain are also achieved.

7.0 ADVANCED WISPR FILTER APPLICATIONS

7.1 Introduction

Several typical applications of the WISPR and related filters have been described in previous sections. Here, a number of advanced applications will be presented that require imagination to realize that fluctuation-based processors are applicable. It is quite possible that many other such applications await discovery, limited only by researchers' familiarization with these processors, time, and resources. There are several tactical decision aids (TDA) commonly used in the Fleet that might benefit from fluctuation-based processors. One of those, the Gram (time history display of spectral tonal content), will be shown to perform with a high level of robustness to masking. Widely used to improve the performance of some TDAs are various noise spectrum equalization (NSE) algorithms. An illustration of WISPR and $AWSUM_4$ to achieve NSE is illustrated for the Gram TDA. Extension of this NSE algorithm to two-dimensional applications is shown to be computationally straightforward.

7.2 Multifrequency Matched-Field Processing

One problem of current interest in matched-field processing (MFP) is the occurrence of relatively high sidelobes in range and depth. It is often very difficult to identify, with high confidence, the true depth and range peak from the multiplicity of range-depth peaks due to range and depth sidelobes. One method of getting around that problem is to generate ambiguity surfaces for many frequencies and then to average them on a range-depth cell basis. The rationale for doing that is that the locations of the sidelobes in range and depth will change with the frequency, but the true range and depth of the target will be the same no matter what the frequency is. Hence, averaging multiple ambiguity surfaces, for different frequencies on a bin-by-bin basis, should not affect the true range and depth peak, but it should reduce the average due to sidelobes by averaging the high levels at some frequencies, with the low background levels at other frequencies. The result should be a reduction in the high sidelobes that tend to confuse a detector.

Through simulations of MFP, cases were generated for SNR levels of –5 and –8 dB, with ambiguity surfaces produced at eight frequencies for each SNR level. Those two SNR cases were processed through the AVGPR and WISPR processors. The upper plots in Fig. 7.1 (–5 dB SNR case) and Fig. 7.2 (–8 dB SNR case) are for AVGPR processing, and the lower plots are for WISPR processing. The peak that corresponds to the target range and depth of 50 km and 110 m, respectively, is clearly evident as the largest peak in each of the plots in those figures. Comparing the background levels in the upper two plots, it is visually lower for the –5 dB SNR case as would be anticipated. Comparing the background in the upper plot of Figs. 7.1 and 7.2 with the corresponding lower plots, it is visually lower in the WISPR-processed plots. Notable visually, the background level for the –8 dB SNR case from WISPR processing is almost equivalent to the AVGPR –5 dB SNR result, an improvement at least.

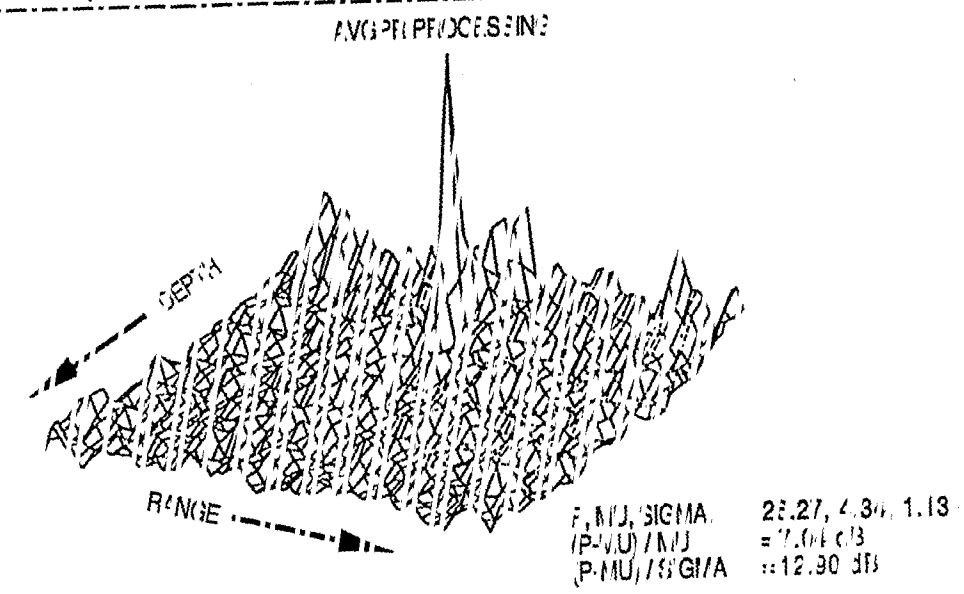

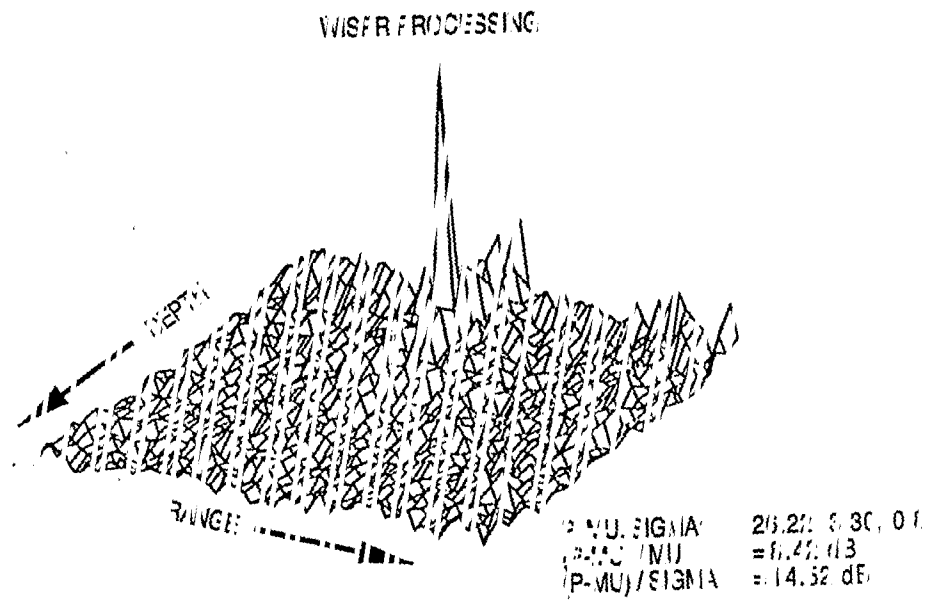

Fig. 7.1 — Multifrequency matched-field processing, SNR = 5 dB, target depth 110 m, target range 50,000 m

The results of these two processors can be compared quantitatively by comparin the target range-depth peak (F), the mean level of the background excluding the peak neighbors (Mu), and the standard deviation of the background levels (Sigma). In bot [illegible] the WISER filter results are about the same. For [illegible] the WISER filter is about 1.0 to 1.1 dB less than the bro generated [illegible]

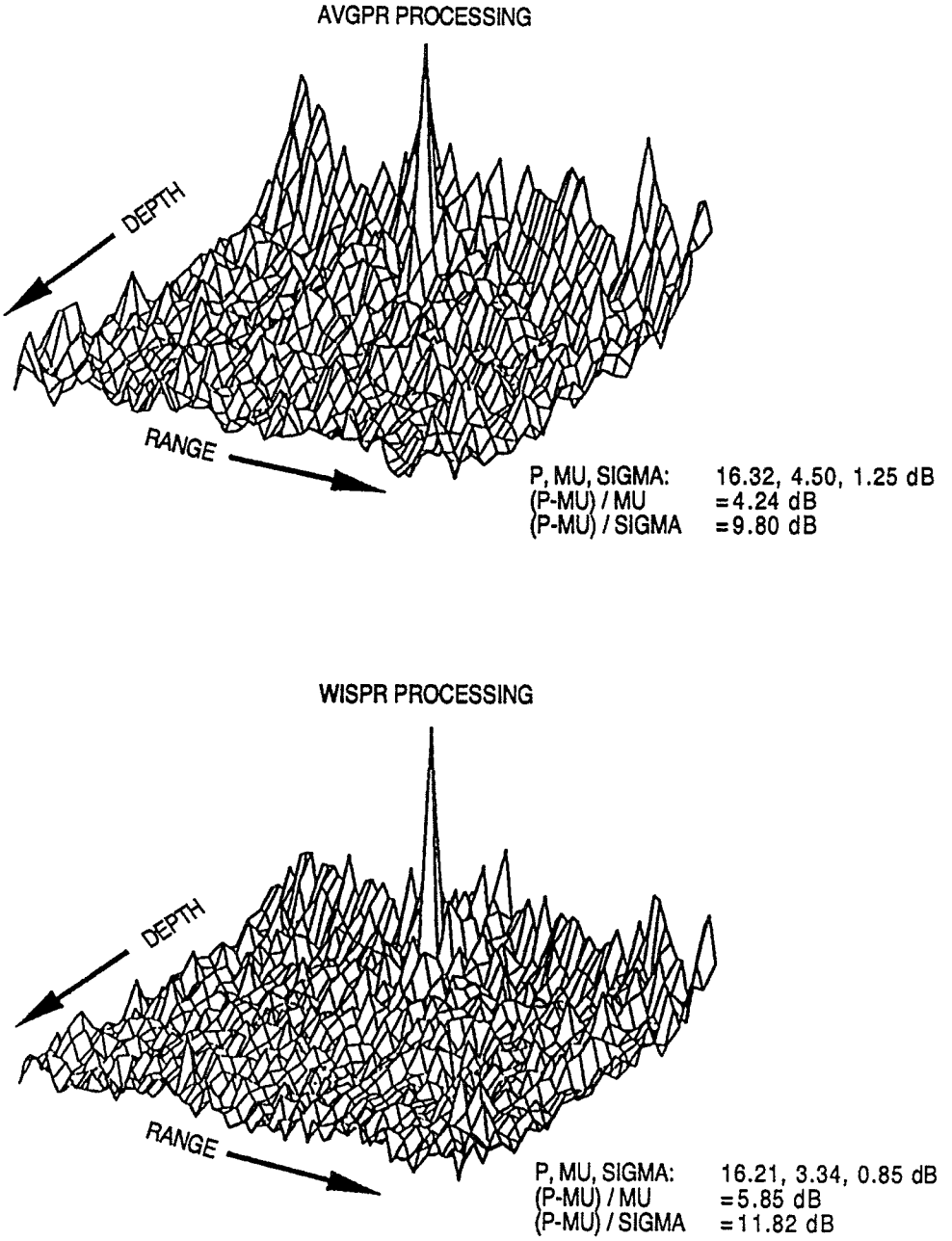

Fig. 7.2 — Multifrequency matched-field processing, SNR −8 dB, target depth 110 m, target range 50,000 m

Two other quantitative comparisons can also be made:

(a) The processor output SNR ratio: SNR = (P − Mu)/Mu

(b) The processor output detection index: DI = (P − Mu)/Sigma

In both cases, the WISPR results outperforms the AVGPR results by about 1 dB and 2 dB for the SNR and DI, respectively. This suggests that the use of the WISPR Filter in place of the linear

average (AVGPR) can be expected to provide a significant enhancement in identifying the location of targets. Even better results (though not presented herein) were achieved using the $AWSUM_4$ Filter instead of the WISPR Filter. It is anticipated that processing of real data, where the effects of natural fluctuations of the medium are also present, would additionally magnify the improvements just discussed.

7.3 WISPR Applied to Frequency Domain Matched Filtering

When the replica signal is sufficiently long in time to generate time histories of narrow-band spectral output, a WISPR-type frequency domain matched filter approach can be taken to detect the returning signal among the reverberation and noise. In doing that, the WISPR Filter equation can be written in the more general form of a path integral:

$$W(f,t,\Theta) = B - 10\log\left[\frac{1}{L_C}\int_C 10^{[A-G(f,t,\Theta)]}dz\right], \tag{7.3.1}$$

where

A, B = constants dependent upon data type,

f = frequency,

t = time,

Θ = steering angle,

C = integration path,

L_C =integration path length, $\int_C dz$,

$G(f,t,\theta)$ = frequency/time/beam number surface.

Using the modifications indicated below, Eq. 7.3.1 also applies to the following cases:

(a) Passive sonobuoy:

$C = C(t)$,

$G(f,t,\theta) = G(f,t)$;

(b) Passive sonar array:

$C = C(t)$ for CW,

$c = c(f,t)$ for transient matched filter,

$f = h(t)$ transient waveform function;

(c) Active sonar array:

$C = C(f,t)$,

$f = h(t)$ signal waveform function.

The application of Eq. 7.3.1 is fairly straightforward and will be discussed in terms of an active sonar array, which involves the most complex form for which this type of processing has been done thus far.

The approach to perform frequency domain fluctuation-based matched filtering for an active sonar array will be demonstrated with a linear frequency modulated (LFM) waveform that is a frequency ramp that increases with time and extends over time for 8 s as it increases linearly in frequency over 16 frequency bins (235 to 250). The surface in Fig. 7.3a is a time after ping versus frequency bin number plot. The time ranges from 0 s after ping at the top to 580 s after ping at the bottom. Frequency bin number increases from left to right. There are three return pings in that plot. The first one is a continuous wave (CW) signal that covers about four frequency bins near bin 253 and arrived at approximately 50 s after start of recording. The next arrival in time is a broadband (BB) signal that extends over frequency bins 235 through 277 at approximately 340 s. The last arriving signal is the LFM return signal that extends from frequency bins 235 to 250 and over time from about 350 to 360 s. These known characteristics can be used to define a matched filter along path C in time frequency space. The path designated LFM SWEEP RETURN in Fig. 7.3c ending at about 351 s coincides with the return of the LFM signal. At each time instance, there are other paths parallel to this one that coincide with the processing paths "C." Of course, they would not all coincide with the LFM signal return.

Now suppose the objective is to detect the LFM signal and to discriminate against all other signals and noise. If one does conventional (AVGPR) processing on the frequency time-of-arrival domain that has been transformed to coincide with path C, the result in Fig. 7.4a is obtained. In that plot, the CW, LFM, and BB signals are clearly evident along with the reverberation (REV). The power average processor has not been able to enhance detection of the LFM signal by reducing the other two to any discernable degree. However, that is not the case for the WISPR frequency domain matched-filter results in Fig. 7.4b. In this case, the matching to the path enabled the WISPR Filter to attenuate everything except the LFM signal. In fact, there is no remaining trace of the BB signal and only a small remnant of the CW signal. Furthermore, the reverberation has been reduced on the average about 8 dB. The LFM signal has been reduced about 3 dB, but there is no doubt that its detectability has been greatly enhanced by the WISPR frequency domain matched filter.

7.4 WISPR and the Active Barrier

One possible means of detecting a submerged target in shallow water is to ensonify a vertical plane between a source and a vertical string of sensors and to identify abnormalities in the received signals that are caused by the target passing through the plane. Such a concept was tested in Dabob Bay. Figure 7.5 shows the plot of the bay where the experiment was conducted and the locations of the source and receivers and the track of the target. Figure 7.6 shows a cross-section of the bay along a vertical plane containing the source and the receiver. The signals from the hydrophones were recorded during the time the projector was operating, which included times before, during, and after the target passed through the ensonified plane between the source and hydrophones. The SNR was always greater than 20 dB.

The signals from each hydrophone were spectrum analyzed to obtain the time series of the power in each source frequency bin. The AVGPR and WISPR Filter results were computed, treating the data for groups of hydrophones at the same instant of time as the data sequence (a vertical spatial sequence in this case as opposed to the time sequences used in most of the earlier examples). The running difference between these two levels (A_{01} processing) was determined. In Fig. 7.7, the time history of the result is compared to the track of the target passing through the ensonified plane using hydrophones 1 through 24. The peak in this figure corresponds to the approximate time that the target passed through the plane. At all other times, the A_{01} level is nearly zero. Similar results were obtained using hydrophones 36 to 48 near the bottom, Fig. 7.8, and also using only three

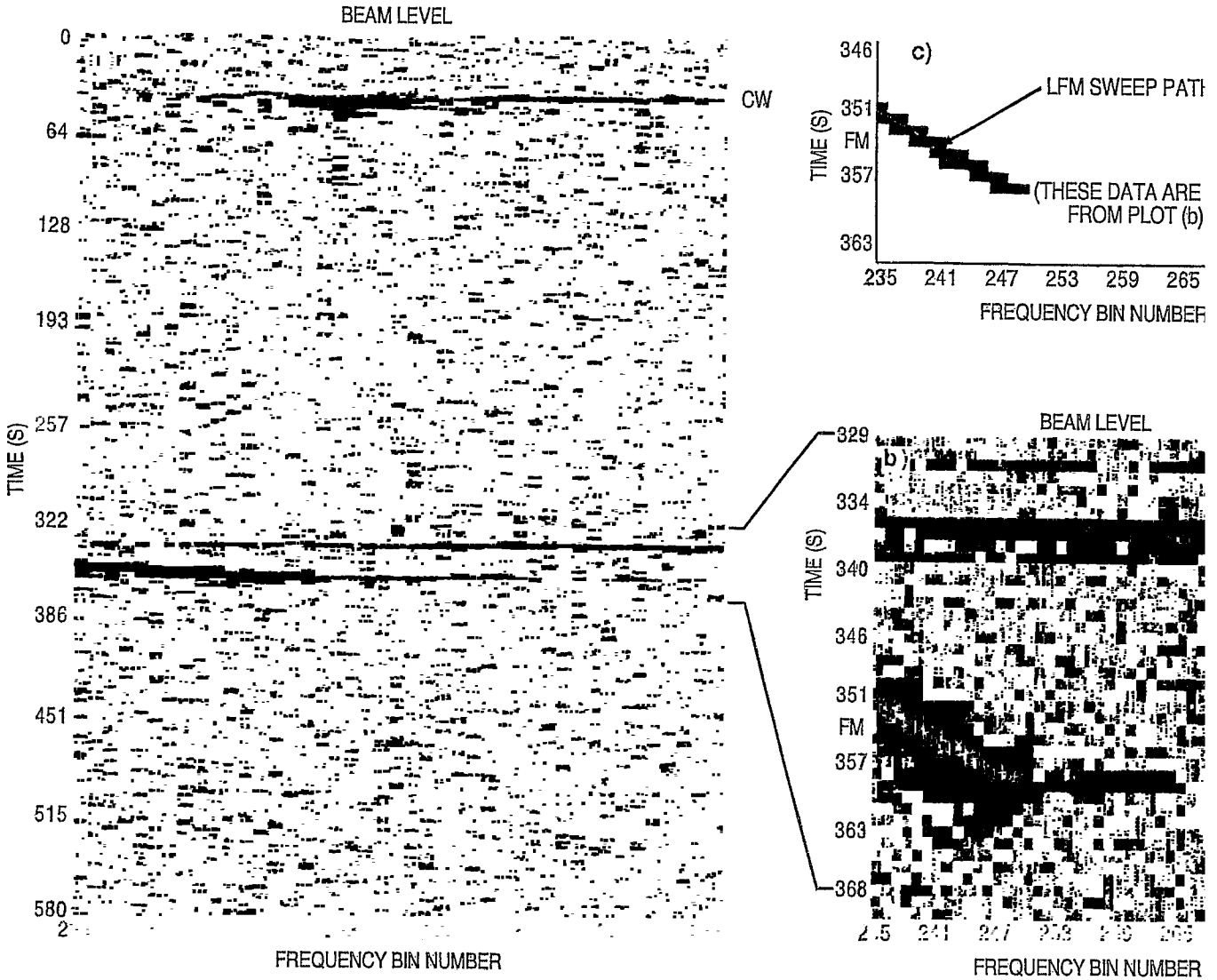

Fig. 7.3 — Frequency domain fluctuation-based matched filtering for an active sonar array

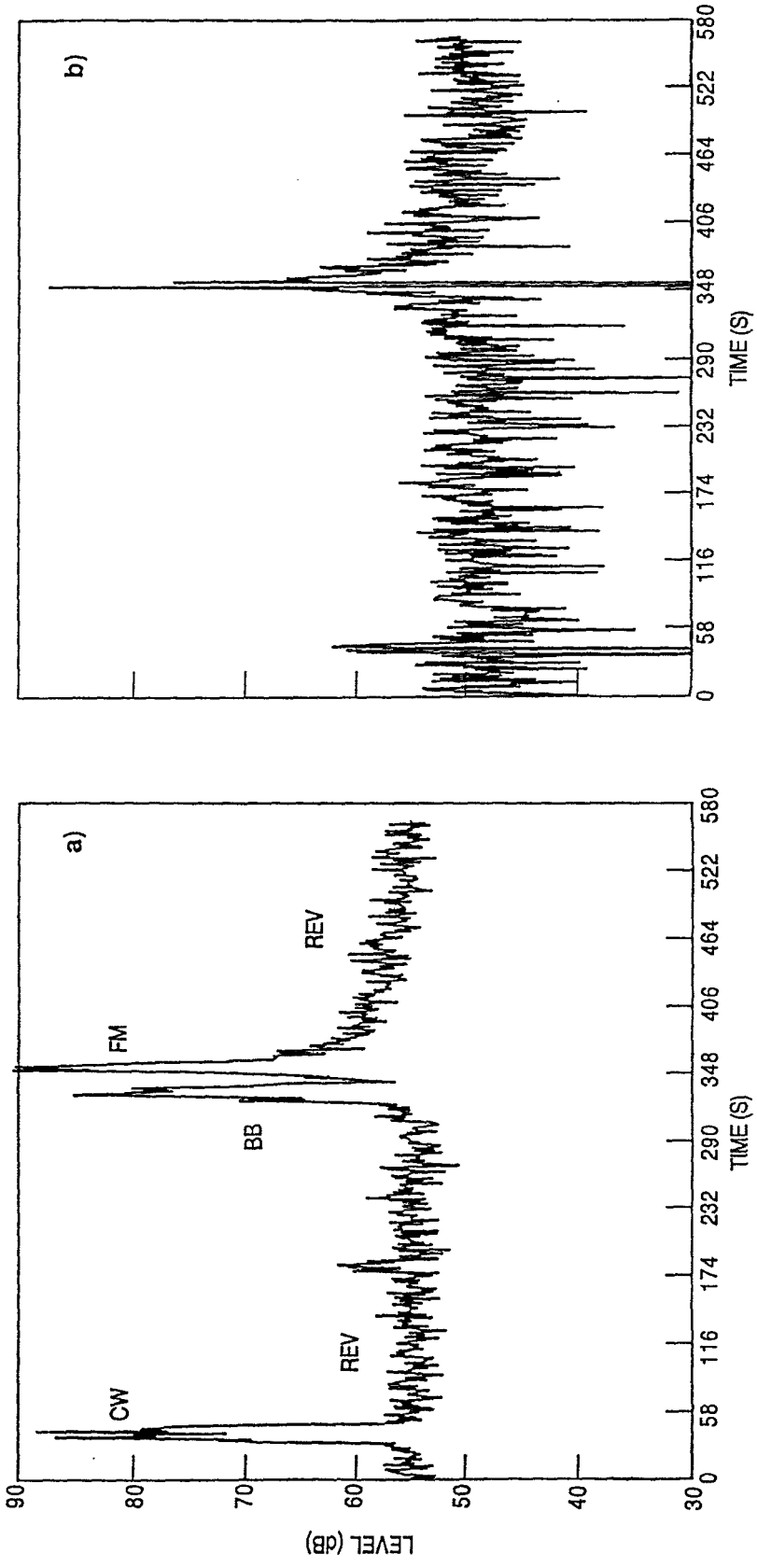

Fig. 7.4 — Matched filter response: (a) power average (FM AVGPR) and (b) FM WISPR

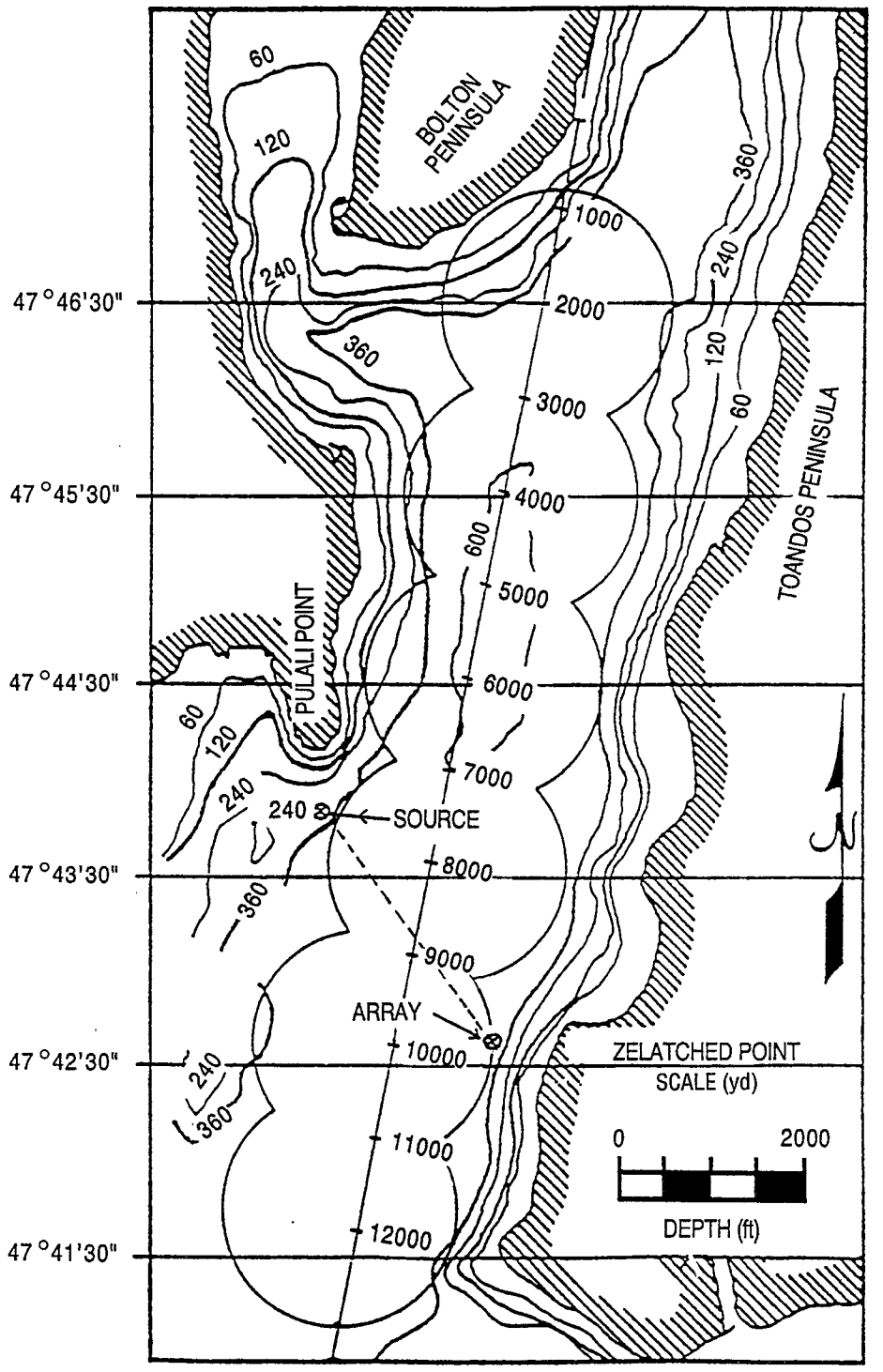

Fig. 7.5 — Target track during Dabob Bay active barrier experiment

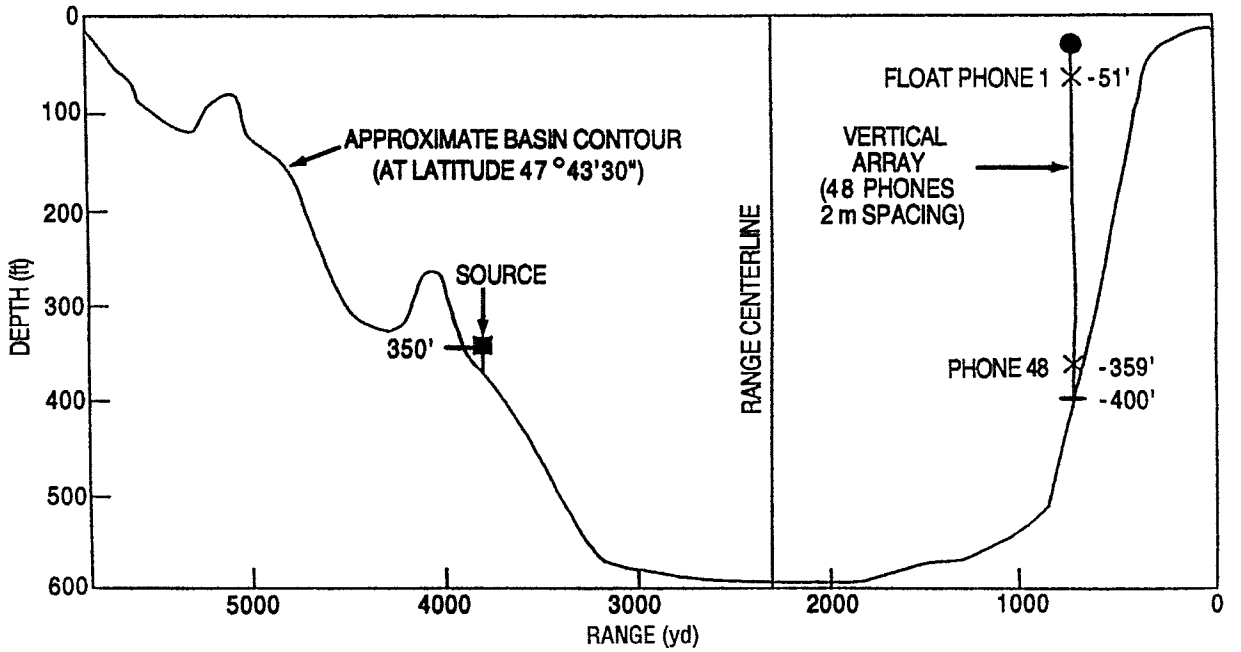

Fig. 7.6 —Dabob Bay profile transverse to the active barrier experiment track

hydrophones, Fig. 7.9. These results suggest that in some shallow-water environments, the WISPR Filter can be used in an active barrier situation to detect the passage of a target.

7.5 WISPR Time History (Gram) Performance/Robustness to Masking

Robustness to masking using WISPR processing will be illustrated with two cases of sonobuoy data. A well-behaved sonobuoy will be used to provide a comparison baseline to data from a sonobuoy during a time when the signal is partially masked by periods where the sonobuoy is operating erratically.

7.5.1 Data from a Well-Behaved Sonobuoy

Figure 7.10 presents some of the analysis products that illustrate WISPR performance for sonobuoy systems. The plot in Fig. 7.10a is the broadband time history trace of a sonobuoy output that covers the time period from approximately 5 min (300 s) after the beginning of data acquisition to about 6.5 min (400 s). The time history trace is "reasonably well behaved." This indicates good data from a well-functioning sonobuoy. The one small "glitch" about two-thirds the way across the trace would have almost no effect on conventional data processing.

The curves in Fig. 7.10c correspond to the first 50 s of data in the time history plot. The spectra were obtained for 23 FFTs (0.25-Hz BW with 50% overlap). The top and middle curves are the AVGPR and WISPR results. The spectral lines and broadband noise are evident in both of these curves. The broadband noise component of the WISPR spectrum is approximately 6 dB less than the AVGPR result. The bottom curve is the A_{01} processor result. When this curve is very close to zero (usually less than 1.5 dB), there exists a stable tonal in the data at that frequency which is characterized as one originating from a submerged source. This happens at the frequencies marked A, B, C, D, and E.

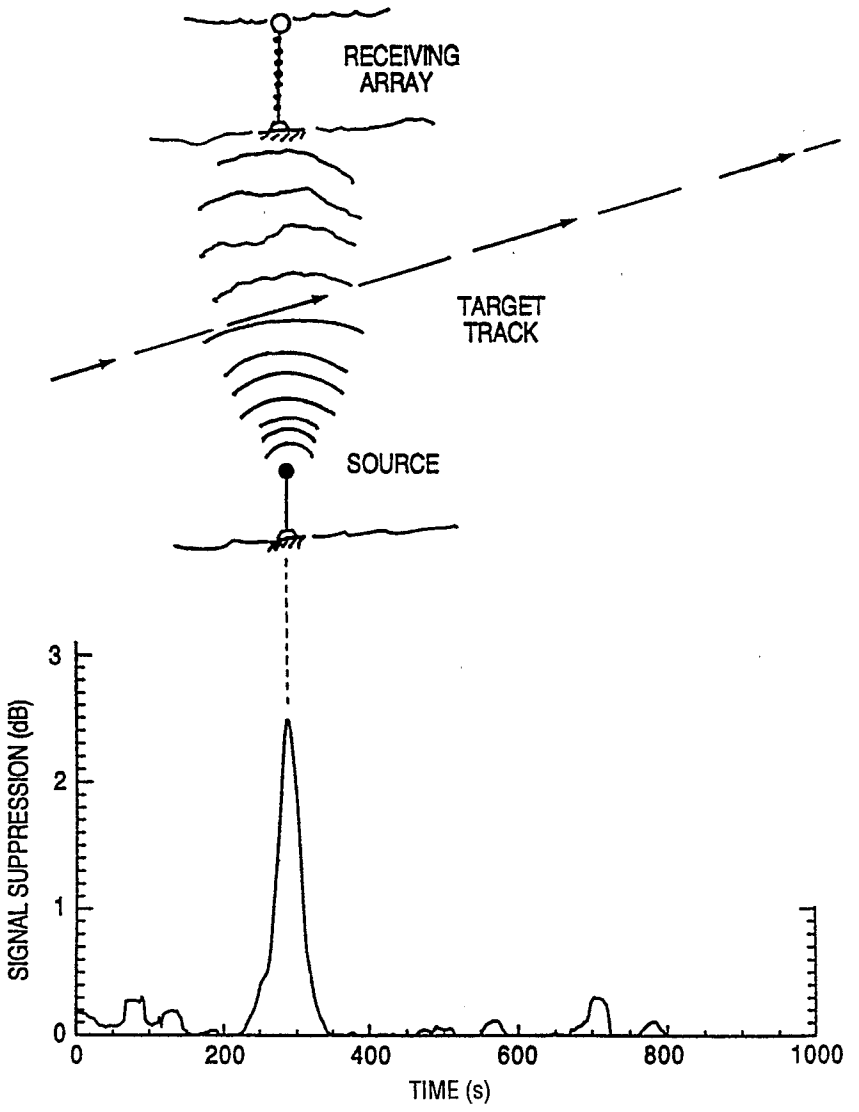

Fig. 7.7 — Dabob Bay active barrier processing results, hydrophones 1 through 24

Figure 7.10b and d contains gram-type time histories of the AVGPR and WISPR result for the first 20 min (labeled 1 to 21 min). The spectral lines appearing on the gram displays are those that pass a particular threshold above the background level after passing the spectral data through an NSE algorithm. Those spectral lines that persist in time appear as linear traces on these grams. Both grams are rich with line structure. The AVGPR results have more lines in the middle range of frequencies, while the WISPR result has more lines in the frequency regime below approximately 30 Hz. Overall, the WISPR results have more line components. Many of the lines the two processors have in common have longer time durations in the WISPR results. Thus, the WISPR processor permits tracking the lines longer and perhaps farther in range due to the 6- to 8-dB SNR enhancement and noise suppression capability of the WISPR Filter.

Figure 7.11 contains two grams. Figure 7.11a is identical to Fig. 7.10b. The gram in Fig. 7.11b was obtained from the A_{01} processor; plotted are only those periods when the submerged source

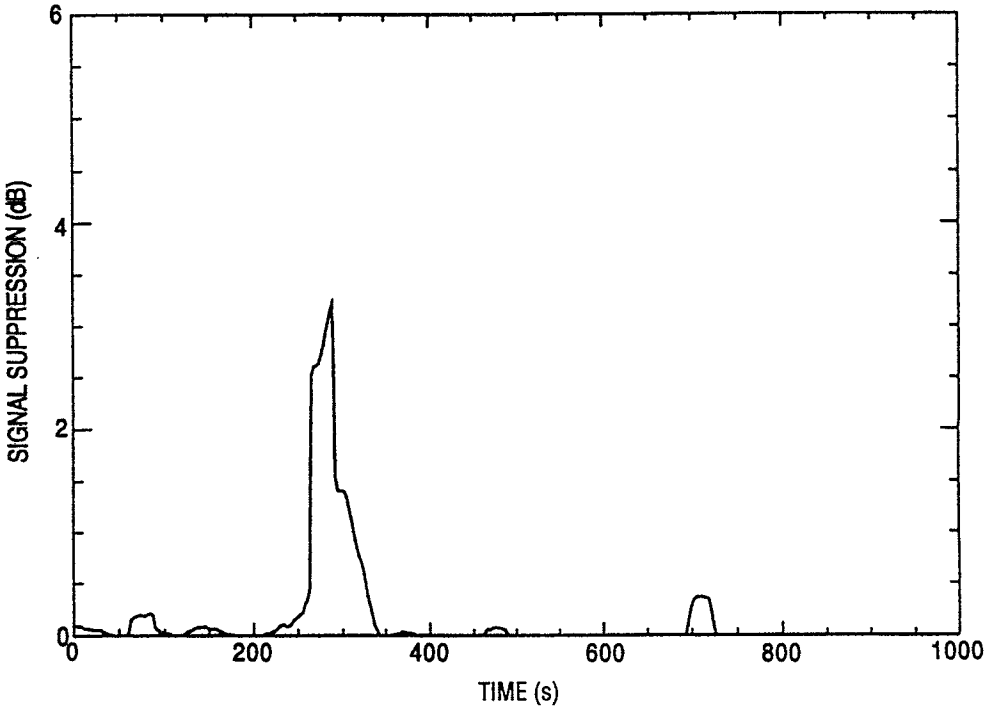

Fig. 7.8 — Dabob Bay active barrier processing results, hydrophones 36 through 48

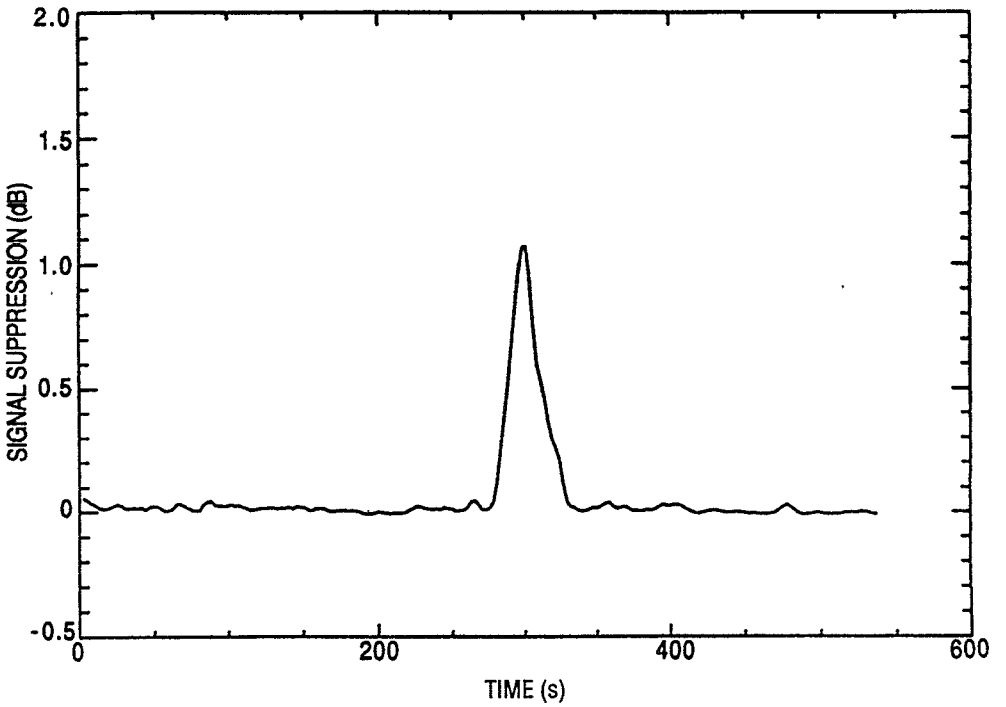

Fig. 7.9 — Dabob Bay active barrier processing results, hydrophones 4, 20, and 36

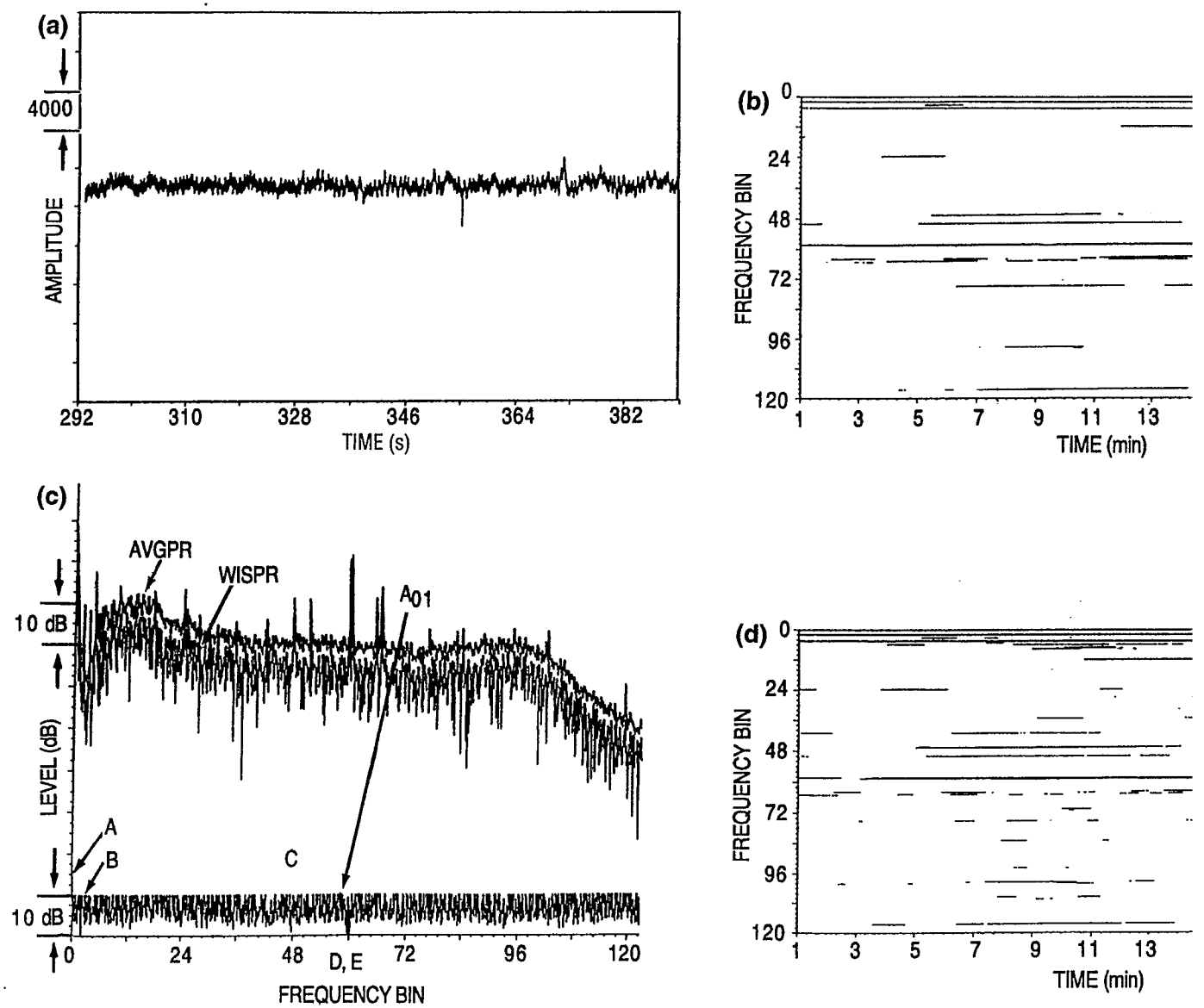

Fig. 7.10 — Gram display of conventional (AVGPR) versus WISPR performance

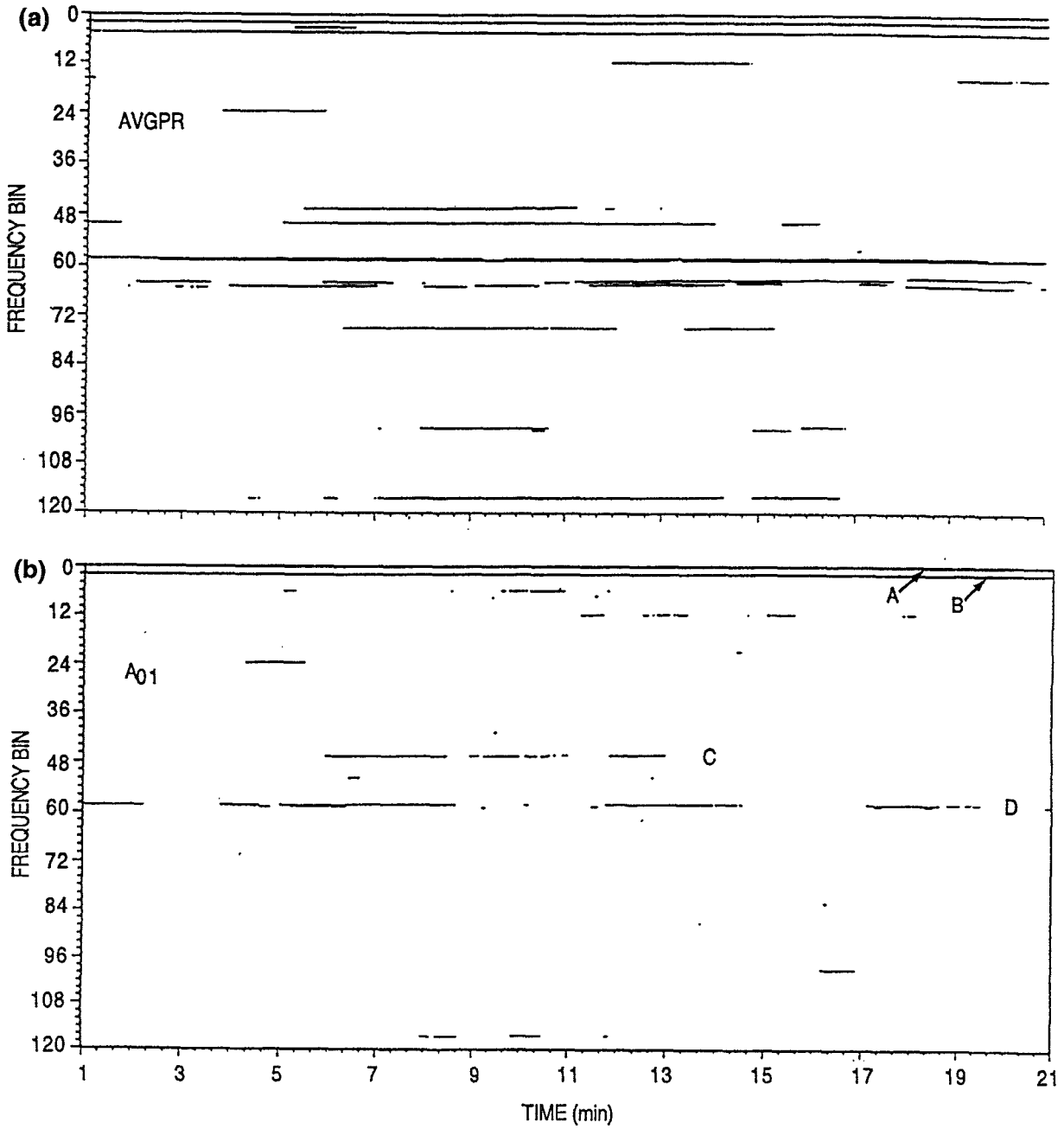

Fig. 7.11 — Gram display of conventional (AVGPR) versus WISPR performance

threshold is exceeded for a given frequency. The A_{01} gram indicates that a submerged source was radiating spectral lines marked at A, B, C, and D for a significant part of the 20 min, and also at a few other frequencies for lesser periods of time. The AVGPR gram possesses more lines than the WISPR difference gram, but using it alone, there is no means to determine which are from submerged sources and which are from surface noise clutter sources.

Some of the lines that occur in the A_{01} results are also in the AVGPR results, but when they are of small duration in the AVGPR results, they are smaller yet in the A_{01} results. One reason for this is that for a line to exist in the A_{01} result it must first exist in the AVGPR result. Therefore, it would be unusual to have an A_{01} line that exceeded the time duration of the corresponding line in the AVGPR result. Another reason is that as the line begins to disappear from the AVGPR result, the noise begins to dominate and the spectral line output takes on the fluctuation character of the noise. In other words, this occurs when the initial SNR is not sufficient to identify the source as one that originated from a submerged source.

7.5.2 Data from a Sonobuoy with Intermittent Noise Masking

Figs. 7.10 and 7.11 correspond to a time period when the sonobuoy system was functioning well. Unfortunately, this is not always the case. It is not unusual for a large percentage of the data to be severely degraded as a result of one or more of the many faults or casualties that can occur. Examples include sonobuoy antenna wash-over due to high seas and loss of transmitted signal due to the aircraft being out of range, or the aircraft being in a turn and shielding its own antenna from the line-of-sight path to the sonobuoy antenna. When things like this happen, the fault appears as a telemetry problem that induces high-level fluctuations in the results. This is illustrated by the time history plot in Fig. 7.12a. One segment of time during which the fluctuations were particularly numerous, identified by the word "masking," was processed to illustrate the power of WISPR to suppress or eliminate the effects of masking or jamming. This was not the only time period of masking, but it was the worst period in the data. These data are a continuation of the previous data in Figs. 7.10 and 7.11 for times when telemetry problems occurred. A spectral plot similar to the one in Fig. 7.10c was obtained by processing the data for the time period identified as the masking segment. (Note: all times after the beginning of the segment identified for illustration were degraded due to the same type of masking.) In this case, there is a large difference between the AVGPR curve and the WISPR curve at the lower frequencies. It is much more than the 6 to 8 dB that might otherwise be expected for the difference. In fact, at one point near the axis, the AVGPR result is about 80 dB and the WISPR result is about 40 dB, a suppression of the masking effects of 40 dB. Furthermore, the line components at these low frequencies are not evident in the AVGPR results, but they are still present in the WISPR results. In other words, WISPR reduced the contamination by 40 dB to leave a low-frequency line sticking up 15 dB above the background ambient noise.

The difference curve in Fig. 7.12c designates only the line component very close to the axis as originating from a submerged source. WISPR processing uncovered other lines above that one. They do not appear in the A_{01} curve even though they were so designated before the onset of masking. The reason for this is that the A_{01} processor requires reasonable results from both the AVGPR and WISPR filters. In this case, most of the AVGPR results are completely destroyed by the masking. In such a case, one would have to rely on a WISPR gram and conventional gram reading techniques. At least with a WISPR gram this is still possible, while with AVGPR gram it is not.

Figures 7.12b and 7.12d give gram representations of the data for the time period immediately before and after the onset of masking. The top gram (Fig. 7.12b) is from the AVGPR processing

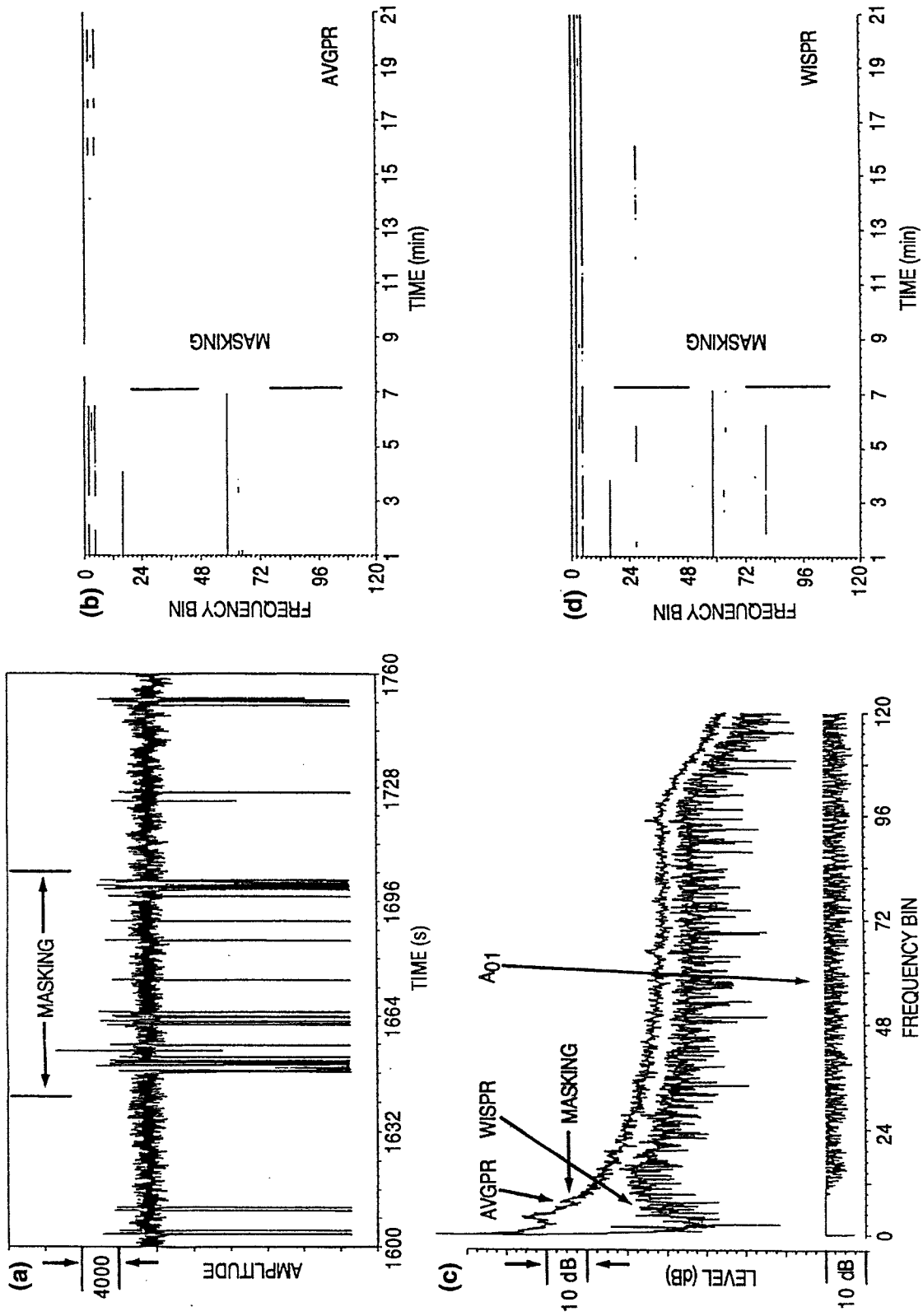

Fig. 7.12 — Gram display of conventional (AVGPR) versus WISPR performance during masking

and the bottom one (Fig. 7.12d) is from the WISPR processing. The AVGPR gram shows only the extremely low frequency line and small traces of two others above it. The WISPR gram shows the first two as continuous, the other one as nearly continuous, and a small trace at much higher frequency. Higher frequencies did not appear in either the AVGPR or the WISPR results. These results clearly demonstrate the value of the WISPR gram in increasing SNR and reducing or eliminating the effects of masking.

Figure 7.13 contains curves similar to Fig. 7.11 except for the masking time period. Figure 7.13a is identical to Fig. 7.12b and has been reproduced to facilitate comparison with the WISPR difference gram in Fig. 7.13b. Lines that appear in the WISPR difference gram are designated as originating from submerged sources. It is interesting to compare the AVGPR gram and its sparse line information with the WISPR difference gram, which contains a wealth of line information at the lower frequencies, all of which have passed the submerged source threshold test.

7.6 Noise Spectrum Equalization (NSE) via Fluctuation-Based Processing to Enhance Submerged Source Detection and Classification

The detection of signals is often determined by the signals exceeding a predetermined threshold. Setting such a threshold, when the background noise has significant variations in level across the frequency band, can be a difficult challenge. That is particularly true in the case of undersea ambient noise, where the noise can vary more than 40 dB across the frequency band from a few hertz to a few kilohertz. The problem is considerably less complicated when the spectrum is prewhitened before the threshold is applied. Such a process removes the large level excursions in the background noise without altering the SNR of the signals that are embedded in the noise. Such algorithms are often called NSE algorithms. It is much easier to set sensible detection thresholds for data that have been prewhitened by an NSE algorithm than data that have not been prewhitened, so much so that it is almost a universal procedure for undersea acoustic data prior to displaying the frequency content on gram displays (time histories of the spectrum analyzed signal data).

There are many different NSE algorithms, each with its advantages and disadvantages. Sometimes the choice of an NSE algorithm is determined by the personal preference of the researcher or by some unique feature or attribute of the algorithm. Here, a new class of fluctuation-based NSE algorithms is introduced that may be more attractive for some applications. The WISPR and AWSUM filters will be used to demonstrate the method of doing this new type of NSE and to illustrate some of the unique and interesting characteristics of the results.

The two new WISPR and AWSUM NSE algorithms are based upon the A_{01} and A_{24} processors, Eqs. 2.5.1 and 2.5.5. Expressed in decibels they become

$$A_{01} = \text{AVGPR} - \text{WISPR}$$

and

$$A_{24} = \text{AWSUM}_2 - \text{AWSUM}_4 .$$

An example of an AVGPR curve, the corresponding WISPR curve, and the resulting A_{01} (difference or NSE) curve is given in Fig. 7.14. The AVGPR curve is the top one, the WISPR curve is in the middle, and the A_{01} curve is at the bottom. Notice that both the AVGPR curve and the WISPR curve are nonwhite (not spectrally flat). However, the A_{01} curve is relatively flat, at least

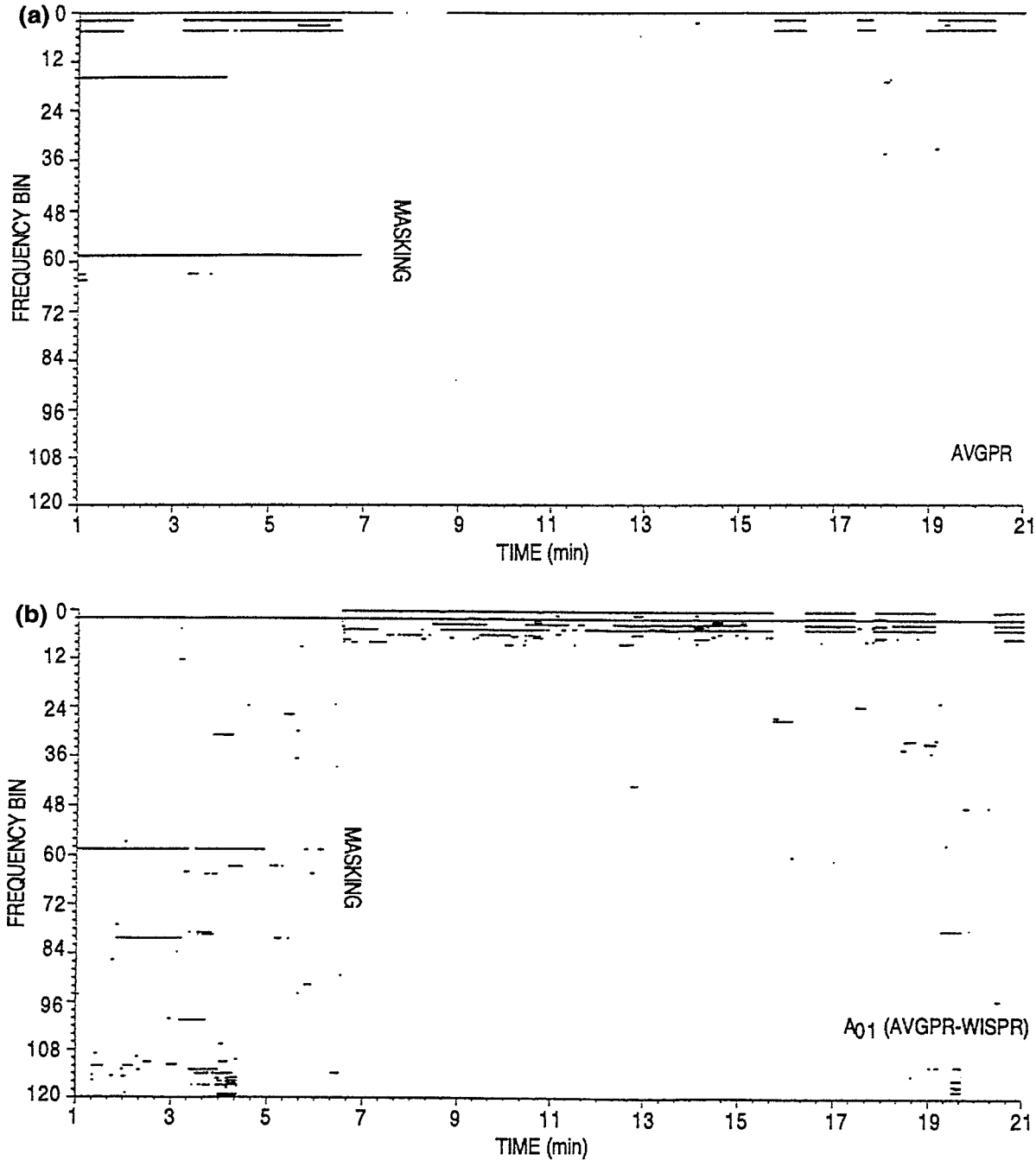

Fig. 7.13 — Gram display of conventional (AVGPR) versus WISPR performance during masking

the bottom part of the envelope is reasonably flat except at the location of the tonal at A. Hence, the final result, A_{01}, is a "white" (flat) curve with a peak extending down from its envelope. The peak at A is significant because it identifies the corresponding signal in the AVGPR spectrum as a highly stable tonal, i.e., a tonal from a submerged source. If the source had not been submerged, the tonal would have been acted upon by the fluctuation generation mechanisms near the surface, and it would have been amplitude modulated and would have had relatively large amplitude fluctuations. In such a case, it would have fallen within the lower amplitudes of A_{01} and been indistinguishable from the noise. Hence, not only did A_{01} processing accomplish the NSE function, it also eliminated the other signals that fluctuated nearly as much as the noise and classified signal A as an amplitude stable, or submerged source, signal.

Figure 7.15 illustrates a case similar to that in Fig. 7.14 except the AVGPR curve is contaminated by high-level transients that occurred during the measurements. The result of the contamination is that there are no tonals visible in the AVGPR spectrum (top curve). The middle curve is the corresponding $AWSUM_4$ result. In this case, the AVGPR and $AWSUM_4$ curves are not separated by a nearly constant amount across the frequency band. Hence, a curve for A_{04} would not be approximately constant. Therefore, A_{04} cannot be used here for NSE. However, a tonal is present in the $AWSUM_4$ curve that is not present in the AVGPR curve. That indicates that something useful can be obtained by using a fluctuation-based signal processor. The bottom curve in Fig. 7.15 is, for display purposes, five times the A_{24}. In this case, the NSE function has been accomplished by the A_{24} NSE algorithm. Furthermore, the A_{24} NSE algorithm was able to identify the tonal at B as one that is highly stable and, therefore, must have originated from a submerged source.

Some very attractive features of the two NSE algorithms (A_{01} and A_{24}) discussed above include:

(a) these NSE algorithms are computationally very efficient,

(b) fluctuating tonals (clutter signals from sources at the sea surface) are eliminated,

(c) tonals from submerged sources are detected and classified as being from a submerged source,

(d) the A_{24} processor provides an NSE algorithm, robust to masking from high-level transients, and

(e) the A_{14} processor has also been successfully used in many applications and is generally preferred over the A_{24} processor. Because of its greater magnitude, a multiplier is not required for display purposes as is necessary with the A_{24} processor.

Spectral plots such as those in Figs. 7.14 and 7.15 show results for a single averaging period. When the results from multiple averaging periods are displayed in a gram type of format, after appropriate NSE, a trace across frequency at a particular time is obtained. Figure 7.16 gives the AVGPR, WISPR, and A_{01} results for a submerged source for a particular time during which grams of the three different statistics (or signal processors) were generated. There are numerous tonals present. Some are from the submerged source and some are from surface ship clutter. Not all tonals from the submerged source are stable enough in amplitude to exceed the submerged source $A_{01} < 1.5$ dB threshold. There are five such tonals, whereas only one would be sufficient to detect the presence of a submerged source.

Along with the clutter, it is possible that some of the submerged source signals were also eliminated because of fluctuations or instabilities in amplitude that were temporary, being induced by either the medium or the temporary instability of the source generation mechanism. Such instabilities come and go with time and are readily apparent when the results are displayed as a gram that covers a significant time period.

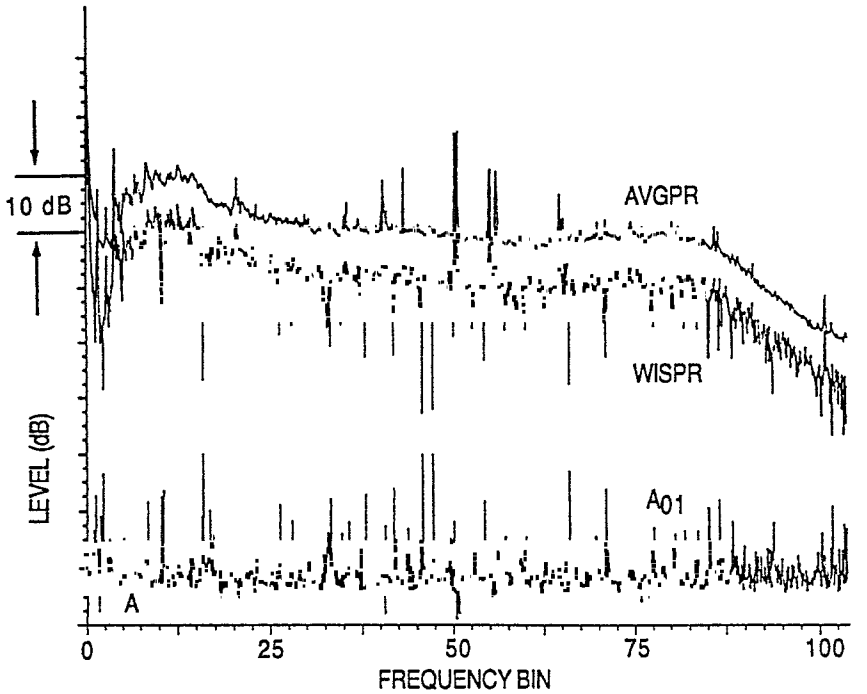

Fig. 7.14 — WISPR used for noise spectrum equalization (NSE) shown for A_{01} processing

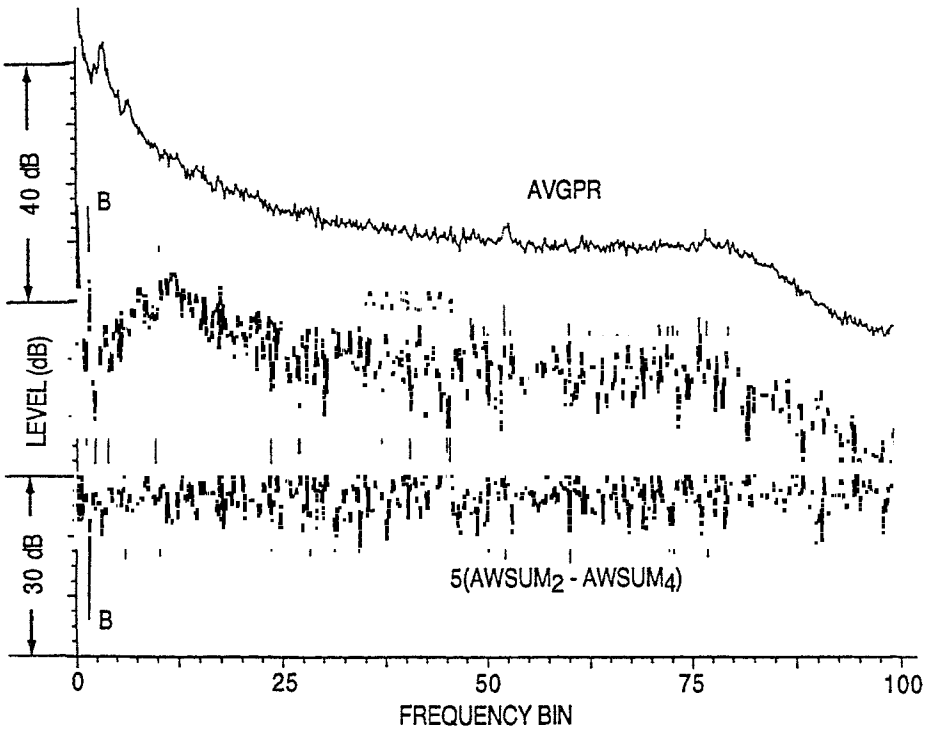

Fig. 7.15 — AWSUM used for noise spectrum equalization (NSE) shown for $5(A_{24})$ processing (these same data are also shown in Fig. 6.3)

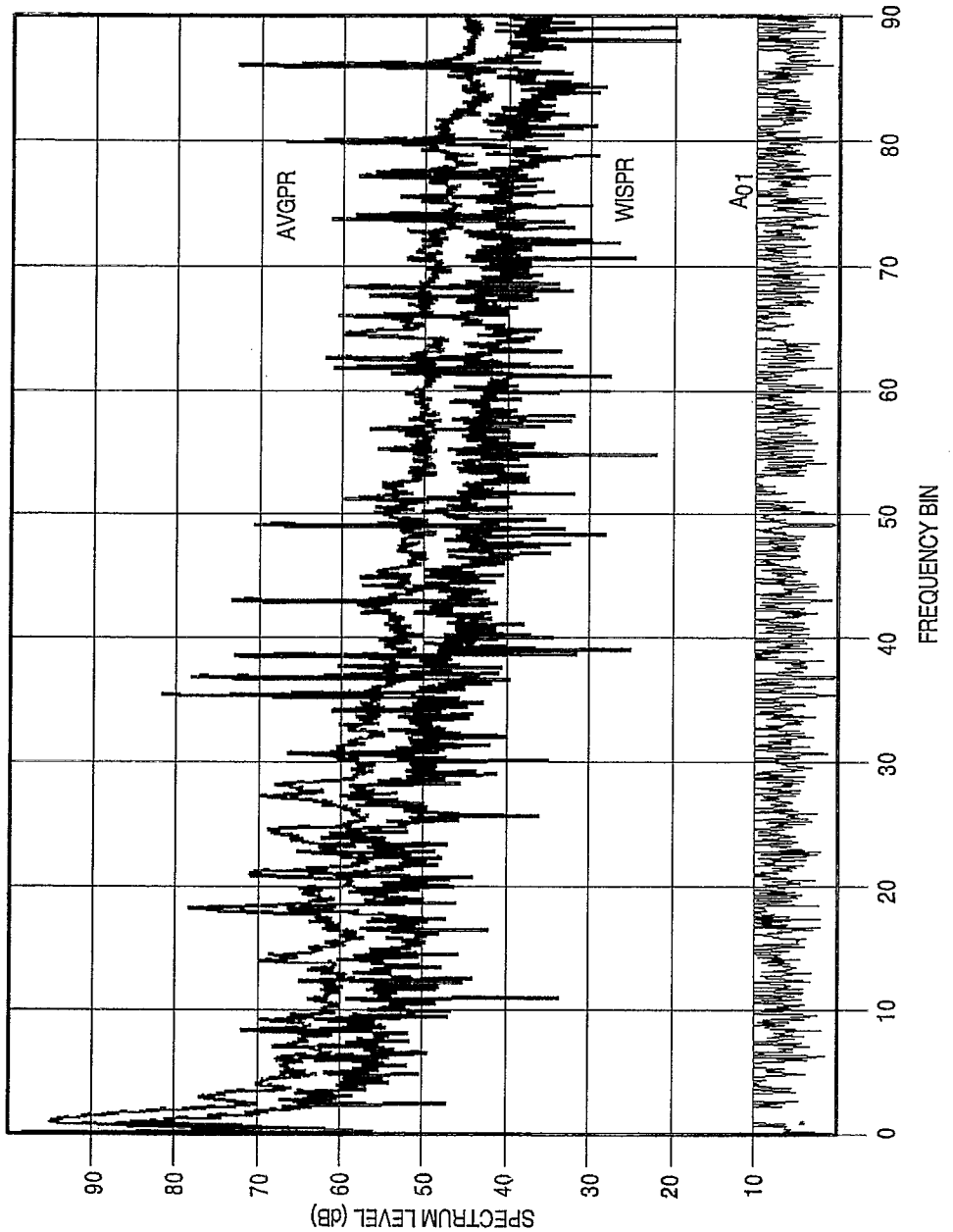

Fig. 7.16 — Spectral results for AVGPR and WISPR processing for a particular time of the gram displays presented in Fig. 7.17

The top three plots in Fig. 7.17 give the gram results for the AVGPR processor (top plot) the WISPR processor (second plot), and the A_{01} processor (third plot). Frequency is on the x-axis and time is on the y-axis. The total time covered is 30 min. Both the AVGPR plot and the WISPR plot show major tonals at a number of frequencies and many minor ones. However, the WISPR plot shows more of each. That is because of the increased resolution of the WISPR processor. The number of tonals plotted can be changed by modifying the threshold level to achieve fewer or more threshold crossings. The previous results to which the WISPR gram are compared were produced using one of the prewhitening filters commonly used to produce a gram.

The A_{01} gram in the third plot is unique as a gram, since it contains only those lines (i.e., tonals) that have passed the submerged source tonal threshold. As a result, the number of lines on the gram are few compared to the many that exist in the previous two grams for the AVGPR (top plot) and the WISPR (second plot) processors. However, each line in the A_{01} plot has a high probability of being from a submerged source. An independent evaluation of the submerged source spectrum by qualified personnel using other analysis products and methods (not included herein) have confirmed that the lines in the A_{01} gram are indeed from a submerged source.

The bottom plot in Fig. 7.17 gives the percent of time that a particular line was present in the A_{01} gram. From that plot, as well as an "eyeball analysis" of the A_{01} gram, it is apparent that some of the tonals received from the submerged source enter and leave periods of high stability. Hence, at any one time, some of the tonals from the submerged source will be amplitude stable and some will not. The time history display provided by the gram format significantly increases the likelihood of detecting an amplitude stable tonal from a submerged source. In addition, the submerged source gram (A_{01} gram) effectively eliminates the clutter and simplifies the detection and classification of the submerged source tonals.

The A_{01} and A_{14} NSE algorithms can be generalized to two dimensions with no change in the nature of the computations with just an increase in the number of cells (or bins) that the equations are applied to. For example, there were 512 frequency cells within which the equations were applied to arrive at the 512 results that made either the A_{01} or the A_{14} curves. Analogously, the beam number spectral surface in Fig. 7.18 contains 200 frequency bins in the vertical (0.1-Hz BW resolution) and 256 beam bins in the horizontal, or about 5×10^4 beam frequency cells. It is then a simple matter to threshold the corresponding A_{01} and A_{14} surfaces generated, as was done in the three previous examples (Figs. 7.14, 7.15, and 7.16) to identify the signals from submerged sources and to eliminate the numerous signals from the surface ships (clutter) that would otherwise dominate the display, as is the case of the top two plots in Fig. 7.17. The result of that thresholding for the A_{01} surface is given in Fig. 7.19. The dot at about 15 Hz, beam number 101, and the bar (a spread-out dot) at 5.2 Hz, beam number 249, correspond to the tonals that are identified as having originated from submerged sources. Indeed, this was independently confirmed to be the case. All of the other signals from the numerous surface ships (see Fig. 7.18) that constitute a considerable clutter problem for other NSE algorithms have been eliminated. Identical results have been obtained by the A_{14} algorithm. The authors know of no other two-dimensional NSE algorithm.

One extremely attractive feature of these NSE algorithms is their simplicity. Normally, one would expect the computational load and the complexity of an NSE algorithm to increase with the square of the dimension. In the case of A_{01} and A_{14}, the computational load increased by that factor, but the complexity didn't increase. Furthermore, they both have the capability of identifying

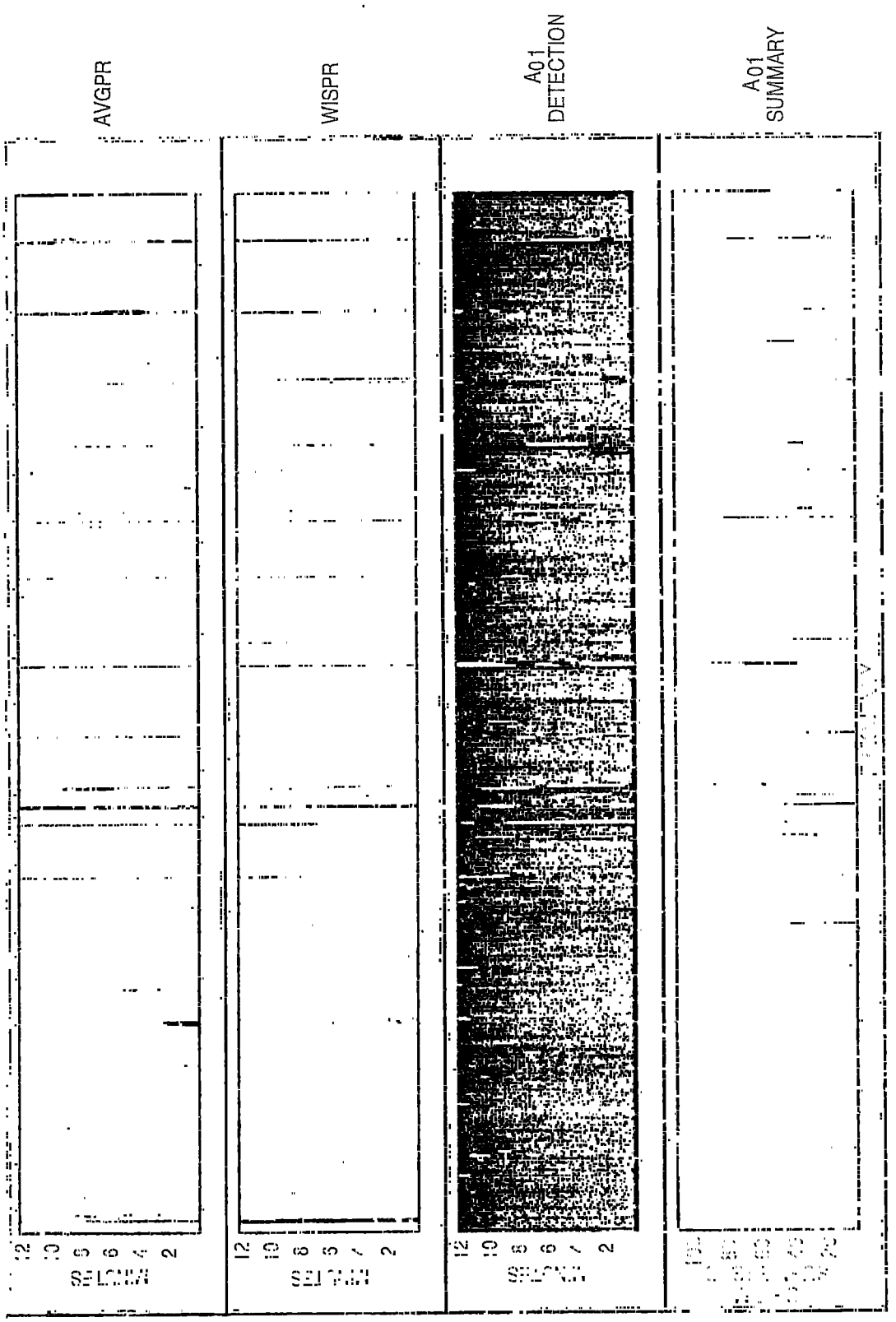

Fig. 7.17 — Gram displays demonstrating results where WISPR processing has been used for noise spectrum equalization (NSE). The top plot is for conventional processing (AVGPR), the second plot is WISPR processing, and the third plot is a display corresponding to the times where the A_{01} difference is above the detection threshold. The bottom plot shows the percentage of time that the A_{01} detection occurred for each frequency in the third gram plot.

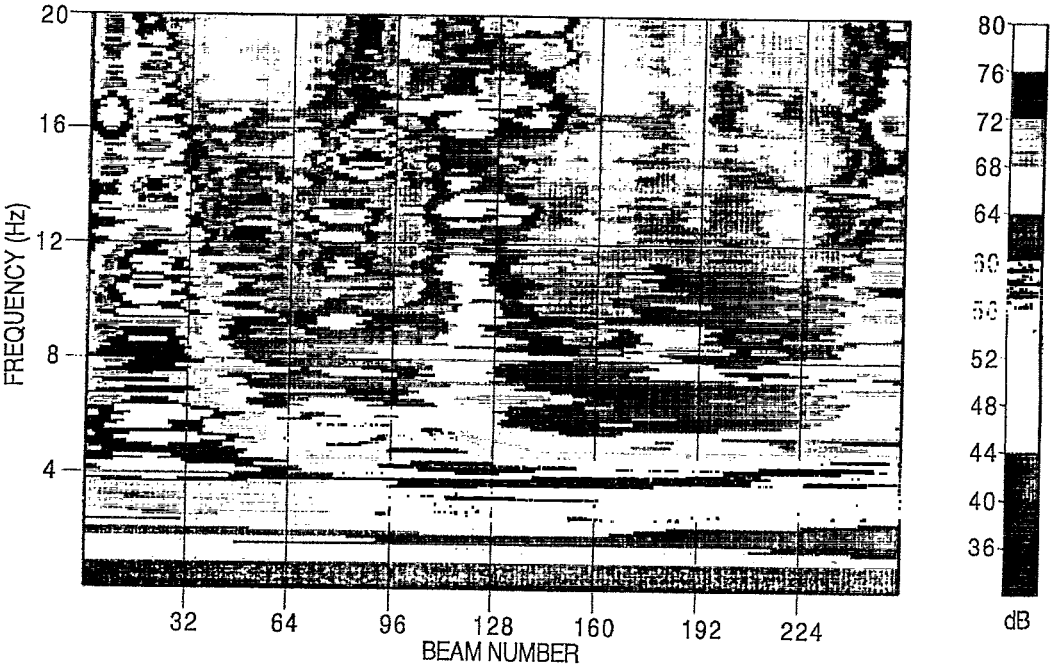

Fig. 7.18 — A two-dimensional representation of the result of conventional processing (AVGPR) presented as a beam number/spectral surface

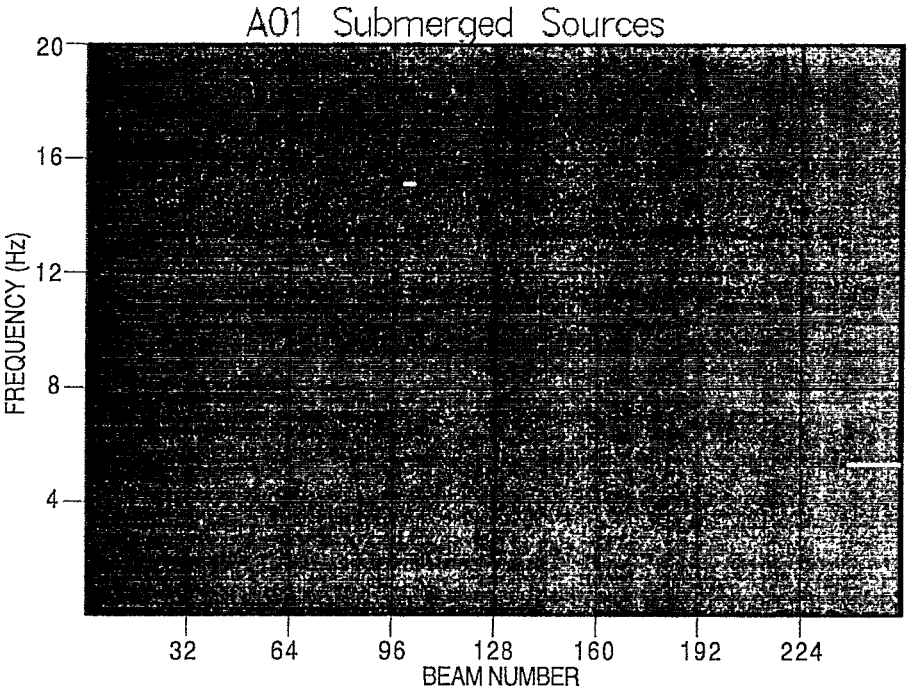

Fig. 7.19 — A two-dimensional representation of the result of A_{01} processing for noise spectrum equalization (NSE) when applied to the beam number/spectral surface. Results are plotted for only those instances passing the submerged threshold test.

tonals from submerged sources, although A_{14} is more robust to contamination than is A_{01} as discussed earlier.

7.7 Summary

These advanced applications presented should provide insight into the far reaching applications of fluctuation-based processors. It is quite possible that these processors can be applied with excellent results in many areas that have not been considered at the present time.

8.0 WISPR FILTER COHERENT PROCESSING APPLICATIONS, WISPR III_k AND A_kCSDM

8.1 Introduction

All of the applications developed in earlier chapters have applied the WISPR and related processors to time sequences of spectral power. In those applications, the spectral results from FFTs or DFTs were converted to power (magnitude squared) before processing. Therefore, the applications discussed earlier were not capable of exploiting information contained in the phase information. Two techniques incorporating the WISPR philosophy that utilize the phase information are the WISPR III_k and the AWSUM Cross-Spectral Density Matrix (A_kCSDM) processors. The WISPR III_k processors achieve coherent summation utilizing a specialized algorithm for phase correction; whereas, the A_kCSDM processors achieve coherent summation through the properties of the cross-spectral density matrix.

8.2 The WISPR III_k Processor

The WISPR Filter, Eq. 2.4.1, is an incoherent signal processor that exploits the fluctuations in amplitude to achieve enhanced performance. The WISPR III_k processor is an analogous processor that has been developed to exploit fluctuations present in the signal phase information as well. The difference between the two is that instead of using only the time histories of the magnitudes as the WISPR Filter does, the time histories are treated as vectors, and thus WISPR III_k utilizes both the magnitude and phase histories. Successive realizations of the vector quantities, shifted appropriately in phase, are added to achieve coherent gain and divided by their magnitude to get fluctuation gain. Powers other than 1 for the magnitude may be used to produce higher order $WISPR_k$ III processors, analogous to extending the WISPR Filter to obtain the higher order $AWSUM_k$ Filters.

One of the key tasks associated with this processor is to determine an appropriate phase shift. Typically, complex spectra from an FFT or DFT of temporal sample sets, or the result from a beamformer, are obtained where each is offset by a fixed time, Δt, which is a function of the sample rate, temporal FFT size, and the percentage overlap. In general, for steady tonal sources, i.e., those tonals with a steady frequency-generating mechanism, the initial phase of the tonal will systematically advance or delay at the beginning of each temporal sample set, a signal processing artifact associated with the discrete sampling. The complex spectral results for those frequency bins nearest to a particular tonal will also partially reflect the systematic phase shift of the tonal. Therefore, to avoid cancellation of out-of-phase segments of the same tonal during a complex summation, any systematic phase shift must be removed from the complex spectral value nearest the tonal frequency. This is necessary regardless of the type of coherent summation that is performed; the conventional summation or ones based on the WISPR philosophy. One method for accomplishing this task is described by George and Wagstaff.[2] In WISPR III_k processing, an algorithm is invoked

to remove the systematic phase shift artifact, enabling subsequent coherent processing. The residual variations in phase constitute the phase fluctuations utilized by this processor.

8.2.1 The WISPR III_k Processor Definition

Let the set $\{z_n\}$ ($n = 1,2,3, ..., N$) denote the phase shifted (to ensure coherent tonal summation) complex spectral values from a single hydrophone or a single beam at a particular frequency, and let Φ_n denote the shifted phase values. The estimate of a signal corresponding to a particular frequency bin for that sample period is represented by

$$z_n = (r_n \cos \Phi_n + jr_n \sin \Phi_n) . \tag{8.2.1}$$

The set average value, s_{avg}, is

$$s_{avg} = \left[\frac{1}{N} \sum_{n=1}^{n=N} \frac{z_n}{r_n^k} \right] . \tag{8.2.2}$$

Using these results, the WISPR III_k processor is defined by

$$WISPR\ III_k = \left[\left(\frac{1}{N} \sum_{n=1}^{n=N} r_n^{-k} \right)^{-1} \sqrt{s_{avg} s_{avg}^*} \right]^2 . \tag{8.2.3}$$

Note: The above three equations are developed in App. A.7 where all terminology is fully defined.

One important feature of the averaging of the WISPR III_1 processor is that the weighted phase factors, z_n/r_n^1, from all N samples lie on the unit circle and contribute equally to the average, regardless of the original sample amplitudes, r_n. This minimizes the effect of large amplitude fluctuations in the noise, allowing the phase factors (due to random noise) to add incoherently and cause significant cancellations of each other. In contrast, as a result of preprocessing to achieve coherent addition of the nearly stable tonal, the phase factors will be relatively constant. This coherent addition will yield a value closely representative of the stable tonal.

In the case of the more general WISPR III_k processor ($k > 1$), the phase factors, z_n/r_n^k, are weighted even more heavily in favor of low amplitudes, r_n. This is expected to provide an even greater selection for the noise phase components and to generate additional noise reduction. This approach still needs to be investigated and offers potential for additional SNR gain through higher suppression of fluctuating signals and noise.

8.2.2 An Example of Processing Using WISPR III_1 as a Beamformer Post Processor

The present formulation of the WISPR III_1 Filter is valid for beamformed output as a post processor similar to the WISPR Filter. This is illustrated by Fig. 8.1, which contains four plots comparing the WISPR Filter and WISPR III_1 Filter results at two different frequencies. Plots (a) and (c) are for the lower frequency, whereas plots (b) and (d) are for the higher frequency. The top curve in each plot is the output of the AVGPR processor. The middle curve in the top two plots is

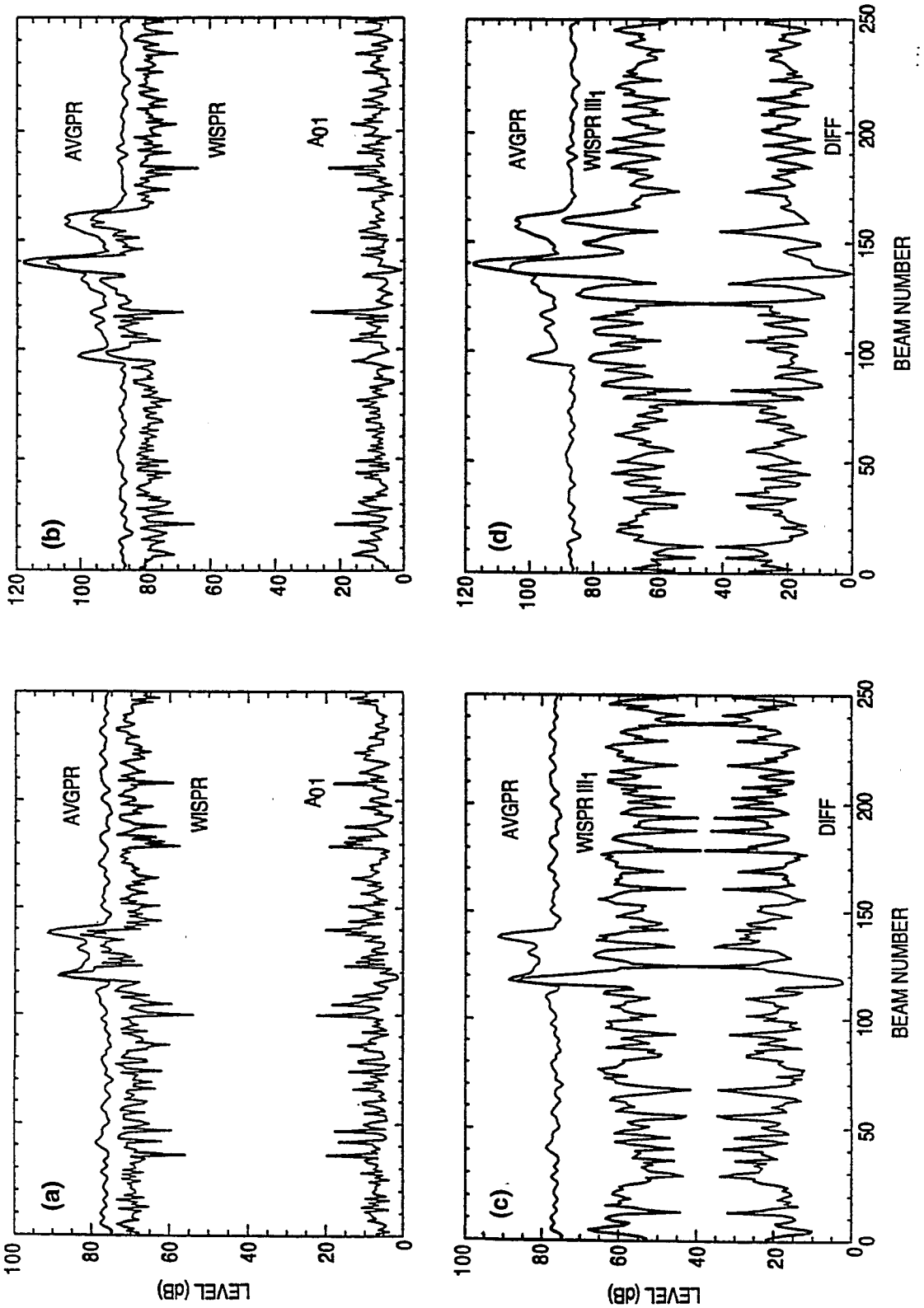

Fig. 8.1 — A comparison of WISPR and WISPR III_1 processing: (a) and (b) AVGPR – WISPR (A_{01}) processing, (c) and (d) AVGPR – WISPR III_1 difference processing

the WISPR Filter result, and in the bottom two plots the WISPR III_1 Filter result. The average SNR gain is obtained from the bottom curves, which is the difference between the other two curves in the same plot. At the lowest frequency, the SNR gain of the WISPR Filter (plot (a)) is about 6 dB, while for the WISPR III_1 Filter (plot (c)) it is about 15 dB, an improvement in gain of about 9 dB due to the coherent nature of the WISPR III_1 Filter. The corresponding gain at the higher frequency is about 6 dB. There was another rather interesting result. At the low frequency, the WISPR III_1 Filter noise attenuation caused the stable signal to remain as the sole prominent peak in plot (c). The results at the higher frequencies in plot (d) were similar but less dramatic.

The excellent noise fluctuation suppression characteristic of the WISPR III_1 Filter suggests that it would make a very attractive automated detection algorithm. As a result of the very high gain achieved, the submerged source detection threshold could probably be set at higher levels than is possible with other processors without generating excessive false alarms.

8.3 The AWSUM Cross-Spectral Density Matrix, A_kCSDM Processor, and the WISPR Cross-Spectral Density Matrix, WCSDM = A_1CSDM Processor

Many forms of signal processing for multiple sensors strive to achieve coherent processing through the properties of the cross-spectral density matrix (CSDM). Successive realizations of the CSDM are averaged to obtain statistically stable results. One application of the CSDM is to form spatial beams with reduced noise and ultimately increased SNR. If an improved CSDM average can be devised, it should be possible to enhance results of processing that is dependent upon the CSDM. This can be accomplished with the A_kCSDM processor, which has objectives similar to those of the WISPR III_k processor previously described. The rationale for the need to ensure that summations of complex spectral values are coherent, presented in App. A.7 for the WISPR III_k processor, applies equally to the A_kCSDM processor. However, coherent processing, in this case, is accommodated via the CSDM formalism.

8.3.1 Processor Definition

Initially consider the quantity, $Z_{l,m}$, the averaged value ordinarily used by a CSDM beamformer just before beam steering and power summation. This quantity for the simplest (conventional) type of average may be defined as

$$Z_{l,m} = \frac{1}{T} \sum_{i=1}^{i=T} Z_{l,m,i} \; . \tag{8.3.1}$$

The A_kCSDM processor is defined by

$$A_k CSDM_{l,m} \equiv \left[\frac{1}{T} \sum_{i=1}^{i=T} r_{l,m,i}^{-k} \right]^{-1} \left[\frac{1}{T} \sum_{i=1}^{i=T} Z_{l,m,i} \, r_{l,m,i}^{-k} \right] . \tag{8.3.2}$$

Note: The above two equations are developed in App. A.8 where all terminology is fully defined.

The A_kCSDM processor, for order k (typically, 1, 2, 3, or 4), is accomplished by the simple replacement of the quantity, $Z_{l,m}$, with the new average $A_k CSDM_{l,m}$, prior to beam steering and

summation to form the beam output. WCSDM is the special case for $k = 1$, i.e., $A_1CSDM_{l,m}$, analogous to the WISPR Filter equalling $AWSUM_1$ as explained in Sec. 2.0.

8.3.2 Comparison of A_1CSDM (or WCSDM) with CSDM Beamforming

One case used to compare the A_1CSDM (or WCSDM) processor with conventional averaging for a CSDM beamformer was generated by the simulation of a 50-channel horizontal array. The signal from an actual single hydrophone was used as the output from all channels to simulate a signal on broadside. Figure 8.2a and b present the conventional CSDM and WCSDM beamformed results for this case, respectively. These results are overlaid in the inset plot in the second figure. The large peak at beam number 125 corresponds to the broadside beam, which is "captured" by the broadside signal. In Fig. 8.2a, the first few sidelobes are evident near the broadside beam and disappear in the relatively uniform noise of the system. The peak sidelobe response is 32 dB down from the main beam arrival, typical of Hann shading. The WCSDM results presented in Fig. 8.2b show the same broadside beam response, but the sidelobes near the main lobe and the system noise are different. The sidelobes near the main lobe are better defined, and the self noise has been significantly reduced along all beam number segments, and more dramatically along some. What remains appears to be some form of sidelobe structure that is well below the conventional results, quite obvious in the inset plot.

In a second case, a similar set of figures was made where the original hydrophone data (without artificially injecting one hydrophone's data as in the previous case) were used. Figure 8.3a and b give the results for the conventional CSDM and the WCSDM, respectively. An insert is likewise included in Fig. 8.3b of the superposition of the two plots. The high-level distributions of energy at the right hand sides correspond to the signal. Although it is not as "clean" as in the previous case, where an identical signal was injected into all channels, the results generated from the WCSDM show that there is substantial reduction in the noise, but not in the signal. Hence, the result is generally an increase in SNR of more than 8 dB, and in particular regions, more than a 20 dB decrease in the noise.

8.3.3 Comparison of WCSDM Beamforming with WISPR and $AWSUM_4$ Processing

Figure 8.4 compares the SNR gains while beamforming with three levels of WISPR type processing. The first column of figures corresponds to WISPR and conventional (power averaging) processing of 144 channels of array data at 29 Hz (top plot) and 13 Hz (bottom plot) for a time when a signal was near broadside (near beam number 128). The top curve in each plot corresponds to the average power level across the array for a 4096-point FFT and a sample rate of approximately 200 Hz. The bottom curve in each plot is the corresponding WISPR curve. The middle column of plots gives similar results for $AWSUM_4$ processing. The last column of plots corresponds to the same 144 channels of hydrophone data that were used to get the previous two sets of plots, but instead, those data were beamformed using a WCSDM beamformer that had the same steering angles as in the two previous columns of plots. As before, the top curve in each row of plots is the average power level. It is identical in all three sets of plots of a given row. The lower curves in the third column of plots, which appears to be a series of signal and noise level spikes, is the corresponding WCSDM result.

There are several important features that these three columns of plots illustrate. First, the signal level (near beam number 128) is about the same for the two different types of processing contained in each of the six plots. Hence, the signal suppression of each of the processors (WISPR, $AWSUM_4$, and WCSDM) compared to the AVGPR is small. Second, the noise is suppressed much more than

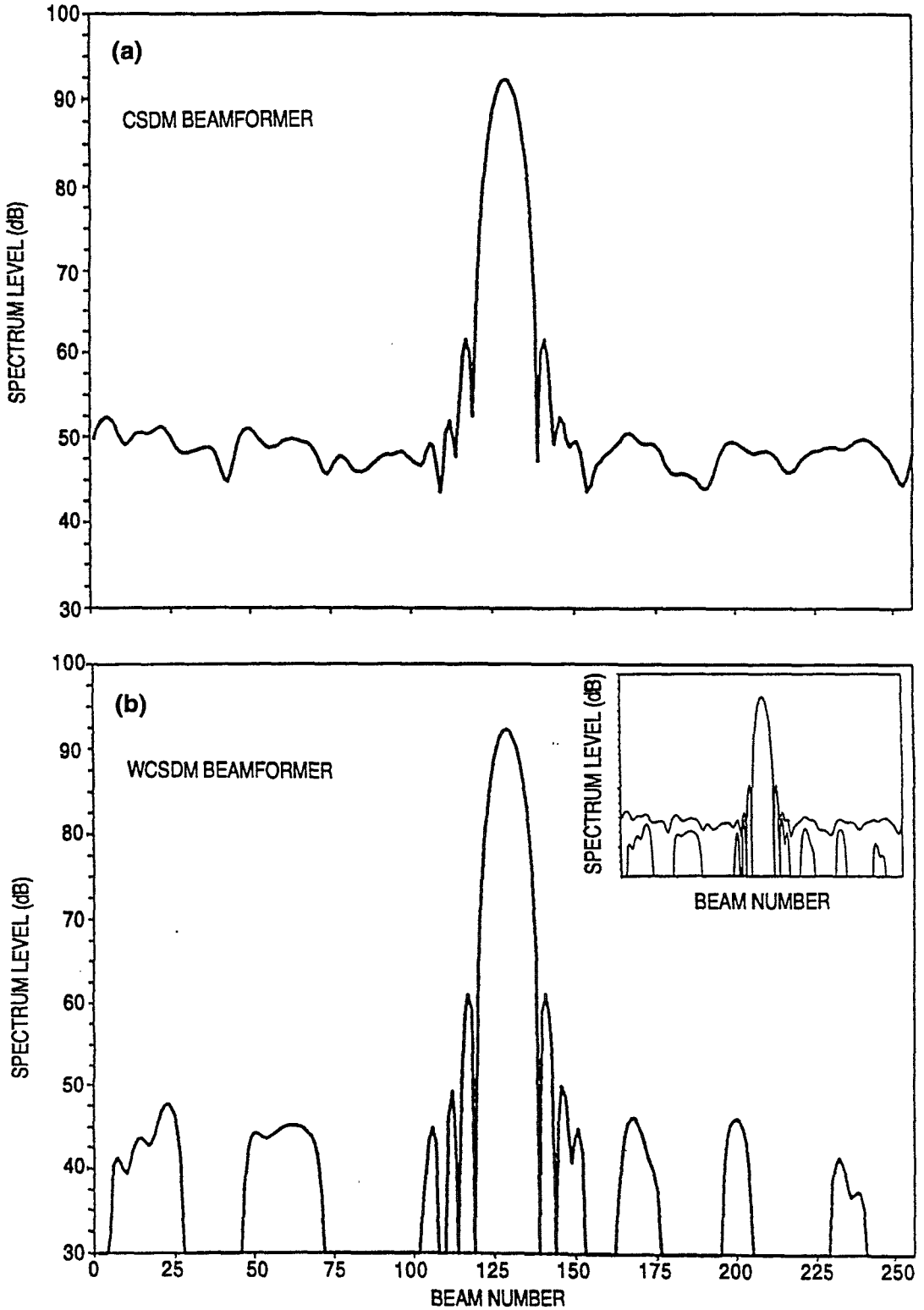

Fig. 8.2 — WISPR processing: WCSDM versus CSDM beamforming

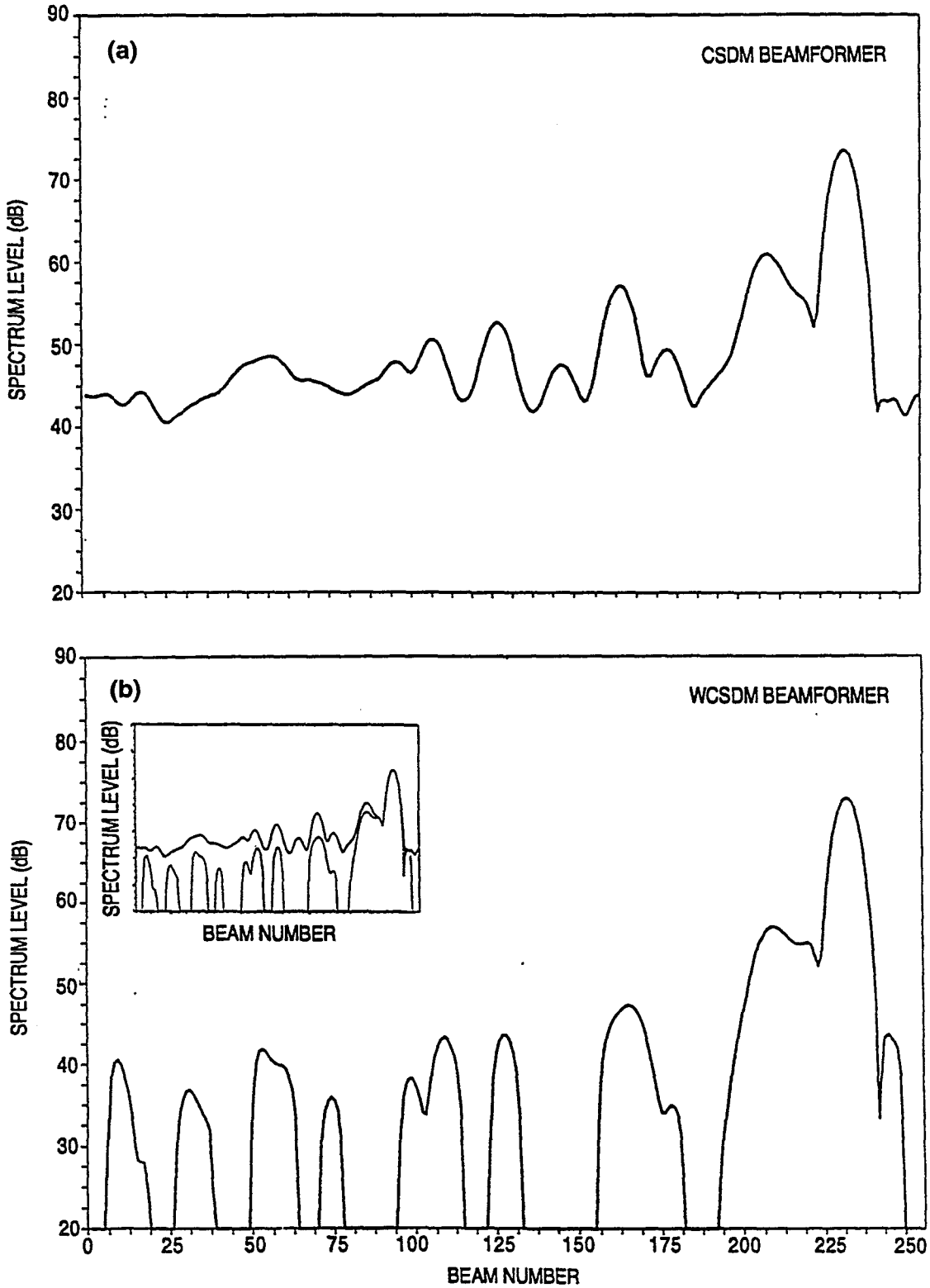

Fig. 8.3 — WISPR processing: WCSDM versus CSDM beamforming

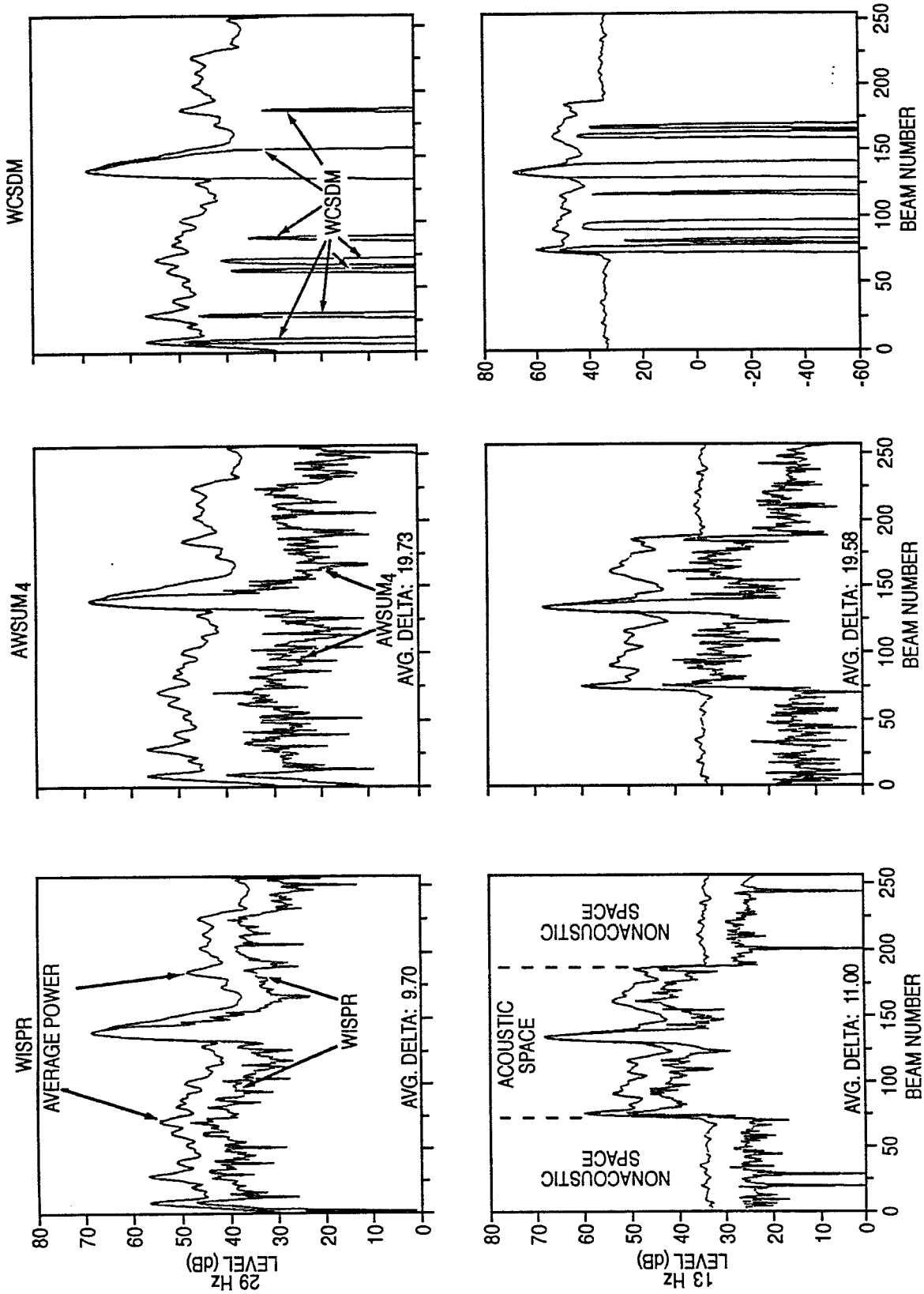

Fig. 8.4 — Three levels of WISPR processing for a 144-element array at 29 and 13 Hz

the signal, which gives a SNR gain to the processors (WISPR, $AWSUM_4$, and WCSDM, bottom curves) compared to the AVGPR. In the case of WISPR processing (first column of plots), the SNR gain is approximately 9.6 dB. For the $AWSUM_4$ processing (second column of plots), it is about 19.6 dB. However, for the WCSDM processing (third column of plots) it is difficult to estimate because most of the WCSDM curve is suppressed more than 100 dB and does not show on the plot. It appears that the majority of the noise is being cancelled by the WCSDM processing, rather than merely being suppressed.

Finally, the overall noise suppression, or elimination capability of the WCSDM processor, is very impressive. There are broad regions in beam number space (related to regions in azimuth) in which the noise is virtually gone. It is especially evident in the 13-Hz results in which approximately 57% of the beams are in the nonacoustic domain. In this example, all of the nonacoustic noise has been eliminated. This characteristic was also the case for other frequency resolutions (0.2 to 0.025 Hz) and other apertures (9, 18, 36, 72, and 128 elements).

9.0 COMBINING THE WISPR FILTER WITH OTHER HIGH-RESOLUTION PROCESSORS

9.1 Introduction

Several algorithms have been developed for the specific purpose of increased resolution in beam number space. Two of these, the Wagstaff-Berrou Broadband (WB^2)[3] signal processor and the newly developed Directivity Improved Estimation Technique (DIET)[4] can be further enhanced when combined with fluctuation-based processors such as the WISPR Filter and other closely related processors to achieve additional SNR gain. Since each of the above techniques are described in detail elsewhere, only the results will be presented here.

9.2 High Gain and Resolution with the Combined WB^2 and WISPR Processors

Combining the WB^2 signal processor algorithm with the WISPR processor simultaneously increases the spatial resolution and SNR gain. The four plots presented in Fig. 9.1 provide interesting examples of this capability. Each plot contains two curves. The top curve represents AVGPR processing results from 200 consecutive outputs from a 64-beam double FFT beamformer. The real acoustic space is contained between beam numbers 32 and 48. The nonacoustic, or virtual, domain lies outside that region. The bottom curves in each plot, labeled WB^2, WISPR, WISPR(WB^2), and $AWSUM_4$(WB^2), correspond to processing results of these same data by those processors. Each of these four plots illustrates specific characteristics of the processors:

(a) Upper left plot – The WB^2 gain achieved for the signal was only about 5 dB. However, that gain is actually a result of confining the source power to a smaller region in beam (or azimuth) space and not a result of a gain against the general background.

(b) Upper right plot – Little spatial resolution enhancement was achieved by WISPR processing near beam number 34, though the SNR gain improvement is obvious, approximately 7 dB. Even though the definition of some of the sources in the background noise has improved slightly, WISPR is far from qualifying as a high-resolution processor. Unlike WB^2, the gain of WISPR is due to suppressing the background noise, not from enhanced resolution. In Sec. 6.3.1, the WISPR Filter was shown to enhance spatial resolution over AVGPR for low SNR signals, equivalent in some cases to arrays of 2× aperture. The spatial resolution enhancement in that case resulted from suppression of fluctuations caused by interference of closely spaced arrivals. This particular example,

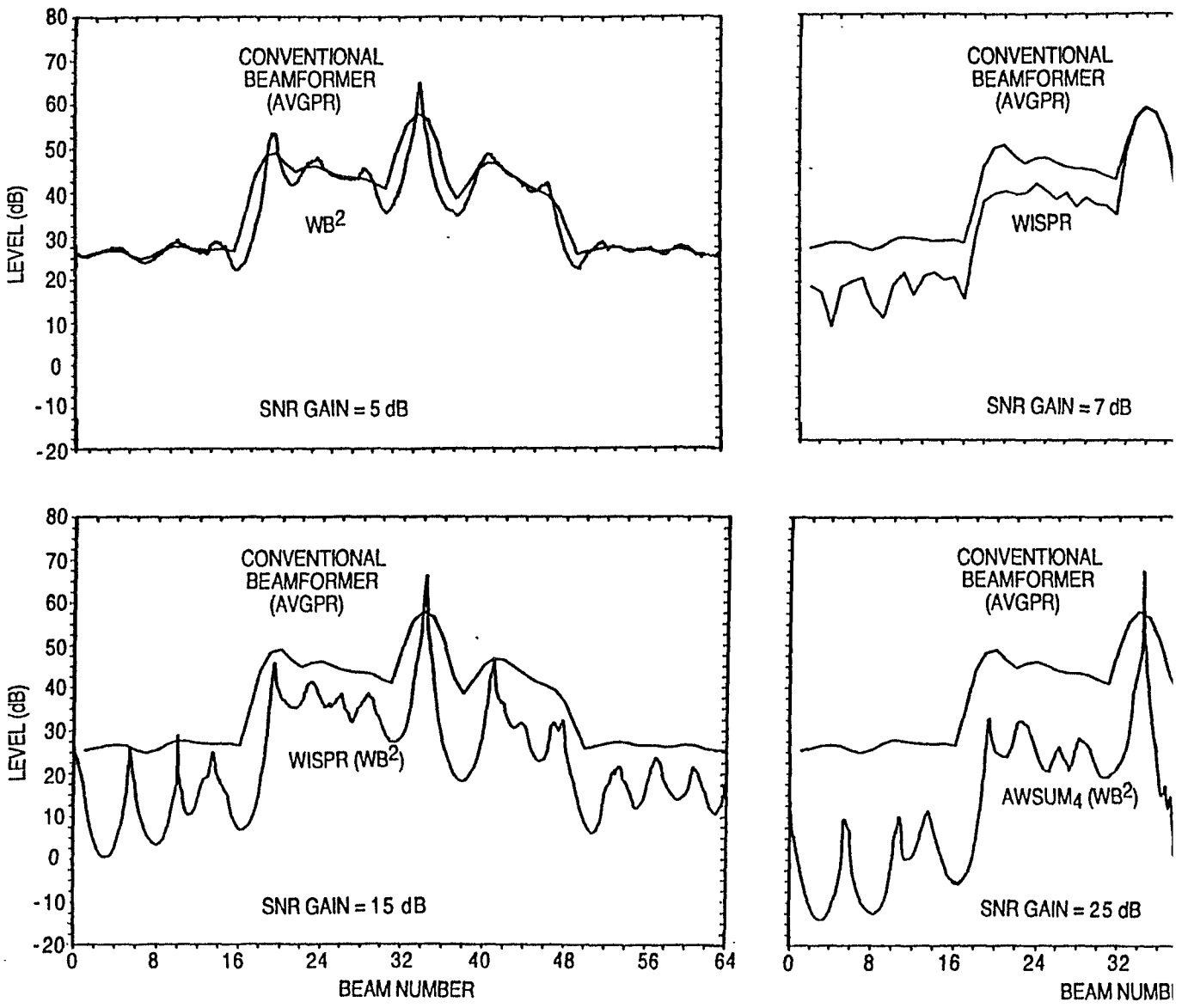

Fig. 9.1 — High resolution – high gain: WISPR (WB^2), $AWSUM_4$ (WB^2)

relatively free from this effect, with a strong single arrival dominating the lobe at beam 34, was selected to enable easy identification of the impact of WB^2 when used in combination with WISPR.

(c) Lower left and lower right plots – A signal processor that provides both high gain and high resolution ought to be an attractive processor for some underwater sonar applications. Since WB^2 provides high resolution and WISPR provides high gain, it seems that the combination of the two could produce high resolution and high gain. This concept was tested on the same data previously discussed, by first forming 200 WB^2 high-resolution estimates and then passing those through either the WISPR Filter or the $AWSUM_4$ Filter. This was done on a beam angle basis, since the original 64 discrete beams are expanded to about 1024 beam noise density points in the WB^2 output. The results for WISPR (WB^2) and $AWSUM_4$ (WB^2) are included as the lower curves in the left and right plots, respectively. In the case of the WISPR (WB^2) result, the SNR gain is about 15 dB, 3 dB better than WISPR (7 dB) plus WB^2 (5 dB), and the resolution is also better than it is for WB^2 alone. The same is true for the $AWSUM_4$ (WB^2) result, but the gain is enhanced by an additional 10 dB over the WISPR (WB^2) result.

Figure 9.2 shows similar results to those of Fig. 9.1 for an array with an aperture approximately 2.5 times longer than the previous one. Hence, the beamwidths are reduced by the same factor. In this case, the corresponding gains go from about 4 dB for WB^2 alone to about 14 dB for WISPR (WB^2) and to about 22 dB for $AWSUM_4$ (WB^2). As the aperture increases and the beamwidths get narrower, the gain achieved by WB^2 is less. That accounts for the WISPR (WB^2) and $AWSUM_4$ (WB^2) gains being less for this case than the previous one. However, it is still rather impressive.

9.3 High Gain and Resolution with the Combined DIET and WISPR Processors

Figure 9.3a gives the temporally averaged output power of the beamformer in decibel levels (designated AVGPR). The x-axis is beam number and the y-axis is decibel level. There are at least six identifiable local maxima, which are due to various sources in the acoustic environment, most likely surface ships. There are two arrows at approximately beam number 480. They mark the location in beam number space of a signal that is due to a submerged source. Given only the AVGPR curve, it would not be possible to detect the presence of the signal or to identify its location in beam number space. Figure 9.3c contains the same AVGPR curve that is in Fig. 9.3a and the arrows that mark the location of the signal. The other curve, labeled WISPR, is the corresponding result from the WISPR processor. The difference between the two curves is the WISPR suppression relative to the average power (AVGPR) that results from WISPR processing. It is referred to herein as the A_{01} algorithm, and its result is plotted in Fig. 9.3b. The source location may be determined from the A_{01} curve. When the A_{01} curve approaches the x-axis (y = 0 dB) within 1.5 dB, the signal is considered to be sufficiently stable in amplitude to have come from a submerged source.

When the WISPR curve in Fig. 9.3c is compared to the AVGPR curve in the beam number region near the arrows, it is evident that the WISPR processor has separated the signal from among the noise and has achieved substantial SNR gain in the process. Furthermore, the spatial resolution of the signal has improved to the point that it can be identified as a separate entity, something that is not the case in the AVGPR curve. However, although the WISPR result provides improved resolution for the signal, it still cannot be considered high gain.

Figure 9.3d contains three curves. One is the AVGPR curve and the other two involve the WB^2 high-resolution algorithm. The top curve is the one that is due to WB^2. The improvements in the resolution at the location of some of the peaks in the AVGPR curve are obvious in the WB^2 result, and the modest amount of gain is also obvious. Unfortunately, the resolution (identification) and

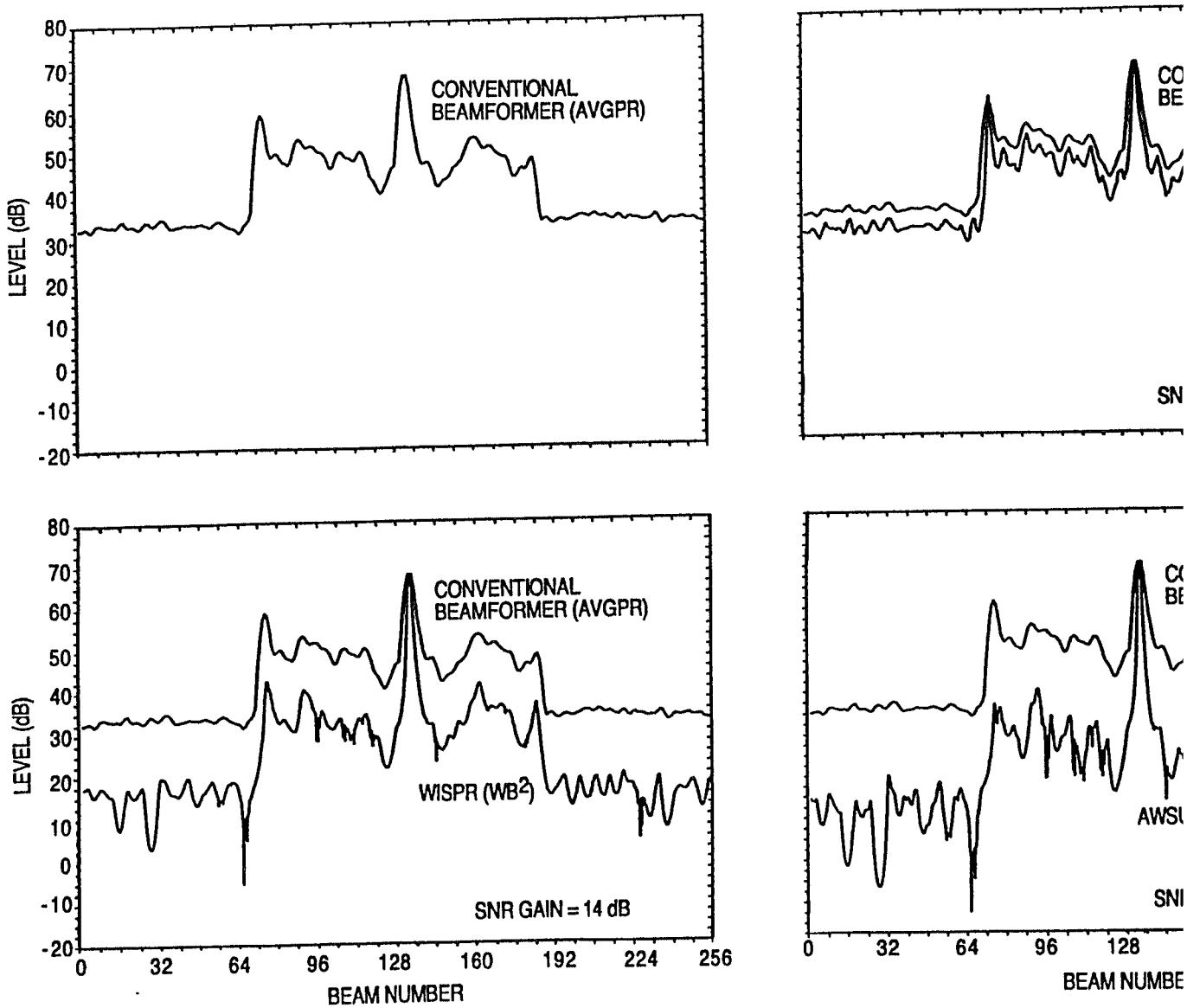

Fig. 9.2 — High resolution – high gain: WISPR (WB^2), $AWSUM_4$ (WB^2)

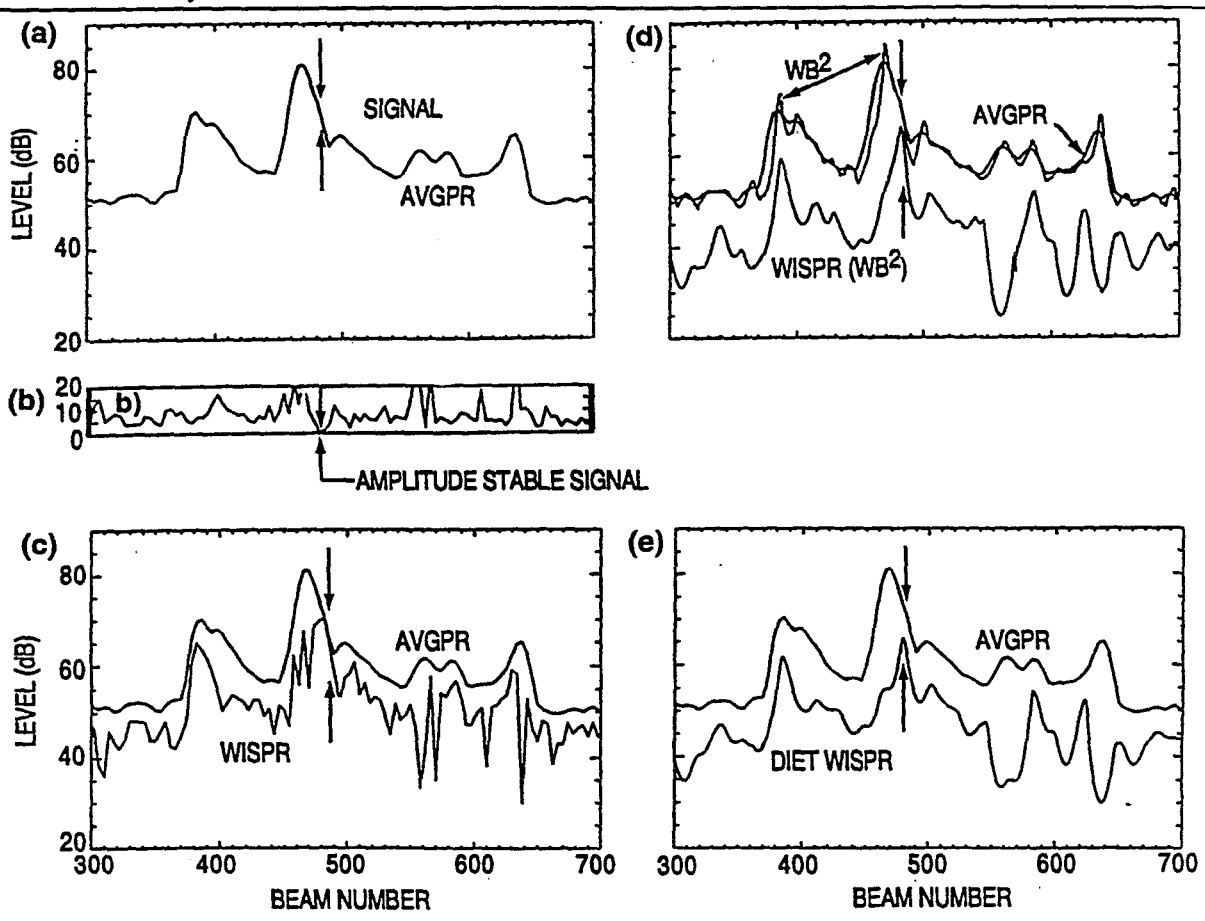

Fig. 9.3 — High gain – high resolution algorithms: WISPR (WB^2) and DIET WISPR

the SNR gain of the buried signal have not been improved by WB^2. Notice the lack of change in the immediate region of the two arrows that identify the location of the submerged source signal.

The bottom curve in Fig. 9.3d, designated WISPR (WB^2), was obtained by combining the WISPR and the WB^2 algorithms. That was accomplished by generating a WB^2 curve for every FFT output and then applying the WISPR algorithm across the set of WB^2 curves at each resolution point across the beam number plot. (Note that the resolution of the WB^2 output across the plot is a factor of four greater than the resolution in beam number.) In this case, the WISPR (WB^2) curve has about the same resolution as the WB^2 curve, but some of the peaks are at different places than in either the AVGPR curve or the WB^2 curve. The reason for this is that the WB^2 and AVGPR algorithms are not sensitive to the fluctuations, while the WISPR (WB^2) algorithm is sensitive to fluctuations. Hence, when a submerged source signal fluctuates less than clutter signals and noise, it will be attenuated less by the WISPR processor than will the clutter signals and the noise. The net effect is that there will be an enhancement in the SNR and a more accurate localization of the stable (i.e., less fluctuating) submerged source signals. For example, the peak in the WB^2 result that is close to the two arrows is actually co-located with the peak in the AVGPR curve. On the other hand, the peak in the corresponding WISPR (WB^2) curve is at the exact location of the arrows, where it needs to be. In addition, it has the approximate magnitude (level) that it should have. Furthermore, the SNR for the real submerged source signal peak (at the arrows) has been increased dramatically by the WISPR (WB^2) algorithm, compared to the AVGPR result where it is not visible at all. The SNR of the submerged source signal in the AVGPR result is obviously <0 dB.

It is still not readily identified in the WISPR results of Fig. 9.3c, but the main peak in the noise beam has been suppressed by about 15 dB. Furthermore, the level of the peak may not be much different from the WISPR result in Fig. 9.3c, but the resolution in the WISPR (WB^2) result has been significantly enhanced.

Figure 9.3e provides a comparison of a new algorithm called the DIET via the WISPR algorithm (DIET WISPR) with the AVGPR result. In this case, the location of the stable signal is identified correctly and the SNR gain has been increased sufficiently to produce a well defined peak where it should be. When the DIET WISPR curve in this figure is compared with the corresponding curve for WISPR (WB^2) in Fig. 9.3d, considerable similarities can be seen. The most important are that the signal has been correctly localized and the SNR gain enhancement has been sufficient to produce a well identifiable peak where there is not a peak in the AVGPR curve.

The similarities between the curves for the WISPR (WB^2) and the DIET WISPR algorithms are rather remarkable. Both algorithms are fluctuation-based signal processors. In other words, both algorithms have been devised or modified to exploit the fluctuations to enhance those algorithms' performances for signals that have lower fluctuation amplitudes. Furthermore, both algorithms correctly localize the stable signal and provide sufficient SNR gain to make it clearly identifiable. The similarity is even more remarkable when the $AWSUM_4$ algorithm is used instead of WISPR to produce the DIET $AWSUM_4$ algorithm. When that is done, the results, presented in Fig. 9.4, are very similar in SNR as the WISPR (WB^2) results, but the resolution is significantly greater. The DIET $AWSUM_4$ results are also enhanced compared to the DIET WISPR results in Fig. 9.3e.

The results in Figs. 9.3 and 9.4 illustrate the important role that fluctuations can play in detecting, identifying, localizing (Figs. 9.3 and 9.4), and enhancing the resolution and SNR of stable signals among clutter signals and background noise.

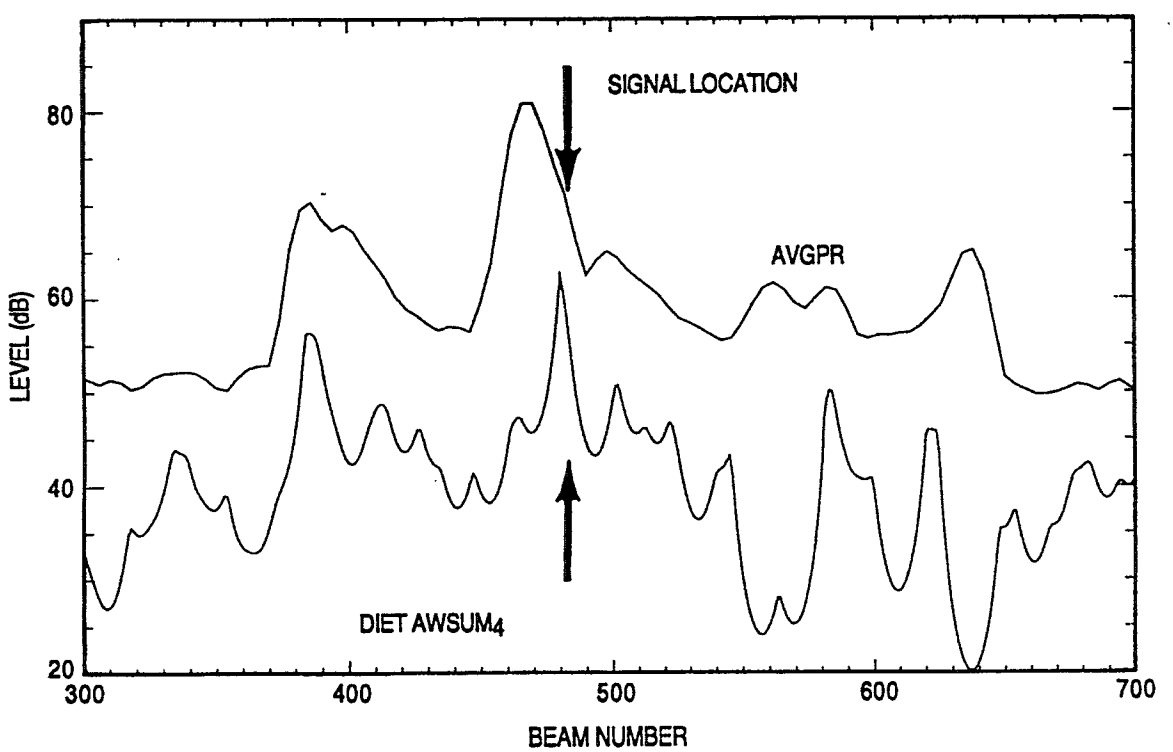

Fig. 9.4 — A comparison of DIET $AWSUM_4$ processing with conventional processing

10.0 MEASURES OF WISPR PROCESSOR PERFORMANCE

10.1 The Problem with the DI as a WISPR Performance Measure

10.1.1 Introduction

Throughout this report, the SNR gain increase has been defined as the signal excess of the fluctuation-based processors (e.g., WISPR, AWSUM, and WISPR II) compared to the signal excess that is achieved by the AVGPR processor. Some signal processing researchers may attempt to "put round pegs into square holes," e.g., try to evaluate an unconventional nonlinear processor such as WISPR according to standards developed to test conventional linear processors. An example is the measurement of the SNR gain of WISPR. A benchmark method that has become accepted by many signal processors for determining the SNR gain improvement of one processor relative to another is the DI, defined in Sec. 10.1.2. The relative SNR gain by this procedure is defined simply as the ratio of the DIs for the two systems to be compared. For example, with A and W for AVGPR and WISPR respectively, the SNR gain of WISPR compared to AVGPR would be

$$SNR_{(Gain:W/A)} = DI_W/DI_A \,. \tag{10.1.1}$$

The main fallacy of this method is that it is incapable of reasonably accounting for gain achieved through differences in signal fluctuations. In fact, when fluctuation gain must be taken into account, this index (at low SNR) can be shown to produce absurd and unusable results. Although not obvious, the evenly distributed noise assumption (locally white noise in the vicinity of the signal) is tacitly required by its definition. In addition, no distinction is made between signals which have variation in fluctuation levels. The main cause of failure is the structure of the index itself. It arises as a direct result of its definition in terms of expectations and implied statistical distributions.

10.1.2 Definition of the Detection Index

Detection Index, DI, as used herein, is

$$DI \equiv \left[\frac{<S+N>-<N>}{\sigma_f}\right]^2 , \tag{10.1.2}$$

where

$< >$ = expectation operator,

N = noise power,

S = signal power,

σ_f = is the power standard deviation, across a group of frequencies, centered around the frequency of signal S, exclusive of itself. It is usually estimated by

$$\sigma_f \approx \left[\frac{1}{n-1}\left[\sum_{j=f-(n/2)}^{j=f-1}(X_j - X_{avg})^2 + \sum_{j=f+1}^{j=f+n/2}(X_j - X_{avg_f})^2\right]\right]^{\frac{1}{2}} , \tag{10.1.3}$$

and

$$X_{avg_f} = \frac{1}{n}\left[\sum_{j=f-(n/2)}^{j=f-1} X_j + \sum_{j=f+1}^{j=f+n/2} X_j\right], \tag{10.1.4}$$

where

n = in this case, an even number of values in the vicinity of the fth item,

j = the index of a spectral bin,

X_j = the jth spectral power, taken in the vicinity of the fth frequency, excluding itself.

Other ad hoc ranges thought to be more typical of the ambient noise could be used with some loss of objectivity for this index.

10.1.3 Discussion of the DI Calculation

If the acoustic local white noise frequency domain world was from a statistically perfect universe, it could be assured that the $\langle N \rangle$ and $\langle S + N \rangle$ (expectations) could be determined easily. With a sufficiently large number of time realizations, by simply taking averages over noise frequency bins, the average would converge to $\langle N \rangle$. Since the idealized world is locally of white noise, the average for noise in a signal bin would also have to converge to $\langle N \rangle$. Additionally, the average for a purported signal bin should converge to $\langle S + N \rangle$. Close examination of Eqs. 10.1.2, 10.1.3, and 10.1.4 reveals that these conditions must be at least approximately true to obtain reasonable estimates for $\langle S + N \rangle$ and $\langle N \rangle$.

The authors are not trying to convince anyone that this is reality; clearly it is not. Yes, noise generated in the sea by many natural processes is broadly distributed in frequency. Yes, transient events, whose time domain signals are processed through the Fourier transform, also produce results broadly distributed in frequency (though hardly ergodic). Man-made signals obviously have some broadband structure. However, many signals of interest generated at power levels sufficient to reach distant receivers are chiefly discrete tonals. Admittedly, some of their power shows up after Fourier transformation as sidelobes in the frequencies near to the tonal frequency. In spite of all this, there is still plenty of opportunity for noise (on the average) to not be absolutely evenly distributed. Thus, some spectral bins may contain much less noise than that indicated by the estimated average value.

10.1.4 Detection Index Fluctuation-Based Performance Study for WISPR Processors

To demonstrate just what the DI would show for typical acoustic data of known characteristics, noise and tonal data have been artificially generated. The result of this simulation is shown in Table 10.1.1.

10.1.4.1 Data Set Generation Method

Typical signal and noise power levels, normally distributed in decibels (equivalent to a log-normal distribution before conversion to decibels), were generated separately for a mean of 70 dB and with the standard deviations (sigma) indicated in Table 10.1.1 (3, 4, 5, and 6 dB) for

Table 10.1.1 — WISPR Class Processor Detection Index Simulation Study

Processor	N-Avg. Across Freq.	% Noise in Bin				% Noise in Bin			
		10	40	70	100	10	40	70	100
		Total Power in Tonal Bins, dB				DI Ratio, Processor/AVGPR			
AVGPR	69.98	70.4	71.5	72.4	72.9	1	1	1	1
WISPR	67.92	70.4	71.4	72.1	72.5	50	8	5	4
$AWSUM_2$	66.90	70.4	71.3	72.0	72.3	63	8	5	3
$AWSUM_3$	65.95	70.4	71.2	71.9	72.2	56	7	3	2
$AWSUM_4$	65.14	70.4	71.2	71.8	72.1	52	6	3	2

Time Sequence Noise Standard Deviation, 3 dB–Time Sequence Tonal Standard Deviation, 1 dB

Processor	N-Avg. Across Freq.	% Noise in Bin				% Noise in Bin			
		10	40	70	100	10	40	70	100
		Total Power in Tonal Bins, dB				DI Ratio, Processor/AVGPR			
AVGPR	70.00	70.4	71.6	72.4	73.0	1	1	1	1
WISPR	66.32	70.3	71.3	71.8	72.2	297	23	12	8
$AWSUM_2$	64.55	70.3	71.2	71.6	72	328	22	11	7
$AWSUM_3$	63.04	70.3	71.1	71.5	71.8	327	20	9	6
$AWSUM_4$	61.90	70.3	71.0	71.4	71.7	375	22	10	6

Time Sequence Noise Standard Deviation, 4 dB–Time Sequence Tonal Standard Deviation, 1 dB

Processor	N-Avg. Across Freq.	% Noise in Bin				% Noise in Bin			
		10	40	70	100	10	40	70	100
		Total Power in Tonal Bins, dB				DI Ratio, Processor/AVGPR			
AVGPR	69.98	70.4	71.3	72.3	72.7	1	1	1	1
WISPR	64.30	70.4	71.0	71.6	71.9	767	102	33	26
$AWSUM_2$	61.70	70.3	70.9	71.4	71.7	799	98	29	22
$AWSUM_3$	59.76	70.3	70.9	71.3	71.5	1030	122	34	26
$AWSUM_4$	58.45	70.3	70.8	71.2	71.4	1424	164	45	33

Time Sequence Noise Standard Deviation, 5 dB–Time Sequence Tonal Standard Deviation, 1 dB

Processor	N-Avg. Across Freq.	% Noise in Bin				% Noise in Bin			
		10	40	70	100	10	40	70	100
		Total Power in Tonal Bins, dB				DI Ratio, Processor/AVGPR			
AVGPR	70.01	70.5	71.2	72.4	73.2	1	1	1	1
WISPR	61.82	70.4	70.9	71.3	71.7	2201	427	107	58
$AWSUM_2$	58.37	70.4	70.8	71.2	71.4	2914	538	126	66
$AWSUM_3$	56.10	70.3	70.8	71	71.2	4884	879	200	102
$AWSUM_4$	54.66	70.3	70.7	70.9	71.1	7496	1325	295	149

Time Sequence Noise Standard Deviation, 6 dB–Time Sequence Tonal Standard Deviation, 1 dB

300 time realizations. (This data set can be considered to apply to any frequency range, since the maximum frequency of real data would be determined by the time domain digital sampling rate.)

(a) The dB values generated were converted to arithmetic power levels and stored.

(b) The noise generated for each of 1024 frequency bins was averaged across time for each bin.

(c) The single tonal generated was averaged across time.

(d) The power level for the entire data set was adjusted so that the noise and tonal arithmetic averages when converted back to decibels would equal 70 dB, an initial SNR of 1.0.

(e) The arithmetic power level for the noise in bins 100, 400, 700, and 1000 was adjusted to 10%, 40%, 70%, and 100% of the former values, respectively.

(f) The single tonal set was then added to the noise in bins 100, 400, 700, and 1000. Note that only bin 1000, with 100% noise, has a 70-dB noise level and a 70-dB signal level, an initial SNR = 1.0 (0 dB).

10.1.4.2 Discussion

The results of processing these simulated data utilizing the AVGPR, WISPR, $AWSUM_2$, $AWSUM_3$, and $AWSUM_4$ processors are shown in Table 10.1.1. Several observations can be made concerning these results:

(a) The reduction in the processor result (Col. 2) systematically decreases as the noise sigma is increased from 3 to 6 dB and systematically decreases as the AWSUM processor order number increases, just as would be anticipated from the previously described properties of these processors.

(b) In contrast to observation (a), there is practically no suppression of the tonal in the 10% noise bin (Col. 3) and only 0.8- to 2.1-dB suppression of the tonal in the highest noise case, the 100% noise bin (Col. 6).

(c) The WISPR DI ratio (SNR gain from Eq. 10.1.1) progresses dramatically upward as the noise content in a signal bin is reduced, e.g., for the 5-dB noise case, the WISPR DI ratio at 100% noise is 26, increasing to 767 at 10% noise. In instances where the average noise and signal are approximately equal, but noise in a particular instance is not manifest in the signal bin, the numerator of Eq. 10.1.2 would become zero when the AVGPR processor is used, producing $DI_A \approx 0$. Since the fluctuation-based processors will dramatically suppress the noise (estimated $\langle N \rangle$) in all bins, but not the steady tonal (estimated $\langle S + N \rangle$) in the signal bin, this numerator would be far from zero. Therefore, the SNR gain would approach infinity, a very unreasonable result. One may think this cannot occur in reality. Examples demonstrating this possibility will be presented shortly for real data.

(d) In any case, an interpretation of the DI results from this data set, constructed to intentionally show its weakness for the evaluation of fluctuation-based processors, leaves one with the question, "Now that I have calculated the DI, how can it be used under similar field conditions in any reasonable manner to evaluate the processors being compared?" The implications are probably more subtle than a reader unfamiliar with these processors is initially willing to admit.

10.1.5 Processor DI Performance for Real Ocean Acoustic Data

10.1.5.1 The Fallacy of AVGPR when SNR = 1 (0 dB) for Real Data

From the point of view of fluctuation-based processors, any fluctuating signal is noise; whereas, steady tonals are viewed as those from submerged sources. In essence, the question to be answered

is, "How well do these processors identify those steady tonal submerged sources?" Note, as discussed earlier, that as a practical matter, the theoretical values for $<S + N>$ and $<S>$ are never known for real data but may only be estimated. With real data, calculation of the DI resorts to a determination of $<S + N>$ as the averaged value (determined with the processor under consideration) in that spectral bin where a signal is purported to be present. Then, from other nearby spectral bins where noise only is purported to be present, $<N>$ is estimated as the average for those bins of the value that was obtained by the processor, e.g., as determined by Eqs. 10.1.3 and 10.1.4.

Example 1: (Note: The figure referred to in the next paragraph was presented in Sec. 4.0)

Clearly, in Fig. 4.6a (with only 50 elements of the array), calculating the detection index for the signal near beam 68 for the AVGPR processor, $<S + N> \approx <S>$, which yields from Eq. 10.1.2 that $DI_A \approx 0$. Any reasonable person, examining the $AWSUM_4$ curve in that plot, would conclude that $<S + N>$ is about 42 dB and the $<N>$ is about 30 dB. Therefore, for the WISPR type processor, $AWSUM_4$ in this case

$$\frac{DI_W}{DI_A} = \left[\frac{<S+N>-<N>}{\sigma_f}\right]_W^2 \Big/ \left[\frac{<S+N>-<N>}{\sigma_f}\right]_A^2$$

$$= \left[\frac{42-32}{\sigma_f}\right]_W^2 \Big/ \left[\frac{\approx 0}{\sigma_f}\right]_A^2 = \rightarrow \infty ,$$

an absurd result. The signal peak at beam number 68, visible on the $AWSUM_4$ curve, is not visible on the AVGPR curve. However, it is difficult to deny that the two curves are actually quite reasonably related. That this peak actually exists, as indicated by the $AWSUM_4$ processor, is ultimately shown in the AVGPR curve when the number of array elements is increased to 100 and to 198 as shown in Fig. 4.6b and c.

Example 2:

Figure 10.1 identifies three tonals that are embedded in background noise at 43, 65, and 80 Hz. The top curve is for AVGPR, the middle curve is for WISPR, and the bottom curve is the difference between the previous two curves (noise suppression A_{01}), truncated at 10 dB. Where this last curve (or set of curves) approaches 0 dB, it indicates the presence of three tonals that are known to have been projected from submerged sources. For the signals at 43 and 65 Hz, it would be possible to calculate the DI. At those frequencies, DI may or may not (dependent upon the actual detailed values) numerically indicate that the AVGPR processor is superior to the WISPR processor. The situation is somewhat different at 80 Hz where there is no discernible signal in the AVGPR curve, but there is in the WISPR result. In this case, the ratio of the DIs approaches infinity as described in Example 1 just presented, indicating that WISPR is far superior. How does one reconcile this ambivalence using the ratio of the DIs for evaluating the two processors? One can't; he/she must simply conclude that the DI definition does not make much sense when applied to fluctuation-based processors; processors that can achieve gain through properties of signals and noise that simple conventional processors fail to utilize. WISPR is clearly better, but the ratio of the DIs can't quantify exactly how much better, or even that it is better.

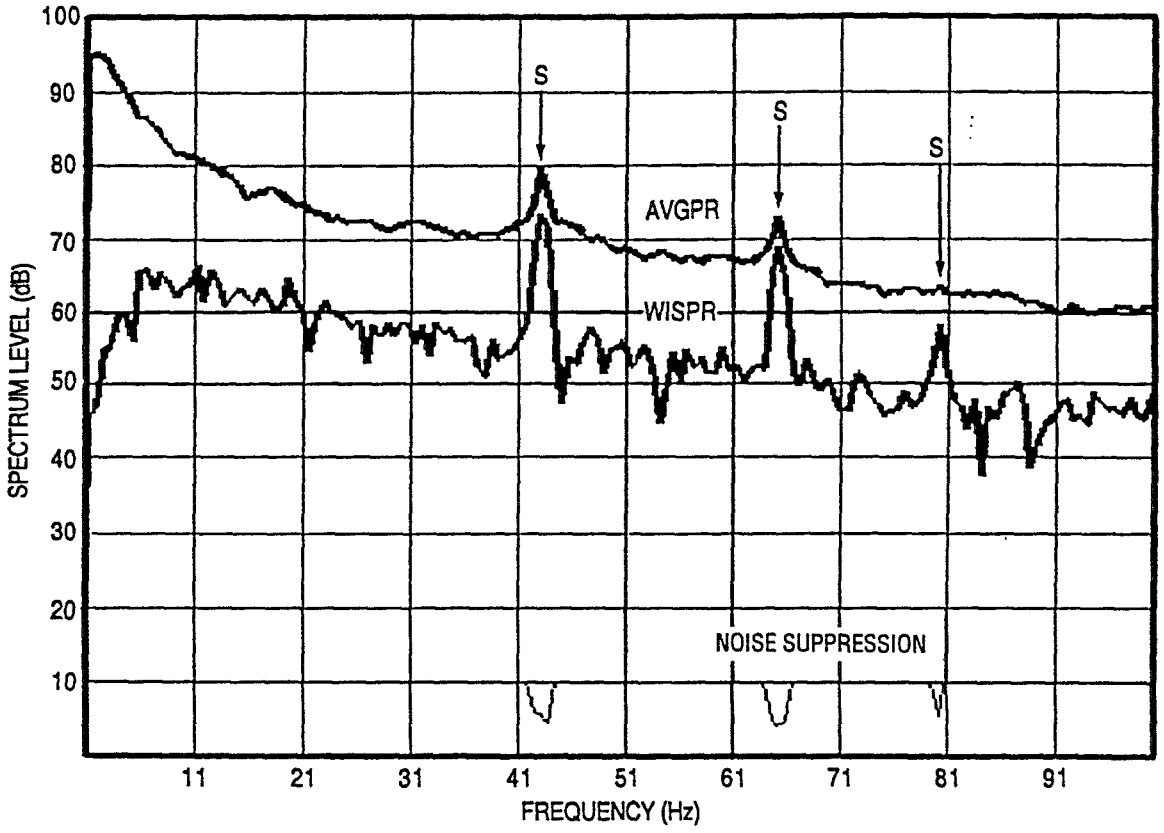

Fig. 10.1 — WISPR processing: SNR <0 at 80 Hz

10.1.6 Summary

It should be obvious from the simulation study and the two examples using real data that if the SNR is too low for the tonal to be detected by the conventional processor, the ratio of the DIs are not valid and cannot be used to compare the two processors. That being the case, the question naturally arises as to when can the ratio of the DIs be used? Furthermore, if it is not a valid measure at low SNR, what then makes it a valid one at higher SNR, and how high must it be? Until those questions are answered, it seems that other criteria need to be devised; criteria that recognize the uniquely different nature of the WISPR processor compared to classical/conventional processors. In devising such criteria, the most important thing to keep in mind is that the WISPR processor is driven by the magnitude of the fluctuations. The actual magnitude of the tonal, for the most part, is not a relevant parameter for the fluctuation-based processors such as the WISPR processor. By contrast, conventional signal processors are driven by the magnitude of the tonal and completely discard a key source of classification information encoded by nature in the acoustical fluctuations of signals and noise.

10.2 WISPR Performance Measured by ROC Curves and the Relationship to DI

Receiver Operating Characteristics (ROC) curves were generated to measure the performance of the WISPR Filter in noise that has a Gaussian distribution in power and in noise that has a Gaussian distribution in the log of power (a log-normal distribution). Figure 10.2, containing plots

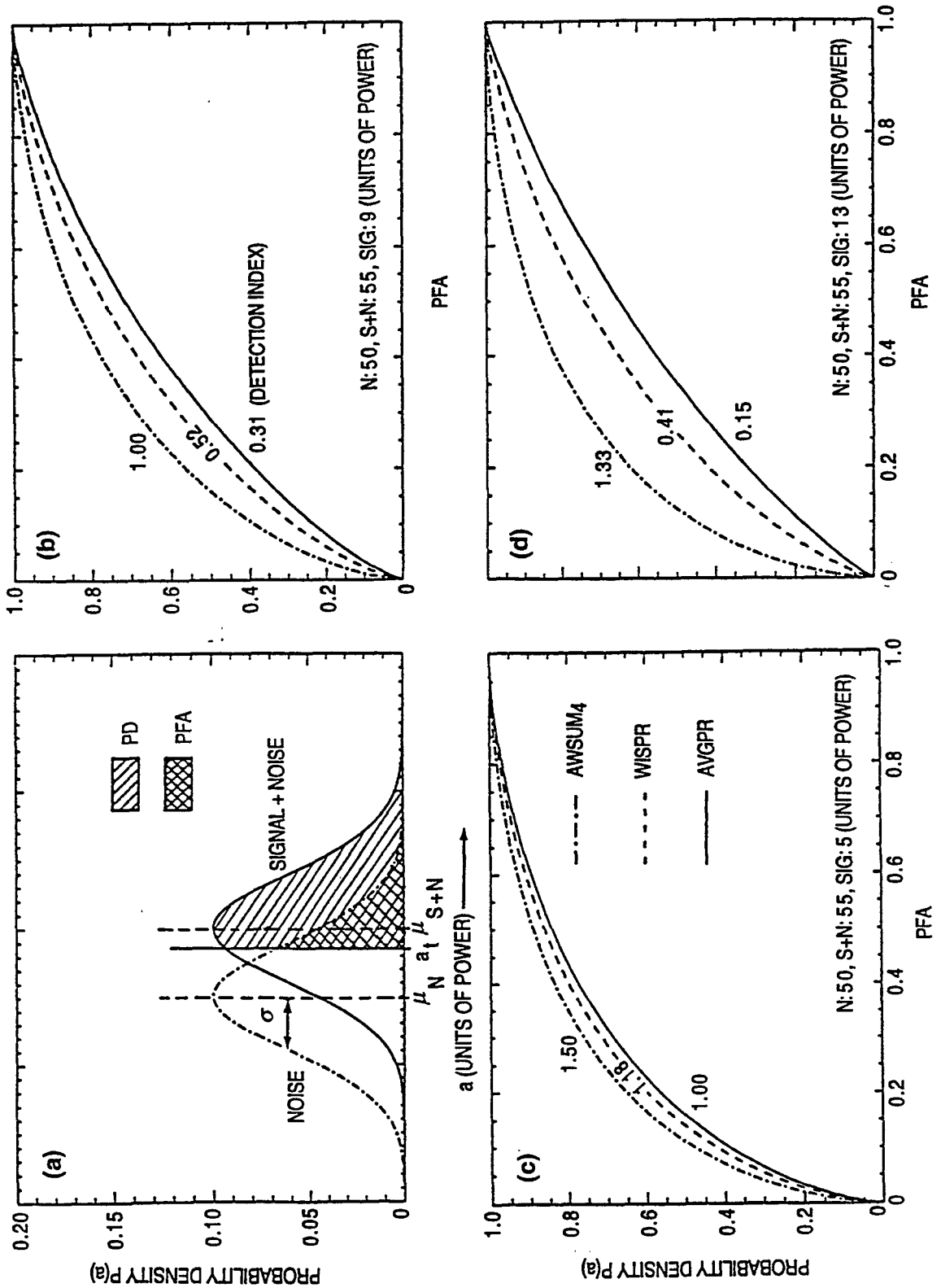

Fig. 10.2 — Receiver operating characteristics (ROC) curves for signal (S) and signal plus noise ($S+N$) for various standard deviations (SIG, σ)

(a), (b), (c), and (d), illustrates the results for the AVGPR (the solid curves), the WISPR Filter results (the dashed curves), and the AWSUM$_4$ Filter results (the dashed-dot curves).

Figure 10.2, plot (a), illustrates the process of generating the ROC curves and the regions under the noise and the signal plus noise curves that are important in the calculations. The mean noise power is μ_N and the mean signal plus noise is μ_{S+N}. The signal is assumed to be an ideal steady tonal with a standard deviation (variously labeled σ, SIG, or SIGMA) of zero and power a_t. The boxes show the type of shading under the noise and signal plus noise probability density curves that correspond to the areas that represent the probability of detection (PD) and the probability of false alarm (PFA). In this case, the signal plus the noise is five units of power more than the noise.

Figure 10.2, plots (b), (c), and (d), give the ROC curves for the three different methods when the standard deviations (units of power) are 9, 5, and 13, respectively. In each case, the WISPR Filter outperforms the AVGPR processor by achieving a larger DI (c.f., Sec. 10.1.2 for the definition of DI) and the AWSUM$_4$ Filter outperforms both of them. For example, in plot (b) the DIs are 0.31, 0.52, and 1.00 for the AVGPR processor, the WISPR Filter, and the AWSUM$_4$ Filter, respectively. The trend is for the DI of the WISPR Filter to exceed that of the AVGPR processor differences to grow as the standard deviation of the noise increases.

The previous illustration shown in Fig. 10.2 was for a highly idealized case where the equivalent standard deviation ranged from about 0.6 dB (plot (c)) to 1.5 dB (plot (d)). The standard deviations of noise in the ocean normally range from about 4.5 to 7 dB, and the probability density curves for the signal and the noise are more nearly log-normal than Gaussian (c.f., Fig. 3.20 and the discussion of that figure).

Results for the AVGPR processor and the WISPR Filter are given in the left and right plots in Fig. 10.3, respectively, for a mean noise level of 70 dB, a standard deviation of 6 dB, and for three different signal levels. The SNRs range from –5 dB to 1 dB.

The results in Fig. 10.3 indicate, as in Fig. 10.2, that the performance of the WISPR Filter, as measured by the DI, exceeds the performance of the AVGPR processor by substantial amounts for all three signal levels (and also SNR). The improvement is approximately a factor of 18 (12.8 dB),

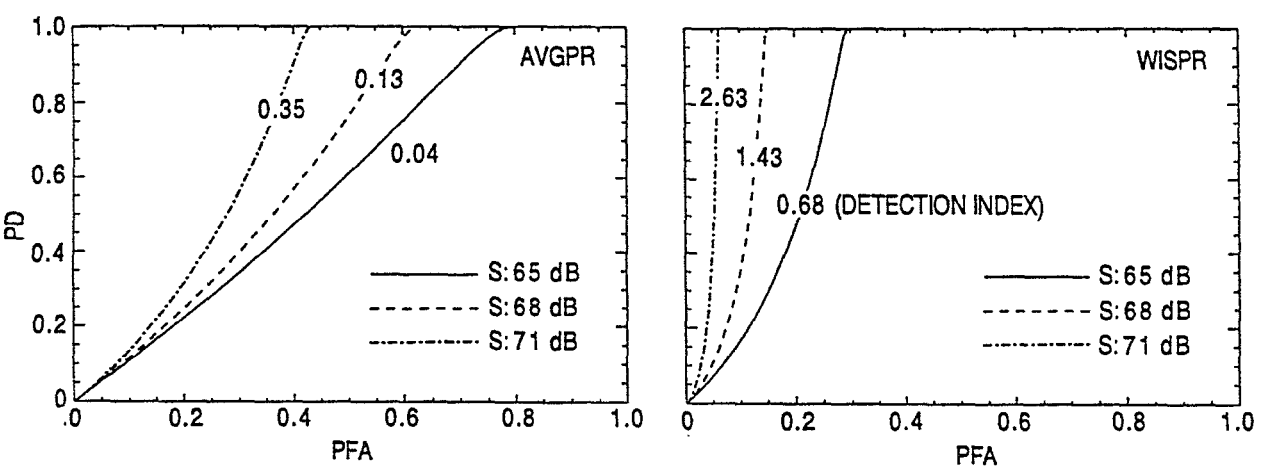

Fig. 10.3 — Sonar system performance for tonal (S) in log-normal noise (N): WISPR (right) versus conventional (AVGPR) processing (left), N: 70 dB, SIGMA: 6 dB

11 (10 dB), and 7 (8.5 dB) for signal levels of 71, 68, and 65 dB, respectively, and for SNR of 1, –2, and –5 dB, respectively. For the case of a steady tonal in noise that is characteristic of undersea ambient noise (Fig. 10.3), the gains in WISPR processing are of the order of 8 to 12 dB for SNR from 1 to –5 dB. However, when the standard deviations are small (Fig. 10.2) and the noise is normally distributed, not at all like the undersea noise, the gains are small enough to be considered insignificant. However, that turns out to be an advantage, since the distribution of an actual submerged tonal has a rather small standard deviation such as the "noise" in Fig. 10.2, and the attenuation by the WISPR Filter would also be small, less than about a decibel.

There is an important point that needs to be made in regard to the ROC curves in Figs. 10.2 and 10.3. They were produced with the assumption that the signal and the noise added in an incoherent manner. For some signals and noise that would not be a valid assumption and a coherent addition would be more appropriate.

11.0 ACKNOWLEDGMENTS

Mr. Tommy Goldsberry of the Office of Naval Research (ONR) Code 321 is gratefully acknowledged for his support under the WISPR Development and Evaluation Project Number 602314.

Appreciation is also expressed for colleagues at the Naval Research Laboratory who contributed to the research reported herein including Ms. Karen Dudley, Mr. Robert Fisher, Ms. Susan D. Gardner, Ms. Stephanie F. Kooney, Mr. Jackson Mobbs, Mr. Joal J. Newcomb, and Mr. E. J. Yoerger. Their contributions include figures used in the report, time contributed to acquire and process data, and contributions to the analysis efforts. For those contributions the authors are sincerely grateful.

The authors also wish to acknowledge with gratitude various forms of assistance provided by Dr. Marshall Bradley of Planning Systems Inc. (especially in modeling) and Laura Hart of Alliant Techsystems (especially in data acquisition and processing) and their highly competent and helpful staff.

12.0 REFERENCES

1. "Encyclopedic Dictionary of Mathematics," Volume II, 2nd Ed., Section 211, p. 807, English translation by the Massachusetts Institute of Technology (1987), United States Library of Congress ISBN 0-262-09026-0, MIT Press.

2. R. A. Wagstaff and J. George, "A New Fluctuation Based Digital Signal Processor Including Phase Variations," patent application submitted, Aug 1995.

3. R. A. Wagstaff and J.-L. Berrou, "A Fast and Simple Nonlinear Technique for High Resolution Beamforming and Spectral Analysis," *J. Acoust. Soc. Am.* **75**(4), 1133–1141 (1984).

4. S. D. Gardner, "A Method for Improving the Signal-to-Noise Ratio and Resolution of Stable Amplitude Signals," MS Thesis, Univ. of New Orleans, Dec 1995.

Appendix A

PROCESSING ALGORITHMS AND RELATED EQUATIONS

A-1.0 INTRODUCTION

To interpret data, particularly when in the form of rapidly acquired real-time data streams, it is both reasonable and necessary to develop methodologies (algorithms) that reduce the original data to more easily interpretable (derived) quantities. The statistical community commonly computes familiar quantities, such as measures of central tendency (e.g., average), standard deviation, and higher order statistics.

Some of the computational methods pertinent to this report are evolved from the generalized function

$$M_r = M_r(a) = \left[\frac{1}{n} \sum_{j=1}^{j=n} a_j^r \right]^{\frac{1}{r}}, \tag{A.1.1}$$

where the data stream is the sequence, a

$$a = (a_1, a_2, a_3, \ldots a_n),\ a_j \geq 0. \tag{A.1.2}$$

Because of the possibility of numerical overflow, use of Eq. A.1.1, when $r < 0$ is restricted to nonzero data values. Two practical approaches that avoid numerical overflow are: (1) Force values near zero to a small numerically convenient value. As A/D converters are not usually significant in the lowest order bits, a logical choice is to set this minimum value of a_j to the value implied by some small multiple of the A/D converter least significant bit. (2) Simply delete any data less than a small numerically convenient value from the original data set. This latter approach is preferred as it also provides for automated removal of data from periods of time where the data acquisition system is malfunctioning or otherwise unavailable without biasing the results obtained from the data actually processed.

Eq. A.1.1 can be used quite generally and for particular choices of r defines several familiar statistical quantities. For example, compare:

When $r = 1$, the average is: $a_{avg} \equiv M_1 = \left| \frac{1}{n} \sum_{j=1}^{j=n} a_j \right|$,

when $r = 2$, the root mean square is: $a_{rms} \equiv M_2 = \left[\frac{1}{n}\sum_{j=1}^{j=n} a_j^2\right]^{\frac{1}{2}}$,

when $r = -1$, the harmonic mean is: $a_{harm} \equiv M_{-1} = \left[\frac{1}{n}\sum_{j=1}^{j=n} a_j^{-1}\right]^{-1}$.

Consider Eq. A.1.1's relationship to the geometric mean.[1]

$$a_{geom} \equiv \left[\prod_{j=1}^{j=n} a_j\right]^{\frac{1}{n}} = M_{r\to 0} = \lim_{r\to 0}\left[\frac{1}{n}\sum_{j=1}^{j=n} a_j^r\right]^{\frac{1}{r}}. \tag{A.1.3}$$

Thus, though not initially obvious, the geometric mean, a_{geom}, is identically equal to M_0.

Another important property that can be shown by mathematical induction[1] is that M_r increases strictly monotonically with increasing r. This is illustrated in Fig. A.1.1 using the arbitrary data sequence $a = (1, 2, 3, \ldots, 10)$. It follows that

$$M_{-1} \le M_0 \le M_1 \le M_2, \text{ i.e., } a_{harm} \le a_{geom} \le a_{avg} \le a_{rms}. \tag{A.1.4}$$

The value of M_r for any particular sequence, a, $a_j \ge 0$, is also bounded

$$M_{r\to\infty} \to a_{max} \text{ and } M_{r\to-\infty} \to a_{min}. \tag{A.1.5}$$

In Fig. A.1.1, it is fairly obvious that $M_{r\to\infty}$ approaches 10, the maximum value, and $M_{r\to-\infty}$ approaches 1, the minimum value.

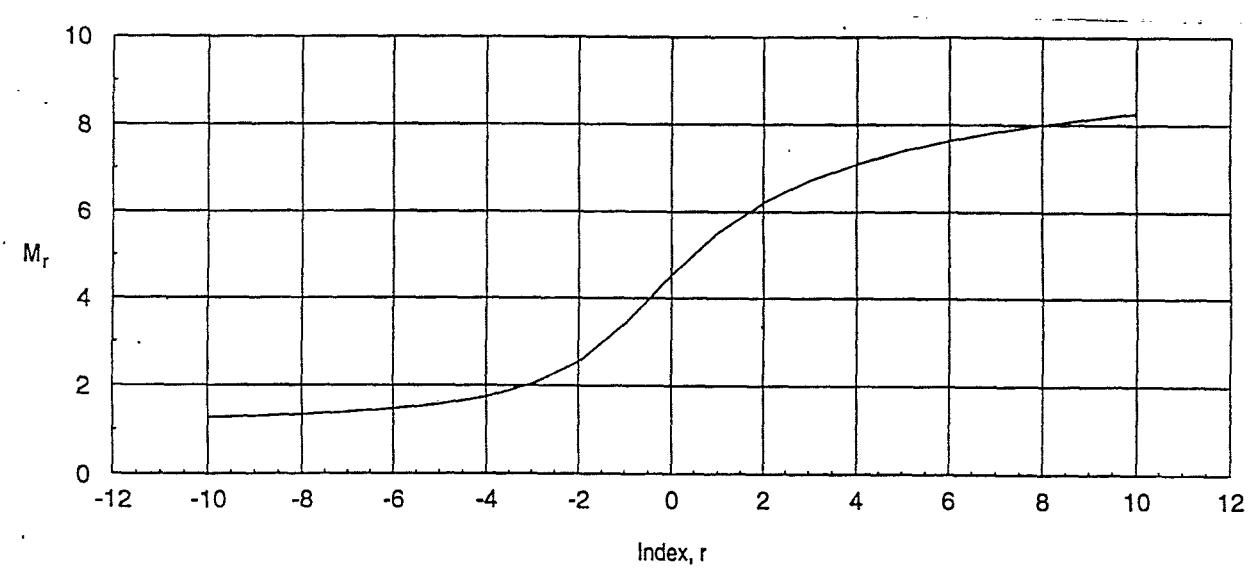

Fig. A.1.1 — The effect of index r on the sequence, $a = (1, 2, 3, 4, 5, 6, 7, 8, 9, 10)$

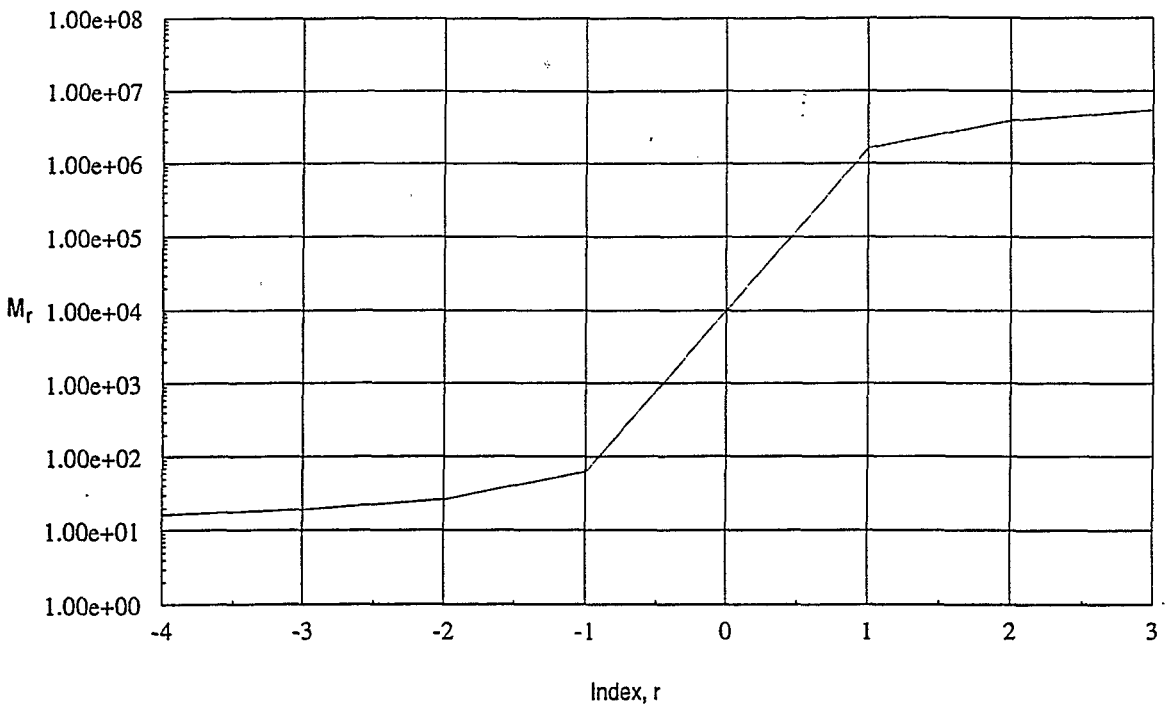

Fig. A.1.2 — The effect of index r on the sequence, $a = (10^1, 10^2, 10^3, 10^4, 10^5, 10^6, 10^7)$

The linearly distributed data shown used to prepared Fig. A.1.1 is not particularly representative of ocean acoustic data. Even though the trend is obvious, the example does not adequately illustrate what happens when data are distributed over a broad range in power. The logarithmically distributed data sequence $a = (10^1, 10^2, 10^3, 10^4, 10^5, 10^6, 10^7)$ used to prepare Fig. A.1.2 provides an example of what occurs for this type of data. With data distributed in this fashion, the negative order (exponent) processor results are almost captured (very strongly influenced) by the smallest two values, 10^1 and 10^2, whereas the positive order processor results are almost captured (very strongly influenced) by the largest two values, 10^6 and 10^7. It is quite simple to verify that if there is no variation in the data, i.e., there are no fluctuations, the result for M_r of all orders, $r = -4, -3, -2, -1, 0, 1, 2, 3, 4$ will be equal. In other words, the greater the fluctuation level, the greater that the negative order filters, M_r, will suppress the final result, whereas, nonfluctuating signals are not suppressed. It is this interpretation of the properties of these fluctuation-based processor algorithms/filters that is the key to successfully understanding the unusual and often very impressive results they achieve on actual measured data.

A.2.0 AVERAGING IN LOGARITHMS OR DECIBELS

A.2.1 Logarithms

Let X_j correspond to the original data values in power, then if

$$a_j = \log(X_j),$$

and noting that $a_{avg} = M_1$, this particular average yields

$$a_{avg\ in\ log} = \left[\frac{1}{n}\sum_{j=1}^{j=n} \log X_j\right].$$

Thus, from Eq. A.1.3

$$\log^{-1}(a_{avg\ in\ log}) = \left(\left[\prod_{j=1}^{j=n} X_j\right]^{\frac{1}{n}}\right) = (X_{geom}).$$

Upon taking the logarithm again

$$a_{avg\ in\ log} = \log\ (X_{geom}). \tag{A.2.1}$$

A.2.2 Decibels

Following the same steps for averaging in decibels, let X_j correspond to the original data values in power, then if

$$a_j = \mathrm{dB}(X_j) = 10\ \log\ (X_j),$$

and noting that $a_{avg} = M_1$, this particular average yields

$$a_{avg\ in\ dB} = \left[\frac{1}{n}\sum_{j=1}^{j=n} 10 \log X_j\right] = 10\left[\frac{1}{n}\sum_{j=1}^{j=n} \log X_j\right].$$

Thus, from Eq. A.1.3

$$\log^{-1}(a_{avg\ in\ dB}) = \left(\left[\prod_{j=1}^{j=n} X_j\right]^{\frac{1}{n}}\right)^{10} = (X_{geom})^{10}.$$

Upon taking the logarithm again and using the result from Eq. A.2.1

$$a_{avg\ in\ dB} = 10\ \log\ (X_{geom}) = 10 a_{avg\ in\ log}. \tag{A.2.2}$$

These results are important computationally, since the obstacles that M_0 cannot be calculated directly and the product, $\prod_{j=1}^{j=n} X_j$, can easily produce numerical overflow when n is large, are avoided.

A.2.3 Magnitude Order

The magnitude order is preserved in decibels, i.e., with the original data in power

$$\mathrm{dB}(a_{harm}) \leq \mathrm{dB}(a_{geom}) = \mathrm{dB}(a_{avg\ in\ dB}) = 10a_{avg\ in\ log} \leq \mathrm{dB}(a_{avg}) \leq \mathrm{dB}(a_{rms}) \ . \qquad \text{(A.2.3)}$$

Similarly, the decibel magnitude order is preserved for other values of r, a property that is extensively utilized by fluctuation-based processors.

A.3.0 THE CONVENTIONAL PROCESSOR - FILTER

The average power is referred to herein as the conventional processor or filter. Thus, when the sequence, a, is power, average power is

$$AVGPR = M_1. \qquad \text{(A.3.1)}$$

A.4.0 FLUCTUATION-BASED PROCESSORS/FILTERS EQUAL TO M_r

A.4.1 The WISPR Filter (Wagstaff's Integration Silencing PRocessor)

When the sequence, a, is power, then

$$WISPR = M_{-1}. \qquad \text{(A.4.1)}$$

It may be noted that *WISPR* is notationally equivalent to $AWSUM_1$ below. It is also known in the literature as the harmonic mean.

A.4.2 The $\mathrm{AWSUM_k}$ Filters (Advanced WISPR SUMmations), Usually for $k = 2$, 3, or 4

When the sequence, a, is power, then

$$AWSUM_k = M_{-k} \ . \qquad \text{(A.4.2)}$$

A.5.0 FLUCTUATION-BASED PROCESSORS/FILTERS, DERIVED FROM M_r

Several processors that are related to the M_r class may be obtained by simple combination of those previously described.

A.5.1 The A_{0k} Processors

Examples for A_{0k} processors, for $k = 1$ and 4, are

$$A_{01} = AVGPR/WISPR = M_1/M_{-1}, \qquad \text{(A.5.1)}$$

$$A_{04} = AVGPR\ /AWSUM_4 = M_1\ /M_{-4}, \qquad \text{(A.5.2)}$$

or more generally,

$$A_{0k} = AVGPR/AWSUM_4 = M_1/M_{-k}. \tag{A.5.3}$$

A.5.2 The A_{jk} Processors

The A_{lk} processors for $j = 1$ and $k > 1$ are defined as

$$A_{1k} = WISPR/AWSUM_k = M_{-l}\ /M_{-k}\ , \tag{A.5.4}$$

and for $j > l$ and $k > j$ are defined as

$$A_{jk} = AWSUM_j/AWSUM_k = M_{-j}/M_{-k}\ . \tag{A.5.5}$$

A.6.0 THE WISPR II_k PROCESSORS

When the data exist in the form of a decibel power spectrum series, an additional statistic that can be used to achieve gain is the modified temporal standard deviation, σ, of the sequence, a, for the ith spectral bin. Care must be taken during overlapped processing to use only the results of the independent time series, i.e., only the nonoverlapped segments should be used to estimate a_j, otherwise the values will be correlated and a value that is lower than the true standard deviation will be found. In particular, σ is for a in decibels

$$\sigma = \left[\frac{1}{n-1}\sum_{j=1}^{j=n}(a_j - a_{avg})^2\right]^{\frac{1}{2}}. \tag{A.6.1}$$

Using this definition for the standard deviation, WISPR II_k becomes

$$WISPR\ II_k \equiv WISPR\ /\ 10^{\left(\frac{k\sigma}{10}\right)}. \tag{A.6.2}$$

A detailed rationale for this processor was developed in Sec. 5.0.

A.7.0 WISPR III_k PROCESSOR OF ORDER k

The WISPR III_k processor has been developed to exploit fluctuations present in the signal phase information. Typically, complex spectra are obtained from an FFT or DFT on temporal sample sets where each is offset a fixed time, Δt, which is a function of the sample rate, FFT size, and the percentage overlap. In general, for steady tonal sources, i.e., those tonals with a steady frequency-generating mechanism, the initial phase of the tonal will systematically advance or delay at the beginning of each temporal sample set, a signal processing artifact associated with discrete sampling. The complex spectral results obtained by FFTs or DFTs for those frequency bins nearest to a particular tonal will reflect that systematic phase shift of the tonal. Therefore, to avoid cancellation of out-of-phase segments of the same tonal during a complex (or coherent) summation,

any systematic phase shift must be removed from the complex spectral value nearest the tonal frequency. This is necessary regardless of the type of coherent summation that is used; the conventional summation or ones based on the WISPR philosophy. In WISPR III_k processing, great care is taken to ensure that the processing is coherent. Once the systematic phase shift has been removed, the residual variations in phase are then considered to be fluctuations.

When a steady tonal, ζ, is generated, with time, t, equal to zero at the beginning of the first data set, it may be represented (even though several mechanisms may subsequently generate fluctuations in amplitude and phase prior to reaching a hydrophone) as

$$\zeta = r_0 e^{\left[j(\Theta_0 + 2\pi f t)\right]}, \tag{A.7.1}$$

where

t is the time since the onset of sampling,

f is the tonal frequency in Hz,

r_0 is the tonal hypothetical steady magnitude, and

Θ_0 is the phase at the onset of sampling.

Alternatively with time, τ, equal to zero at the beginning of each temporal data set

$$\zeta = r_0 e^{\left[j\left(\Theta_0 + 2\pi f(n-1)\Delta t + 2\pi f \tau\right)\right]} = r_0 e^{\left[j\left(\Theta_n + 2\pi f \tau\right)\right]}, \tag{A.7.2}$$

where

τ is the time since the beginning the temporal data set,

Δt is the sample offset time (time between temporal data sets), and

Θ_n is the phase at the beginning the temporal data set.

Defining signal summation as the addition (in the time domain) of the sampled tonal, after a sufficient number of samples, the summation would result in zero due to out-of-phase summations, not a very useful result. Even if fluctuations in magnitude and phase have been generated prior to reaching the sensor that samples the tonal, on the average, the effect of out-of-phase cancellations is still present. Coherent summation avoids the effect of cancellation by shifting the phase of the sample segment to Θ_0, i.e., by subtracting $(2\pi f(n-1)\Delta t$ from Θ_n. Normally, the actual phases would all be reduced numerically modulo 2π.

Discrete numerical operations, equivalent to those just presented, are more conveniently accomplished in the frequency domain. A somewhat subtle, and sometimes overlooked point, is that the complex spectral values generated by an FFT or DFT of even noise-free data, in general, (1) do not have bin boundaries that correspond exactly to the tonal frequencies actually present; thus, the tonal frequencies are not known exactly and (2) do not reproduce the phase of the tonal itself at the beginning of the temporal sample set, but rather the phase of the frequency corresponding to the frequency at the upper bin boundary. Therefore, it is not possible to achieve coherent

processing by simply using the frequency of the nearest spectral bin boundary to calculate the offset.

If the BW is sufficiently narrow to isolate tonals, the systematic phase shift of the tonal is reflected closely (though not exactly) for the frequencies of the nearest spectral bins. Any algorithm used must be capable of extracting a reasonable estimate of the required phase shift, even in the face of these obstacles and in the presence of noise. Although the success of the WISPR III_k processor, at least in part, depends on removal of the phase shift discrete sampling artifact, the actual technique used to determine the correct shift has little bearing the development of the WISPR III_k processor and, thus, is omitted from this discussion.

The discussion just presented from the point of view of time series data from a hydrophone would also apply to output from a beamformer with only minor modifications in terminology. Let the set $\{v_n\}$ ($n = 1,2,3, \ldots, N$) denote the shifted phase (to ensure coherent summation) complex spectra values from a single hydrophone or a single beam at a particular frequency. Let Φ_n denote the new phase values determined by a suitable phase-shifting algorithm, then the estimate of the signal corresponding to a particular bin frequency for that sample period is represented by

$$v_n = r_n e^{\left[j\left(\Theta_n + 2\pi f t\right)\right]}, \tag{A.7.3}$$

and has the Fourier transformed value

$$z_n = (r_n \cos\Phi_n + j r_n \sin\Phi_n) . \tag{A.7.4}$$

The set average value, s_{avg}, is

$$s_{avg} = \frac{1}{N} \sum_{n=1}^{n=N} \frac{z_n}{r_n^k} .$$

Using these results, the WISPR III_k processor is defined by

$$WISPR\ III_k = \left[\left(\frac{1}{N} \sum_{n=1}^{n=N} r_n^{-k} \right)^{-1} \sqrt{s_{avg} s_{avg}^*} \right]^2 . \tag{A.7.5}$$

A.8.0 WISPR CROSS-SPECTRAL DENSITY MATRIX BEAMFORMING, A_kCSDM OF ORDER k

Beamformers that are based upon the cross-spectral density matrix (CSDM) are referred to as CSDM beamformers. Input data required are the complex spectral values for each hydrophone from FFTs or DFTs at several sequential temporal realizations. Let the complex spectral value for a particular frequency bin for hydrophones l and m, at time index, i, be represented by

$$z_{l,i} = x_{l,i} + j y_{l,i} \text{ and } z_{m,i} = x_{m,i} + j y_{m,i} ,$$

then the CSDM quantity, $Z_{l,m,i}$ for hydrophones l and m, is

$$Z_{l,m,i} = z_{l,i} z^*_{m,i} = (x_{l,i} + jy_{l,i})(x_{m,i} - jy_{m,i}) \ .$$

The typical CSDM beamformer uses averages of these complex data according to some specific procedure prior to beam steering and summation to form the beam output; e.g., the simplest average is

$$Z_{l,m} = \frac{1}{T} \sum_{i=1}^{i=T} z_{l,m,i} \ .$$

The A_kCSDM beamformer utilizes a new average resulting from the WISPR philosophy, substituting this "average" for the conventional ones. Let the magnitude of $Z_{l,m,i}$ be $r_{l,m,i}$, i.e.,

$$r_{l,m,i} = +\sqrt{Z_{l,m,i} Z^*_{l,m,i}} \ .$$

The A_kCSDM beamformer, for order k (typically, 1, 2, 3, or 4), is accomplished by the simple replacement of the quantity, $Z_{l,m}$, with the new average $A_k CSDM_{l,m}$, prior to beam steering and summation to form the beam output. $A_k CSDM_{l,m}$ is defined as

$$A_k CSDM_{l,m} \equiv \left[\frac{1}{T} \sum_{i=1}^{i=T} r^{-k}_{l,m,i} \right]^{-1} \left[\frac{1}{T} \sum_{i=1}^{i=T} \frac{Z_{l,m,i}}{r^{k}_{l,m,i}} \right] . \tag{A.8.1}$$

WCSDM beamforming is the special case for $k = 1$, i.e., $A_1 CSDM_{l,m}$, analogous to WISPR being equivalent to $AWSUM_1$.

A.9.0 TIME AND FREQUENCY DOMAIN WISPR MATCHED FILTERS

These applications simply use the standard WISPR Filter processors. The only difference is the type of data that are actually processed. A description of the type of data processed is provided in Secs. 7.2 and 7.3.

A.10.0 WISPR(WB^2)

The WB^2 processor[1] is a processor that utilizes an iterative technique to enhance the spatial and spectral resolution from the output of a conventional processor. It is possible to enhance this technique by utilizing the output of other processors, e.g., the fluctuation-based processors described herein. When combined in this manner, the resulting processors are referred to as

$$\text{WISPR}(\text{WB}^2) \ ,$$

or more generally for the AWSUM higher order processors as

$$\mathrm{AWSUM_k(WB^2)}\ .$$

This application is discussed in Sec. 9.2.

A.11.0 DIET WISPR AND DIET AWSUM$_k$

The DIET AWSUM$_k$ processor of order k is a self-consistent, high-resolution, high-gain estimate of the spatial density. The special case where $k = 1$ is referred to as DIET WISPR^2. The generalized form of the unnormalized processor is defined as

$$DIET\,AWSUM_k(x_i) \equiv \left[\sum_{t=1}^{T} \sum_{j=1}^{J} \left\{ B_{j,t} / R_{j,t}(x_i) \right\}^{-k} \right]^{-\frac{1}{k}} , \qquad \text{(A.11.1)}$$

where

i is the spatial density index,

j is the beam number index,

t is the time index,

k is the processor order, $k > 0$,

x_i is the spatial density variable,

$B_{j,t}$ is the beamformer output powers for the jth beam for time sample t,

$R_{j,t}(x_i)$ is the beam power spatial response of the jth beam at the ith location in spatial density space for time sample t,

J is the number of beams, and

T is the number of time samples.

To compare the output of this processor to other accepted standards, normalization is required. However, as this process (though a little tedious numerically) is straightforward, it is omitted from this discussion.

The form of the DIET WISPR processor presented here applies to spatial beamforming applications similar to those described in Sec. 9.3. Using a rationale parallel to that which has resulted in defining Eq. A.11.1, a similar equation can be developed for improved spectral resolution. This remains an area needing additional research to fully develop its capability.

Appendix B

LIST OF RELATED PUBLICATIONS

B.1.0 PATENTS

1. R. A. Wagstaff, "Signal Processing for Increasing Signal-to-Noise Ratio," Navy Case No. 72548, Jan 1993.

2. R. A. Wagstaff, "Advanced WISPR Summation (AWSUM) Processor," Navy Case No. 74838, application submitted to NPO, Sep 1994.

3. R. A. Wagstaff and J. George, "A New Fluctuation Based Digital Signal Processor Including Phase Variations," application submitted to NPO, Dec 1996.

4. R. A. Wagstaff, "A_kCSDM: A General Fluctuation Sensitive Cross Spectral Density Matrix for High Gain Beamforming and Signal Processing," Navy Case No. 78,266, submitted Naval Research Laboratory, Jan 1997.

B.2.0 JOURNAL ARTICLES

1. R. A. Wagstaff, "The WISPR Filter: A Method for Exploiting Fluctuations to Achieve Improved Sonar Signal Processor Performance," submitted to *J. Acous. Soc. Am.*, Sep 1995.

2. R. A. Wagstaff and S. D. Gardner, "Exploitation of Acoustic Fluctuations to Enhance Signal-to-Noise Ratio and Resolution of Amplitude Stable Signals," submitted to *J. Acous. Soc. Am.*, Oct 1995.

3. R. A. Wagstaff, "WISPR Processing: The Key to Accessing a New Source of Signal-to-Noise Gain," unpublished manuscript, Oct 1995.

4. J. George and R. A. Wagstaff, "Enhanced Target Detection in the Dabob Bay Active Acoustic Barrier Using the WISPR Filter," unpublished manuscript, Oct 1995.

5. J. George and R. A. Wagstaff, "WISPR Filter Performance Measured in the Presence of Signal Fluctuations and Ambient Noise," unpublished manuscript, Oct 1995.

6. R. A. Wagstaff, "AWSUM: A Digital Filter for Achieving Increased Signal-to-Noise Ratio and Other Signal Processor Enhancements," unpublished manuscript, Apr 1996.

7. R. A. Wagstaff and K. J. Dudley, "Trend Removal to Improve the Performance of the WISPR Processor for Detecting Submerged Sources," unpublished manuscript, Oct 1995.

8. R. A. Wagstaff and S. F. Kooney, "The AWSUM Filter: A 20-dB Gain Fluctuation Based Processor,"*IEEE J. Oceanic Eng.* **22**, 119–127 (1996).

9. R. A. Wagstaff, "WISPR II and Other Enhanced Fluctuation Based Processors," submitted to *J. Acous. Soc. Am.*, Mar (1997).

10. S. D. Gardner and R. A. Wagstaff, "DIET AWSUM: A Technique for Exploiting Fluctuations to Enhance Signal-to-Noise Ratio and Resolution," *IEEE J. Oceanic Eng.* **22**, 110–118 (1997). Jan 1997.

11. R. A. Wagstaff and J. George, "A New Fluctuation Based Processor Including Phase Variations," unpublished manuscript, Apr 1996.

12. J. George, "Performance Evaluations of a Fluctuation Sensitive Processor Using Synthetic and Measured Data," submitted to *J. Acous. Soc. Am.*, Mar 1996.

13. R. A. Wagstaff and J. A. Mobbs, "Pseudo-Operational Unalerted Detection Classification Test of the WISPR Filter," unpublished manuscript, Oct 1996.

14. R. A. Wagstaff and R. F. Fisher, "Mitigating the Adverse Effects of Transients in Acoustic Parameter Estimation," submitted to *J. Acous. Soc. Am.*, Apr 1997.

15. R. A. Wagstaff, "A_kCSDM: Fluctuation Sensitive Beamformers for the Enhancement of Low-Fluctuation-Amplitude Signals," submitted to *IEEE J. of Oceanic Eng.*, Jan 1997.

16. R. A. Wagstaff and W. E. Avera, "Nonacoustic Detection of Submerged Sources Using the WISPR and AWSUM Filters to Exploit Amplitude Fluctuations," unpublished manuscript, Nov 1996.

17. R. A. Wagstaff, "Increasing the Resolution and Gain of High-Resolution Signal Processors for Low Fluctuation Amplitude Signals by Increasing Their Sensitivity to Fluctuations," submitted to *IEEE J. of Oceanic Eng.*

18. J. George, "Physical Mechanisms to Explain the Observed Features of Ambient Noise in Shallow Water," *J. Acous. Soc. Am.* **99**, 3439–3444 (1996).

19. R. A. Wagstaff and J. A. Mobbs, "Exploiting the Sequential Order-Dependence of Amplitude Fluctuations to Enhance Acoustic Parameter Estimation," submitted to *J. Acous. Soc. Am.*, Jun 1997.

B.3.0 REPORTS

1. J. George and R. A. Wagstaff, "Enhanced Shallow Water Barrier Detection Using WISPR and its Application to Dabob Bay," unpublished manuscript, 1993.

2. J. George and R. A. Wagstaff, "Variations of WISPR Levels and Average Power Levels with Standard Deviation," NRL/MR/7176--93-7077, Naval Research Laboratory, Stennis Space Center, MS, 1994.

3. J. George and R. A. Wagstaff, "Target Detection in the Fixed-Fixed III Experiment Using the WISPR Algorithm," unpublished manuscript, 1994.

4. J. George and R. A. Wagstaff, "WISPR Performance Measured by ROC Curves," NRL/MR/7176--94-7559, Naval Research Laboratory, Stennis Space Center, MS, 1994.